

Microwave Electronics

**HEXAGONAL DIELECTRIC RESONATOR ANTENNA – A  
NOVEL DR ANTENNA FOR WIRELESS COMMUNICATION**



**Thesis Submitted**

by

**V. HAMSAKUTTY**

*In partial fulfilment of the requirements for the degree of*

**DOCTOR OF PHILOSOPHY**

**MICROWAVE TOMOGRAPHY AND MATERIALS RESEARCH LABORATORY  
DEPARTMENT OF ELECTRONICS,  
FACULTY OF TECHNOLOGY  
COCHIN UNIVERSITY OF SCIENCE AND TECHNOLOGY  
KOCHI-682 022, INDIA**

**MARCH 2007**

**Dedicated**

**“To the two who gave me life” and**

**To the one who taught me love**

## CERTIFICATE

This is to certify that the thesis titled **Hexagonal dielectric resonator antenna - A novel DR antenna for wireless communication** is a bonafide record of the research work carried out by Mr. V. Hamsakutty under my supervision in the Department of Electronics, Cochin University of Science and Technology. The results embodied in this thesis or parts of it have not been presented for any other degree.



**Dr. K.T. Mathew**

(Supervising Guide)

Kochi- 22

Professor

16-03-2007

Department of Electronics

Cochin University of Science and Technology

## DECLARATION

I hereby declare that the work presented in this thesis titled **Hexagonal dielectric resonator antenna - A novel DR antenna for wireless communication** is based on the original work done by me under the supervision of Dr. K.T. Mathew, in the Department of Electronics, Cochin University of Science and Technology, and no part thereof has been presented for the award of any other degree.

Kochi – 22

16-03-2007



V. HAMSAKUTTY

## Heartfelt thanks...

How little can mere words reveal of what our hearts most deeply feels...It's natural that a lot of thanks come with this thesis.

First I thank and praise the Lord Almighty for his mercy, sustenance, and uncountable blessings.

I would like to express my gratitude to my Guide Professor K.T Mathew, who poured over every fine aspect of the thesis with painstaking attention to details and made a semi-infinite number of helpful suggestions. My special thanks go to Professor & Head of the department Dr. K. Vasudevan for his help and advice. Many thanks to Dr. P.Mohanan, Dr. C.K. Aanandan, Dr. K.G Balakrishnan, Dr. P.R.S Pillai, Dr. Tessamma Thomas, Mr. James Kurian and Mrs. Suppriya who helped me in various ways.

A thoughtful act and a kindness shown to others is never forgotten, but remembered for ever - Dr. Joe Jacob, Sr. Lecturer Newman's College, Thodupuzha, you are one of those people. I thank you from the bottom of my heart. A bouquet of thanks to my colleagues Dr. Jaimon yohannan, Mr. A.V Praveen Kumar, Mr. Rohith K. Raj, Mr. Anil Lonappan, Mr. Vinu Thomas, Mr. Robin Augustine, Mr. Cyriac M.O, Mr. Anupam R. Chandran and Mr. Abdullah for their continuous advice and help during the past several years.

Let me also remember at this moment, all the teaching, non teaching staffs and research scholars of the DOE for their continuous companionship. Now I wish to acknowledge the financial support of the UGC through FIP fellowship during the course of my doctoral studies.

I would also like to express my gratitude and thanks to the members of my family, each of whom helped me in innumerable ways. My parents were a constant source of inspiration and moral support. Their

sacrifices and continuous prayers helped me throughout my life. Thanks to my wife for her support, encouragement and prayers throughout all the uncertain times. Her sacrifices helped me to complete this work. Special thanks to my fathers-in-law and mothers-in-law, who gave me constant support and encouragement, and also to all my dears and nears.

I would like to express my thanks and appreciation to the Manager, and Principal Dr. A. Abdul Latheef of W.M.O College, Wayanad who permitted me to undertake the research under FIP. Last but not least, I would like to thank all the colleagues at W.M.O College for their continuous encouragement and support.

Though busy, you all had time to spare for me, to listen to me, to discuss with me, to help me and to guide me. I want you (all) to know how very grateful I am...

*Thank you*

# CONTENTS

Preface

1

---

## CHAPTER I INTRODUCTION

---

1.1	Developments in Electromagnetics and Microwaves	7
1.1.1	Predecessor to Microwaves: Wireless and Radio	9
1.1.2	The Physicist's War: World War II	13
1.1.3	Microwaves and Telecommunication	16
1.2	Antennas	19
1.3	Dielectric resonator antennas	21
1.3.1	Features of dielectric resonator antenna	24
1.3.1.1	Resonant Frequency	24
1.3.1.2	Q-Factor	25
1.3.1.3	Bandwidth	26
1.3.1.4	Different geometries	28
1.4	Coupling methods to DRAs	29
1.4.1	Coaxial probe	30
1.4.2	Slot/Aperture coupling	31
1.4.3	Microstrip transmission line/proximity coupling	32
1.4.4	Coplanar feed	32
1.4.5	Waveguide feed	33
1.4.6	Conformal strip feed	32
1.5	Theoretical Considerations: Dielectric Resonators	35
1.5.1	Field Modes	35
1.6	Numerical Methods	37
1.6.1	Overview	37
1.6.2	Finite Difference Method	39
1.6.3	Variational Methods	40
1.6.3.1	Method of Moments (MoM)	40
1.6.3.2	Finite Element Method (FEM)	41
1.6.4	Method of Lines	41
1.6.5	Finite Difference Frequency Domain Method	42
1.6.6	Spectral Domain Approach	43
1.6.7	Mode Matching Method	43
1.6.8	Transmission Line Method	43
	References	44

---

## CHAPTER II      REVIEW OF THE PAST WORK

---

2.1	Introduction	46
2.2	Different geometries of DRA	47
2.3	Different coupling methods to DRA	47
2.4	Theoretical Analysis of DRA	47
2.5	Miniaturisation of DRA	49
2.6	Bandwidth Enhancement Techniques	49
2.7	Circular polarization	50
2.8	Antenna Gain	52
2.9	Air gap Effect	52
2.10	Multi-frequency Operation	52
2.11	Conclusion	53
	References	53

---

## CHAPTER III      METHODOLOGY

---

3.1	Introduction	62
3.2	Basic facilities utilized	62
3.2.1	HP 8510C Vector Network Analyzer	62
3.2.2	Anechoic chamber	64
3.2.3	Automated turn table assembly for far field measurements	65
3.3	Experimental set up	65
3.4	Measurement procedure	67
3.4.1	S-parameters, Resonant frequency and Bandwidth	68
3.4.2	Radiation patterns	69
3.4.3	Gain	70
3.4.4	Polarization pattern	71
3.5	Ansoft HFSS	72
	References	73



---

## CHAPTER IV SYNTHESIS OF DIELECTRIC RESONATORS

---

4.1	Introduction	74
4.2	Preparation of DR Pellet	74
4.2.1	Weighing and mixing	75
4.2.2	Pre-heating	75
4.2.3	Binder addition and dry pressing	75
4.2.4	Sintering	79
4.2.5	Finishing	79
4.3	Microwave characterization of DR	80
4.3.1	Method of measuring the permittivity	80
4.3.2	Hakki and Coleman method	81
4.3.3	Cavity perturbation technique	84
	References	86

---

## CHAPTER V EXPERIMENTAL STUDY OF HEXAGONAL DIELECTRIC RESONATOR ANTENNA

---

5.1	Introduction	88
5.2	Coaxial fed HDRA	88
5.2.1	Antenna Configuration	88
5.2.2	Effect of coaxial probe length on the performance of HDRA	90
5.2.3	Effect of DR height on the performance of HDRA	91
5.2.3.1	Results and discussion	92
5.2.4	Effect of variation of Coaxial feed position on HDRA	96
5.2.4.1	Results and discussion	97
5.3	Microstrip fed HDRA	118
5.3.1	Antenna Configuration	118
5.3.2	Effect of microstrip feed position on HDRA	118
5.3.2.1	Results and discussion	120
5.4	Radiation efficiency of the HDRA	133
5.5	Comparison of antenna performance between HDRA and conventional Cylindrical DRA	133
5.6	Conclusion	133
	References	135

## CHAPTER VI THEORETICAL ANALYSIS-FDTD

---

6.1	Introduction	136
6.2	Electromagnetic Analysis	138
6.2.1	Governing Equations	138
6.2.2	Finite difference equations	139
6.2.3	Normalized Maxwell's equations	142
6.2.4	The Perfect Matched Layer (PML)	145
6.3	Description of the microstrip fed HDRA	158
6.3.1	Modeling the materials	160
6.3.2	Boundary conditions	162
6.3.3	Source	163
6.3.4	Resistant source FDTD excitation	164
6.3.5	Flow chart for the simulation of HDRA	167
6.3.6	FDTD Results	170
	6.3.6.1 Calculation of Return loss	170
	6.3.6.2 Calculation of electric field distribution	176
6.4	Description of Coaxial Fed HDRA	177
6.4.1	Modeling the material	180
6.4.2	FDTD Results	182
	6.4.2.1 Calculation of return loss	182
6.5	Conclusion	185
	References	186

---

## CHAPTER VII CONCLUSION AND FUTURE SCOPE OF THE WORK

---

7.1	Highlights of the work	194
7.2	Possible applications	195
7.3	Scope of future work	195
7.4	Concluding remarks	196

---

## APPENDIX-A

---

A-1	Introduction	197
A-2	Antenna structure	198
A-3	Experimental results	199
A-4	Conclusion	202
	References	202

---

## APPENDIX-B

---

B-1	Introduction	204
B-2	Sample preparation	206
B-3	Experimental procedure and set up	206
B-4	Theory	208
B-5	Results and discussion	209
B-6	Conclusion	214
	References	215
	<b>List of Publications</b>	<b>216</b>
	<b>Resume</b>	<b>220</b>

---

## **PREFACE**

---

IN an age when access to information, communication and infotainment, any time, any place, anywhere has become a pre-requisite for modern life, it is not surprising that the wireless technology has been the focus of attention of technocrats and scientists.

The field of wireless communication has been undergoing a revolutionary growth for the last decade. This is attributed to the invention of portable mobile phones some fifteen years ago. The access of the second generation (2G) cellular communication services motivates the development of wideband third generation (3G) cellular phones and other wireless products and services, including wireless local area networks, home RF, bluetooth, wireless local loops, local multipoint distributed networks etc. The crucial component of a wireless network or device is the antenna. We can see our cities are flooded with antennas of different kinds and shapes. On the other hand for safety and portability reasons, low power, multi functional and multiband wireless devices are highly preferred. All these stringent requirements demand the development of highly efficient, low profile and small size antennas that can be embedded into wireless products.

In the last two decades, two classes of novel antennas have been investigated. They are the Microstrip Patch Antenna (MPA) and the Dielectric Resonator Antenna (DRA). Both are highly suitable for the

development of modern wireless communications. The use of dielectric resonator antenna was first proposed by Prof. S. A. Long in the early nineteen eighties. DRA has negligible metallic loss, and hence it is highly efficient than its counterpart when operated in microwave and millimeter wave frequencies. Also low loss dielectric materials are now easily available commercially at very low cost, which attracts more system engineers to choose dielectric resonator antenna to design their wireless products.

Dual or multifrequency operation is highly attractive in current wireless communication systems. If a single DRA can support multiple frequencies, then there is no need for multiple single frequency antennas. Applications requiring different frequency bands can be addressed simultaneously with one radiating element. This reduces the circuit size and leads to compact systems. In addition, when multiple frequencies are located close to each other, the antenna may have a broad operating bandwidth. Many investigators have reported on DRA with dual frequency operation using various approaches. But in all these cases dual frequencies are achieved by using either dual feed lines or multiple radiating elements or hybrid radiating structure, which causes design complexity and large size.

In this thesis, the author proposes a new geometry of hexagonal shape DR to the DR antenna community - Hexagonal Dielectric Resonator Antenna (HDRA) for multi frequency operation with a single feed of excitation, which is the highlight of this work. These multiple frequency bands are suitable for Digital Cordless Telephones (DCT), Personal

Communication Systems (PCS) and Wireless Local area Networks (WLAN) bands.

This thesis is organized into seven chapters which describe the problem addressed, methodology adopted, results obtained, comparison between measured and theoretical results, and conclusions arrived at.

First chapter explains the development of electromagnetism, microwaves and its application from the origin. Also describes the dielectric resonator antennas (DRAs), its features over conventional microstrip antennas, different coupling methods used for exciting the DRAs and different geometries of DRAs already developed. The last section of this chapter gives a comparative study of different numerical methods used for modeling the antenna.

Chapter II provides the review of dielectric resonator antennas from its beginning to the current development. It includes the different coupling mechanism used to excite the DRAs, various geometries of DRAs developed, different techniques for improving the bandwidth, gain and the sequential theoretical analysis of DRAs. The diverse methods for producing circular polarization, air gap effect on resonant frequency and bandwidth, variety of techniques for producing multi frequency operation are reviewed in chronological order.

Chapter III describes the research methodology opted for this work. The experimental setup used for measuring the return loss, radiation pattern, gain and polarization is explained. Moreover it describes the

simulation software used for characterizing the hexagonal dielectric resonator antenna.

The step-by-step development of hexagonal dielectric resonator antenna from the basic material is explained in chapter IV. It includes weighing, mixing, sintering, pressing, shaping etc. The setup used for measuring the dielectric permittivity of the material is also explained.

In Chapter V, the first part introduces the new hexagonal shaped dielectric resonator antenna with coaxial feed as excitation. The optimizations of coaxial probe length, probe feed location and aspect ratio of HDRA are performed experimentally. Besides, it explains the radiation pattern, gain and polarization of the antenna for different bands using the coaxial feed excitation. The second part explains the HDRA characteristics using microstrip feed excitation. A comparison of experimental results with the simulated results, using Ansoft HFSS, is also included in this chapter.

The theoretical study using finite difference time domain (FDTD) method for modeling the microstrip fed and coaxial fed HDRA is explained in chapter VI. It describes the theoretical concepts of FDTD in electromagnetics and the perfect matched layer (PML) concepts for absorbing boundary condition (ABC). All the necessary equations for three-dimensional electric and magnetic field variables are derived from the fundamental Maxwell's curl equations and are given in this chapter. It also uses Lubber's feed techniques for reducing the number of time steps

required for modeling the whole structure. The FDTD results are compared with the measured values.

Chapter VII provides the conclusions and highlights drawn from this work. Advantages of new geometry hexagonal DRA and its possible applications in wireless communication are specified. Furthermore, it gives the future scope of the work in this area.

There are two Appendices included.

In Appendix – A, a metal-coated cylindrical dielectric resonator antenna for producing multiple resonances is given. Coaxial probe is used for exciting the cylindrical DRA. All the characteristics of the antenna are explained in this section.

In Appendix – B, the development of a novel coupling media and phantom material constituent for microwave medical imaging applications using sodium meta silicate gel is explained. Dielectric parameters, heating and absorption coefficient of this material are studied and discussed. Comparative studies of the suitability of gel with various biological tissues are also given in the last part.

In view of the fact that, microwave medical tomography is promising a novel non- hazardous method of imaging for the detection of tumors in soft tissues. The tomographic set up consists of antennas, coupling media and the object to be imaged. The antenna must be operated at ISM frequency. The purpose of coupling media is to enhance the coupling of electromagnetic energy between the antenna and the object to be imaged.



The object is placed at the center of the imaging set up from where the scattered microwave data is collected and analyzed at the various locations of the receiver and the orientation of the object. As the HDRA developed in the core work of the thesis operates at 2.4 GHz-ISM frequency can as well be used in tomographic set up.

## **Chapter I    INTRODUCTION**

---

### **1.1    Developments in electromagnetics and microwaves**

Microwaves are electromagnetic waves with wavelengths longer than those of Terahertz but relatively shorter than radio waves and have wavelengths approximately in the range of 30cm to 1mm. Although scientists knew a good deal about both electricity and magnetism by 1750, no one yet suspected that there was any connection between the two. We know that both the electric force that attracts bits of paper to a comb and the magnetic force that attracts a steel paper clip to a magnet are different aspects of the same force, the “electromagnetic” force. Electricity and magnetism are intimately related in a complex way, and it took a number of geniuses in the 1800s to figure it out.

In 1820, the Danish physicist Hans Christian Oersted found that if he moved a wire carrying an electric current near a magnetic compass needle, the needle tended to turn at right angles to the wire. This was the first direct evidence that electricity and magnetism were related. In the following four decades, physicists like Michael Faraday and Joseph Henry studied this relationship in more detail. Many of them tried to develop a theory to explain exactly how electricity and magnetism were related, but they encountered great mathematical and experimental problems.

$$\oint H \cdot dl = I + \epsilon \frac{d}{dt} \iint E \cdot ds$$

*Ampere's Law*

$$\oint E \cdot dl = -\mu \frac{d}{dt} \iint H \cdot ds$$

*Faraday's Law*

$$\epsilon \oiint E \cdot ds = \iiint q_v \cdot dv$$

*Gauss' Law*

$$\mu \oiint H \cdot ds = 0$$

*The Fourth Equation*

*Maxwell's four equations define the entire field of electromagnetics.*

The man who overcame these problems and developed a comprehensive theory of electromagnetism was Scottish physicist James Clerk Maxwell.

During the 1860s he devoted several years to the problem of electromagnetism, and published his results in their complete form in 1873. At the time few physicists could understand Maxwell's work, but when the years passed the world recognized that Maxwell had written down the

essential laws of electrodynamics, which is how the electromagnetic force operates. Today Maxwell's discovery can be expressed in four short equations called Maxwell's Equations, although he did not originally write them in that form.

Maxwell's Equations allowed for the existence of invisible electromagnetic waves with much longer wavelengths than light. No one had imagined the existence of such waves but physicists began to look for them. In a series of experiments that began in 1886, the German physicist Heinrich Hertz proved that these long electromagnetic waves were real. He showed this when he generated what we now call radio waves with an

electric spark, transmitted them the length of his laboratory, and made them produce a smaller spark at his receiver. By showing that these “Hertzian waves” traveled in beams and could be focused like light rays, Hertz convinced the scientists of his time that he had discovered the long electromagnetic waves that Maxwell’s equations predicted. In the 1890s, other physicists repeated and expanded Hertz’s experiments. The Indian physicist Jagadish Chunder Bose produced and experimented with waves as short as 5 millimeters (less than a quarter of an inch, but still much longer than light).

### **1.1.1 Predecessor to Microwaves : Wireless and Radio**

The technology of microwaves has its roots in the earlier technology of radio communication. The first form of radio was called “wireless telegraphy,” because when it was invented around 1900, people thought of it as an improved form of the telegraph. Wireless telegraphy was used to send messages from point-to-point. Although it is still used that way today, we are more familiar with “radio telephony” and radio “broadcasting”. Radio telephony was simply a wireless form of the telephone, while voice broadcasting employed a single station that transmitted to a multitude of receivers scattered across a wide geographic area.

In the late 1890s, when radio began, most physicists believed that radio signals could not travel great distances. In a series of experiments that began in 1894, radio pioneer Guglielmo Marconi proved them wrong.

Marconi successfully transmitted radio signals across increasingly long distances and in 1901 he transmitted radio signals across the Atlantic. When Marconi proved that radio waves could be transmitted over very long distances, physicists around the world took note. Marconi's equipment used rather long waves, which did not make sense to physicists of the day. The problem that alarmed them was that of radio waves, like light waves, were supposed to travel in straight lines. We can't see beyond the horizon with light waves, so how could radio waves travel beyond the horizon? As a possible answer to the puzzle, American Arthur E. Kennelly and Englishman Oliver Heaviside proposed that a layer of ions (charged atoms and molecules) high in the atmosphere might reflect radio waves back to earth. This layer was later proven to exist and became known as the ionosphere. Long waves bounced back and forth between the ionosphere and the earth's surface as they traveled outward from their point of origin. These reflections allowed them to follow the curvature of the earth.

One problem of using those long waves was that once more and more radio stations came into service, they interfered with each other. In order to reduce that interference, stations were assigned particular frequencies on which to broadcast. Using the shorter wavelengths (what today is the AM broadcasting band) proved to be a good solution to the problem of overcrowding. There was a lot more room in the shorter wavelengths for more stations, and these shorter waves tended to fade

after a few hundred kilometers (or usually much less), so that even if two stations were given the same frequency to operate in, as long as they were located far from each other they would not interfere. The “medium waves” as they were later known still serve us today as the AM radio band. “Short waves” were also opened up for broadcasting, and these proved suitable for international broadcasts. The military, television stations, police departments, and others are also assigned various frequencies in this part of spectrum.

In order to accomplish all these, improved equipment was developed that was not available back in Marconi’s day. The change from dot-dash wireless telegraphy in the early 1900s to voice broadcasts was first demonstrated on Christmas Eve, 1906, when Canadian inventor Reginald A. Fessenden broadcast the first music and voice program over long distances. Transmitted from Massachusetts, Fessenden’s broadcast was received as far away as Virginia. Fessenden’s broadcast proved that radio waves could be transmitted more than just the dots and dashes of Morse Code. However, it was not until the 1920s that regular voice broadcasts began.

Fessenden used an electromechanical device called an alternator to produce the waves he used for broadcasting. Another approach to generating radio waves (the one that ultimately succeeded) was to use an electron tube circuit. One of the first electron tubes was the Audion, invented in 1906 by Lee De Forest. The Audion was intended to amplify

radio waves, not to generate them, but it turned out that it could do both. After many years of development, the Audion were employed to generate high frequency radio waves for radio and television stations.

Armed with improved equipment, professional researchers and radio amateurs found that short radio waves could travel around the world as well as or better than longer radio waves under certain conditions. But it took improved electron tube equipment to make use of the shorter waves. The short waves had lengths from about 100 meters down to 10 meters (300 to 30 feet) long. Their frequency was between 3 million cycles per second or “megahertz” (MHz) and 30 MHz. Amateurs found that with an inexpensive transmitter putting out only a few watts of power, they could talk to another station halfway around the world. Besides improvements in electron tubes, researchers developed new scientific techniques to understand the way radio waves traveled through space or along transmission lines such as coaxial cables. One such development was the “Smith chart” proposed by Phillip Smith. The usefulness of short waves for radio communication made some researchers curious about what awaited them at wavelengths shorter than 10 meters (30 feet) and higher in frequency than 30 MHz. Throughout 1930s, scientists and engineers began experiments with what they called “ultra-short waves” or “micro waves.” Their efforts led to discovery of various microwave bands, the classification of which is given below in **Table 1.1**

Table 1.1

Microwave frequency bands	
Designation	Frequency range
L band	1 to 2 GHz
S band	2 to 4 GHz
C band	4 to 8 GHz
X band	8 to 12 GHz
K <sub>u</sub> band	12 to 18 GHz
K band	18 to 26.5 GHz
K <sub>a</sub> band	26.5 to 40 GHz
Q band	30 to 50 GHz
U band	40 to 60 GHz
V band	50 to 75 GHz
E band	60 to 90 GHz
W band	75 to 110 GHz
F band	90 to 140 GHz
D band	110 to 170 GHz

### 1.1.2 The Physicist's War: World War III

World War II (1939-1945) was the first major war in which nations systematically recruited their scientists and engineers to develop weapons and other military technology. Because of this new reliance on technology and invention it is sometimes referred to as the Physicists' War. All sorts of inventions and discoveries, from the atomic bomb to improved antibiotics and medical care, came about during those few short years. The war led to tremendous advances in microwave technology as well, and the reason can be summed up in one word: radar.

Radar works by sending out radio waves toward an object to be detected. The time a wave takes to reach an object and come back is a measure of how far away the object is. If the waves are focused in a narrow beam, moving the beam from side to side and noting the angle



where the received signal is strongest can determine the direction of the object. Since radio waves travel just as easily in the dark as in the daytime, radar is a way of seeing things in the dark, and through clouds and fog. The prospect of detecting enemy planes and ships and of navigating across land and sea with the aid of invisible radio waves attracted the attention of military researchers as early as the 1920s. In the 1930s, several laboratories developed early versions of radar sets. They gave a vital early warning of air attacks across the English Channel and showed that radar was a promising new technology for military use.

British researchers also developed one of the most useful electron tubes for radar, the cavity magnetron. This tube generated hundreds of watts of power at microwave frequencies with wavelengths about 10 centimeters (four inches) long, enough to produce echoes from objects many miles away. Britain lacked the large-scale manufacturing facilities to mass-produce the magnetron, and hence in 1940, one was shipped in secrecy to the United States. There, researchers at the Massachusetts Institute of Technology (MIT) Radiation Laboratory (Rad Lab) and elsewhere developed many production versions of the magnetron as well as a wide variety of radar sets that used them. The ordinary wires and cables that could carry radio waves were inefficient for carrying microwaves, so a technology called the waveguide was developed for World War II (and later) radars. This type of waveguide was a hollow metal pipe through which the microwaves traveled.

Airborne radars were used in bombers as an aid to night flying. Large antennas would not fit on airplanes, so airborne radars used small antennas only a couple of feet across and short microwave wavelengths of about three centimeters (one inch). These radars could show the pilot a “map” of the region he was flying over at night or in fog. Ground-based flight control radars made it easier for pilots to land at hastily constructed airfields during the war. After 1945, researchers used the knowledge and equipment they had gained during the war to find new uses for microwaves. These were not long in coming, and included technologies such as satellite communications and the ubiquitous microwave oven. Finally, microwaves are used by the military in global positioning systems or GPS. GPS receivers use microwave beams from satellites to find positions almost anywhere on Earth. In certain circumstances GPS can locate a target within a few yards of its location. A more speculative use of microwaves is so-called “death rays.” Since the 1930s, rumors spread about secret weapons that use powerful microwave beams to form death rays. Most experts agree that if one wants to make a death ray, microwaves are a poor choice; lasers and other devices that use even shorter wavelengths would be better. High-power microwaves, however, do have growing military value as a non-lethal weapon, a direct contradiction of a “death ray.”

### **1.1.3 Microwaves and Telecommunication**

Every time two people anywhere in the world have a telephone conversation, a two-way electronic path has to be established between them. Telecommunications is the technology of providing these paths reliably at a reasonable cost, and telecommunications often depends on microwaves. The first major use of microwaves in telecommunications came after World War II. Microwave technology that was developed during the war was used to send large numbers of long-distance telephone calls around the United States and other countries. Microwave “repeater” towers used for the transcontinental television network in the 1950s were also useful for carrying telephone calls. These repeater towers were spaced about every 40 kilometers (30 miles) and formed a chain on which the microwaves traveled.

Because there is often more bandwidth available in the electromagnetic spectrum at microwave frequencies than at lower radio frequencies, a single microwave link (chain of repeaters) can simultaneously carry hundreds or thousands of telephone conversations. Before World War II there were ways of sending several conversations at once over a buried cable, but microwave links proved to be both cheaper and higher in transmission capacity. From the 1950s through the 1970s, microwave link networks were built over land in many parts of the world to carry long-distance telephone traffic. In the 1980s fiber-optic cable began replacing microwaves as the long-distance transmission method of

choice. A single optical fiber has thousands of times the information-carrying capacity of a microwave link. As optical fiber cables began connecting cities together, using them became cheaper than maintaining the limited-capacity microwave networks. But as long-distance applications for microwaves decreased new short-range applications emerged. These included wireless computer and data networks and cell (or mobile) phones. A cell-phone system breaks up a large area into smaller cells, each with its own base station and antennas (often on a tower or tall building). When you make a call from your cell phone, your phone transmits a microwave signal in the 1-2 GHz frequency range to the base station closest to you. Once communication is established, the base station works with your phone to set the lowest power of transmission that will let the call go through just to that base station. Doing so ensures that your signal doesn't carry much farther than the cell you are in. This means you don't interrupt other people in other parts of the city who are using the same band of microwave frequencies. This also reduces the power drain on the battery in your phone and maximizes the battery's life.

The growth of the Internet and computer communications has increased the demand for both fiber-optic and microwave communications systems. As useful as fiber-optic cables are, you cannot walk around or drive while connected to one. For this reason, it is likely that microwaves will continue to be used in many kinds of mobile and wireless applications in the future, from telephones to portable computers, personal digital

assistants, and other devices that haven't even been invented yet. Global wireless band is shown in **Fig. 1.1**

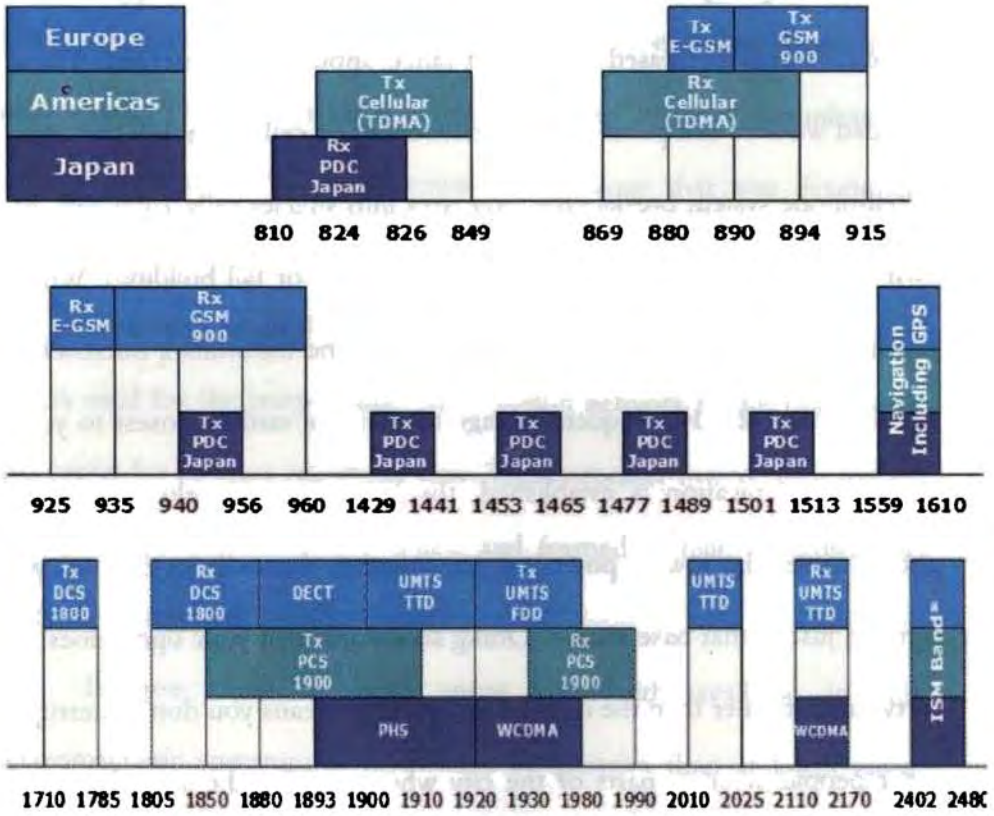
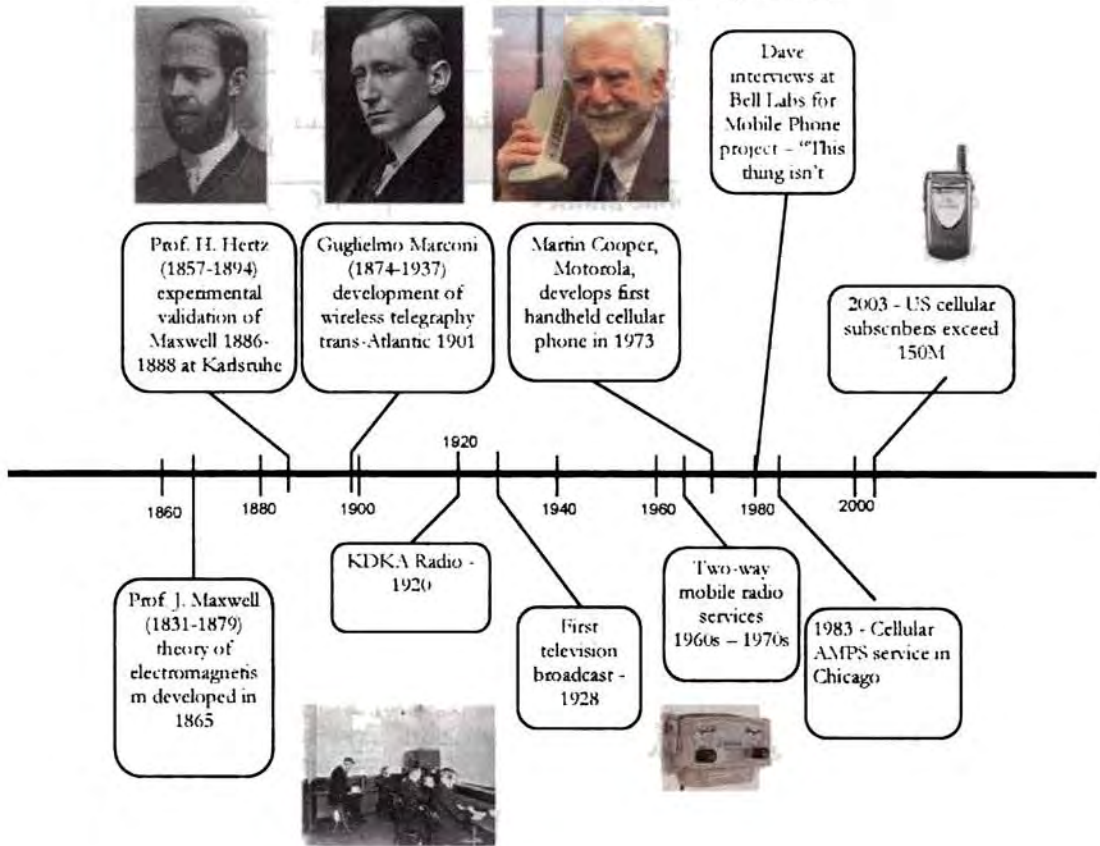


**Fig. 1.1** Global Wireless Frequency Bands

*The development of wireless communication since 1860.....at a glance*

*Timeline of Wireless Communications Development . . .*



**1.2 Antennas**

An antenna or aerial is defined as a means for radiating or receiving radio waves. An antenna is used to radiate or receive electromagnetic energy efficiently in or from desired directions. Antennas act as matching systems between sources of electromagnetic energy and space. The goal in using antennas is to optimize this matching. Brief history of antennas is shown in **Table II.**

Table II

History/ Evolution/ Trends in Antennas		
Antenna	Type	Frequency
Early 20th century	Radio antennas	~ MHz
Mid- 20th century	TV	100's MHz
Late 20th century	Mobile phones	~ 1 GHz
Early 21st century	Bluetooth/WLAN (Wireless systems)	2-5 GHz
Next??	Future generation (?)	20-50 GHz (?)

Here is a list of some of the properties of antennas

1. Field intensity for various directions (antenna pattern)
2. Total power radiated when the antenna is excited by a current or voltage of known intensity
3. Radiation efficiency, which is the ratio of power radiated to the total power
4. The input impedance of the antenna for maximum power transfer (matching)
5. The bandwidth of the antenna or range of frequencies over which the above properties are nearly constant

Different Types of Antennas used are Dipole Antennas, Monopole, Loop Antennas, Aperture Antennas, Reflector Antennas, Horn, waveguide, Reflector Printed antennas, Array Antennas, Multiple Element Dipole

Antennas, Yagi Antennas, Flat Panel antennas, Parabolic Dish antennas, Helix, Slotted Antennas, Microstrip Antennas, Phased array antenna and Dielectric resonator antennas. In this work the author is interested in dielectric resonator antennas and is explained in the following section.

### **1.3 Dielectric resonator antennas**

Dielectric Resonator Antennas (DRAs) are fabricated from Low-loss dielectric material of various shapes, whose resonant frequencies are functions of the size, shape and permittivity of the material.

The fact that dielectric resonators radiate energy was proven by Richtmyer [1] in 1939; however practical application did not take place until the 1960's [2] when suitable dielectric compounds became available. Initially there was very little interest in applying this technology at the popular frequencies of interest. First antennas were in the MHz ranges, which were adequately handled with inefficient, bulky but simple rigid structures. Dielectric resonators were first popular as filter element devices and oscillators in microwave circuits [3] with the first reported use as a radiating element not until the early 1980's when the smaller size potential and higher frequency applications boosted the research into the dielectric resonator antenna. [4]

The DRA offers several advantages over the Microstrip Patch Antennas (MPAs). At millimeter and near millimeter frequencies, the conductor loss of metallic antennas becomes severe and the efficiency of



the antennas is reduced significantly. Conversely the only loss for a DR is that due to the imperfect dielectric material, which can be very small in practice. It was found that the dielectric resonator antenna (DRAs) operating at their fundamental mode radiate like magnetic dipole independent of their shapes. Since the DRA is a non-metallic structure, there are no conduction or surface wave losses; therefore their radiation efficiency is very high ( $> 98\%$ ) [5]. They can be simply coupled to many types of transmission lines and are easily integrated with microstrip integrated circuits (MICs). Various resonator shapes are possible (rectangular, cylindrical, hemispherical, triangular, conical, tetrahedron), and a variety of feed mechanisms can be utilised (probe, aperture, slot, microstripline), which allows great flexibility in the design process. The bandwidth is inherently larger than MPAs, and is controllable through the permittivity. Permittivity can also be used to control the relative size of the resonator, since the wavelength within the dielectric is shorter than that in free space. The DR is normally made of high-permittivity material, with dielectric constant  $\epsilon_r > 20$ . The unloaded Q factor is usually between 50 and 500, but can be high as 10000. High permittivity allows for smaller resonators, while low permittivity results in higher bandwidth. Also, rectangular DRAs are not as susceptible to tolerance errors as are MPAs, especially at higher frequencies [6]

DRA design requires accurate information on the basic antenna parameters, such as resonant frequency, bandwidth, internal field

distribution and radiation pattern. To date, however, there is no comprehensive work published in order to assist in the design Process. For the most part, much of the current work is hampered by the requirement for approximation methods, since many of the structures cannot be analytically determined through closed form solutions. Literature surveys indicate that considerable preliminary work has been conducted in determining resonant frequencies and Q factors, however there was little consideration given to radiated fields or mode structures.

DR was usually treated as an energy storage device rather than as a radiator. Open DRs were found applications as radiators many years ago. As compared to the microstrip antenna, the DRA has a much wider impedance bandwidth. This is because, the microstrip antenna radiates only through two narrow radiation slots, whereas the DRA radiates through the whole DRA surfaces except the ground part. ~~Avoidance of surface waves is another attractive advantage of the DRA over the microstrip antenna.~~

Nevertheless, many characteristics of the DRA and microstrip antenna are common because both of them behave like resonant cavities. For example, since the dielectric wavelength is smaller than the free-space wavelength by a factor of  $\sqrt{\epsilon_r}$ , both of them can be made smaller in size by increasing  $\epsilon_r$ . Moreover virtually all excitation methods applicable to the microstrip antenna can be used for the DRA.

1.3.1 Features of dielectric resonator antenna

1.3.1.1 Resonant Frequency

The resonant frequency of the  $npm$  mode of a basic cylindrical DRA can be found as

$$f_{npm} = \frac{1}{2\pi a \sqrt{\mu \epsilon}} \sqrt{\left\{ \begin{matrix} X_{np}^2 \\ X'_{np}{}^2 \end{matrix} \right\} + \left[ \frac{\pi a}{2d} (2m + 1) \right]^2} \dots\dots\dots (1.1)$$

Where  $a$  = radius of the cylindrical DRA,  $d$ = height of the DRA,  $m$  = mode,  $\mu$  and  $\epsilon$  are the permeability and permittivity of DRA respectively.

In practical applications, the fundamental (dominant) mode is of interest, which has the lowest resonant frequency .It is found that the fundamental mode is  $TM_{110}$  mode, with the resonant frequency given by

$$f_{TM_{110}} = \frac{1}{2\pi a \sqrt{\mu \epsilon}} \sqrt{X_{11}^2 + \left( \frac{\pi a}{2d} \right)^2} \dots\dots\dots (1.2)$$

Where  $X'_{11} = 1.841$ .

The above equation can be written as

$$f_{110} = \frac{c}{2\pi a \sqrt{\epsilon_{ra}}} \sqrt{1.841^2 + \left( \frac{\pi a}{2d} \right)^2} \dots\dots\dots (1.3)$$

where  $\epsilon_{ra}$  is the permittivity of DR.

Where  $c$  is the velocity of light in free space. For a low- profile disk antenna,  $a/h \gg 1.841$  and therefore this expression can be further simplified as

$$f_{110} = \frac{c}{4d\sqrt{\epsilon_{ra}}} \dots\dots\dots (1.4)$$

This is identical to the corresponding simplified expression for low-profile rectangular resonators.

### 1.3.1.2 Q-Factor

The concept of Q-factor (or Quality factor) is used to describe the antenna as a resonator. A high Q-factor means a sharp resonance and narrow bandwidth. The Q-factor can be expressed as:

$$Q = \frac{\text{antenna reactance}}{\text{antenna resistance}}$$

Usually in circuit design we want elements to have a high Q-factor in order to reduce the circuit loss. However, talking about antennas we want a low Q-factor because the “loss” involved is the radiation we really want. A low-Q antenna is easier to match and tune, and have a wider bandwidth.

If the antenna can be placed inside a sphere of radius  $a$ , the minimum Q-value for a loss-less antenna is

$$Q_{\min} = \frac{1}{(ka)^3}$$

where

$$k = \frac{2\pi}{\lambda}$$

This expresses the absolute minimum Q value the antenna can take. Unfortunately, the theory does not tell us how to implement a minimum Q antenna. The antenna Q can of course be reduced by introducing loss (a resistor) in addition to the radiation resistance, but this would reduce the antenna efficiency, see below. The concept of Q-value is very useful when considering small antennas. The Q-value of the small antenna is high due to the low radiation resistance and the high reactance. The smaller the antenna, the higher Q-value we expect. Hence, the bandwidth of a small antenna will be small, more difficult to match and more susceptible to de-tuning by surrounding objects.

The radiation Q- factor of the DRA is determined using

$$Q = \frac{2 W_e}{P_{rad}} \dots\dots\dots (1.5)$$

Where  $W_e$  and  $P_{rad}$  are the stored energy and radiated power, respectively.

**1.3.1.3 Bandwidth**

In general, all resonant antennas will have a limited bandwidth of operation due to their resonant nature. The input impedance of the antenna usually defines this bandwidth limitation since it is the quantity, which changes most rapidly with frequency. The radiation pattern can also be used to define the bandwidth, in terms of the gain, beam width, cross-polarization levels, or side lobe levels. Several techniques can be used to increase the operational bandwidth of resonant antennas, which have inherently narrow bandwidth. Several methods for reducing the inherent

Q-factor of the resonant antenna are available. For microstrip patch antennas for instance, one of the simplest technique is to lower the dielectric constant of the substrate. Since the Q-factor is related to the dielectric constant, a decrease in the dielectric constant will cause decrease in the Q-factor and thus an increase in the bandwidth. Although this is a simple solution, there are some drawbacks. As the dielectric constant is reduced, the size of the resonant antenna will increase, for a given frequency. This may not be desirable for many applications where a compact or low profile antenna is required. Also the coupling to the antenna may become more difficult. Another method for lowering the Q-factor involves loading the antenna. The advantage of this approach is that, there is no significant increase in the dimensions. Impedance matching networks can be used to increase the bandwidth of a resonant antenna by transforming its input impedance to better match that of the coupling circuit. These matching networks are usually external to the antenna, occurring after the coupling mechanism, but sometimes these networks can be incorporated within the antenna itself. The final approach to increasing the bandwidth of resonant antenna involves the use of multiple resonant configurations. By using two or more resonators, each designed at a somewhat different frequency; the resonators can be combined to give wideband or multi-band operation. The advantage of this approach is that each resonator can be tuned more-or less independently. The disadvantage

lies in the added area required which may preclude some of these configurations from being used in an array environment.

The bandwidth of the DRA is related to the Q-factor by

$$BW = \frac{S-1}{Q\sqrt{S}} \cdot 100\% \dots\dots\dots (1.6)$$

Where S is the desired VSWR at the input port of the DRA. The Q-factor occurs for small values of dielectric constant. In theory, a DRA with a dielectric constant of one would have the lowest Q-factor and therefore the widest bandwidth. In practice, however, there is a lower limit on the values of the dielectric constant required to contain the fields within the DRA in order to resonate. A considerable degree of bandwidth control is possible by adjusting the aspect ratio of the DRAs. As the DRA volume increases, the bandwidth initially decreases until it reaches a minimum value, and then increases with volume.

#### 1.3.1.4 Different geometries

Various shapes of DRAs already investigated are shown in **Fig. 1.2**;

- a) Cylindrical b) Half cylindrical c) Triangular d) Rectangular
- c) Spherical d) Hemi spherical d) e) Conical f) Tetrahedron.



**Fig. 1.2** Various geometries of DRAs

#### **1.4 Coupling methods to DRAs**

Energy can be coupled in to the DRA in numerous ways as described below. Coupling mechanisms can have a significant impact on the resonant frequency and Q-factor of the DRA.

##### **1.4.1 Coaxial probe**

The coaxial probe can either be located adjacent to the DRA or can be embedded within it. Adjusting the probe height and the DRA location can optimize the amount of coupling. Also, depending on the location of the



probe, various modes can be excited. For the probe located adjacent to the DRA, as in Fig. 1.3, the broadband  $HE_{118}$  mode of the cylindrical DRA is excited (which radiate like a transverse horizontal magnetic dipole). For a probe located in the center of a cylindrical DRA, the  $TM_{018}$  mode is excited (radiating like a vertical electric dipole). Another advantage of using probe coupling is that one can couple directly into a  $50 \Omega$  system, without the need for a matching network. Probes are useful at lower frequencies where aperture coupling may not be practical due to the large size of the slot required.

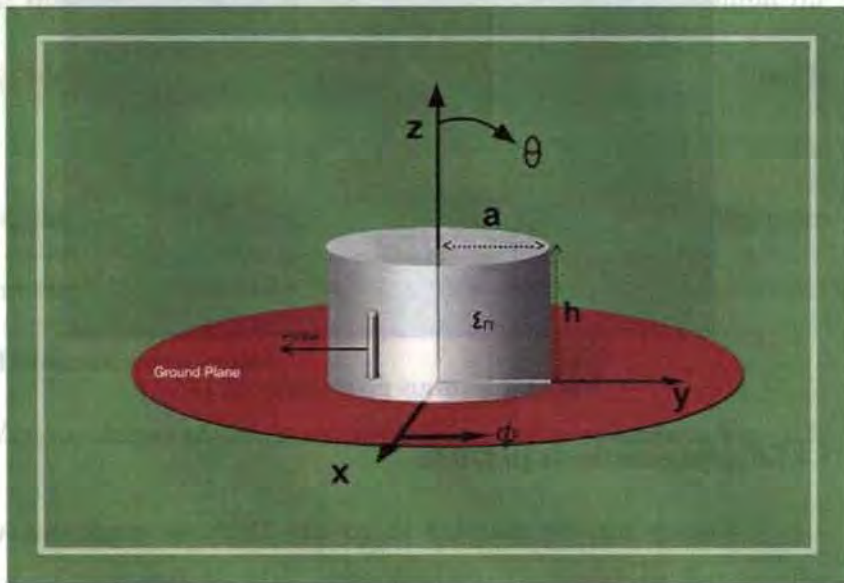


**Fig.1.3** Dielectric resonator antenna with coaxial probe feed

#### 1.4.2 Slot/Aperture coupling

**Fig. 1.4** below depicts a DRA fed by an aperture. The aperture behaves like a magnetic current running parallel to the length of the slot, which

excites the magnetic fields in the DRA. The aperture consists of a slot cut in a ground plane and fed by a microstrip line beneath the ground plane. This coupling mechanism has the advantage of having the feed network located below the ground plane, thus avoiding spurious radiation. The microstrip stub can be designed to cancel out the reactive component of the slot, thus allowing for an impedance match to the DRA. Moreover,

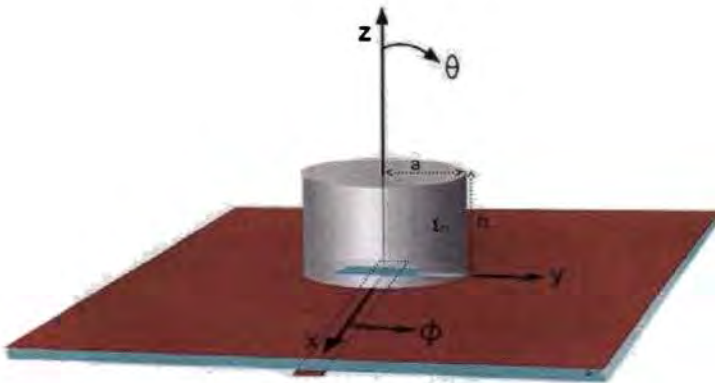


**Fig.1.4** Aperture- fed DRA

slot coupling is an attractive method for integrating DRAs with printed feed structures. The-coupling level can be adjusted by moving the DRA with respect to the slot.

### 1.4.3 Microstrip transmission line/proximity coupling

Another common method for coupling to dielectric resonators in microwave circuits is by proximity coupling to microstrip lines. This approach is equally applicable to DRAs as shown in **Fig. 1.5**. Microstrip

coupling will excite the magnetic fields in the DRA to produce the short horizontal magnetic dipole mode. The level of coupling can be adjusted by the lateral position of the DRA with respect to the microstrip line and on the relative permittivity of the DRA. For lower permittivity values (necessary for DRAs requiring wide bandwidth), the amount of coupling is generally quite small.

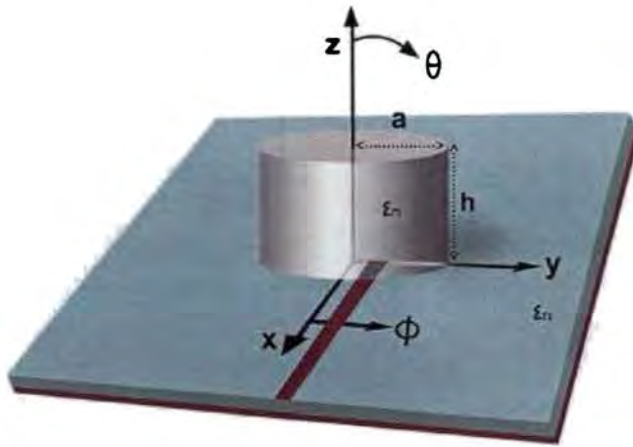


**Fig.1.5** Dielectric resonator antenna with microstrip feed

#### 1.4.4 Coplanar feed

Coupling to DRAs can also be achieved using co-planar feeds. Fig. 1.6 shows a cylindrical DRA coupled to a co-planar loop. The coupling level can be adjusted by positioning the DRA over the loop. The coupling behavior of the co-planar loop is similar to that of the coaxial probe, but the loop offers the advantage of being non obtrusive. By moving the loop

from the edge of the DRA to the center, one can couple into either the  $HE_{11\delta}$  mode or the  $TE_{011}$  mode of the cylindrical DRA.

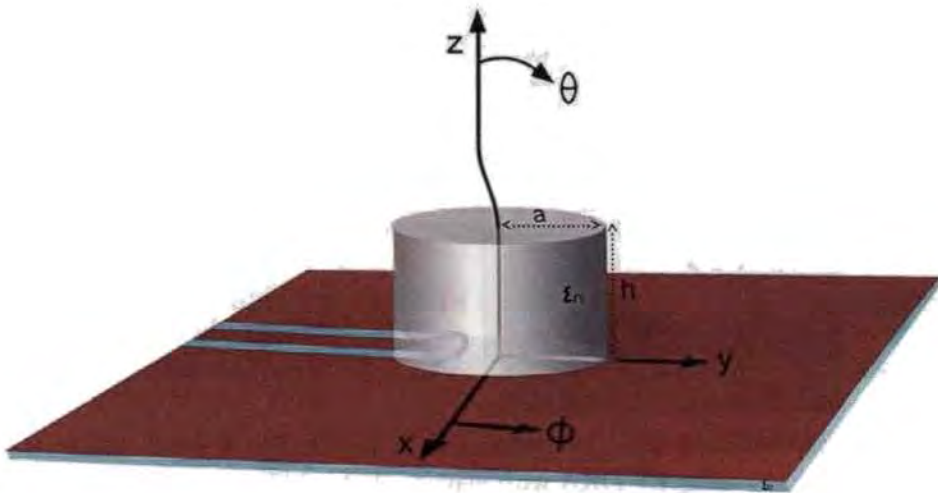


**Fig.1.6** DRA with co-planar feed

#### 1.4.5 Wave guide feed

Fig. 1.7 shows the waveguide fed DRA. Here the DRA is placed over a waveguide. A coaxial probe penetrating through the waveguide excites the antenna. Here the coupling is done by adjusting the length of the coaxial probe. These types of feed techniques improves the bandwidth

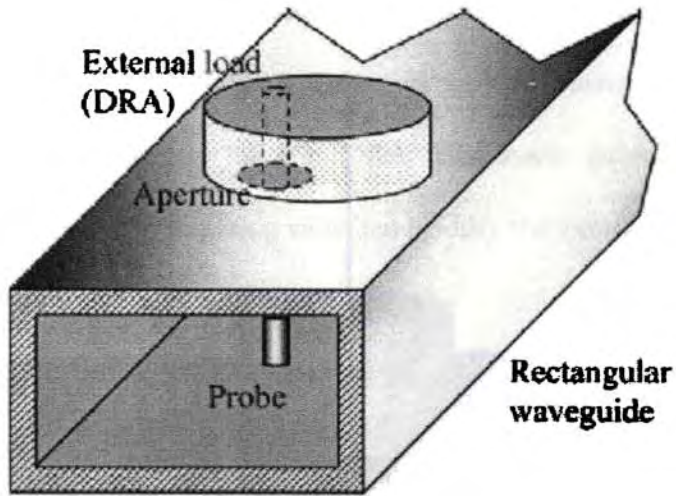
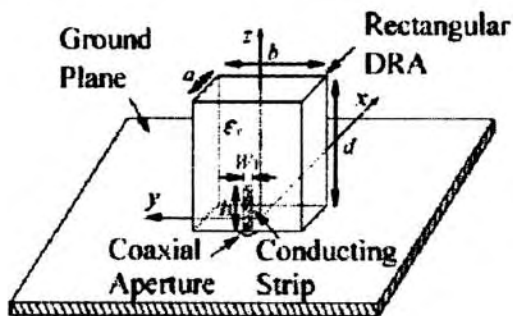


Fig.1.7 DRA with waveguide feed [7]

#### 1.4.6 Conformal Strip feed

Fig. 1.8 shows the conformal strip fed DRA. Here a metal strip is pasted on DRA which is used for improving the bandwidth. Here the coupling is adjusted by adjusting the width and length of the strip.



Configuration of the strip-fed rectangular DRA.

Fig.1.8 DRA with conformal strip feed [8]

### **1.5 Theoretical Considerations: Dielectric Resonators**

As previously mentioned, dielectric resonators have been known to radiate since the work conducted by Richtmyer in 1939, however, this information was not pursued as the then current application for dielectrics was as energy storage devices and not as radiators. In the 1980's, antenna research was being conducted at microwave and millimeter wave frequencies. Conductor losses limited the use of metallic structures; therefore research into dielectric materials became popular. Dielectric resonator antennas could be made smaller than their microstrip patch counterparts through the use of high permittivity materials, since the guided wavelength is inversely proportional to the permittivity of the dielectric material,

$$\lambda_{dielectric} = \frac{\lambda_0}{\sqrt{\epsilon_{dielectric}}} \text{-----} (1.7)$$

#### **1.5.1 Field Modes**

All resonators have a series of resonant modes or field structures, which are determined by their electrical characteristics and the boundary conditions. Van Bladel [9, 10] investigated DRAs of arbitrary shapes with very high permittivity, and concluded that there were two field modes in which the DRA could be classified. These are the confined and non-confined modes. The classification criteria are that at all interface boundaries the following conditions are met.

$$\text{a. } \mathbf{E} \cdot \mathbf{n} = 0; \quad \dots\dots\dots(1.8)$$

and

$$\text{b. } \mathbf{n} \times \mathbf{H} = 0 \quad \dots\dots\dots(1.9)$$

In eqn.1.7, where  $\mathbf{E}$  denotes the electric field intensity and  $\mathbf{n}$  denotes the normal to the surface of the resonator, is satisfied for both confined and non-confined modes. This condition states that there is no electric field intensity normal to the boundary. In eqn.1.8, where  $\mathbf{H}$  denotes the magnetic field intensity, is only satisfied for confined modes. This condition indicates that the magnetic field is normal to the boundary. He further states that the lowest order non-confined and confined modes act like magnetic and electric dipoles respectively. Finally, he has shown that confined modes can only be supported by dielectric elements exhibiting axial-symmetric properties.

These modes or field structures are often classified as H and E modes. The H modes, corresponding to the non-confined case above, have a large magnetic field perpendicular to the interface, with the lowest order mode resembling a magnetic dipole in field structure. The E modes, confined, do not have this large magnetic field and the lowest order mode resembles an electric dipole. Okaya and Barash first classified the H mode to belong to the transverse magnetic (TM) family and the E modes to the transverse electric (TE) family [9], however, later work by Yee [12] used the opposite notation. This second convention continues to be used today, with two or three subscripts to identify the specific mode order. The

subscripts denote the field variations in the appropriate orthogonal component, dependent on the co-ordinate system used, spherical, cylindrical or rectangular. Cylindrical and spherical DRAs support both TE and TM modes, which, when combined together form an additional hybrid family of modes. These degenerate modes, in which, two modes exhibit the same resonant frequency, and thus interact with each other result in a lack of mode purity.

Various configurations of dielectric materials have been investigated [13], with the theoretical emphasis placed on cylindrical or hemispherical shapes. The reason for this is the ability to generate closed form analytical solutions for axial-symmetric shapes. Since the focus of this thesis is Hexagonal DRAs, the discussion and analysis will deal solely with this geometric shape.

## **1.6 Numerical Methods**

### **1.6.1 Overview**

Numerical solutions became popular in the 1960's with the invention of high-speed digital computers. Today's modern technology has brought these methods more into the forefront, with some methods made more efficient, while others that originated in other disciplines are being applied to electromagnetic analysis. Until numerical methods became common, problems were solved through the classical separation of variables analytical method or through integral equation solutions. If these methods proved unwieldy, or closed form solutions were not possible, one



of two outcomes was possible. The first was to make appropriate assumptions in order to bypass the gridlock, and the second was to halt any analytical analysis. The assumptions deemed adequate for previous low frequency applications do not meet the requirements of today's millimeter wave integrated circuits. The ability to tune or weak the circuit characteristics after fabrication is virtually impossible, unlike that of the previous technology. This has increased the necessity of the computer-aided design (CAD) process, thus the reliance on these numerical methods.

Numerical solutions allow the tedious, time-consuming computations to be carried out by the computer. Accuracy, computer efficiency, memory requirements, analytical processing and versatility have been used as criteria to assess numerical method performances. The numerical computations are based on several well-known methods, as shown in **Table 1.2**, some of which will be briefly discussed in the following paragraphs.

The first three methods form **Tables 1.2** are useful in solving geometries with arbitrary shapes, while the remainders have applications in specific areas. The integral equation method, for example, is useful to solve DRA geometries exhibiting axial symmetric symmetry. The numerical method chosen for evaluating the electromagnetic characteristics in this thesis are the finite difference method, which will be discussed in more detail.

**Table 1.2:** Numerical Methods and their applicability [14]

Method	Storage requirements	CPU Usage	Generality	Pre-processing requirements
Transmission line matrix	Moderate to large	Moderate to large	Very good	small
Finite element	large	Moderate to large	Very good	small
Finite difference	large	large	Very good	Nil
Method of lines	Moderate	Small	Good	Moderate
Mode matching	Moderate	Small to Moderate	Good	Moderate
Integral equation	Small to Moderate	Small to Moderate	Good	Moderate
Spectral domain	small	small	Marginal	large

### 1.6.2 Finite Difference Method

First developed in the 1920's by A. Thom under the title "method of Squares" it was used to solve hydrodynamic equations. Finite difference techniques are based on discretisation approximations, which allow for the replacement of differential equations by finite difference equations, hence the name. These approximations relate the value of the dependent variable at a point in the solution region to the values at some neighboring point. A finite difference solution process consists of dividing the solution region into a grid of nodes, and applying the approximations to each point in the grid. The differential equations are then solved subject to the boundary

and/or initial conditions of the structure. The finite difference approximations are essentially numerical estimates of the derivatives- The finite difference time domain (FDTD) is a common technique that uses this method, approximating the differential equations in the time domain.

This method is well known to be the least analytical. Mathematical pre-processing is minimal, and the method can be applied to a wide variety of structures, even those with odd shapes. Numerical efficiency however, is not good. Open region problems truncated to a finite size can produce problems and mesh points must lie on boundary regions for accurate solutions.

### **1.6.3 Variational Methods**

This method allows a problem of integrating a differential equation to be reduced to an equivalent variational problem. The variational problem finds a function that gives a minimum value for some integral. This method forms the basis for the Method of Moments (MOM) and Finite Element Method (FEM).

#### **1.6.3.1 Method of Moments (MoM)**

MOM is a method of weighted residuals applicable for solving both integral and differential equations. The procedure usually involves four steps.

1. The appropriate integral or differential equation is derived.
2. This equation is discretized into a matrix equation using basis (or expansions) functions and weighting (or testing) functions.

3. The matrix elements are evaluated.
4. The matrix equation is solved and the parameters of interest obtained.

This method owes its name to the process of taking moments by multiplying by appropriate weighting functions, and integrating. Its use has been successfully applied to a wide variety of EM problems.

### **1.6.3.2 Finite Element Method (FEM)**

Finite element analysis consists of discretising the solution region into a finite number of sub regions or elements. Governing equations are then derived for a typical element. All elements in the solution region are assembled and the system of equations solved for. The finite difference and moment methods are conceptually simpler and easier to program than the finite element method, however the FEM is more powerful and versatile for handling complex geometries and inhomogeneous media. General-purpose computer programs can be created to solve a wide range of problems, due to the systematic nature of this method. Care must be taken at the truncation points when this method is applied to open region problems.

### **1.6.4 Method of Lines**

This method solves three-dimensional problems by reducing the problem to a single dimension through the use of discretisation in two of the three dimensions. Analytical solutions are then sought for the remaining dimension. Similar to the mode matching technique and the finite difference method, the biggest difference is the simplification in that

all but one independent variables are discretised to obtain a system of ordinary differential equations.

### 1.6.5 Finite Difference Frequency Domain Method

Although conceptually the Finite Difference Frequency Domain (FDFD) method is similar to the Finite Difference Time Domain (FDTD) method, from a practical standpoint it is more closely related to the finite element method. Like FDTD, this technique results from a finite difference approximation of Maxwell's curl equations. However, in this case the time-harmonic versions of these equations are employed,

$$\nabla \times E = -j\omega\mu H \text{ ----- (1.10)}$$

$$\nabla \times H = (\sigma + j\omega\epsilon)E \text{ ----- (1.11)}$$

Since, there is no time stepping it is not necessary to keep the mesh spacing uniform. Therefore optimal FDFD meshes generally resemble optimal finite element meshes. Like the moment-method and finite-element techniques, the FDFD technique generates a system of linear equations. The corresponding matrix is sparse like that of the finite element method. Although it is conceptually much simpler than the finite element method, very little attention has been devoted to this technique in the literature. Perhaps this is due to the head start that finite element techniques achieved in the field of structural mechanics. There are apparently very few codes available that utilize this technique. A notable exception is the FDFD module that is included in the GEMACS software marketed by Advanced Electromagnetics [15].

### **1.6.6 Spectral Domain Approach**

This is a Fourier-transformed version of the integral equation method, which is applied to microstrip or printed line structures. An efficient but restricted method, it can only handle well shaped structures that involve infinitely thin conductors.

### **1.6.7 Mode Matching Method**

Typically applied to the problem of determining the scattering characteristics in a wave-guide structure on both sides of any discontinuity, the fields on both sides of the discontinuity are expanded with respect to their various modes. Boundary conditions are applied along with the concept of field continuity in achieving the desired solution.

### **1.6.8 Transmission Line Method**

This method is used for solving field problems using circuit equivalents. It is based on the equivalence between Maxwell's equations and the equations for voltages and currents on a mesh of continuous two-wire transmission Lines. The main feature of this method is the simplicity of formulation and programming for a wide range of applications.

Originally proposed by Johns and Beurle in 1971 in order to analyze 2-D field problems, the model is based on Huygen's principle, which states "each particle in any wave front acts as a new source of disturbance, sending out secondary waves combined to form a new wave front. [16]. In 1975 Ahtarzad and Johns expanded the 2-D analysis to 3-D. This increases the complexity, however not the general procedure.

Complexity is increased since the 3-D node consists of 12 transmission line sections while the 2-D node encompassed only 4 transmission lines.

Waves propagate on a mesh of transmission lines interconnected at nodal points spaced a distance  $\delta l$  apart. At each node, the incident fields are redirected outward based on the impedance seen on the respective transmission lines. The disturbance then propagates outward, joining together to form a secondary wave front as Huygen's theory stipulates. This procedure continues through the structure, repeating the process at each and every node.

### **References**

1. R.D. Richtmyer, Dielectric Resonators, Journal of Applied Physics, Vol 10, pp 391-398, June 1939.
2. A.K. Okaya & L.F. Barash, The Dielectric Microwave Resonator, IRE Proceedings, Vol 50, pp 2081 –2092, October 1962.
3. J.K. Plourde, Chung-Li Ren, Application of Dielectric Resonators in Microwave Components, Microwave theory and techniques, vol-29, No 8, pp 754-770, Aug 1981.
4. M.T. Birand & R.V. Gelsthorpe, Experimental Millimetric Array Using Dielectric Resonators Fed by means of a Dielectric Waveguide, Electronic Letters, Vol 17, No 18, pp 633-635, Sept 1981.
5. R.K. Mongia, A. Ittipiboon, M. Cuhaci, Measurement of Radiation Efficiency of Dielectric Resonator, IEEE Microwave and Guided Wave Letters, Vol 4, No 3, pp 80-82, March 1994.
6. R.K. Mongia, Theoretical and Experimental Investigations on Dielectric Resonators Ph.D Thesis, Centre for Applied Research in Electronics, Indian Institute of Technology, Delhi, 1988.
7. Islam A. Eshrah, Ahmed A. Kishk, Alexander B. Yakovlev, and Allen W. Glisson, Equivalent Circuit Model for a Waveguide Probe With Application to DRA Excitation, IEEE transactions on Antennas and Propagation, Vol. 54, No. 5, pp. 1433-1441, May 2006.
8. Bin Li, and kwok Wa Leung, Strip-fed rectangular dielectric resonator antennas with/without a parasitic patch, IEEE

- transactions on Antennas and Propagation, Vol. 53, No. 7, pp 2200-2207. July 2005.
9. J. Van Bladel, The Excitation of Dielectric Resonators of Very High Permittivity, MTT-23, No 2, February 1975, pp 208-218.
  10. J J. Van Bladel, On the Resonances of a Dielectric Resonator of Very High Pennitivity, MTT-23, No 2, pp 199-208, February 1975.
  11. A.K. Okaya & L.F. Barash, The Dielectric Microwave Resonator, IRE Proceedings, Vol 50, pp 2081 –2092, October 1962.
  12. H.Y. Yee, Natural Resonant Frequencies of Microwave Dielectric Resonators, Microwave Theory and Techniques, Vol. 13, pp 256, March 1965.
  13. R.K. Mongia & P Bhartia, A Review and General Design Relations for Resonant Frequency and Bandwidth, International Journal of Microwave and Millimeter-Wave Cornputer Aided Engineering, Vol 4, No 3, pp 230-247,1994.
  14. T. Itoh, edn., Numencal Techniques for Microwave and Millimeter-Wave Passive Structures, John Wией and Sons, New York, 1989.
  15. GFMACS, software available from Advanced Electromagnetics, 5617 Palomino Dr. NW, Albuquerque, NM 87120.
  16. E.C Jordan and KG. Balmain, Electromagnetic Waves and Radiating Systems, Prentice-Hall, New Jersey, pp 188, 1968.



## **Chapter II      REVIEW OF THE PAST WORK**

---

### **2.1      Introduction**

Dielectric Resonators (DRs) have been primarily used in microwave circuits such as in oscillators and filters for many years [1]. The DR is normally made of high permittivity material, with dielectric constant  $\epsilon_r > 20$ . The unloaded Q factor is normally among 50 to 500, but can be as high as 10000. Because of these traditional applications, the DR was usually treated as energy storage device rather than radiators. Although open DRs were found to radiate many years ago [2-4], the idea of using DR as antenna had not been accepted until the first original paper on the cylindrical dielectric resonator antenna (DRA) [5] was published in 1983. At that time it was observed that the frequency range of interest for much system had generally progressed upwards to the millimeter and near millimeter range (100-300 GHz). At these frequencies the conductor loss of metallic antennas becomes severe and the efficiency of the antennas is reduced significantly. On the other hand, the only loss for a DRA is that due to the imperfect dielectric material, which can be very small in practice.

### **2.2      Different DRA geometries**

Subsequent to the cylindrical DRA, Long and his colleagues investigated the rectangular [6] and hemispherical [7] DRAs. This work

created the foundation for future investigations of the DRA. Kishk et al. studied the radiation characteristics of cylindrical DRA with new applications [8]. Many other shapes such as triangular [9], spherical-cap [10], cylindrical ring [11-12], conical [13], and tetrahedron [14] were also studied. The basic principle and mode nomenclatures of the DRA were discussed in the review paper [15].

### **2.3 Different coupling methods to DRA**

Different methods are used for exciting the antenna, which are coaxial probe [5-7], aperture coupling with a microstrip feedline [9,10, 16-24], aperture coupling with coaxial feed line [25, 26], direct microstrip feed line [27, 28], coplanar feed [29], soldered through probe [12], slot line [30], strip line [31], conformal strip [32-34], dielectric image guide [35] and waveguide probe [105].

### **2.4 Theoretical Analysis of DRA**

Leung et al [36] carried out the first theoretical analysis of the input impedance for the hemispherical DRA. The detailed analysis is explained in [37]. The variation of input impedance with frequency for different probe length is described in [38]. It is found that the input impedance increases significantly and resonant frequency shifts slightly with probe length. The variation of input resistance (increases) of the  $TE_{111}$  mode as a function of permittivity is explained in [38, 39]. An experiment was carried out in [40] to verify the hemispherical DR theory. Leung et al. [41] studied the cross polarization characteristics of a probe fed hemispherical DRA,

which is excited in  $TE_{111}$  mode. It should be noted that as DRAs of different shapes show very similar behavior and hence knowledge of hemispherical DRA can be used to anticipate the characteristics of other shapes. Leung et al [42] studied the aperture coupled hemispherical DRA with a thick ground plane, the antenna excite with the fundamental broad side  $TE_{111}$  mode. The theoretical analysis of slot coupled hemispherical DRA was also investigated [43]. When the DRA is fed axially, TM modes are excited; a rigorous and simple general solution can be obtained in [44].

The rectangular DRA is analyzed with dielectric wave guide model and is explained in [45-48]. In this approach, the top surface and two sidewalls of the DRA are assumed to be perfect magnetic walls, whereas the two other sidewalls of the DRA are imperfect magnetic walls. The fields of the DR are explained in TE and TM modes using the mode expansion method. A more accurate, but time consuming, approach is to use the FDTD method, which was adopted by Shum and Luk [16] in analyzing the aperture coupled rectangular DRA. The aperture coupling excitation method is applied to rectangular DRA in [49]. Mongia et al. demonstrated the radiation characteristics of a low profile rectangular DRA with very high permittivity [50]. An excellent impedance matching was obtained with 3% impedance bandwidth. Latter low profile high permittivity circular [51] and triangular [52] DRAs were investigated and similar results were obtained. Low permittivity low profile DRAs were also investigated by Esselle [53].

## **2.5 Miniaturisation of DRA**

Apart from using high permittivity material, Mongia [54] inserted a shorted metallic cylinder at the center of a cylindrical DRA to reduce the antenna size. Also the DRA size can be reduced by utilizing a metal plate perpendicular to the conducting ground plane [55, 56]. A half cylindrical DRA was placed against the vertical metal plate, by virtue of image effect the size of DRA was reduced by one half. Tam and Murch [57] extended the method to the annular sector DRA to reduce the size.

## **2.6 Bandwidth Enhancement Techniques**

Bandwidth enhancement techniques for the DRA have been of interest to the antenna engineers and scientists. In 1989 Kishk et al [58] stacked two different DRAs on top of one another. Since the DRAs had different frequencies, the configuration had a dual resonance operation, broadening the antenna bandwidth. Sangiovanni et al. [59] employed the stacking method with three DRAs to further increase the antenna bandwidth. Leung et al. [60] introduced an air gap between the stacking (high permittivity low profile DRA) and active DRA elements, good results were obtained. Junker et al. [61] analyzed the stacking configuration that employs a conducting or high permittivity loading disk. Simon and Lee [62] used another method in which two parasitic DRs were placed beside the DRA to increase the impedance bandwidth. Again Leung et al. [63] used the dual disk method to enhance the bandwidth of the low profile DRA of very high permittivity. In all the above technique require more

than one DR element. Wong et al [64] introduced an air gap inside a hemispherical DRA to widen the impedance bandwidth. Ittipiboon et al. [65] performed a similar work with the rectangular DRA. Shum and Luk [66] placed an air gap between the DRA and ground plane to broaden the bandwidth. Leung [67] investigated the case where the air gap between the DRA is replaced by a conductor. Chen et al [68] added a dielectric coating to the DRA to increase the impedance bandwidth. Similar work was also carried out by Shum and Luk [69]. A parasitic conducting patch has been used to increase the impedance bandwidth of the DRA [70, 71]. Kishk et al modified the geometry so as to obtain various shapes such as, conical [13] and tetrahedron [14] for wide bandwidth. Tayeb A. Denidni et al. [72] proposed an inverted L-shaped DRA for improving the bandwidth up to 38%. Later Quinjiang Rao et al. [73] modified the above geometry to a T-shaped DRA with two equilateral triangle cross section and improved bandwidth to more than 60%. Recently a hybrid DRA structure comprises a rectangular DR and a coplanar wave guide inductive slot is also proposed to increase the bandwidth [74]. Reducing radiation Q- factor of a cylindrical DRA for achieving broad bandwidth has been also reported [106].

## **2.7 Circular polarization**

For long time, studies on DRAs have concentrated on producing linear polarization. However for sometimes systems using circular polarization are preferred because they are insensitive to the transmitter

and receiver orientations. In some applications such as satellite communications, it also offers less sensitivity to propagation effects. In contrast, linearly polarized signal cannot be received properly when the transmitter is orthogonal to the received field and hence more effort has been developed to the CP DRA in recent years. The first CP DRA was presented in 1985 by Haneishi and Takazawa [75]. They truncated two opposite corners of a rectangular DRA to produce CP fields. After 10 years Mongia et al [76] studied a CP DRA that employed a quadrature feed. Later some other CP DRAs with quadrature feeds were demonstrated [77-79]. The quadrature feeding method gives a wide axial ratio (AR) bandwidth, but it substantially increases the size and complexity of the feed network. Petosa et al. [80] employed a cross shaped slot coupled DRA to excite CP fields. Oliver et al. [81] and Esselle [82] used a conventional rectangular DRA with the coupling slot inclined at  $45^\circ$  with respect to DRA to obtain a CP DRA. This method however is not applied to circular circumferences. Huang et al [83] produced CP using a cross-slot to the above geometries. A CP excitation method that utilized a pair of parasitic conducting strips was proposed by Lee et al. [84]. Leung and Ng [85, 86] and Long et al. [71] found that a single parasitic patch can also be used to excite CP fields. Recently Leung and Mok [87] used a perturbed annular slot to excite a CP DRA. By using sequential rotation CP fields can be obtained by using LP elements [88].

## **2.8 Antenna Gain**

Antenna gain is another important parameter for antenna designers. Different types of rectangular and cylindrical DRA arrays [89-94] have been studied for increasing the antenna gain. Some researchers have increased the gain by using a double layered DRA [95] i.e. by using the DR as a non radiating dielectric guide antenna.

## **2.9 Air gap Effect**

Junker et al [96, 97] have studied the air gap effect between the probe and DRA for the broadside  $HEM_{1,1\delta}$  ( $TM_{1,1\delta}$ ) mode of the cylindrical DRA and noted that the air gap increases the operational frequency, lowers the resonance impedance and has not significant effect on 3db bandwidth. The air gap between bottom of the DRA and ground plane was investigated by Junker [97, 98], the resonant mode was the end fire  $TM_{0,1}$  and noted that the resonant frequency increases and the 3dB bandwidth is significantly broadened when the size of air gap become larger. Drossos et al [99] studied the effect of air gap between the DRA and microstrip substrate for a microstrip fed DRA.

## **2.10 Multi-frequency Operation**

Dual or multi-frequency operation is highly desirable in modern wireless communication. If a single dielectric resonator antenna (DRA) can support dual frequencies, then the need for two single frequency antennas is not necessary. Applications requiring different frequency bands can be operated simultaneously with one radiating element. This reduces the

antenna size and makes the system compact. Many investigations have been reported on DRA with dual frequency operation using various approaches [100-103]. Recently a novel-coupling aperture feed technique with hybrid DRA is developed for multi-frequency operation [104]. But in all the cases dual frequencies are obtained by using either dual feed lines or a hybrid radiating structure, which may cause design complexity.

## **2.11 Conclusion**

This work proposes a novel hexagonal shaped DR antenna with unique characteristics. The detailed analysis follows in the coming chapters. The study reveals that the main attraction of this geometry is its multiple resonances with a single feed excitation, irrespective of coaxial or microstrip feeding, which eliminates the use of multiple antennas for multiple frequencies and results in the miniaturization of the total system.

## **References**

1. D.Kajfez and P. Guillon, Eds., Dielectric Resonators, Norwood, MA: Artech house, 1986.
2. R.D. Richmyer, Dielectric Resonators, J. appl. Phys., vol. 10, pp. 391-398, June 1939.
3. M. Gastine, L. Courtois and J. L. Dormann, Electromagnetic resonances of free dielectric Spheres, IEEE transactions on Microwave theory Tech., Vol. 15, pp.694-700, Dec. 1967.
4. O. Sagar and F. Tisk, On eigenmodes and forced resonance modes of dielectric spheres, Proc. IEEE, pp. 1593-1594, Sept. 1968.
5. S.A Long and M.W McAllister and L.C. Shen, The resonant cylindrical dielectric cavity antenna, IEEE Trans. Antennas Propagat., vol. 31, pp. 406-412, May 1983.
6. M.W McAllister, S.A Long and G.L Convey, Rectangular dielectric resonator antenna, Electron. Lett., vol. 19, pp.218-219, March 1983.
7. M.W McAllister and S.A Long, Resonant hemispherical dielectric antenna, Electron. Lett., vol. 20, pp.657-659, Aug. 1984.



8. A.A.Kishk, H.A. Auda and B.C. Ahn, Radiation characteristics of cylindrical dielectric resonator antennas with new applications, *IEEE Antennas Propagat. Soc. Newsletter*, vol. 31, pp. 587-589, 1989.
9. A. Ittipiboon, R.K. Mongia, Y.M.M. Antar, P. Bhartia and M. Cuhaci, Aperture fed rectangular and triangular dielectric resonators for use as magnetic dipole antennas, *Electron. Lett.*, vol. 29, pp.2001-2002, Nov. 1993.
10. K.W. Leung, K.M. Luk and E.K.N Yung, Spherical cap dielectric resonator antenna using aperture coupling, *Electron. Lett.*, vol. 30, pp.1366-1367, Aug. 1994.
11. R.K. Mongia, A. Ittipiboon, P. Bhartia and M. Cuhaci, Electric monopole antenna using dielectric ring resonator, *Electron. Lett.*, vol. 29, pp.1530-1531, Aug. 1993.
12. K.W. Leung, K.Y. Chow, K.M. Luk and E.K.N Yung, Excitation of dielectric resonator antenna using a soldered through probe, *Electron. Lett.*, vol. 33, pp.349-350, Feb.1997.
13. A.A. Kishk, Yan Yin and A.W. Glisson, Conical dielectric resonator antenna for wideband applications, *IEEE Trans. Antennas Propagat.*, vol. 50, pp. 469-474, April 2002.
14. A.A. Kishk, Wideband truncated tetrahedron dielectric resonator antenna excited by a coaxial probe, *IEEE Trans. Antennas Propagat.*, vol. 51, pp.2913-2917, Oct. 2003.
15. R.K. Mongia, and P. Bhartia, Dielectric resonator antennas – A review and general design relations for resonant frequency and bandwidth, *International journal of Microwave and Millimeter wave computer aided engg.*, vol. 4, pp.230-247, 1994.
16. K.M.Luk, K.W. Leung and S.M. Shum., Numerical study of dielectric resonator antenna, *Advances in microstrip and printed antennas* (editors: K.F. Lee and W. Chen), chapter 11, pp. 553-592, John Wiley, 1997.
17. J.T.H. St. Martin, Y.M.M. Antar, A.A.Kishk and A. Ittipiboon, Dielectric resonator antenna using aperture coupling, *Electron. Lett.*, vol. 26, pp.2015-2016, Nov. 1990.
18. G.P. Junker, A.A Kishk and A.W Glisson, Input impedance of aperture coupled dielectric resonator antennas, *IEEE Trans. Antennas Propagat.*, vol. 44, pp.600-607, May 1996.
19. K.W. Leung, W.C. Wong, K.M.Luk, and E.K.N.yung, Annular slot coupled dielectric resonator antenna, *Electron. Lett.*, vol. 34, pp.1275-1277, June. 1998.
20. K.W. Leung, and K.M.Luk, Radiation characteristics of aperture coupled hemispherical dielectric resonator antenna, *Microw. And Opt. Techn. Letters*, vol. 7, pp.677-679, Oct. 1994.

21. K.W. Leung, and M.W.To, Aperture coupled dielectric resonator antenna with a perpendicular feed, *Electron. Lett.*, Vol. 33, pp.1000-1001, June. 1997.
22. K.W. Leung, and M.W.To, Slot coupled dielectric resonator antenna using proximity feed on a perpendicular substrate, *Electron. Lett.*, Vol. 33, pp.1665-1666, Sept. 1997.
23. K.W. Leung, Analysis of Aperture coupled hemispherical dielectric resonator antenna with a perpendicular feed, *IEEE Trans. Antennas Propagat.*, vol. 48, pp.1005-1007, Jun. 2000.
24. G.P Junker, A.A. Kishk, D. Kajfez, A.W. Glisson and J.Guo, Input impedance of microstrip slot coupled dielectric resonator antenna mounted on thin dielectric layers, *International journal of Microwave and Millimeter wave computer aided engg.*, vol. 6, pp. 174-182, 1996.
25. K.Y. Chow and K.W. Leung, Theory and experiment of the cavity backed slot excited dielectric resonator antenna, *IEEE Trans. Electromagnetic Compatibility*, vol. 42, pp. 290-297, Aug. 2000.
26. K.Y.Chow, K.W. Leung, K.M. Luk and E.K.N. Yung, Input impedance of the slot fed dielectric resonator antenna with/without a backed cavity, *IEEE Trans. Antennas Propagat.*, vol. 49, pp.307-309, Feb. 2001.
27. R.A. Karaneburg and S.A.Long, microstrip transmission line excitation of dielectric resonator antenna, *electron. Lett.*, vol. 24, pp. 1156-1157, Sept. 1988.
28. K.W. Leung, K.Y. Chow, K.M. Luk, and E.K.N. Yung, Low profile circular disk DR antenna of very high permittivity excited by a microstripline, *Electron. Lett.*, Vol. 33, pp.1004-1005, June. 1997.
29. R.A. Karaneburg, S.A.Long and J.T.Williams, coplanar waveguide excitation of dielectric resonator antenna, *IEEE Trans. Antennas Propagat.*, vol. 39, pp. 119-122, Sept. 1991.
30. H.Y.Lo, K.W. Leung and K.M. Luk, slot line excited equilateral triangular dielectric resonator antenna of very high permittivity, *Microw. And Opt. Techn. Lett.*, vol. 29, pp. 230-231, Apr. 2001.
31. K.W. Leung, M.L. Poon, W.C. Wong, K.M. Luk, and E.K.N. Yung, Aperture coupled dielectric resonator antenna using a stripline feed, *Microw. and Opt. Techn. Lett.*, vol. 24, pp.120-121, Jan. 2000.
32. K.W. Leung, Conformal strip excitation of dielectric resonator antenna, *IEEE Trans. Antennas Propagat.* vol. 48, pp. 961-967, June. 2000.
33. K.W. Leung, Simple result for a conformal strip excited hemispherical dielectric resonator antenna, *Electron. Lett.* vol. 36, pp. 933-935, May. 2000.

34. H.Y. Lo and K.W. Leung, Excitation of low profile equilateral triangular dielectric resonator antenna using a conducting conformal strip, *Microw. And Opt. Lett.*, Vol. 29, pp. 317-319, June 2001.
35. M.T. Birand and R.V. Gelsthorpe, Experimental millimetric array using dielectric radiators fed by means of dielectric waveguide, *Electron. Lett.*, vol. 17, pp. 633-635, Sept. 1981.
36. K.W. Leung, K.M. Luk, K.Y.A. Lai, and D. Lin, input impedance of hemispherical dielectric resonator antenna, *Electron. Lett.*, vol. 27, pp.2259-2260, Nov. 1991.
37. K.W. Leung, K.M. Luk, K.Y.A. Lai, and D. Lin, Theory and experiment of a coaxial probe fed dielectric resonator antenna, *IEEE Trans. Antennas Propagat.*, vol. 41, pp.1390-1398, Oct. 1993.
38. K.W. Leung, Rigorous analysis of dielectric resonator antenna, Ph.D Dissertation, The Chinese University of Hong Kong, Hong Kong, May 1993.
39. E Collin, *Field theory of guided waves*, New York: MacGraw Hill, pp. 260-261, 1960.
40. K.W. Leung, K.M. Luk, K.Y.A. Lai, and D. Lin, On the  $TM_{101}$  mode of dielectric resonator antenna, *Microw. And Opt. Lett.*, vol. 6, pp.626-629, Sept. 1993.
41. K.W.Leung, K.K. Tse, K.M.Luk, and E.K.N. Yung, Cross polarization characteristics of a probe fed hemispherical dielectric resonator antenna, *IEEE Trans. Antennas Propagat.*, Vol. 47, pp.1228-1230, July. 1999.
42. K.W.Leung, K.M.Luk, K.Y.A. Lai and D. Lin, Theory and experiment of aperture coupled hemispherical dielectric resonator antenna, *IEEE Trans. Antennas Propagat.*, vol. 43, pp. 1192-1198, Nov. 1995.
43. K.W.Leung and K.W.Ng, Efficient computation for structures consisting of a slot and a metallic/ dielectric hemisphere cavity, *IEEE Trans. Antennas Propagat.*, Vol. 46, pp.457- 458, Mar. 1998.
44. K.W.Leung, General solution of a monopole loaded by a dielectric hemisphere for efficient computation, *IEEE Trans. Antennas Propagat.*, Vol. 48, pp.1267- 1268, Aug. 2000.
45. R.K. Mongia, Theoretical and experimental resonant frequencies of rectangular dielectric resonator antenna, *IEE Proc.-H.* vol. 139, pp. 98-104, Feb. 1992.
46. R.K. Mongia, and A. Ittipiboon, Theoretical and experimental investigations on rectangular dielectric resonator antenna, *IEEE Trans. Antennas Propagat.*, vol. 45, pp.1348-1356, Sept. 1997.

47. Y.M.M. Antar and Z. Fan, Theoretical investigations of aperture coupled rectangular dielectric resonator antenna, *IEEE Trans. Antennas Propagat.*, Vol. 143, pp.113-118, Apr. 1996.
48. A. Petosa, N.R.S. Simon, R. Siushansian, A. Ittipiboon and M. Cuhaci, Design and analysis of multi segment using dielectric resonator antenna, *IEEE Trans. Antennas Propagat.*, vol. 48, pp.738-742, May 2000.
49. M.G. Keller, D.J. Roscoe, M.B.Oliver, R.K Mongia, Y.M.M. Antar and A.Ittipiboon, Active aperture coupled rectangular dielectric resonator antenna, *IEEE Micro. And Guided Wave Lett.*, vol. 43, pp.376-378, Nov. 1995.
50. R.K Mongia, A. Ittipiboon and M. Cuhaci, Low profile dielectric resonator antennas using a very high permittivity material, *Electron. Lett.*, vol. 30, pp.1362-1363, Aug. 1994.
51. K.W.Leung, K.M.M Luk, E.K.N. Yung and S. Lai, Characteristics of low profile circular disk DR antenna with very high permittivity, *Electron. Lett.*, vol. 31, pp. 417 - 418, Mar. 1995.
52. H.Y. Lo, K.W.Leung, K.M. Luk and E.K.N. Yung, Low profile equilateral triangular dielectric resonator antennas of very high permittivity, *Electron. Lett.*, vol. 35, pp.2164-2166, Dec. 1999.
53. K.P Esselle, A low profile rectangular dielectric resonator antennas, *IEEE Trans. Antennas Propagat.*, vol. 44, pp.1296-1297, Sept.1996.
54. R.K Mongia, Small electric monopole mode dielectric resonator antenna, *Electron. Lett.*, vol. 32, pp. 947-949, May1996.
55. M.T.K. Tam and R.D. Murch, Half volume dielectric resonator antenna, *Electron. Lett.*, vol. 33, pp.1914-1916, Nov.1997.
56. A. Petosa, A. Ittipiboon, Y.M.M. Antar, D.Roscoe and M. Cuhaci, Recent advances in dielectric resonator antenna technology, *IEEE Antennas Propagat. Magaz.*, vol. 40, pp.35-48, June 1998.
57. M.T.K. Tam and R.D. Murch, Compact Circular sector and annular sector dielectric resonator antenna, *IEEE Trans. Antennas Propagat.*, vol. 47, pp.837-842, May 1999..
58. A.A. Kishk, B.Ahn and D. Kajfez, Broadband stacked dielectric resonator antenna, *Electron. Lett.*, vol. 25, pp.1232-1233, Aug.1989.
59. A. Sangiovanni, J.Y. Dauvignac and Ch. Pichot, Stacked dielectric resonator antenna for multifrequency operation, *Microw. And Opt. Techn. Lett.*, vol. 18, pp.303-306, July 1998.
60. K.W.Leung, K.M. Luk, K.Y. Chow and E.K.N. Yung, Bandwidth enhancement of dielectric resonator antenna by loading a low profile dielectric disk of very high permittivity, *Electron. Lett.*, Vol. 33, pp. 725 -726, Apr. 1997.
61. G.P. Junker, A.W. Glisson and A.A. Kishk, input impedance of dielectric resonator antenna top loaded with high permittivity and

- conducting disks, *Microw. And Opt. Techn. Lett.*, Vol.9, pp.204-207, July 1995.
62. R.N. Simons and R.Q. Lee, Effect of parasitic dielectric resonators on CPW/aperture coupled dielectric resonator antennas, *IEE Proc.-H.* vol. 140, pp. 336-338, Oct. 1993.
  63. K.W. Leung, K.Y. Chow, K.M. Luk and E.K.N. Yung, Offset dual disk dielectric resonator antenna of very high permittivity, *Electron. Lett.*, vol. 32, pp. 2038-2039, Oct. 1996.
  64. K.L. Wong, N.C. Chen and H.T. Chen, Analysis of a hemispherical dielectric resonator antenna with an air gap, *IEEE Microw. And guided wave lett.*, vol. 3, pp.355-357, Oct. 1993.
  65. A. Ittipiboon, A. Petosa, D.Roscoe and M. Cuhaci, An investigation of a novel broadband dielectric resonator antenna, *IEEE Antennas Propagat. Society international symposium digests*, Baltimore, USA, pp.2038-2041, July 1996.
  66. S.M. Shum, and K.M.Luk, characteristics of dielectric ring resonator antenna with an air gap, *Electron. Lett.*, vol. 30, pp. 277-278, Feb. 1994.
  67. K.W. Leung, Complex resonances and radiation of hemispherical dielectric resonator antenna with a concentric conductor, *IEEE Trans. Microw. Theory and Techn.*, vol. 49, pp.524-531, Mar. 2001.
  68. N.C. Chen, H.C. Su, K.L. Wong and K.W. Leung, Analysis of a broadband slot coupled dielectric coated hemispherical dielectric resonator antenna, *Microw. And Opt. Techn. Lett.*, Vol. 8, pp.13-16, Jan. 1995.
  69. S.M. Shum, and K.M.Luk, Numerical study of a cylindrical dielectric resonator antenna coated with a dielectric layer, *IEEE Proc. Microw. Antennas propagation*, Vol. 142, pp.189-191, Apr. 2005.
  70. H.K. Ng and K.W. Leung, Conformal strip excited dielectric resonator antenna with a parasitic strip, *IEEE Antennas Propagat. Society international symposium digests*, Salt lake city, USA, vol. 4, pp.2080-2083, July 2000.
  71. R.T. Long, R.J. Dorris, S.A. Long, M.A. Khayat and J.T. Williams, Use of parasitic strip to produce circular polarization and increased bandwidth for cylindrical dielectric resonator antenna, *Electron. Lett.*, vol. 37, pp. 406-408, Mar. 2001.
  72. Tayed A. denidni, Qinjiang Rao and Abel R. Sebak, Broadband L-shaped dielectric resonator antenna, *IEEE Antennas and Propagation Letters*, vol. 4, pp. 453-454, 2005.
  73. Qinjiang Rao, Tayed A. denidni and Abel R. Sebak, Broadband compact t-shaped DRA with equilateral triangle cross section, *IEEE Microw. And wireless comp. Letter.*, vol. 16, pp.7-9, Jan. 2006.

74. Yuan Gao, Ban-Leong Ooi, Wei-Bin Ewe, Alexandre P. Popov, A compact wideband hybrid Dielectric Resonator Antenna, *IEEE Microw. And wireless comp. Letters*, vol. 16, pp.227-229, Apr. 2006.
75. M. Haneishi and Takazawa, Broadband circularly polarized planar array composed of a pair of dielectric resonator antenna, *Electron. Lett.*, vol. 21, pp. 437-438, May 1985.
76. R.K Mongia, A. Ittipiboon, M. Cuhaci, and D. Roscoe, Circularly polarized dielectric resonator antenna, *Electron. Lett.*, vol. 30, pp. 1361-1362, Aug. 1994.
77. G. Drossos, Z. Wu and L.E. Davis, Circular polarized cylindrical dielectric resonator antenna, *Electron. Lett.*, vol. 32, pp. 281-283, Feb. 1996.
78. G. Drossos, Z. Wu and L.E. Davis, Switchable cylindrical dielectric resonator antenna, *Electron. Lett.*, vol. 32, pp. 862-864, May 1996.
79. K.W.Leung, W.C.Wong, K.M. Luk and E.K.N. Yung, Circular polarized dielectric resonator antenna excited by dual conformal strips, *Electron. Lett.*, vol. 36, pp. 484-486, Mar. 2000.
80. A. Petosa, A. Ittipiboon and M. Cuhaci, Array of circular polarized cross dielectric resonator antenna, *Electron. Lett.*, vol. 32, pp. 1742-1743, Sept. 1996.
81. M.B. Oliver, Y.M.M. Antar, R.K Mongia and A. Ittipiboon, Circularly polarized rectangular dielectric resonator antenna, *Electron. Lett.*, vol. 31, pp. 418-419, Mar. 1995.
82. K.P. Esselle, Circularly polarized higher order rectangular dielectric resonator antenna, *Electron. Lett.*, vol. 32, pp. 150-151, Feb. 1996.
83. C.Y. Huang, J.Y. Wu and K.L. wong, Cross slot coupled microstrip antenna and dielectric resonator antenna for circular polarisation, *IEEE Trans. Antennas Propagat.*, vol. 47, pp. 605-609, 1999.
84. M.T. Lee, K.M. Luk, E.K.N. Yung and K.W.Leung, Microstrip line feed Circular polarized cylindrical dielectric resonator antenna, *Microw. And Opt. Techn. Lett.*, vol. 24, pp.206-207, Mar. 2000.
85. K.W. Leung and H.K. Ng, Theory and experiment of Circularly polarized dielectric resonator antenna with a parasitic patch, *IEEE Trans. Antennas Propagat.*, Vol. 51, pp. , Feb. 2003.
86. H.K. Ng and K.W. Leung, Excitation of CP aperture coupled dielectric resonator antenna with a parasitic patch, *IEEE Antennas Propagat. Society international symposium digests, Boston, USA*, vol. 4, pp.202-205, July 2001.
87. K.W.Leung and S.K. Mok, Circularly polarized dielectric resonator antenna excited by a perturbed annular slot with a backing cavity, *Electron. Lett.*, vol. 37, pp. 934-936, Jul. 2001.
88. k.K.pang, H.y. Lo, K.W.Leung, K.M.Luk and F.K.N. Yung, Circularly polarized dielectric resonator antenna subarrays, *Microw. and Opt. Techn. Lett.*, vol. 27, pp.377-379, Dec. 2000.

89. G.D. Loos and Y.M.M. Antar, A new aperture coupled rectangular dielectric resonator antenna array, *Microw. and Opt. Techn. Lett.*, vol. 7, pp.642-644, Oct. 1994.
90. K.Y. Chow, K.W. Leung, K.M. Luk and E.K.N. Yung, Cylindrical dielectric resonator antenna array, *Electron. Lett.*, vol. 31, pp. 1536-1537, Aug. 1995.
91. K.W. Leung, H.Y. Lo, K.M. Luk and E.K.N. Yung, Two dimensional cylindrical dielectric resonator antenna arrays, *Electron. Lett.*, vol. 34, pp. 1283-1285, Jun. 1998.
92. G. Drossos, Z. Wu and L.E. Davis, Aperture coupled cylindrical dielectric resonator antennas forming four element linear arrays, *Microw. and Opt. Techn. Lett.*, vol. 20, pp. 151-153, Jan. 1999.
93. A. Petosa, R.K. Mongia, A. Ittipiboon and J.S. wight, Design of microstrip fed series array of dielectric resonator antenna, *Electron. Lett.*, vol. 31, pp. 1306-1307, Aug. 1995.
94. A. Petosa, A. Ittipiboon, M. Cuhaci and R. Larose, Bandwidth improvement for a microstrip fed series array of dielectric resonator antennas, *Electron. Lett.*, vol. 32, pp. 608-609, Mar. 1996.
95. Y. Hwang, Y.P. Zhang, K.M. Luk and E.K.N. Yung, Gain enhanced miniaturized rectangular dielectric resonator antennas, *Electron. Lett.*, vol. 33, pp. 350-352, Feb. 1997.
96. G.P. Junker, A.A. Kishk, A.W.Glisson and D. Kajfez, Effect of an air gap around the coaxial probe exciting a cylindrical dielectric resonator antenna, *Electron. Lett.*, vol. 30, pp.177-178, Feb. 1994.
97. G.P. Junker, A.A. Kishk, A.W.Glisson and D. Kajfez, Effect fabrication imperfections from ground plane backed dielectric resonator antenna, *IEEE Antennas Propagat. magazine*, vol. 37, pp.40-47, 1995.
98. G.P. Junker, A.A. Kishk, A.W.Glisson and D. Kajfez, Effect of an air gap on cylindrical dielectric resonator antenna operating in  $TM_{01}$  mode, *Electron. Lett.*, vol. 30, pp. 97- 98, Jan. 1994.
99. G.Drossos, Z. Wu and L.E. Davis, The air gap effect on a microstrip coupled cylindrical dielectric resonator antenna, *Microw. And Opt. Techn. Lett.*, Vol. 20, pp. 36-40, Jan. 1999.
100. Y. Sung, C. S. Ahn, and Y.-S. Kim, "Microstripline fed dual frequency dielectric resonator antenna", *Microwave and optical technology letters*, vol. 42, no. 5, pp. 388-390, 2004.
101. Tayeb A. Denidni, and Qinjiang Rao, Hybrid Dielectric Resonator Antennas with Radiating Slot for Dual-Frequency Operation, *IEEE Antennas and wireless propagation letters*, vol. 3, pp. 321-323, 2004.
102. Z.Fan and Y. M. M. Antar, Slot coupled DR antennas for dual frequency operation, *IEEE transactions on antennas and propagation*, vol. 45, no. 2, pp. 306-308, 1997.

103. Qinjiang Rao, Tayeb A. Denidni, and Abdel R. Sebak, Hybrid Resonator Antenna suitable for wireless communication applications at 1.9 and 2.45GHz, *IEEE Antennas and wireless propagation letters*, vol. 4, pp. 341-343, 2005.
104. Qinjiang Rao, Tayeb A. Denidni, and Ronald H. Johnston, A novel feed for multifrequency Hybrid Resonator Antenna, *IEEE Microwave and wireless components letters*, vol. 15, pp. 238-240, April 2005.
105. Islam A. Eshrah, Ahmed A. Kishk, Alexander B. Yakovlev, and Allen W. Glisson, Equivalent Circuit Model for a Waveguide Probe With Application to DRA Excitation, *IEEE transactions on antennas and propagation*, vol. 54, no. 5, pp. 1433-1441, 2006.
106. A.V. Praveen Kumar, V. Hamsakutty, Jaimon Yohannan and K. T. Mathew, A Wideband Conical Beam Cylindrical Dielectric Resonator Antenna's, *IEEE Antennas and Wireless Propagation Letters*, Vol.6, 2007.



### **3.1 Introduction**

The methodology adopted and the facilities used for the study of antenna characteristics of the hexagonal shaped dielectric resonator antenna are discussed in this chapter. The details regarding the different sophisticated equipments used to analyse the performance of the antenna are presented. Description of the fabrication of the hexagonal pellet is also given. The chapter also includes the methods and experimental set up used to study the important characteristics of the antenna such as reflection characteristics, radiation pattern, gain, polarisation and other associated parameters.

### **3.2 Basic facilities utilized**

A full description of the equipments and amenities utilized for the measurement of antenna characteristics is presented.

#### **3.2.1 HP 8510C Vector Network Analyzer**

HP 8510 C Vector Network Analyzer (VNA) is versatile equipment capable of making rapid and accurate measurements in the frequency and time domain. It consists of the 32 bit micro controller MC68000 and has 1MB RAM and 512 KB ROM. The NWA can measure the magnitude and phase of scattering (S) parameters for frequencies up to 50 GHz with a resolution of 1Hz. It has the optional ability to take inverse Fourier transform of the measured frequency data to give the time domain response. The NWA consists of a microwave generator, S parameter test

set, signal processor and the display unit, as shown in figure 3.1. The synthesized sweep generator, HP83651B, uses an open loop YIG tuned element to generate the RF stimulus. It can synthesize frequencies from 10 MHz to 50 GHz. The frequencies can be synthesized in step mode or ramp mode depending on the desired measurement accuracy [1].

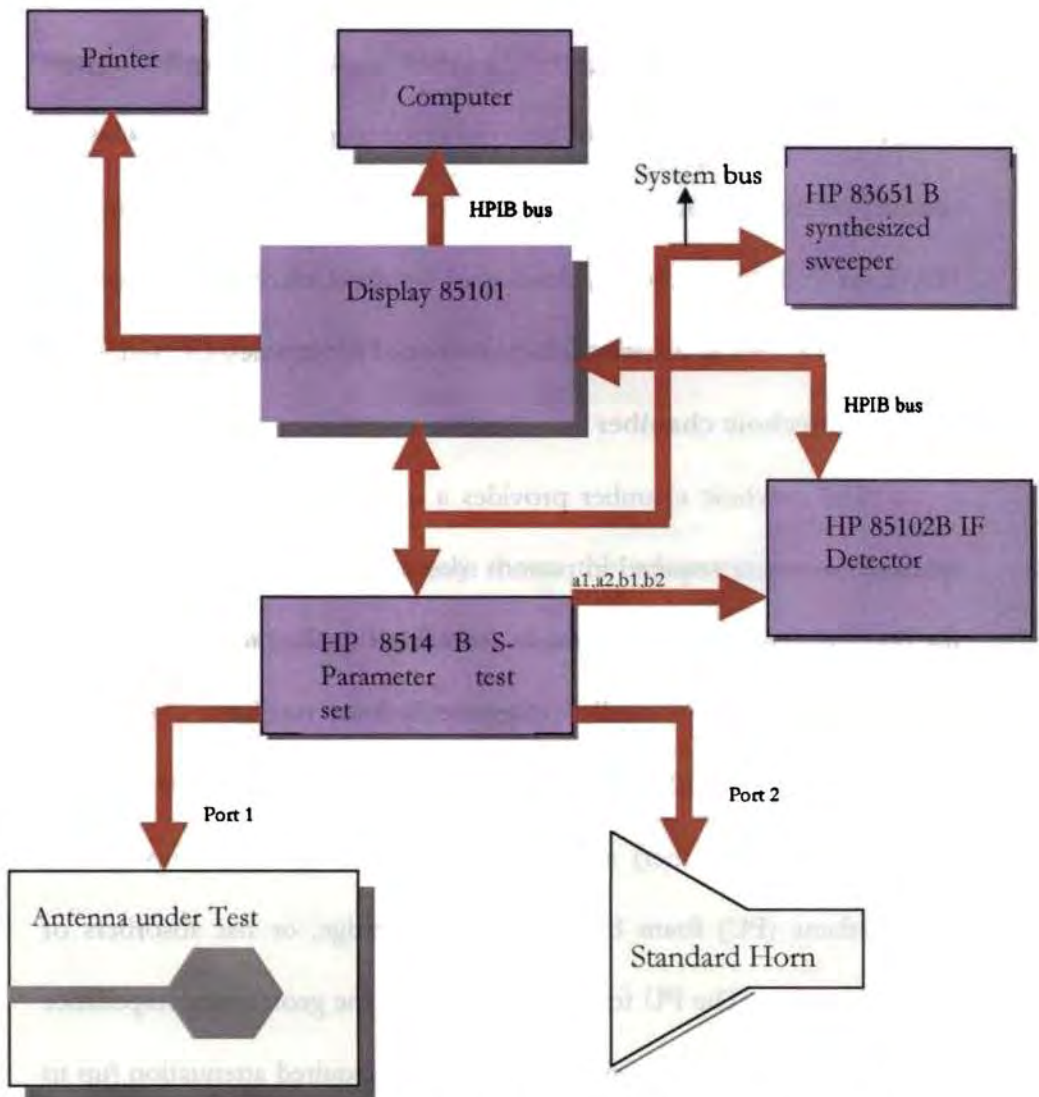


**Figure 3.1** Schematic diagram of HP8510 C Network Analyzer

The antenna under test (AUT) is connected to the two-port S parameters test unit HP8514B. This module isolates the incident (test), reflected and/or transmitted signals (namely  $a_1$ ,  $b_1$ ,  $a_2$ ,  $b_2$ ) at the two ports. The signals are then down converted to an intermediate frequency of 20MHz and fed to the IF detector. These signals are suitably processed to display the magnitude and phase information of S parameters in Log magnitude, linear magnitude, smith chart or polar formats. These constituent modes of the NWA are connected using GPIB system bus. A completely automated data acquisition is made possible using the MATLAB<sup>TM</sup> based software, developed by the Center for Research in Electromagnetics and Antennas, Department of Electronics, CUSAT.

### **3.2.2 Anechoic chamber**

The anechoic chamber provides a quiet zone needed to simulate space environment required in pattern measurements. The absorbers used for building the chamber are made from high quality, low-density form impregnated with dielectrically/ magnetically lossy medium. The wall of the chamber (24' X 12' X 10' ) used for the measurements is properly shaped (tapered chamber) and covered with carbon black impregnated poly urethane (PU) foam based pyramidal, wedge, or flat absorbers of appropriate sizes. The PU foam structure gives the geometrical impedance matching while the dispersed carbon gives the required attenuation (up to -40 dB) for a wide frequency (500 MHz to 18 GHz) range. The chamber is made free of EMI by surrounding with thin aluminium sheet.

### **3.2.3 Automated turn table assembly for far field measurements**

The turntable kept in the quiet zone consists of a stepper motor driven rotating platform, for mounting the antenna under test (AUT). The microcontroller based antenna positioner, STIC 310 C is used for rotating the AUT, for studying the radiation characteristics. The AUT is used as a receiver and a standard wideband (1-18 GHz) ridged horn antenna is used as transmitter for measurements of radiation pattern. Properly shielded cables connect the antennas to NWA. Antenna positioner is interfaced to the computer and the antenna can be rotated  $360^\circ$  in CW or CCW direction with any stepping angle ( $\geq 1^\circ$ ) using the software.

### **3.3 Experimental set up**

**Fig. 3.2** and **Fig. 3.3** respectively shows the schematic set up used to measure the reflection and radiation characteristics of the antenna. A thorough investigation of the input characteristics<sup>↺</sup> followed by pattern measurement inside anechoic chamber.

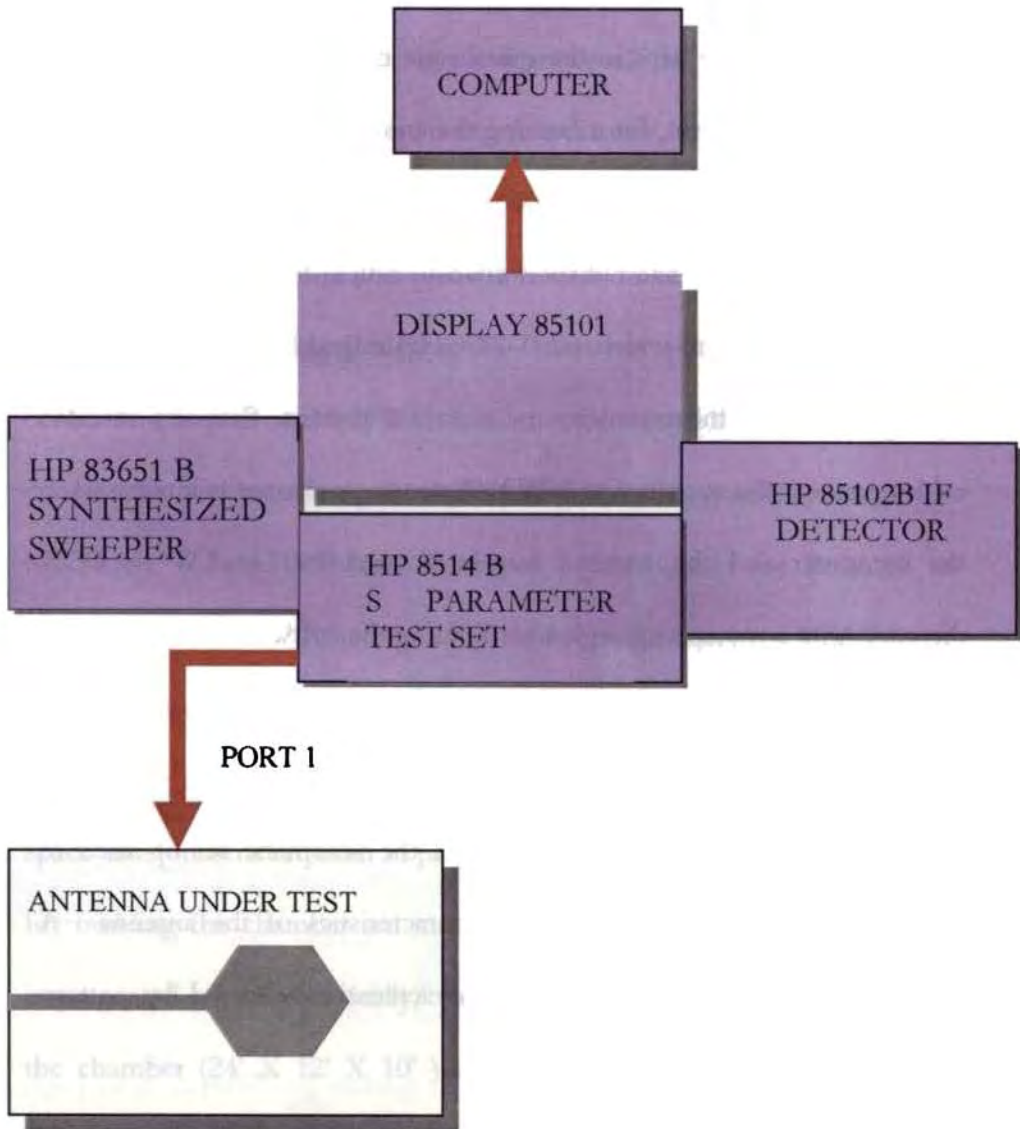


**Fig. 3.2** Setup for measuring the reflection characteristics using HP8510C Network Analyzer

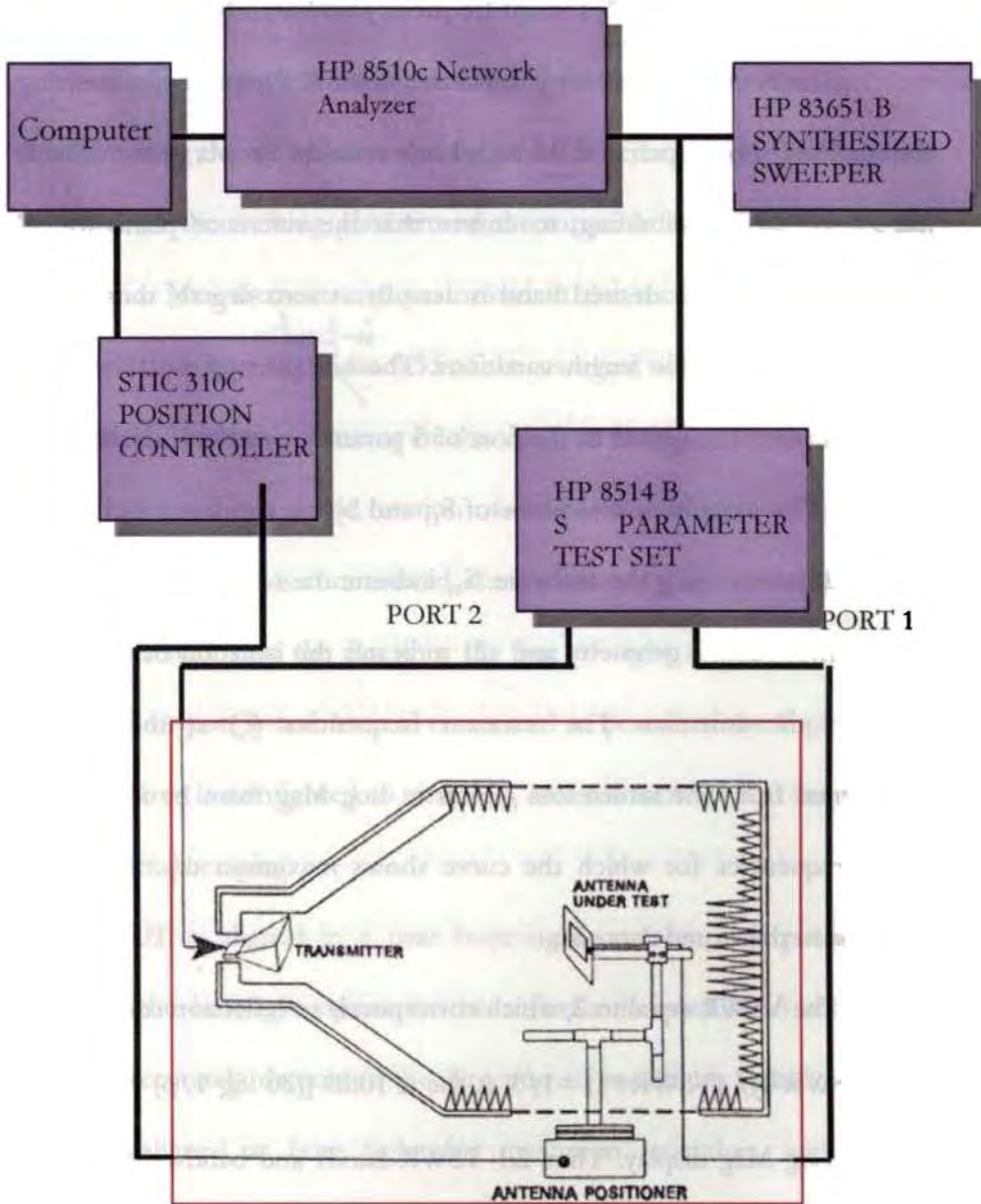


**Fig. 3.3** Set up for measuring radiation pattern using 8510 C Network Analyzer

### 3.4 Measurement procedure

The experimental procedure followed in determining various antenna parameters is discussed below:

### 3.4.1 S-parameters, Resonant frequency and Bandwidth

The Network analyzer is calibrated for full 2 ports by connecting the standard short, open and through loads suitably. Proper phase delay is introduced while calibrating, to ensure that the reference plane for all measurements in the desired band is actually at zero degree, thus taking care of probable cable length variations. The one port of the Hexagonal antenna is then connected to the port of S parameter test unit as shown in **Fig. 3.3**. The magnitude and phase of  $S_{11}$  and  $S_{21}$  are measured and stored in ASCII format using the software.  $S_{11}$  indicate the return loss at the one port of the antenna geometry and  $s_{21}$  indicates the isolation between the ports of the antennas. The resonant frequencies ( $f_r$ ) at the port is determined from the return loss curves in Log Mag form by identifying those frequencies for which the curve shows maximum dip. It can be noted from the stored data also.

The VSWR equal to 2, which corresponds to reflection coefficient,  $\rho = (VSWR-1)/(VSWR+1) = 1/3$ , is the  $\cong 10\text{dB}$  [ $(20 \log 1/\rho) = -9.5\text{dB}$ ] level in Log Mag display. Thus 2:1 VSWR bands and bandwidths at the one port is determined by observing range of frequencies ( $\Delta f_r$ ) about the resonant frequency for which the return loss curves, show  $\leq -10\text{dB}$ . The fractional bandwidth is calculated as  $\Delta f_r/f_r$ . The input impedance at resonant frequency is determined directly from the smith chart display in the network analyzer, where the center point corresponds to  $50\Omega$ .

### 3.4.2 Radiation patterns

Radiation pattern measurement is performed within the anechoic chamber using the set up shown in figure 3.4. The hexagonal DR Antenna mounted on the rotating platform of the turntable assembly kept in the quiet zone. Measurements are performed in the receiving mode for the AUT, which is kept in the far field of the standard wideband ridged Horn antenna. The radiation patterns of the AUT at multiple frequency points can be measured in a single rotation of the positioner using the software. Before measurement is commenced, the transmitter (Tx) and receiver (Rx) are aligned such that the Rx is in the line of sight of the Tx. AUT is connected to port 1 and horn is connected to port 2 of the S parameter test. Analyzer is configured to make  $S_{21}$  measurement in the Step mode with proper Averaging.

AUT is aligned in a near bore sight position with polarization matched; the boresight option in the software is invoked to rotate the AUT to accurately determine the direction of maximum radiation. With antennas aligned at bore sight for maximum reception, and *through* response calibration is performed for the frequency band of interest and saved in the Cal set. Switching to the time domain, *gate* is turned on in the analyzer with a gate span depending on the largest dimension of the AUT. This procedure eliminates the spurious reflections from neighborhood that are likely to corrupt the measured data. After the above sequence, the calibrate option prompts for the frequency band and the number of



frequency points within the band for which  $S_{21}$  cal is to be done for pattern measurements of the AUT.

The position controller is then set to home. The analyzer switched back to frequency domain, and the controlling software for pattern measurement is invoked which prompts for the start, stop and step angle and the software sequences the operations:

- a) Rotate the AUT in the horizontal plane by the specified step angle.
- b) Measure  $S_{21}$  at each frequency step within the specified start and stop frequency range.
- c) Acquire data and rotate the AUT by the step angle to cover the full  $360^\circ$

Measurements are repeated in the principal planes for both the co planar and cross polar orientations of the AUT and Horn, with calibration on. The gated response at each angular position is therefore normalized with respect to boresight trace. From the stored data, half power beam width, cross-polar level, back lobe level etc. in the respective planes are estimated.

### **3.4.3 Gain**

The gain of the AUT is measured in the boresight direction. Gain transfer method utilizing a reference antenna of known gain is employed to determine the absolute gain of the AUT [2-4]. The experimental set up and measurement procedure for determining the gain is similar to radiation pattern measurement. A standard antenna with known gain  $G_R$  operating in

the same band as AUT is used as reference antenna.  $S_{21}$  measurements done using reference antenna (as receiver) and the wideband Horn (as transmitter), is saved as the reference power. A THRU RESPONSE calibration is performed for the frequency band of interest and saved in new Cal set. This acts as the reference (0 dB) gain response. The reference antenna is replaced with AUT, retaining the physical alignment.  $S_{21}$  is measured then with the new calibration on and the power received ( $P_r$  in dB) is recorded. Display on the network Analyzer indicates the relative power in dB of the AUT with respect to the reference antenna. The gain  $G_r$  of the AUT is calculated from the stored data based on Friiss transmission formula as

$$G_r \text{ (dB)} = G_R \text{ (dB)} + P_r \text{ (dB)} \text{ ----- (3.1)}$$

### 3.4.4 Polarization pattern

Polarization of an antenna in a given direction is the polarization of the wave radiated (or transmitted) by the antenna, which is that property of an electromagnetic describing the time varying direction and relative magnitude of the electric field vector at a fixed location in space, and the sense in which it is traced as observed along the direction of propagation [2-3]. The polarization a characteristic of an antenna is represented by its polarization pattern which is the special distribution of the polarization of the field vector radiated by an antenna measured over the radiation sphere.

To measure the polarization pattern along the axis of the antenna beam, the linearly polarized standard horn antenna and test antenna are

aligned so that orientation of AUTs co polar electric field matches with that of the Horn. The AUT connected to port 1 of the S parameter test set up is kept stationary, while the Horn antenna mounted on the turntable is rotated about its axis using the position controller. The horn antenna is connected to port 2 of the S parameters test set and  $S_{21}$  measurement is performed after each rotation of the Horn. The data so acquired is plotted in polar coordinates with respect to angle of rotation to reveal the polarization pattern of the AUT. The ellipse drawn inscribed within the polarization pattern is the polarization ellipse for the antenna in the specified direction.

### **3.5 Ansoft HFSS<sup>TM</sup>**

HFSS [4] stands for High Frequency Structure Simulator is a high performance full wave electromagnetic field (EM) simulator for arbitrary volumetric passive device modeling. It employs Finite Element Method (FEM), adaptive meshing and brilliant graphics to give unparalleled performance and insight to all 3D EM problems. Since it is an interactive simulation system whose basic mesh element is tetrahedron, allows solving any arbitrary 3D geometry with complex curves and shapes and provides solutions to EM problems quickly and accurately. Hence HFSS is used to simulate the characteristics of the hexagonal dielectric resonator antenna which will be explained in Chapter V.

## References

1. HP8510C network Analyzer, operating and service manual, Hewlett Packard company, Santa Rosa, CA, USA.
2. C.A. Balanis, Antenna Theory: Analysis and Design, Second edition, John Wiley & Sons, Inc., Singapore, 2004.
3. C.G. Christodoulou and Praveen F. Wahid, fundamentals of Antennas: Concepts and applications, Prentice Hall India, New Delhi, India, 2001.
4. HFSS high frequency structure simulator 10, Ansoft Corporation.

## **Chapter IV                      SYNTHESIS OF DIELECTRIC RESONATORS**

---

### **4.1      Introduction**

With the recent progress in the field of mobile telephony and satellite communication, the development of microwave dielectric materials having low dielectric loss (high Q), high dielectric constant and small temperature coefficient of resonance frequencies has gained significance. Recently much of the developments in microwave ceramics have been in the field of dielectric resonator antennas and filters.

Titanates ( $\text{TiO}_2$ ) have many uses in electronic and material industry due to its piezoelectric, ferroelectrics and other properties. This chapter explains the method of preparation and characterization of  $\text{TiO}_2$  pellets to be used as dielectric resonators.

### **4.2      Preparation of DR pellet**

The preparation process consists of many steps such as weighing, mixing, calcination, sintering etc. During these processes we can minimize the free energy of the material and redistribute the atoms. The minimization involves the reduction of internal surface area and an increase in the grain size.

The different stages of preparation of DR pellets are detailed below

- (i)      Weighing and mixing
- (ii)     Preheating
- (iii)    Binder addition and dry pressing

- (iv) Sintering
- (v) Finishing

#### **4.2.1 Weighing and mixing**

The first step in the preparation consists of weighing a fixed quantity of  $\text{TiO}_2$  powder in a mortar container. It is then ground to make a fine powder.

#### **4.2.2 Pre-heating**

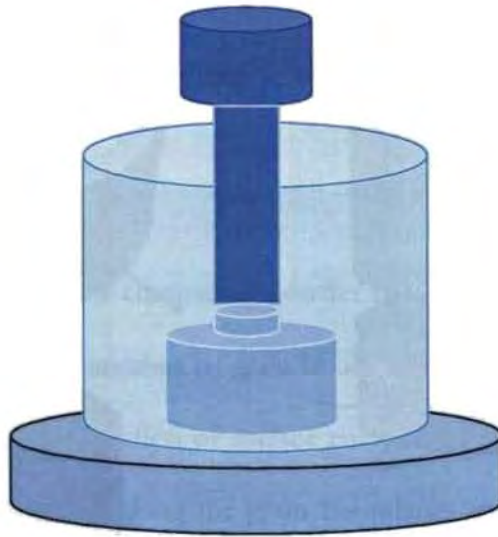
The well ground powder is heated to more than  $100^\circ\text{C}$  to eliminate moisture and other volatile impurities.

#### **4.2.3 Binder addition and dry pressing**

Unless the material concerned contain substantial quantity of clay, it is necessary to incorporate an organic binder. The primary function of the binder is to provide the dried sample sufficient strength to survive the handling between shaping and sintering, but it may also be essential to the method of shaping. One of the most important requirements for a binder is that it should be possible to eliminate from the compact without any disruptive effect. When particles are in high concentration in a fluid they tend to form a continuous network with point of contact between them. These points of contact remain when a binder is burned out and provide sufficient strength to resist the disintegrating effect of small stress. So the preheated powder is again crushed and ground finely again. Then an appropriate quantity of polyvinyl alcohol is added and is mixed well with the powder.

Dry pressing is carried out in a dye with movable top and bottom punches. A cavity is formed with the bottom punch in a low position and this is filled with free flowing granulated powder, which is then struck off level with the top of the dye. The top punch then descends and compresses the powder to a predetermined volume or, in more elaborate presses, to a set pressure. Both punches then move upwards until the bottom punch is level with the top of the dye and the top punch is clear of the powder feeding mechanism. The compact is then removed, the bottom punch is lowered and the cycle is repeated.

Shapes with a uniform section in the pressing direction are the easiest to produce by dry pressing. Pieces that vary in section require very careful powder preparation and may need special press facilities such as floating dyes where the dyes are free to move relative to the punches, or dyes that split open to allow easy extraction of the compact. The time taken for a pressing on an automatic machine varies from 0.2s, for pieces of diameter around 1mm, to 5s for large complex shapes. The schematic diagram and photo of cylindrical and hexagonal dyes are shown in **Figs. 4.1 and 4.2**. **Fig. 4.2 (c)** shows the hexagonal DR pellets



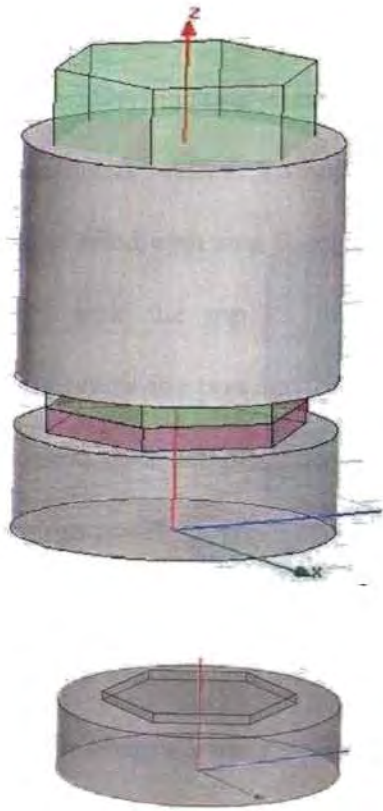
(a)



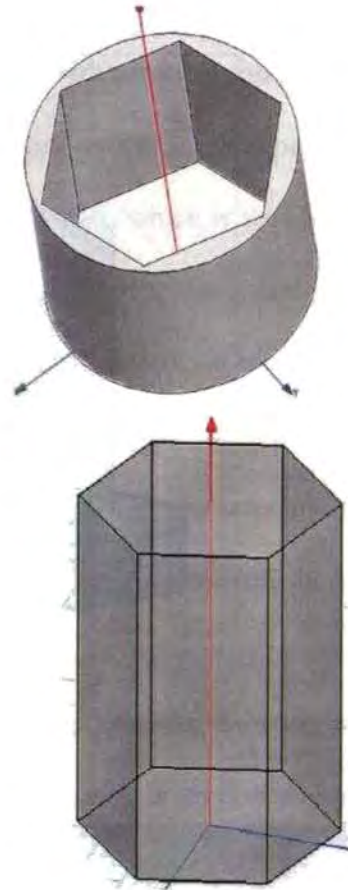
(b)

**Fig. 4.1** (a) Schematic diagram and (b) photo of cylindrical Dye's





Movable bottom punch



Movable top punch

(a)



(b)



(c)

**Fig. 4.2** (a) Schematic diagram and (b) photo of hexagonal Dye's (c) hexagonal DR pellets

This dye can be used to apply a pressure up to 7000-kg/inch squares. Using these dyes shown in above figures, cylindrical/hexagonal pellets can be easily made, by filling it with the powder and applying appropriate pressure.

#### **4.2.4 Sintering**

Sintering converts a compacted powder into a denser structure of crystallites jointed to one another by grain boundaries. The energetic basis for sintering lies in the reduction of surface energy by transferring matter from the interior of grains along the grain boundaries to adjacent pores, which are eventually filled. In simplest situations there are two heating schedule commonly used in sintering experiments. In many cases the powder compact is heated rapidly at a fixed sintering temperature, held at this temperature for the required time and finally cooled at room temperature. This schedule is referred to as isothermal sintering. The other case is known as constant heating rate sintering, the compact is heated at a fixed rate to the required temperature; after which it is cooled. In the present case isothermal sintering is used. The green pellet, which is placed in alumina crucible, is sintered at a temperature of 1200°C for 6 hours and then cooled at the room temperature.

#### **4.2.5 Finishing**

Tool wear during shaping and variations in shrinkage during drying and sintering contribute to the variations of 1%-2% in the dimensions of pieces taken from the furnace. For experimental studies, especially in the

case of measurements of dielectric parameters, the surface of the sample needs to be smoothed or polished. It is done by lapping the dense sample with abrasives such as silicon carbide, diamond powder etc. Here we use a silicon carbide water proof paper for lapping.

### **4.3. Microwave characterisation of DR**

#### **4.3.1 Method of measuring the permittivity**

There are different conventional techniques for measuring the complex permittivity of materials at microwave frequencies. Generally, the methods can be classified into;

- (i) that depends on the standing wave field within the dielectric
- (ii) that depends on waves reflected from the dielectric
- (iii) that depends on transmitted waves
- (iv) resonance methods

The choice of a method or a combination, will depend on the frequency, the value of  $\epsilon_r$  and  $\tan\delta$ , the amount of material available, the accuracy required, and the purpose of measurements.

Method (i) is suitable for liquid dielectrics, while the method (ii) leads to considerable errors while measuring the complex voltage reflection coefficient when the dielectric constant becomes large. The method (iii) is suitable for the measurement of large values of dielectric constant but have the disadvantage that they require carefully prepared specimens. When used in a wave guide the specimens have to be well polished and carefully fitted to avoid air gaps. Hakki and Coleman method [1] and Cavity

perturbation techniques [2] are the two methods mainly used for measuring dielectric parameters of DRs. Since in the present case the dielectric constant of the material is large Hakki and Coleman method is the best choice. Cavity perturbation technique is preferred for measurements on low permittivity material.

#### **4.3.2 Hakki and Coleman method**

The Hakki and Coleman configuration consists of a cylindrical dielectric post sandwiched between two infinite conducting plates. Using the  $TE_{0n\delta}$  modes, the effect of the air gap between the dielectric and the conducting plates becomes negligible since the electric fields tend to be zero at this point. The fields outside the dielectric decay very rapidly and hence, the use of conducting plates of finite dimensions still provides a good approximation to the theoretical model. This method restricts most of the stored energy to the dielectric and allows the experimental configuration to closely approximate the analytical model. Hakki and Coleman method is usually used for measuring high dielectric constant while the  $TE_{011}$  mode is propagating. For samples of low dielectric constants a second method, which also overcomes the air gap at the dielectric-to-conductor interface can be used. This method utilizes a dielectric post fitted in a cutoff circular wave-guide whose dimensions are such that the circular electric mode is cutoff in the air region of the guide.

The construction of the sample holder is shown in **Fig. 4.3**. The top and bottom plates are the two shorting plates, which turn the dielectric

rod transmission line into a resonant structure. The top plate can be raised or lowered to accommodate various lengths of samples; both the top and center plates are gold plated. Coupling to the sample is achieved through two E-field probes, which can be moved in and out radially with respect to the sample thereby varying the coupling coefficients.

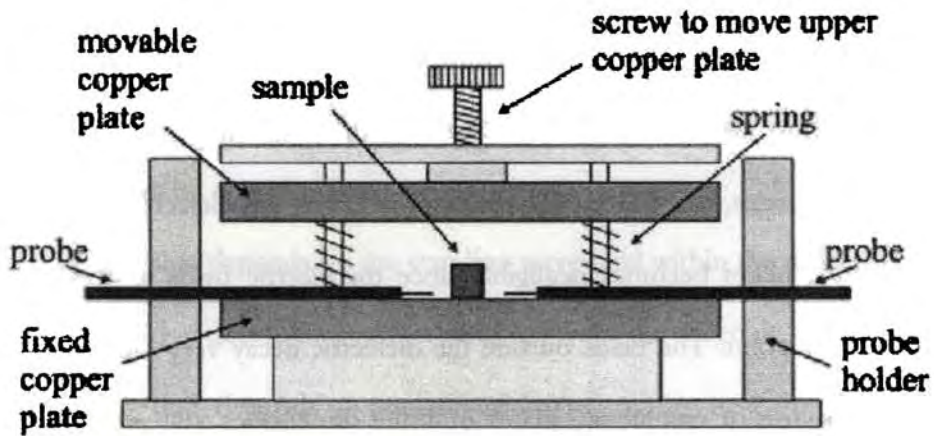


**Fig. 4.3** set up for Hakki and Coleman methods for measuring dielectric constants

Placing the specimen exactly at the center is not critical; it merely needs to be placed approximately symmetrical with the two probes. The coupling of each probe is reduced until no change is detected in the resonant frequency. If the sample is isotropic the  $TE_{011}$  mode can be identified by finding the second low frequency mode. Further proof that this is a  $TE_{0n8}$  mode is obtained adjusting the top plate. As the plate is fine

adjusted, the TM modes move rapidly to higher frequencies while the TE<sub>011</sub> mode remains stationary.

The structure can be essentially treated as a shorted dielectric waveguide in the form of a finite length of a cylindrical dielectric rod. Waveguide is shorted by placing conducting plates at each end thereby turning the transmission line into a resonator. The characteristic equation for the normal modes is well known

It is

$$\left[ \frac{\epsilon_r J_m'(\alpha) + K_m'(\beta)}{\alpha J_m(\alpha) + \beta K_m(\beta)} \right] \left[ \frac{J_m'(\alpha) + K_m'(\beta)}{\alpha J_m(\alpha) + \beta K_m(\beta)} \right] = m^2 \left[ \frac{\epsilon_r}{\alpha^2} + \frac{1}{\beta^2} \right] \left[ \frac{1}{\alpha^2} + \frac{1}{\beta^2} \right] \quad \text{----- (4.2)}$$

Where,

$$\alpha = \frac{\pi D}{\lambda} \left[ \epsilon_r - \left( l\lambda / 2L \right)^2 \right]^{1/2}, \quad \text{----- (4.3)}$$

$$\beta = \frac{\pi D}{\lambda} \left[ \left( l\lambda / 2L \right)^2 - 1 \right]^{1/2}, \quad \text{----- (4.4)}$$

Where  $J_m(\alpha)$ ,  $K_m(\beta)$  are Bessel functions of the first and second kind, respectively,  $\lambda$  is the free-space wavelength,  $D$  is the diameter,  $L$  is the length of the dielectric specimen, and  $l=1,2,3,\dots$ etc., corresponds to

the multiple half-wavelengths in the cavity along the axial direction of the cylindrical specimen.

The equations for  $\alpha$  and  $\beta$  can be rewritten for the TE<sub>011</sub> mode

$$\epsilon_r = 1.0 + \left( \frac{c}{\pi D f_1} \right)^2 (\alpha_1^2 + \beta_1^2), \quad \text{----- (4.5)}$$

Where  $\alpha_1, \beta_1$  are the first roots of the characteristic equation with  $m=0, l=1$ , and  $f_1$  is the resonant frequency. Hence by measuring the frequency of the TE<sub>011</sub> mode and knowing the dimensions of the specimen, the real part of the dielectric constant can be found out.

### 4.3.3 Cavity perturbation technique

The cavity perturbation technique consists of a transmission type S-band rectangular cavity resonator with network Analyzer HP 8714ET as shown in **Fig. 4.4 (a)**. The cavity resonator is excited in the TE<sub>10p</sub> mode. The S-band rectangular cavity resonator is shown in **Fig. 4.4(b)**. Initially, the resonant frequency  $f_0$  and the quality factor  $Q_0$  of each resonant peak of the cavity resonator at the maximum of electric field are determined. The DR sample pellet is designed in the form so as to facilitate its entry and easy movement through the cavity slot. It is introduced into the cavity resonator through the non-radiating slot. For a resonant frequency of the sample-loaded cavity, the position of the sample is adjusted for maximum perturbation (i.e. maximum shift of resonant frequency with minimum amplitude for the peak). The new resonant frequency  $f_s$  and the quality

factor  $Q$ , are determined. The dielectric parameters at this frequency are calculated. The procedure is repeated for other resonant frequencies.

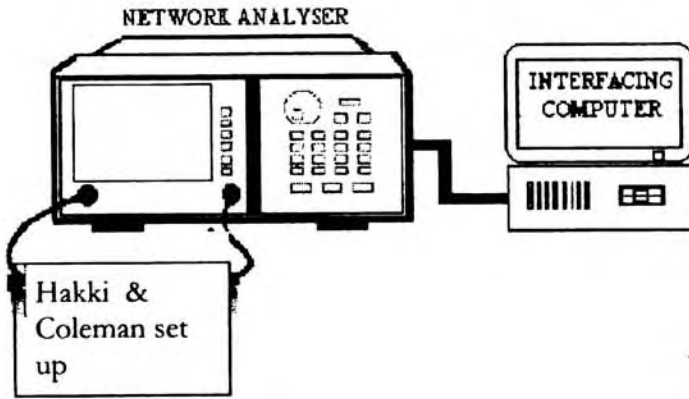


**Fig. 4.4 (a)** Experimental full set up for measuring dielectric parameters

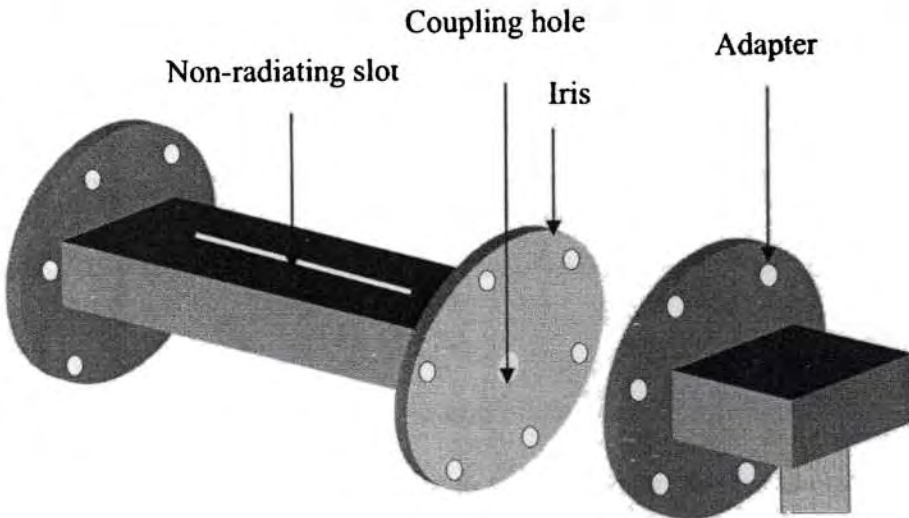


**Fig. 4.4 (b)** Rectangular cavity for measuring dielectric parameters

### Theory

According to the theory of cavity perturbation, the real and imaginary parts of the complex permittivity [2] are given as



$$\epsilon_r' - 1 = \frac{f_o - f_s}{2f_s} \left( \frac{V_c}{V_s} \right) \text{----- (4.6)}$$

$$\epsilon_r'' = \frac{V_c}{4V_s} \left( \frac{Q_o - Q_s}{Q_o Q_s} \right) \text{----- (4.7)}$$

Here,  $\bar{\epsilon}_r = \epsilon_r' - j\epsilon_r''$ ,  $\bar{\epsilon}_r$  is the relative complex permittivity of the sample,  $\epsilon_r'$  is the real part of the relative complex permittivity, which is known as dielectric constant.  $\epsilon_r''$  is the imaginary part of the relative complex permittivity associated with the dielectric loss of the material.  $V_s$  and  $V_c$  are the volumes of the sample and the cavity resonator respectively.

**References**

1. Darko Kajfez, P. Guillon, Dielectric Resonators, Artech House, June 1986
2. K.T Mathew, Encyclopedia of RF and Microwave Engineering, WILY-VCH Publication, Vol. 4, pp. 3725-3735, 2005.

## **Chapter V EXPERIMENTAL STUDY OF HEXAGONAL DIELECTRIC RESONATOR ANTENNA**

---

### **5.1 Introduction**

The results of the experimental studies on the return loss, impedance, gain and radiation characteristics of the new geometry Hexagonal Dielectric Resonator Antenna (HDRA) is discussed in this chapter. The important radiation characteristics such as radiation pattern, half power beam width(HPBW), cross polar level and gain for the coaxial and microstrip feed excitation are presented under subsequent sections. Results related to the optimization of coaxial probe length, antenna height (or aspect ratio) and coaxial probe location are discussed in the beginning part of this chapter. Results related to the optimization of HDRA with microstrip feed excitation is explained in the last part of this chapter. A comparative study of the experimental results with the simulation results, using Ansoft HFSS<sup>TM</sup>, is given at the end of each section.

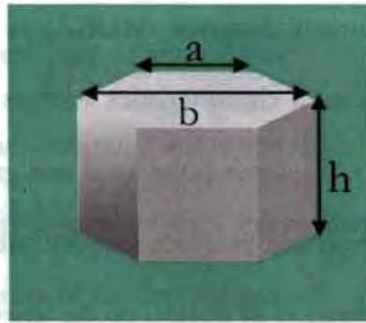
### **5.2 COAXIAL PROBE FED HDRA**

In this section, the optimization of the coaxial probe length and aspect ratio of the antenna are done first, followed by the coaxial probe location. The diameter of the coaxial probe used is 0.6mm.

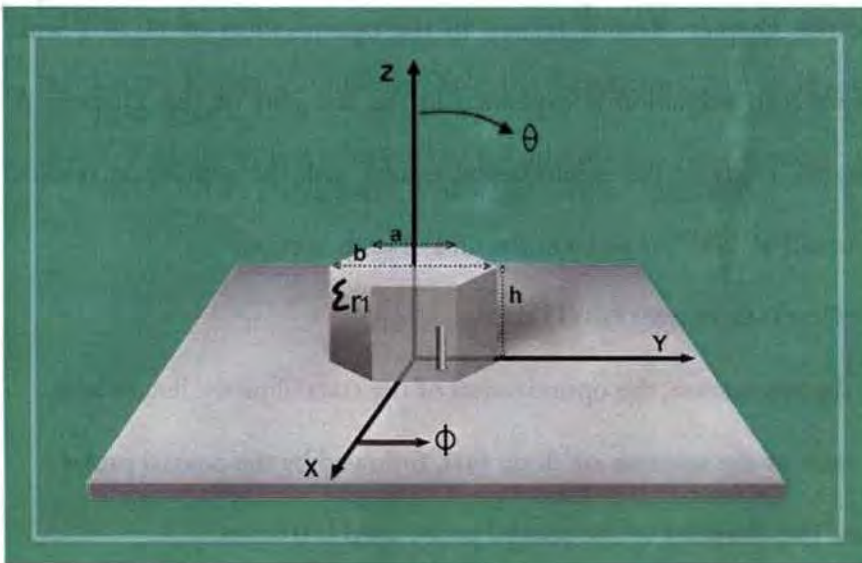
#### **5.2.1 Antenna configuration**

**Fig 5.1 (a)** shows the geometry of the hexagonal pellet and **Fig. 5.1 (b)** shows the coaxial-coupled hexagonal dielectric resonator antenna. The

dielectric constant of the hexagonal dielectric resonator (HDR) used for the study is  $\epsilon_r = 69$ , hexagonal side length,  $a = 14.4$  mm, diagonal length 30.4mm and heights are  $h=13$  mm, 11 mm and 8 mm. The HDRA is placed on a rectangular metal ground plane of dimension 180 mm x 140 mm.



(a)



(b)

Fig. 5.1 (a) geometry of the Hexagonal pellet (b) coaxial-coupled hexagonal dielectric resonator antenna

### 5.2.2 Effect of coaxial probe length on the performance of HDRA

The effect of coaxial probe length variation on the return loss of HDRA is shown in Fig. 5.2 (a). When the length of the probe ( $f_l$ ) is varied from 4mm to 7mm with a step of 1mm, it is found that the impedance varies and hence the return loss also. The probe length is optimized to 6mm, since it gives a minimum return loss of -24dB. The coaxial probe is fed at 13mm ( $f_w$ ) from the center towards one corner of HDRA as shown in Fig 5.2(b). The height of HDRA used is  $h=11$ mm.

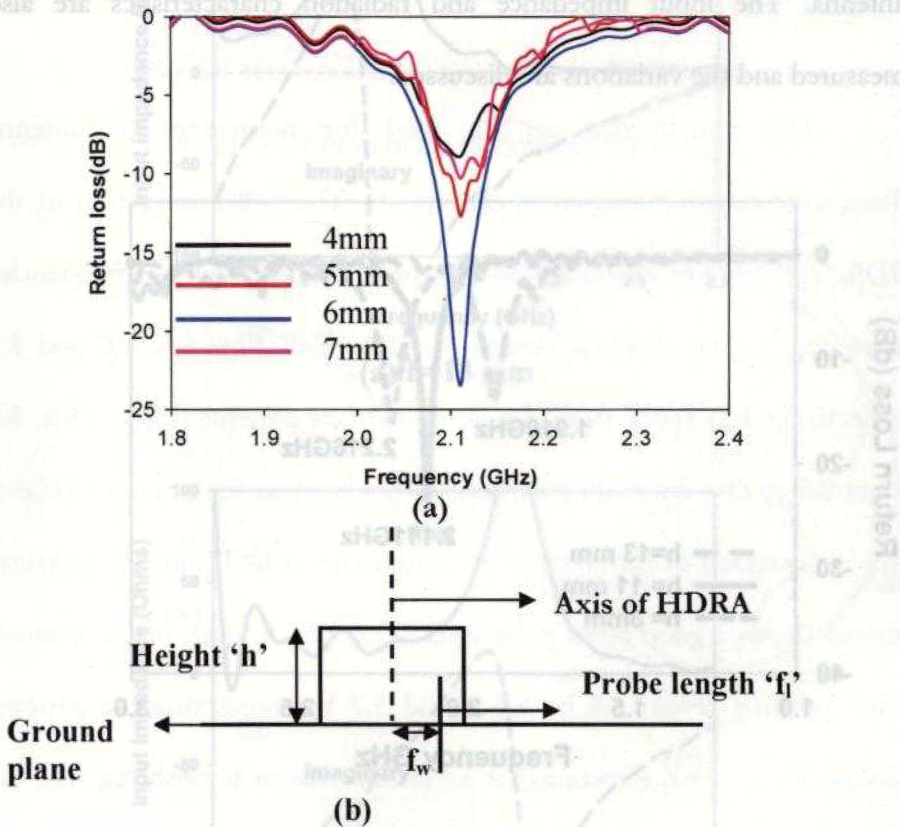


Fig. 5.2 (a) Return loss variation with probe length (b) schematic diagram of hexagonal dielectric resonator showing probe length and probe location (side view).

### 5.2.3 Effect of DR height on the performance of HDRA

The effect of height and hence aspect ratio ( $b/2h$ ) variation on the resonant frequency and impedance bandwidth ( $S_{11} < -10\text{dB}$ ) of a hexagonal dielectric resonator antenna (HDRA) is investigated in this section. The antenna is excited by inserting a probe of length ( $f_i$ ) 6 mm at a distance ( $f_w$ ) of 13 mm from the center ( $Z$  axis) to one corner of the HDRA and the variation in resonant frequency for different heights are studied. Also it is observed that the bandwidth varies with the variation of height of the antenna. The input impedance and radiation characteristics are also measured and the variations are discussed.

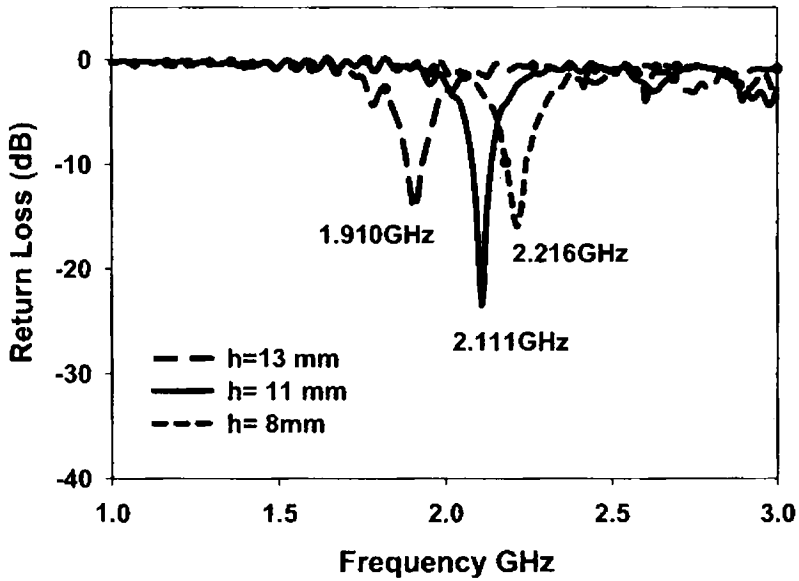
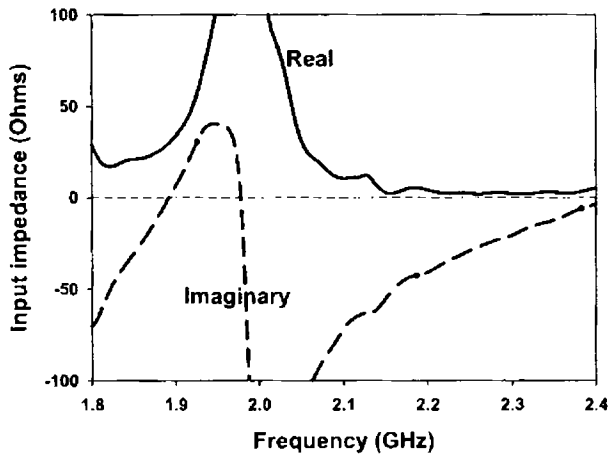


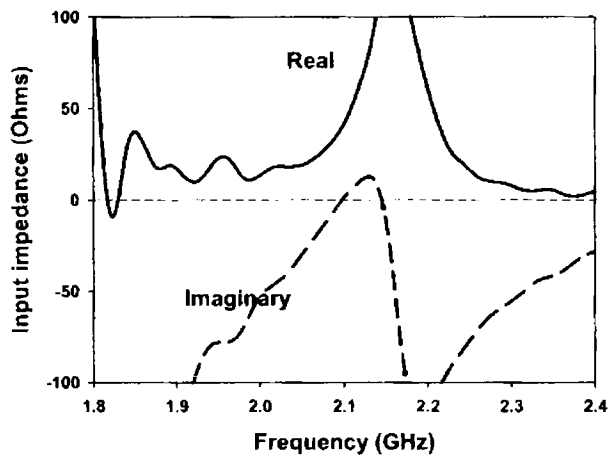
Fig. 5.3 Variation of return loss  $|S_{11}|$  with height of HDRA

### 5.2.3.1 Results and Discussion

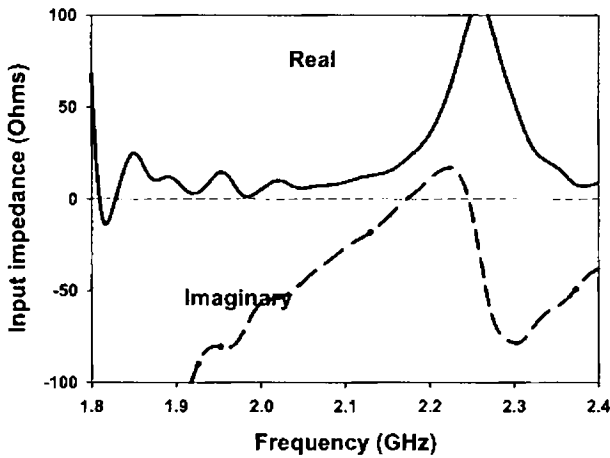
Fig.5.3 shows the variation of return loss with height of HDRA. It is observed that the resonant frequency varies from 1.910 GHz to 2.216 GHz when the height of antenna changes from 13 mm to 8 mm. Impedance variations for the three DRs are shown in Figs. 5.4 (a)-(c). It is also observed that a height of 11 mm provides good matching over the band.



(a)  $h=13$  mm



(b)  $h=11$  mm



(c)  $h = 8 \text{ mm}$

Fig. 5.4 Variation of input impedance with frequency

The experimental set up used for measuring the antenna characteristics was explained in chapter III. The radiation pattern of the HDRAs in the elevation and azimuth planes at the resonant frequencies corresponding to different heights are shown in Figs.5.5, 5.6 and 5.7 respectively. It is found from the elevation plane patterns (Figs. 5.5 a, 5.6 a and 5.7 a) that the cross-polar levels worsen when the height of HDRA ('h') is decreased or increased from 11mm and at  $h=11\text{mm}$  the radiation pattern shows a good cross polar level of  $-22\text{dB}$ . A study of the azimuth plane patterns (Figs. 5.5 b, 5.6 b and 5.7 b) shows that the patterns become more omni directional at  $h=11\text{mm}$ . Also it is observed that the polarization in all the cases is linear. All the characteristics of the antenna are summarized in Table 5.2

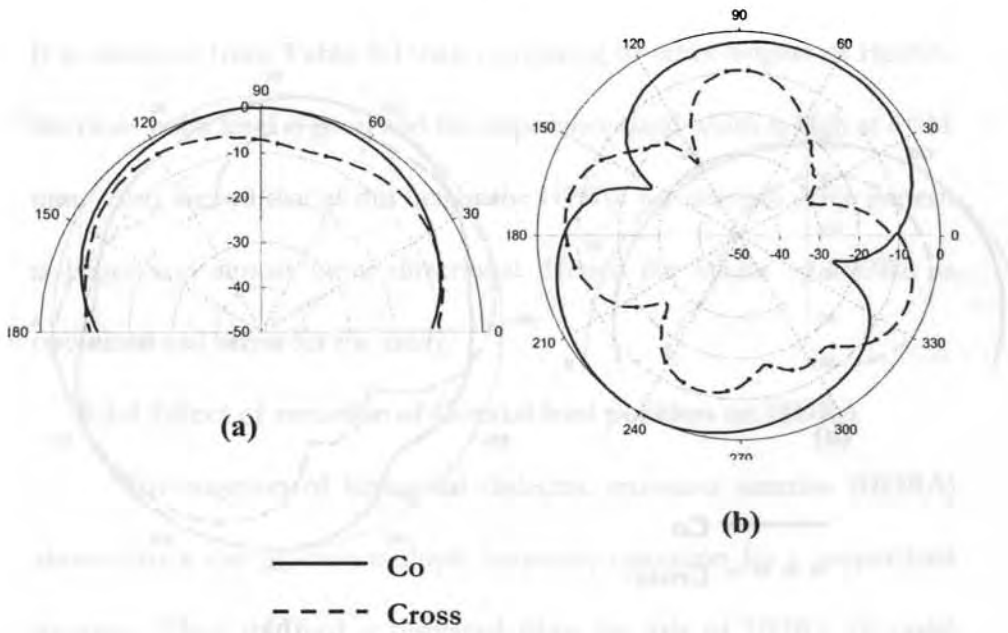


Fig 5.5 Measured radiation patterns at  $h=13$  mm

a) Elevation plane b) Azimuth plane

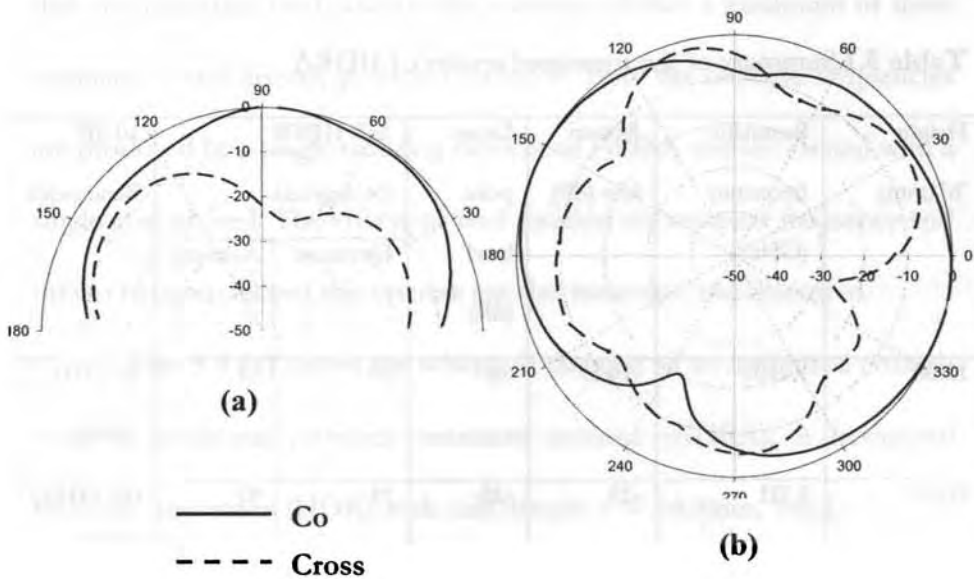
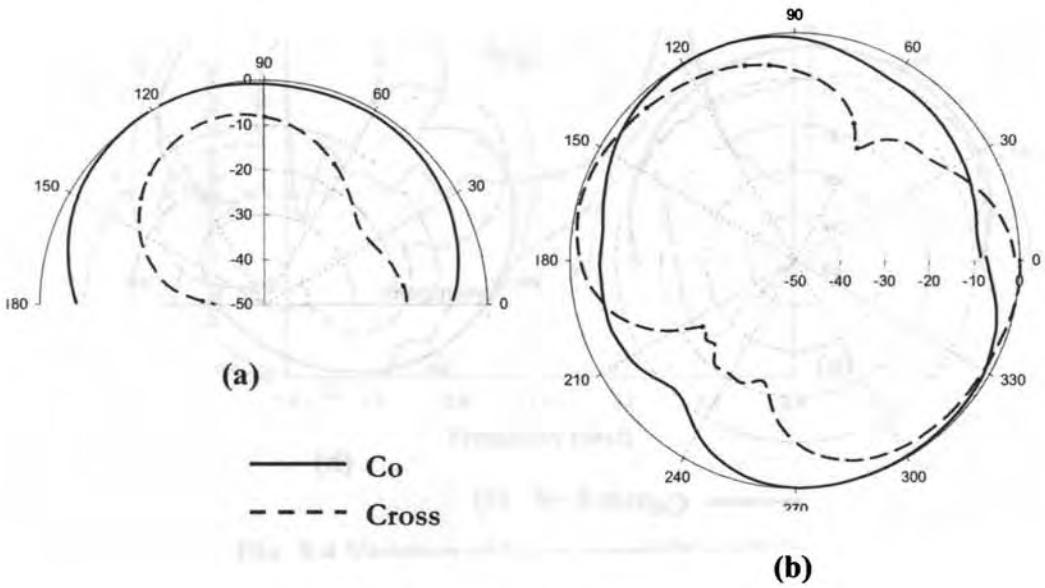


Fig.5.6. Measured radiation patterns at  $h= 11$  mm

a)Elevation plane b) Azimuth plane





**Fig.5.7.** Measured radiation patterns at  $h=8$  mm

a) Elevation plane b) Azimuth plane

**Table 5.1** Summary of the measured results of HDRA

Height 'h' (mm)	Resonant frequency (GHz)	Return loss (dB)	Cross- polar level (dB)	3dB HPBW (in degrees)		10 dB Bandwidth
				Elevation	Azimuth	
13.00	1.910	-14.1	-8	90	77	40 MHz / 2.09 %
<b>11.00</b>	<b>2.111</b>	<b>-23</b>	<b>-22</b>	<b>75</b>	<b>97</b>	<b>60 MHz/ 2.84 %</b>
8.00	2.216	-16	-9	125	90	50 MHz/ 2.25 %

It is observed from **Table 5.1** that, comparing to other heights of HDRA, the cross polar level is good and the impedance band width is high at  $h=11$  mm. Also viewed that at this height the HPBW for azimuth plane pattern is larger and almost omni directional. Hence the height of HDRA is optimized as 11 mm for the study.

#### **5.2.4 Effect of variation of Coaxial feed position on HDRA**

Investigation of hexagonal dielectric resonator antenna (HDRA) shows that it can produce multiple frequency operation for a proper feed location. When the feed is displaced from the axis of HDRA (Z- axis) towards the corner, the characteristics such as return loss, input impedance, radiation patterns and gain are found to vary. It is observed that at a particular feed position the antenna exhibits a maximum of three resonances with linearly polarized radiation. Here the multiple frequencies are produced by a single radiating element of HDRA and are excited with a single coaxial feed. The effects of feed location on resonant frequency and other characteristics of the antenna are also measured and discussed.

**Fig. 5.8 (a)** shows the schematic diagram of an optimized coaxial-coupled hexagonal dielectric resonator antenna (HDRA). A hexagonal dielectric resonator (HDR) with side length  $a = 14.4\text{mm}$ , height  $h = 11$  mm, diagonal length  $b=30.4$  mm and dielectric constant  $\epsilon_r = 69$  is placed on a rectangular ground plane (180mm X 140mm). The HDRA has an aspect ratio ( $h/b$ ) less than unity and it is excited by inserting a probe of length 6mm at different locations on the X- axis as shown in **Fig. 5.8 (b)**.

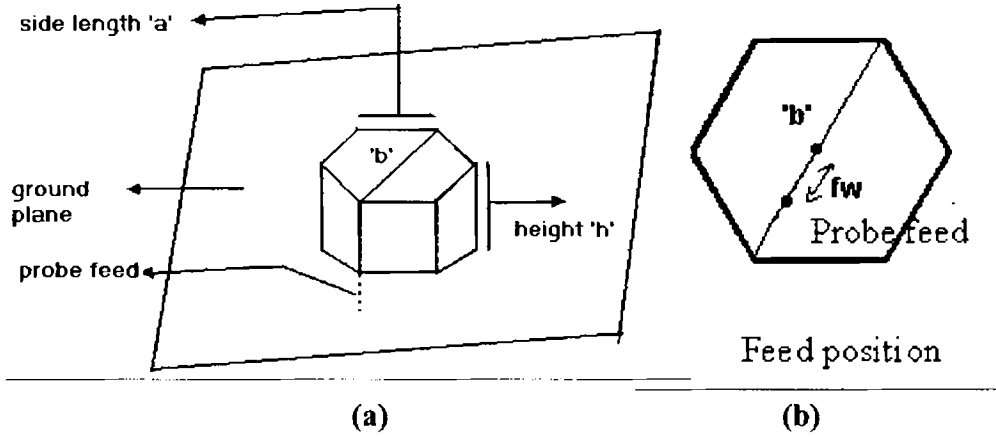
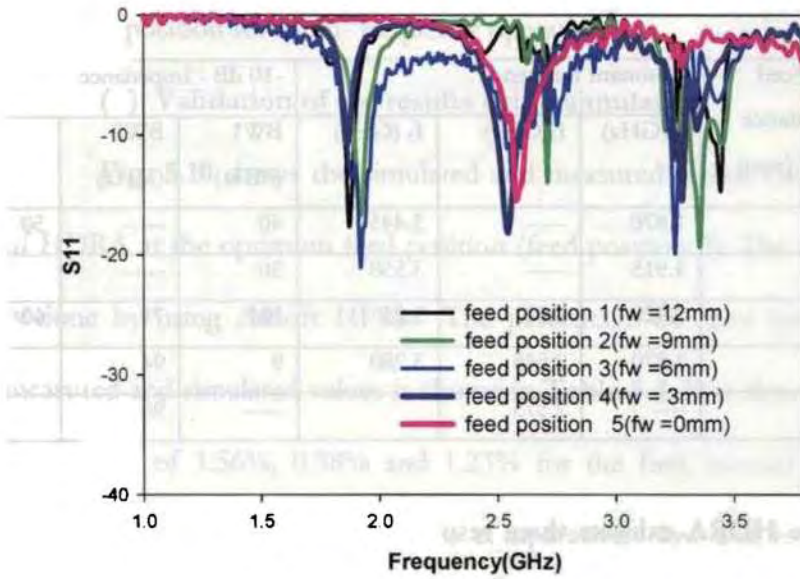


Figure 5.8 (a) schematic diagram of the HDRA (b) feed location

#### 5.2.4.1 Results and discussion

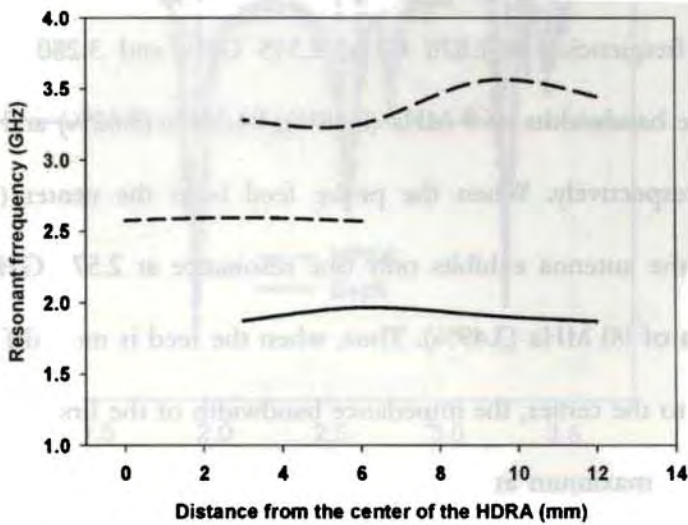
##### (i) Optimization on feed position

Experimental set up was explained in chapter III. Fig.5.9 (a) shows the return loss of HDRA for different feed positions and Fig. 5.9(b) the variation of resonant frequency as function of feed distance ( $f_w$ ) from the center. Table 5.2 shows the variation of resonant frequency and bandwidth with feed location. It is found that, near the periphery, i.e. at 1<sup>st</sup> feed position; there are only two resonant frequencies at 1.870 GHz and 3.445GHz with an impedance bandwidth of 40 MHz (2.14%) and 50 MHz (1.45%) respectively. But when the feed is at 2<sup>nd</sup> position, the dominant resonant frequencies are at 1.915 GHz and 3.550 GHz with impedance bandwidths 30 MHz (1.57%) and 230 MHz (6.48%). A non-radiating resonance at 2.7 GHz is also present.



(a)

Figure 5.9 (a) Variation of return loss against frequency for various feed location



(b)

Figure 5.9 (b) Variation of resonant frequency with feed positions

**Table 5.2** Variation of resonant frequency and bandwidth with feed location

Feed position	Feed distance $f_w$ (mm)	Resonant frequency			-10 dB - Impedance bandwidth		
		$f_1$ (GHz)	$f_2$ (GHz)	$f_3$ (GHz)	BW1 (MHz)	BW2 (MHz)	BW3 (MHz)
1	12	1.870	-----	3.445	40	-----	50
2	9	1.915	-----	3.550	30	-----	230
3	6	<b>1.920</b>	<b>2.57</b>	<b>3.25</b>	<b>104</b>	<b>71</b>	<b>60</b>
4	3	1.870	2.545	3.280	9	94	20
5(center)	0	----	2.575		----	90	----

The HDRA exhibits three resonances at 1.920 GHz, 2.570 GHz and 3.250 GHz with impedance bandwidths of 104 MHz (5.42%), 71 MHz (2.76%) and 60 MHz (1.85%) respectively when the feed is at 3<sup>rd</sup> position, which is along the diagonal, at the central point between axis and the periphery. When the feed is at position 4, the antenna again exhibits three resonant frequencies at 1.870 GHz, 2.545 GHz and 3.280 GHz with impedance bandwidths of 9 MHz (0.48%), 94 MHz (3.62%) and 20 MHz (0.61%) respectively. When the probe feed is at the center (5th feed position) the antenna exhibits only one resonance at 2.575 GHz with a bandwidth of 90 MHz (3.49%). Thus, when the feed is moved from near periphery to the center, the impedance bandwidth of the first resonance  $f_1$  increases to maximum at the third feed position though there is a slight change in resonant frequency. Likewise the bandwidth of the second frequency  $f_2$  increases to a maximum at the fourth feed position and, that of the third resonance  $f_3$  increases to a maximum at the second feed

position. From **Table 5.3** it is clear that the third feed position is the optimum position for multi- frequency operation.

**(ii) Validation of the results using simulation**

**Fig. 5.10** shows the simulated and measured return loss variation of HDRA at the optimum feed position (feed position 3). The simulation is done by using Ansoft HFSS. The percentage of error between the measured and simulated values is shown in **Table 5.4**. It is clear that there is an error of 1.56%, 0.38% and 1.23% for the first, second and third frequency respectively. This error is comparatively low and is attributed due to the air gap between the coaxial probe and HDRA while doing experiment.

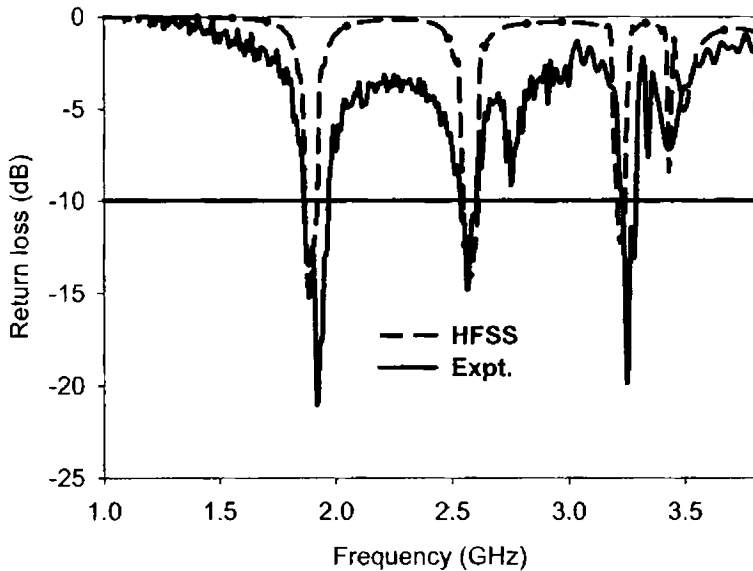


Fig. 5.10 comparison of simulated and measured return loss of HDRA at the optimum feed position

**Table 5.4** Percentage of error in return loss of simulated and measured values

Antenna Position	Measured Frequency(GHz)			Simulation HFSS Frequency(GHz)			% error HFSS over Experiment		
	f1	f2	f3	f1	f2	f3	f1	f2	f3
3	1.92	2.57	3.25	1.89	2.56	3.21	1.56	0.38	1.23

**(iii) Input impedance**

The variation of input impedance with frequency for all the resonant bands at the optimized feed position are given in **Fig. 5.11** (a)-(c), shows better impedance matching over the bands.

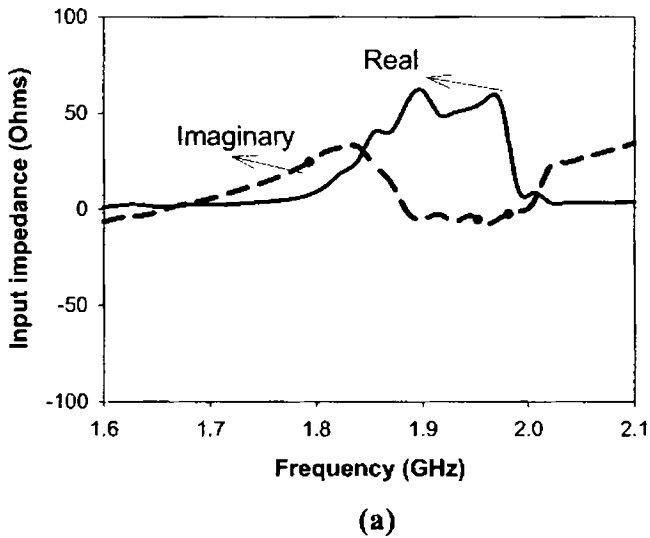


**Figure 5.11 (a)** Variation of impedance with frequency for the first band

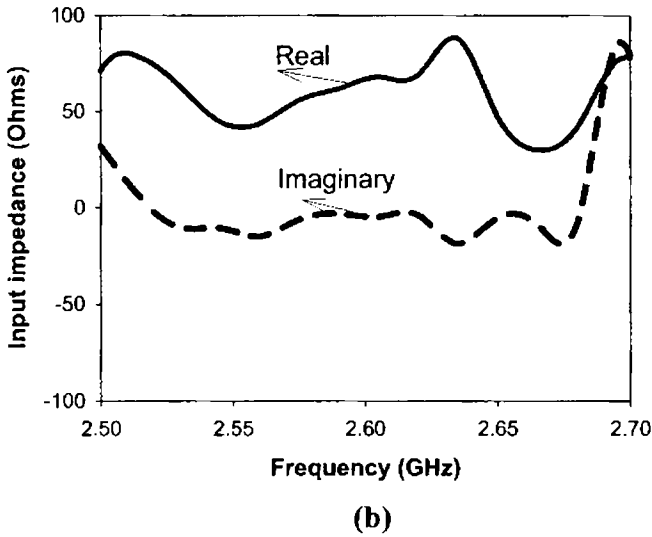


Figure 5.11 (b) Variation of impedance with frequency for second band

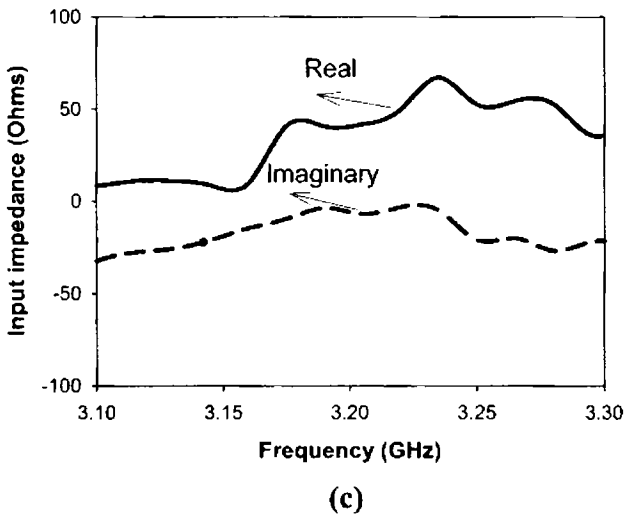


Figure 5.11 (c) Variation of impedance with frequency for third band

(iv) Effect of feed position on radiation pattern

Radiation patterns in elevation and azimuth planes for all the resonant frequencies are shown in Figs. 5.12 (a)-(k) and Figs. 5.13 (a)-



(k) respectively and are found to be similar over the entire band. It is observed from the patterns that the antenna is linearly polarized. Figs.5.12 (a) – (e), (g), (h) and (j) show that the patterns are broad. This is due to the excitation of broad  $HE_{m\delta}$  modes which was explained by Kishk et al. [1]. The half power beam widths are shown in Table 5.5. But in Figs. 5.12 (f) and 5.12(i) a dip at the on axis is observed, which is due to  $HE_{12\delta}$  modes [1]. In Fig. 5.12(k), the same effect is observed on the polarized pattern of the center fed HDRA for which the mode of excitation is  $TM_{01\delta}$  [2]. This pattern is similar to the radiation pattern of a dipole, i.e. the energy is distributed on either side.

The modes corresponds to the three frequencies at the optimum feed location (feed position 3) are referred to as  $HE_{11\delta}$  (Fig. 5.12 (e)),  $HE_{12\delta}$  (Fig. 5.12 (f)), and  $HE_{13\delta}$  (Fig. 5.12 (g)). The first index of the subscripts presents the order of the azimuth variations and is the only index that can be controlled and surely known. The other two indexes cannot be controlled, and in fact there is no unique definition for them when the geometry differs from the cylindrical shape. Here these indexes are used in a similar manner as used in the cylindrical shapes, because the geometry of HDRA is close to that of cylindrical shape, and hence the second index is referred to as variation along radial direction and the third index presents the order of variation along the z direction. This variation is normally  $0.5 < \lambda < 1$  and therefore the symbol  $\delta$  is used.

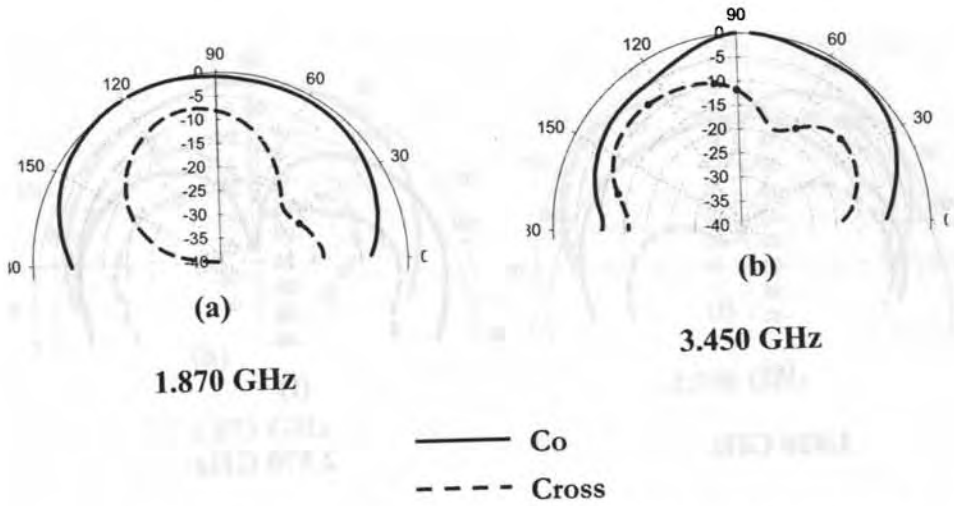


Fig. 5.12 (a) & (b) Elevation plane patterns for feed position 1

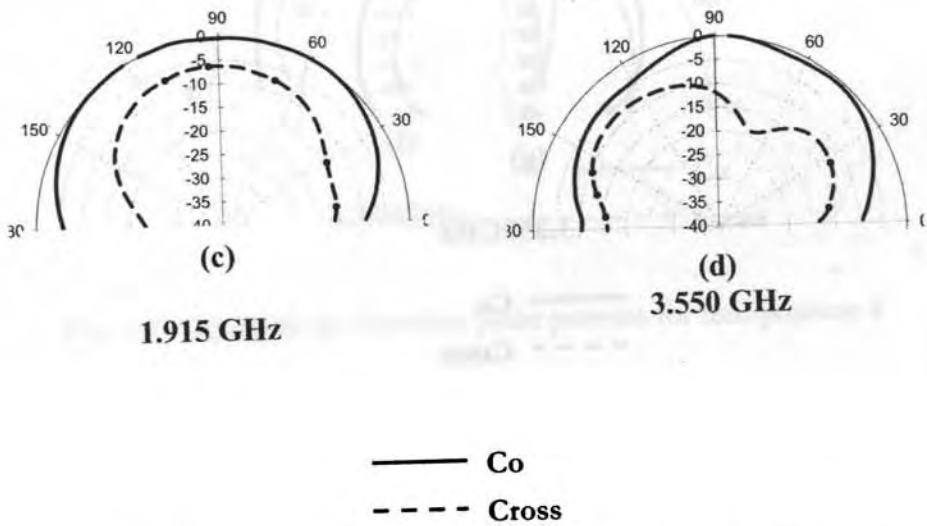


Fig. 5.12 (c) & (d) Elevation plane patterns for Feed position 2

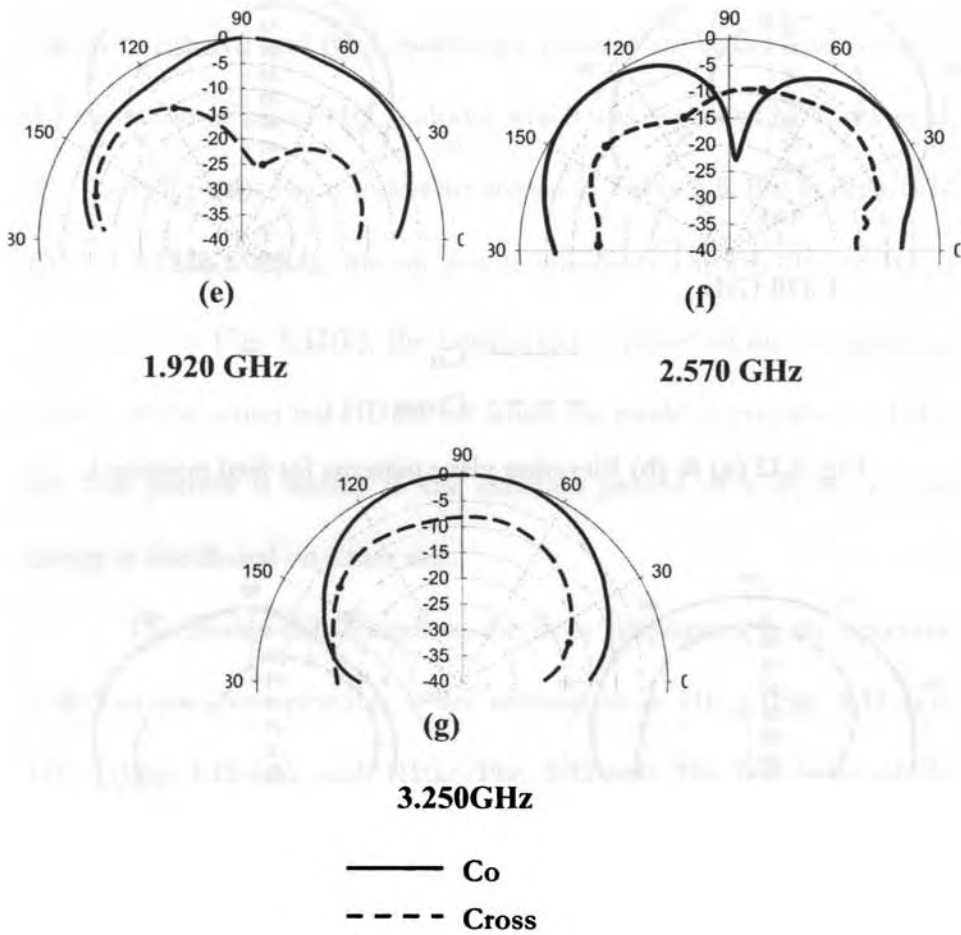


Fig. 5.12 (e), (f) & (g) Elevation plane patterns for Feed position 3

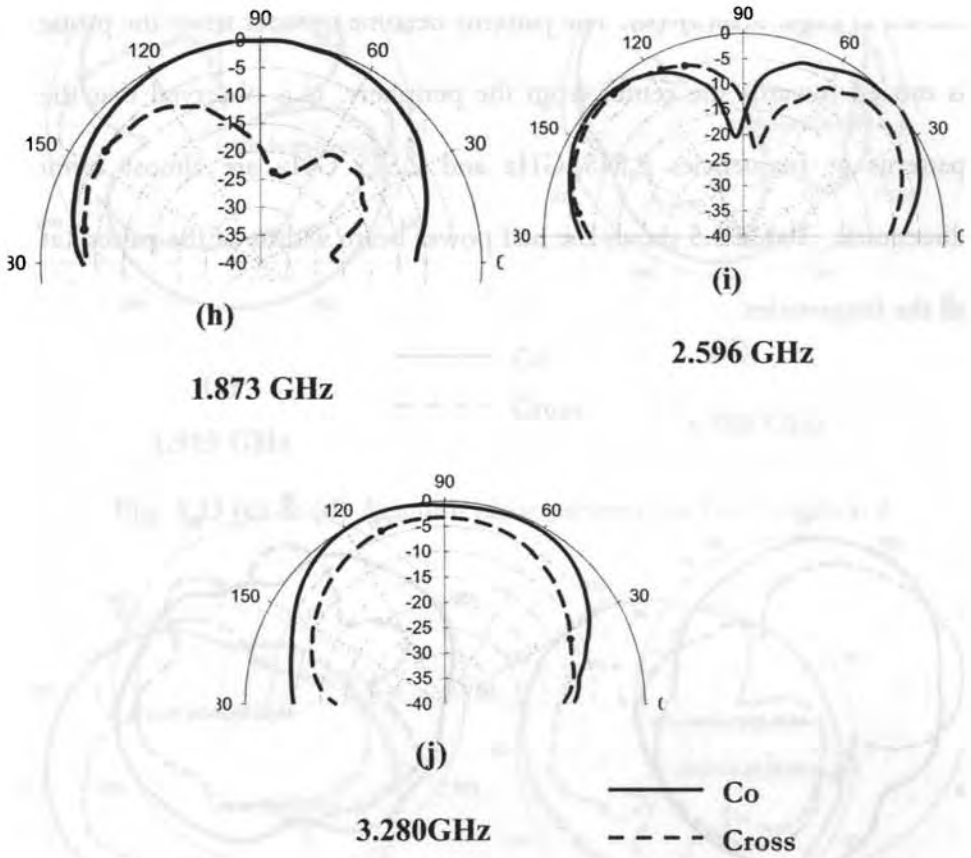


Fig. 5.12 (h), (i) & (j) Elevation plane patterns for feed position 4

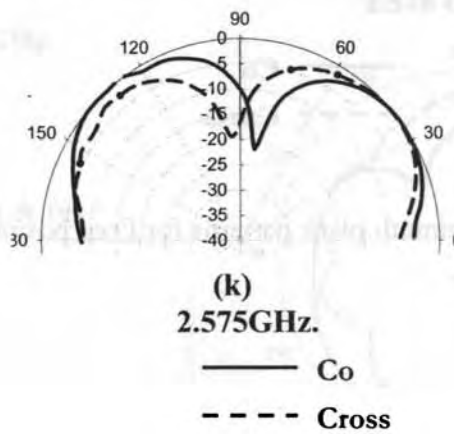
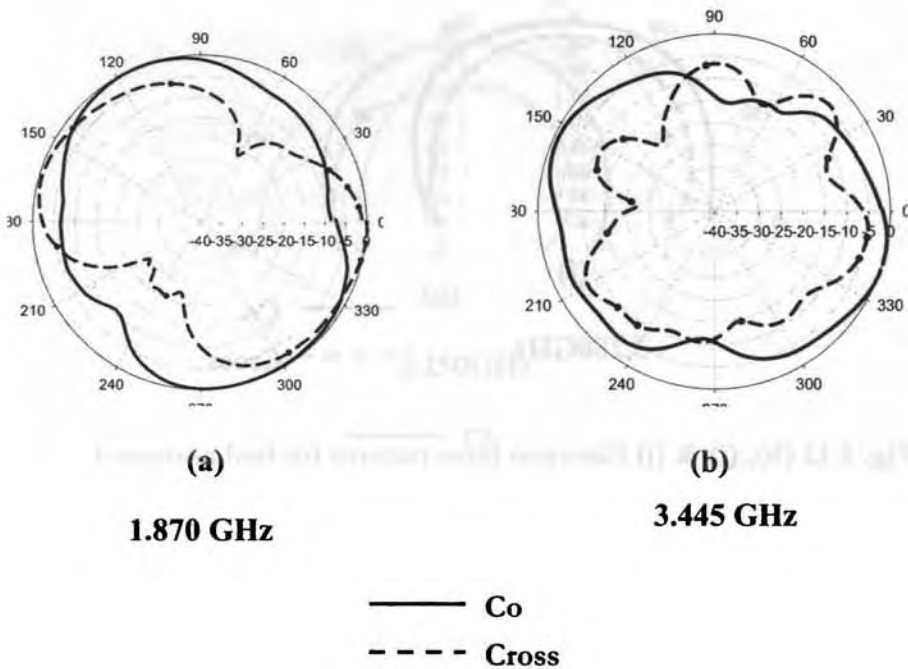


Fig. 5.12 (k) Elevation plane patterns for feed position 5

The azimuth plane radiation patterns at all the frequencies are shown in **Figs. 5.13(a)-(k)**. The patterns become broader when the probe is moved towards the center from the periphery. It is observed that the patterns at frequencies 2.545 GHz and 2.575 GHz are almost omnidirectional. **Table 5.5** shows the half power beam widths of the pattern at all the frequencies.



**Fig. 5.13 (a) & (b)** Azimuth plane patterns for Feed position 1

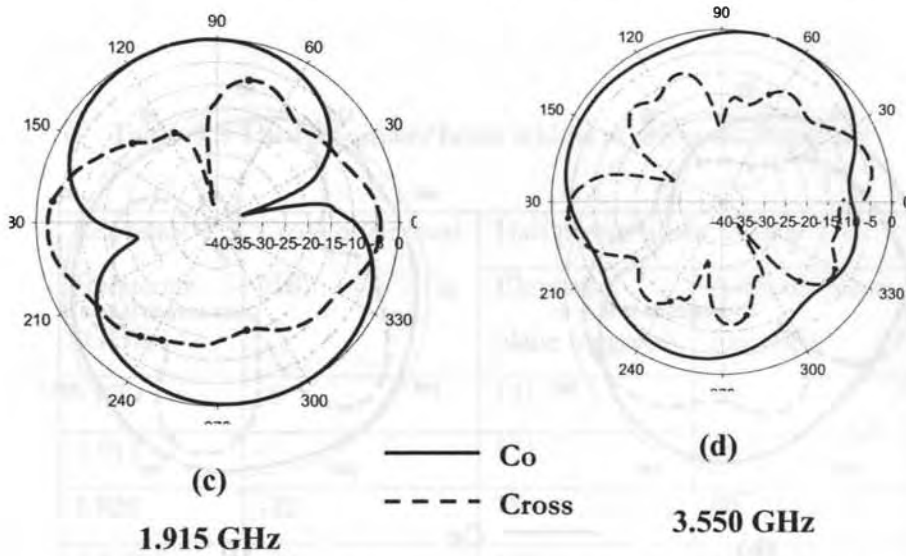


Fig. 5.13 (c) & (d) Azimuth plane patterns for Feed position 2

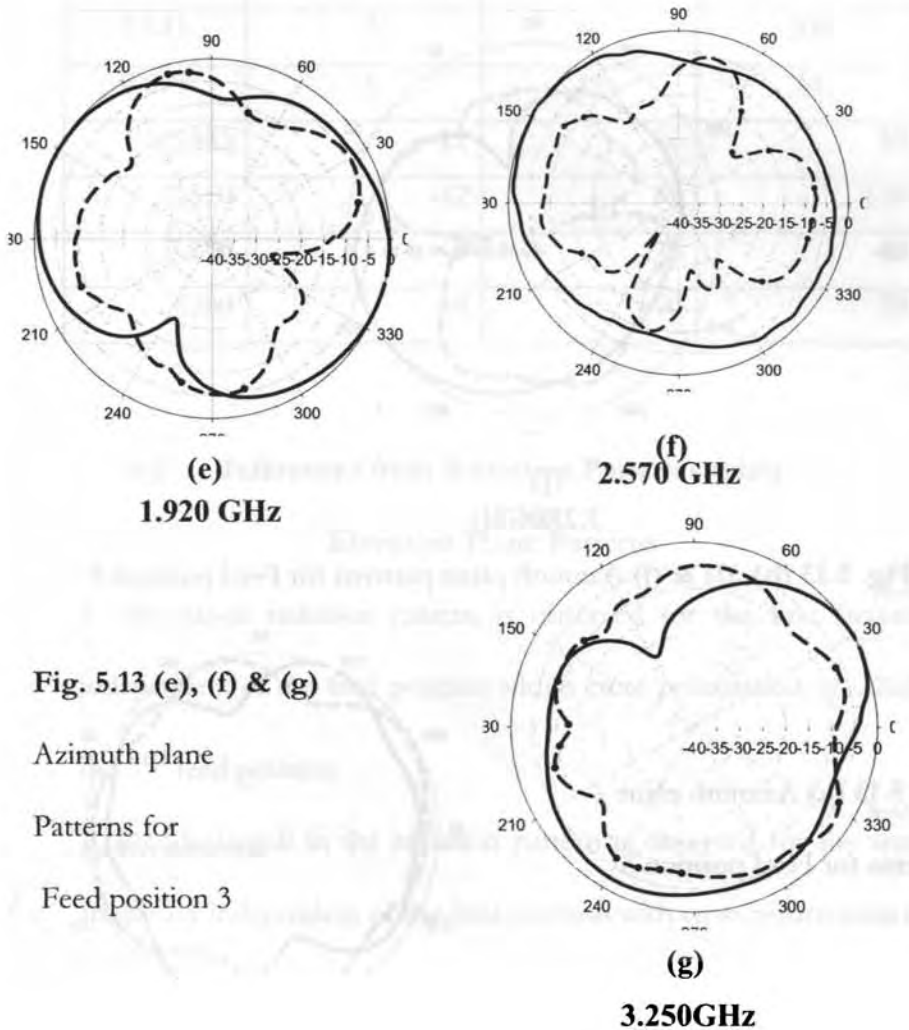


Fig. 5.13 (e), (f) & (g)  
Azimuth plane  
Patterns for  
Feed position 3

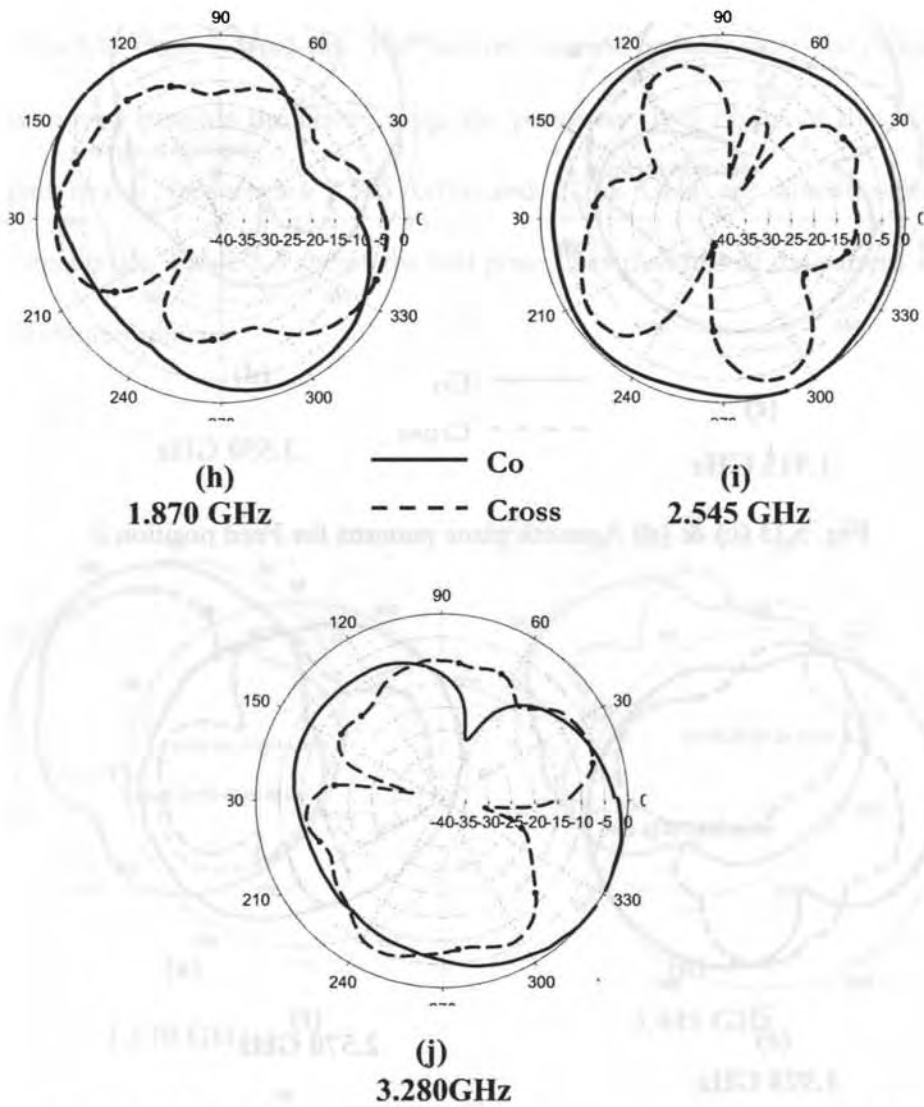
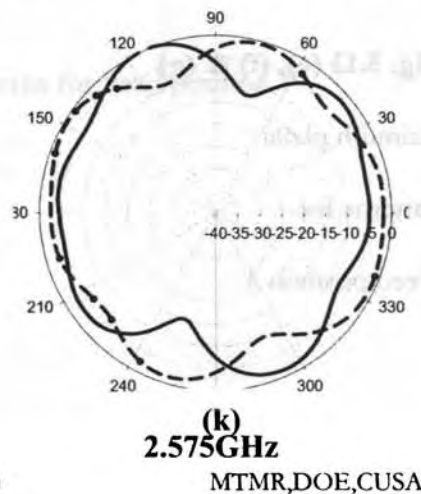


Fig. 5.13 (h), (i) & (j) Azimuth plane patterns for Feed position 4

Fig. 5.13 (k) Azimuth plane patterns for Feed position 5



**Table 5.5** The half power beam widths at different frequency

Resonant frequency (GHz)	Cross polar level (dB)	Half power beam widths	
		Elevation plane (degrees)	Azimuth plane (degrees)
1.870	-8	121	90
1.915	-7	131	96
<b>1.920</b>	<b>-22</b>	<b>75</b>	<b>80</b>
1.870	-20	106	81
<b>2.570</b>	<b>-10</b>	<b>50</b>	<b>65</b>
2.545	-7	40	200
2.575	-5	45	54
3.445	-12	76	50
3.550	-12	85	135
<b>3.250</b>	<b>-9</b>	<b>75</b>	<b>40</b>
3.280	-4	90	70

**(v) Inferences from Radiation Pattern studies**

**Elevation Plane Patterns**

1. Broadside radiation pattern is observed for the first frequency independent of the feed position with a cross polarization of -22dB at the 3<sup>rd</sup> feed position.
2. Broadside-null in the radiation pattern is observed for the second frequency independent of the feed position with cross polarization of -10dB at the 3<sup>rd</sup> feed position.



3. Broadside radiation pattern is observed for the third frequency independent of the feed position with a cross polarization of -9 dB at the 3<sup>rd</sup> feed position.

### Azimuth Plane Patterns

For the 3<sup>rd</sup> feed position the radiation patterns for first and second frequencies are almost omnidirectional but not so good for the third frequency.

#### (vi) 3D Radiation pattern

The 3D radiation pattern drawn using Ansoft HFSS at the optimum feed position (feed position 3) for frequencies 1.89GHz, 2.56 GHz and 3.21 GHz are shown in **Figs. 5.14 (a)-(c)** respectively. **Figs. 5.14 (a) and (c)** shows broadside radiation pattern while **Figs. 5.14 (b)** shows a broadside null pattern. This is in agreement with experimental results.

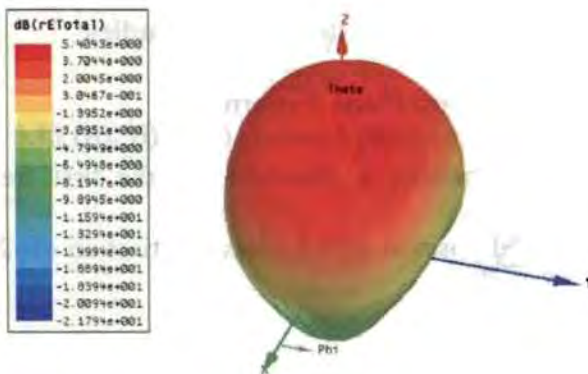


**Fig. 14 (a)** 3D radiation pattern for frequency 1.89 GHz

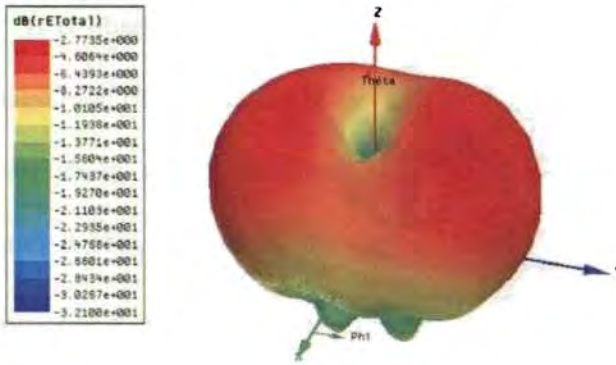


Fig. 14 (b) 3D radiation pattern for frequency 2.56 GHz

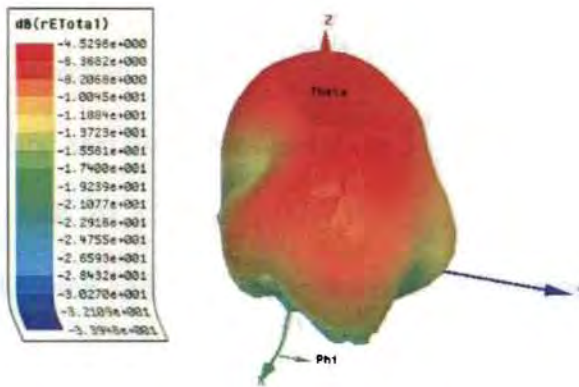
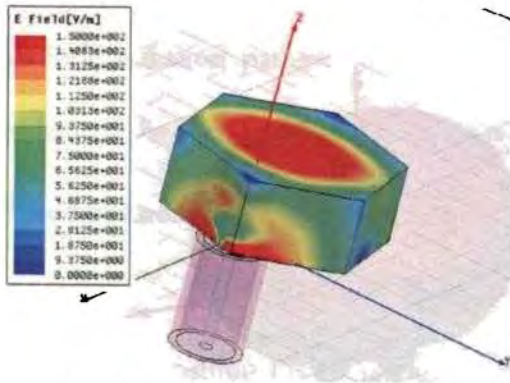


Fig. 14 (c) 3D radiation pattern for frequency 3.21 GHz

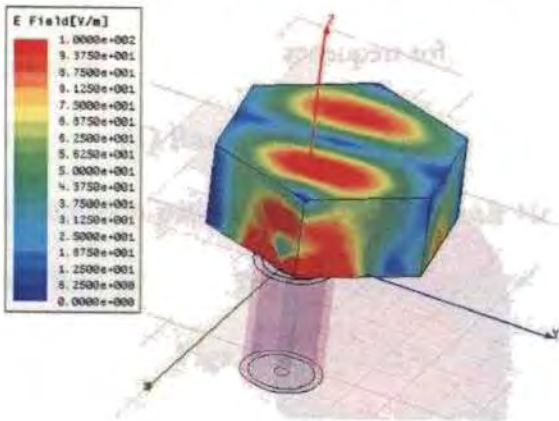
(vii) Mode analysis using HFSS simulation

**Magnitude of Electric field distribution**

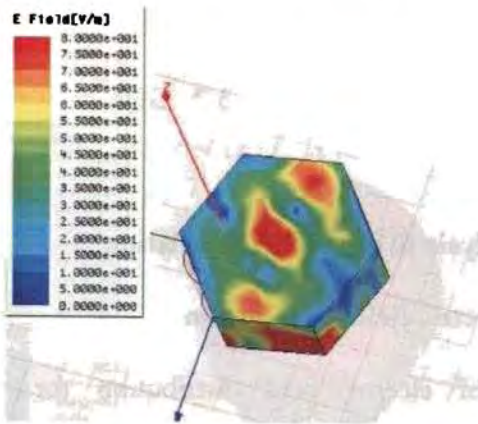
The magnitude of electric field distribution for the three frequencies at the optimum feed position is simulated using HFSS and are shown in Fig. 5.15 (a) - (c).



(a) 1.89 GHz  $HE_{118}$  mode



(b) 2.56 GHz  $HE_{128}$  mode



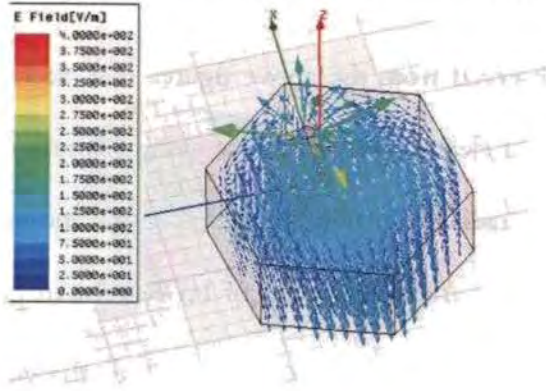
(c) 3.21 GHz  $HE_{138}$  mode

**Fig 5.15** (a)-(c) Magnitude of electric field distribution with the optimum feed position

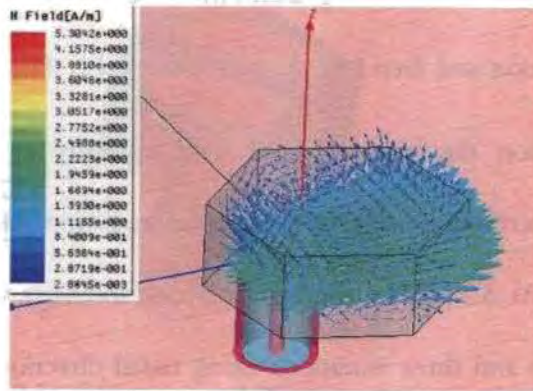
It is observed from the above figures that, at 1.89 GHz, there is one magnitude of electric field variations along azimuth direction and one variation along radial direction and hence the mode excited at this frequency is  $HE_{11\delta}$ . Also on the top of HDRA the magnitude of electric field intensity is maximum at the center and thus the radiation pattern at this frequency is broad sided. At the second frequency, 2.56 GHz, there is only one intensity variation along azimuth direction and two variations along radial direction and therefore the mode excited is  $HE_{12\delta}$ . Besides, in the radial direction the magnitude of field intensity at the center is minimum and therefore at this frequency the radiation pattern shows a broad side null. At 3.21 GHz, there is only one intensity variation along azimuth direction and three variations along radial direction and thus the mode excited is  $HE_{13\delta}$ . In addition, on the top of HDRA the magnitude of electric field intensity is maximum at the center and therefore the radiation pattern at this frequency is broad sided.

The E and H vector field on the top of HDRA for all the frequencies at the optimum field position are shown in **Figs. 5.16 (a)-(f)**. It is clear from Vector E patterns that, the modes excited at the three frequencies corresponds to 1.89 GHz, 2.56 GHz and 3.21GHz are  $HE_{11\delta}$ ,  $HE_{12\delta}$  and  $HE_{13\delta}$  modes respectively. These modes are confirmed from the literature [3]

*Experimental Study of Hexagonal Dielectric resonator antenna*

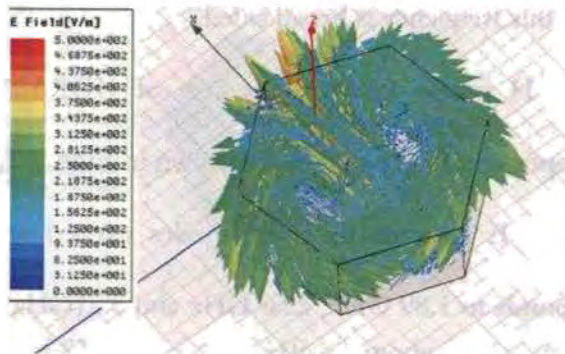


**(a) Vect-E (1.89GHz)**

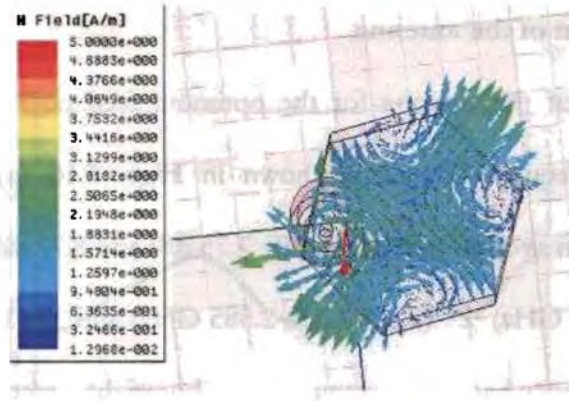


**(b) Vect-H (1.89GHz)**

Fig 5.15 (a) & (b) Vector- E and Vector- H variation for 1.89GHz (HE<sub>118</sub> mode)

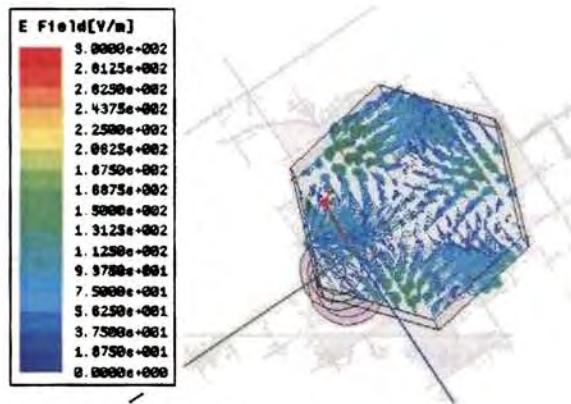


**(c) Vect-E (2.56 GHz)**

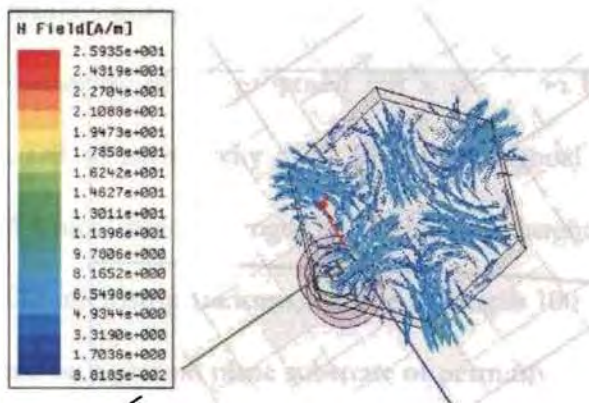


(d) Vect-H (2.56 GHz)

Fig 5.15 (c) & (d) Vector- E and Vector- H variation for 2.56GHz (HE<sub>128</sub> mode)



(e) Vect-E (3.21 GHz)

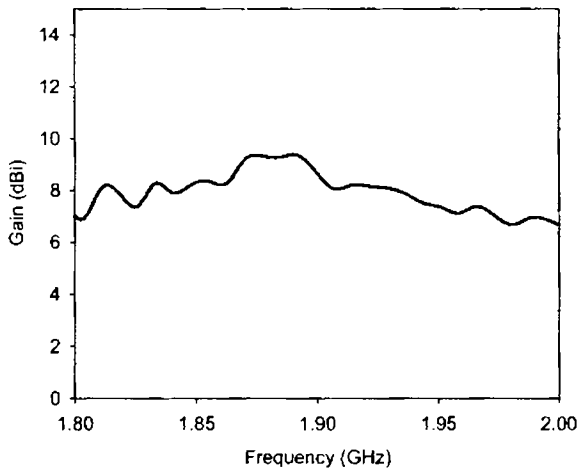


(f) Vect-H (3.21 GHz)

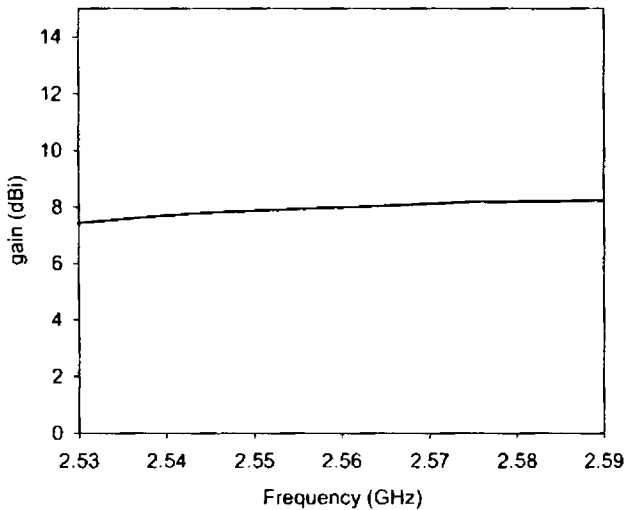
Fig 5.15 (e) & (f) Vector- E and Vector- H variation for 1.89GHz (HE<sub>138</sub> mode)

**(viii) Gain of the antenna**

The gain of the antenna for the optimum feed position for the three resonant frequency bands is shown in **Figs. 5.16 (a)-(c)**. The antenna exhibits an average gain of 6.9 dBi, 7.75 dBi and 8.72 dBi in the 1<sup>st</sup> (1.863 GHz-1.967 GHz), 2<sup>nd</sup> (2.535 GHz-2.585 GHz) and 3<sup>rd</sup> (3.220 GHz-3.280 GHz) frequency bands respectively in the boresight direction.



**(a)**



**(b)**

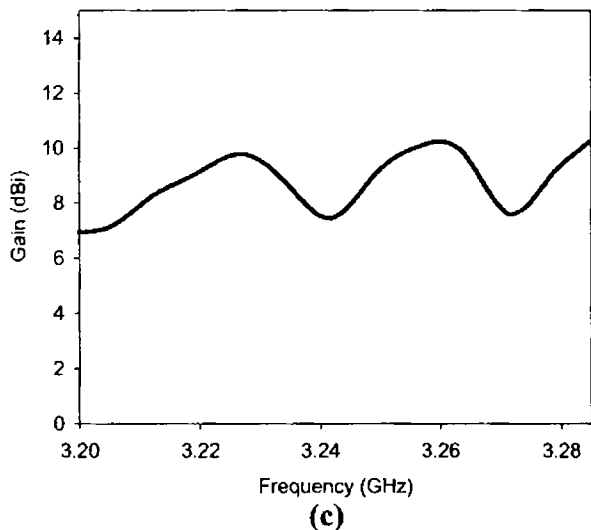


**Fig. 5.16** Gain of the antenna a) 1<sup>st</sup> Band b) 2<sup>nd</sup> Band c) 3<sup>rd</sup> Band

### **5.3 MICROSTRIP FED HDRA**

In this section a microstrip feed is used for exciting the HDR antenna and the corresponding characteristics are studied.

#### **5.3.1 Antenna Configuration**

The geometry of the proposed DR is shown in **Fig.5.17 (a)**. It consists of a DR of permittivity  $\epsilon_{r1} = 69$  with hexagonal geometry, side length  $a = 14.4$  mm, diagonal length  $b=30.4$ mm and height  $h = 11$  mm is fed with a  $50\Omega$  microstrip transmission line of length 100 mm and width 3mm, mounted on a ground plane substrate of permittivity  $\epsilon_{r2} = 4$  and size 140 mm x 110 mm x 1.64 mm.

#### **5.3.2 Effect of microstrip feed position on HDRA**



The schematic diagram of a microstrip fed HDRA is given in **Fig. 5.17 (b)**. For optimizing the feed the HDRA position is varied along x and y direction, where x and y are defined respectively as the vertical and horizontal distances from the strip line end to the DR as shown in **Fig. 5.17 (b)**.

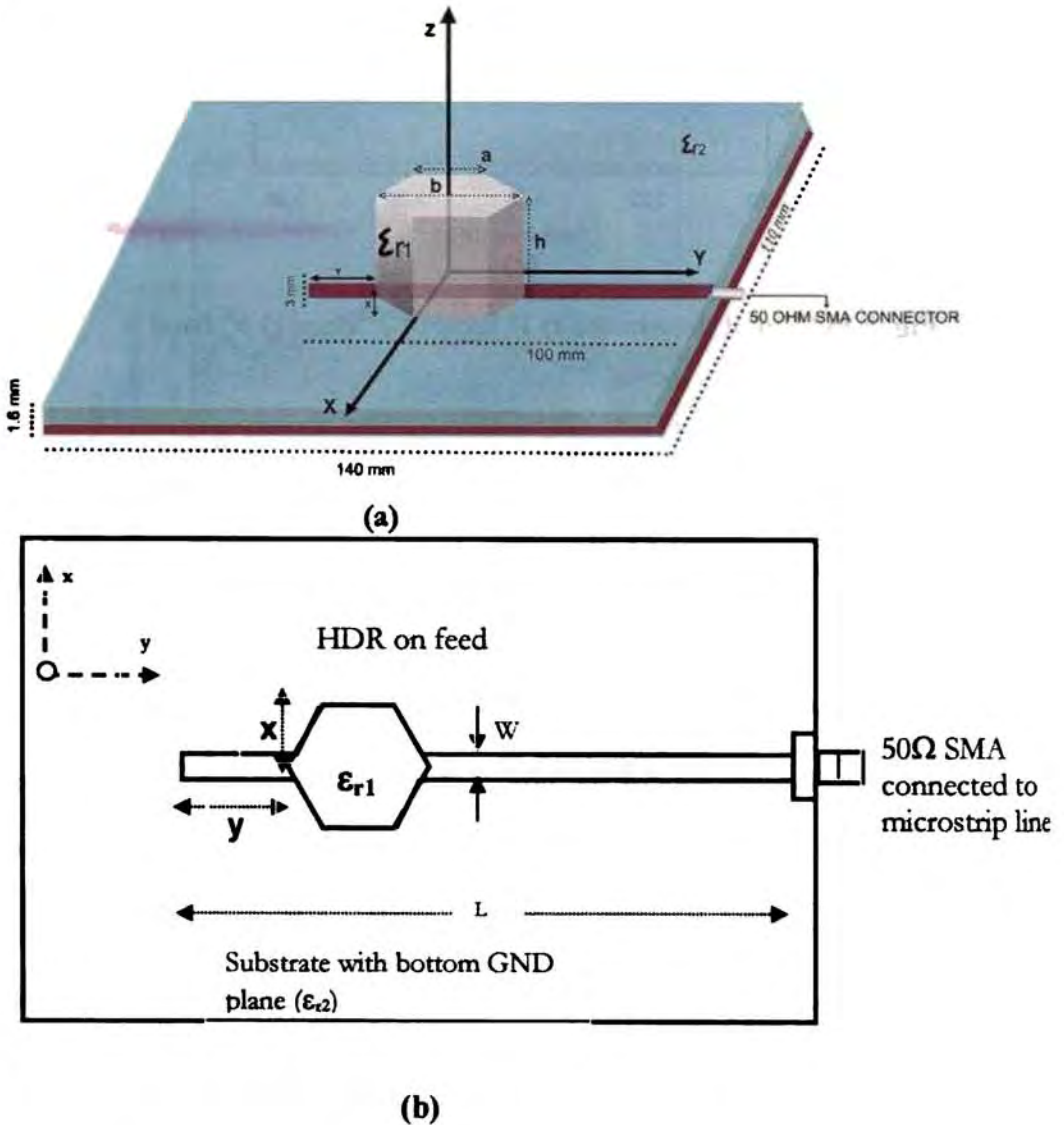
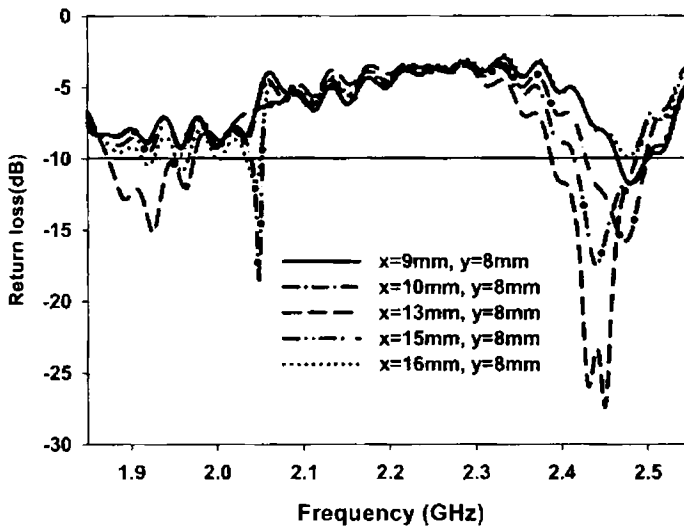


**Fig.5.17** Geometry of the Antenna (a) Hexagonal DR  
(b) Schematic sketch of the antenna

### 5.3.2 Results and discussion

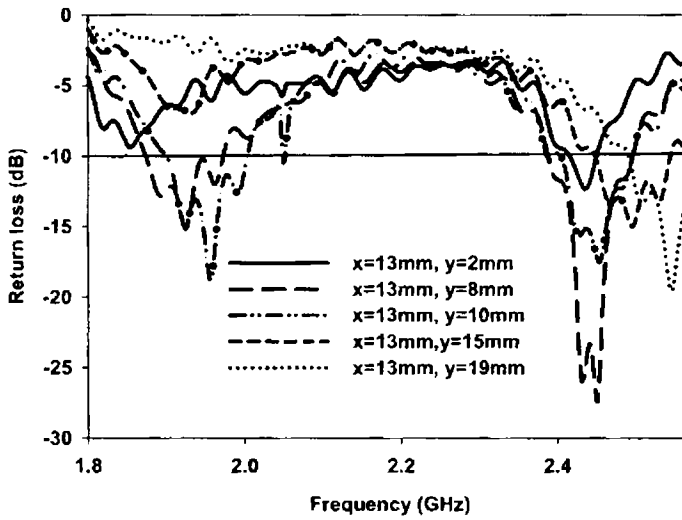
#### (i) Optimization on feed position

The experimental set up used for the measurement consists of an HP 8510 C Vector Network Analyzer as explained in chapter III. The variation of return loss  $|S_{11}|$  with position  $x$  and  $y$  is plotted in **Figs. 5.18 (a) and (b)**. It is observed that when the positions  $x$  and  $y$  are varied the nature of resonance frequency also varies from single resonance to dual resonance. The optimized feed position at  $x_0=13\text{mm}$  and  $y_0=8\text{mm}$  corresponds to a dual frequency operation. The HFSS simulated and measured return loss at the optimum position is compared in Fig. 5.18 (c).



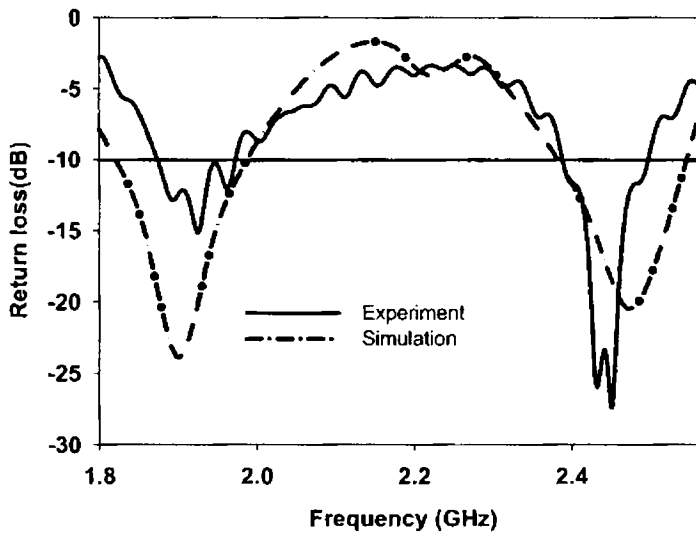
(a)

**Figs. 5.18 (a)** variation of return loss against frequency with the position 'x' by keeping position 'y' as constant



(b)

Figs. 5.18 (b) variation of return loss against frequency with position 'y' by keeping position 'x' as constant



Figs. 5.18 (c) Measured and simulated return loss at the optimized feed position

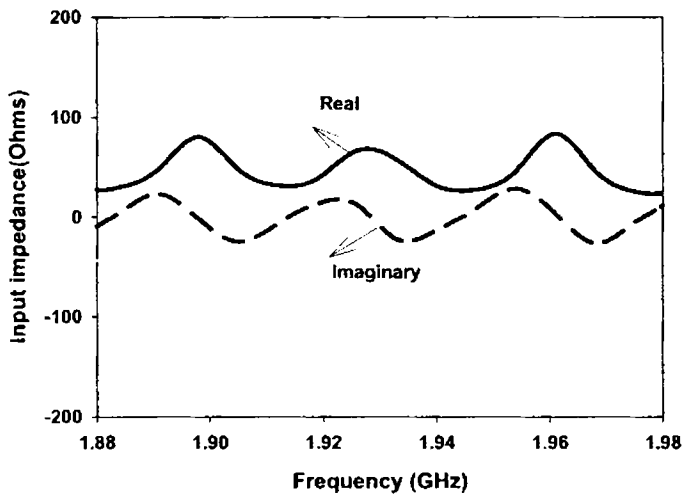
It is noted experimentally that the return loss is minimum at 1.926 GHz and 2.451 GHz. The antenna has a 2:1 SWR bandwidth of 5.2 % ranging from 1.875 GHz to 1.975 GHz and 4.2 % ranging from 2.395 to 2.5 GHz respectively. A comparison between the measured and simulated results is shown in **Table 5.6**. It is clear that there is an error of 1.4% and 0.78% for the first and second frequencies respectively and hence a good agreement between them was observed.

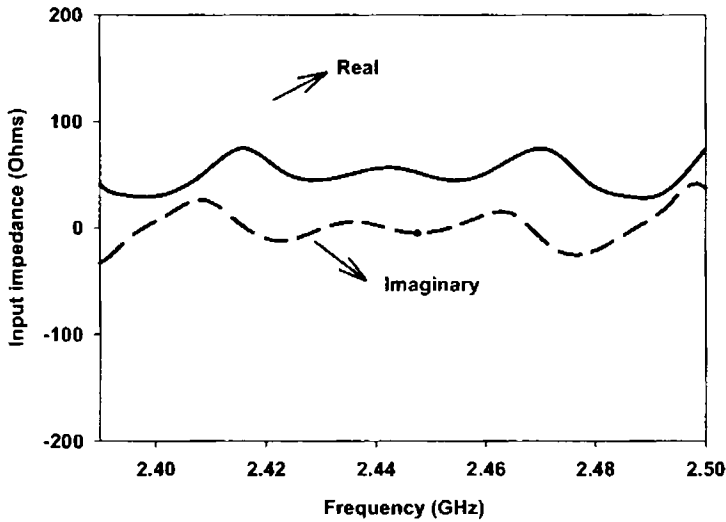
**Table 5.6** comparison of return loss obtained for simulated and measured values

Antenna Position		Experimental Frequency(GHz)		Simulation HFSS Frequency (GHz)		% error HFSS & Experiment	
X0	Y0	f1	f2	f1	f2	f1	f2
13mm	8mm	1.926	2.451	1.899	2.432	1.4	0.78

(ii) Input impedance

Measured input impedances, shown in **Fig.5.19 (a) and (b)** justifies good and steady matching between the feed and the antenna corresponding to the two frequency bands for the optimum feed position.





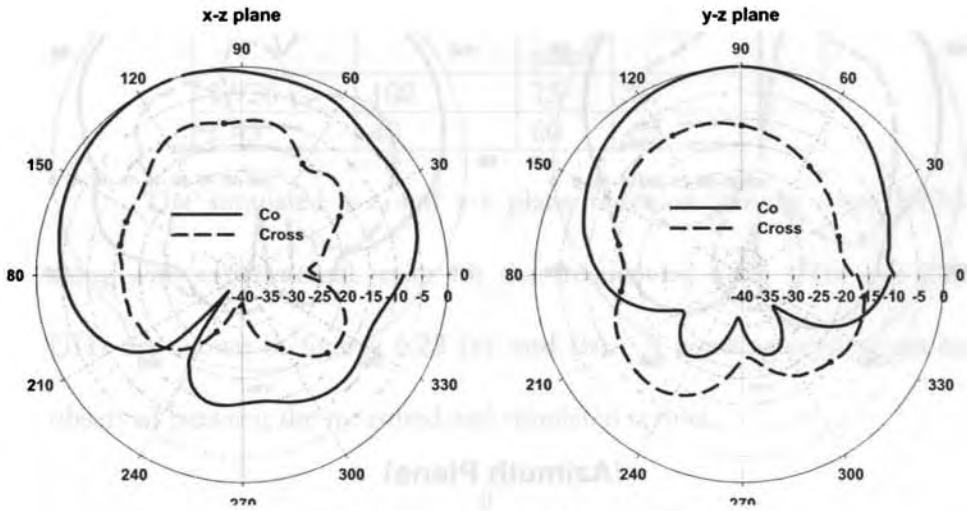
(b)

Fig.5.19 Measured Input Impedance corresponding to (a) I<sup>st</sup> band and (b) II<sup>nd</sup> band

(iii) Radiation Pattern

Measured radiation patterns at 1.926 GHz and 2.451 GHz are shown in Figs.5.20 and 5.21 respectively and are found to be linearly polarized. It is found from Fig. 5.20 that the elevation plane patterns (x-z and y-z plane) corresponds to the mode  $HE_{116}$  are broad with moderate cross-polar levels and the azimuth plane pattern (x-y plane) are also broad on either side. Whereas from Fig. 5.21, the elevation plane patterns (x-z and y-z plane) shows a dip at the on axis, which is due to the excitation of  $HE_{126}$  mode. The azimuth plane pattern (x-y plane) is observed to be omnidirectional. Radiation patterns at other frequencies in the band are also seen to have similar characteristics. The half power beam widths are shown in Table 5.7.

(Elevation Planes)



(Azimuth Plane)

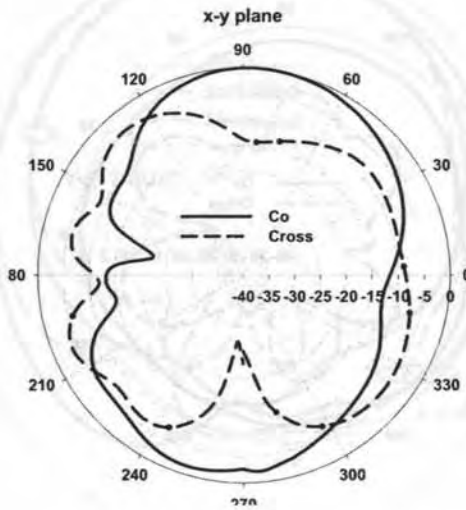
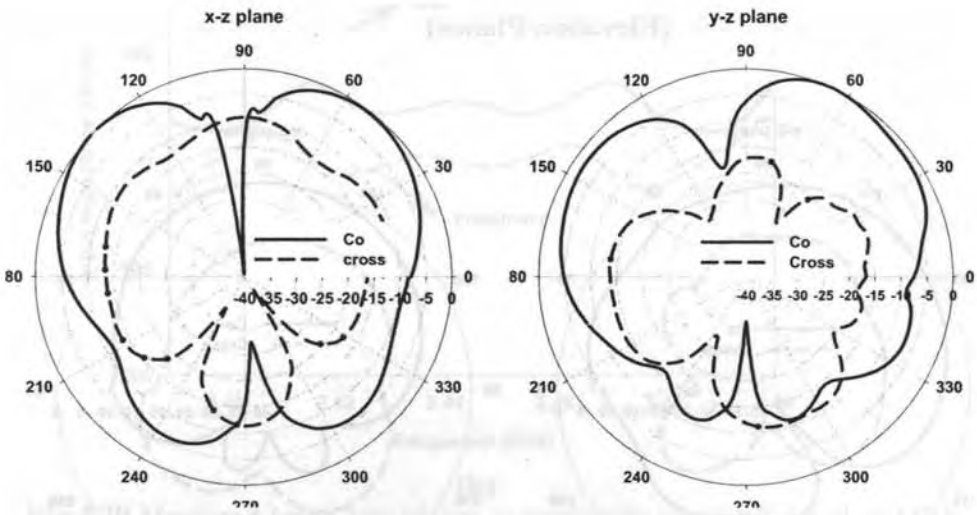


Fig. 5.20 Radiation patterns measured at 1.926 GHz

(Elevation Planes)



(Azimuth Plane)

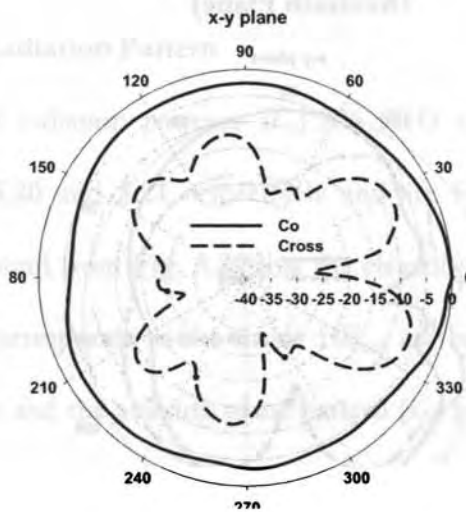
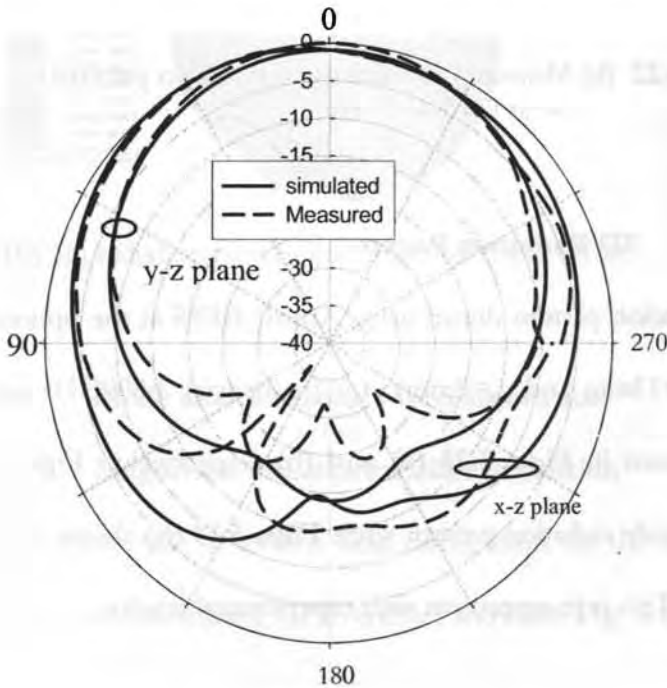


Fig. 5.2.6 Radiation patterns measured at 2.451 GHz

**Table 5.7.** The half power beam widths at the two frequencies

Frequency (GHz)	Half power beam widths		
	Elevation plane (degrees)		Azimuth plane
	x-z plane	y-z plane	x-y plane
1.926	100	75	70
2.45	40	60	60

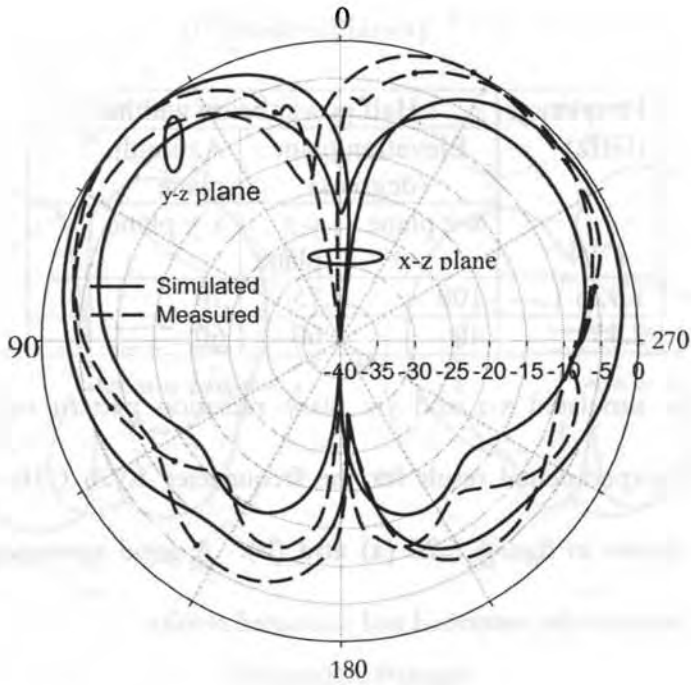
The simulated x-z and y-z plane radiation pattern using HFSS along with experimental result for the frequencies 1.926 GHz and 2.45 GHz are shown in figures 5.22 (a) and (b). A good agreement can be observed between the measured and simulated results.



(a)

Fig. 5.22 (a) Measured and simulated radiation patterns at  $f = 1.926\text{GHz}$ .





(b)

Fig. 5.22 (b) Measured and simulated radiation patterns at  $f = 2.451\text{GHz}$ .

#### (iv) 3D Radiation Pattern

The 3D radiation pattern drawn using Ansoft HFSS at the optimum feed position ( $x_0=13\text{mm}$  and  $y_0=8\text{mm}$ ) for frequencies 1.899GHz and 2.432 GHz are shown in **Figs. 5.23 (a) and (b)** respectively. **Figs. 5.13 (a)** shows broadside radiation pattern while **Figs. 5.14 (b)** shows a broadside null pattern. This is in agreement with experimental results.

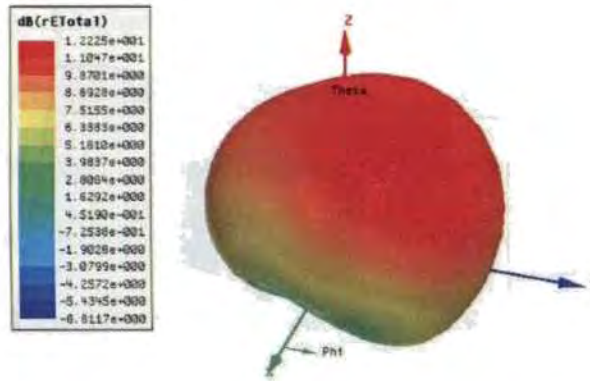


Fig. 23 (a) 3D radiation pattern for frequency 1.899 GHz

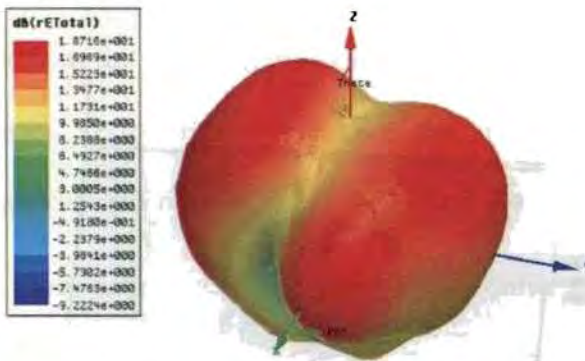
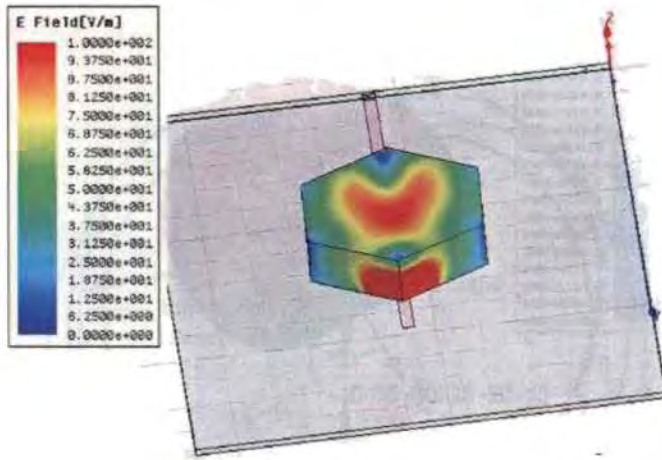


Fig. 23 (b) 3D radiation pattern for frequency 2.432 GHz

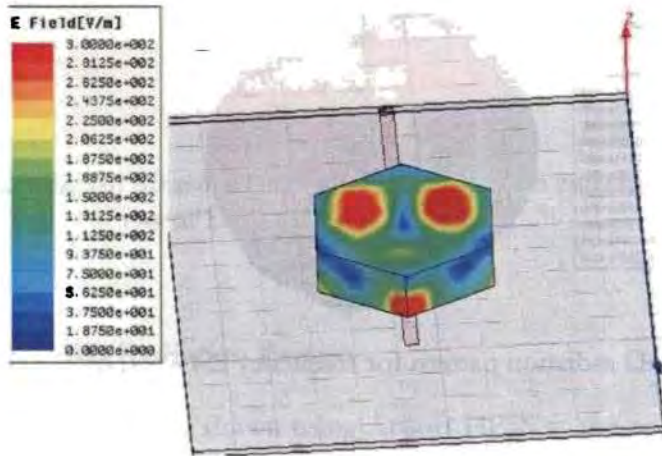
(v) Mode analysis using HFSS simulation

Magnitude of Electric field distribution

The magnitude of electric field distribution for the two resonant frequencies is simulated using HFSS and are shown in Fig. 5.23 (a) - (b).



(a) 1.899 GHz  $HE_{118}$  mode



(b) 2.432 GHz  $HE_{128}$  mode

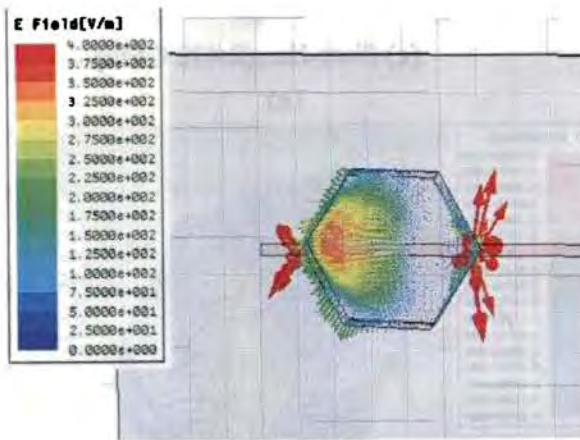
**Fig 5.23** (a)-(b) Magnitude of electric field distribution at the optimum position

It is observed from the above figures that, at 1.899 GHz, there is one magnitude of electric field variation along azimuth direction and one variation along radial direction and hence the mode excited at this frequency is  $HE_{118}$ . Also on the top of HDRA the magnitude of electric

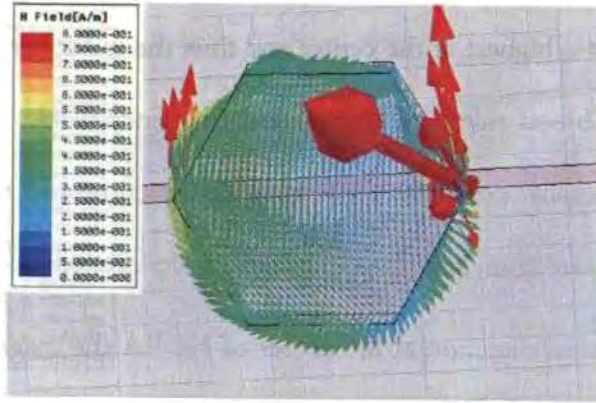
field intensity is highest at the center and thus the radiation pattern at this frequency is broad sided. At the second frequency, 2.432 GHz, there is only one intensity variation along azimuth direction and two variations along radial direction and therefore the mode excited is  $HE_{12\delta}$  mode. Besides on radial direction at the center of HDRA the magnitude of field intensity is minimum and thus at this frequency the radiation pattern shows a broad side null.

The E and H vector field on the top of HDRA for the two frequencies at the optimum position are shown in **Figs. 5.24 (a)-(d)**. It is clear from Vector E patterns that, the modes excited at the two frequencies corresponds to 1.899 GHz and 2.432 GHz are  $HE_{11\delta}$  and  $HE_{12\delta}$  mode respectively. These modes are confirmed from the literature

[3]

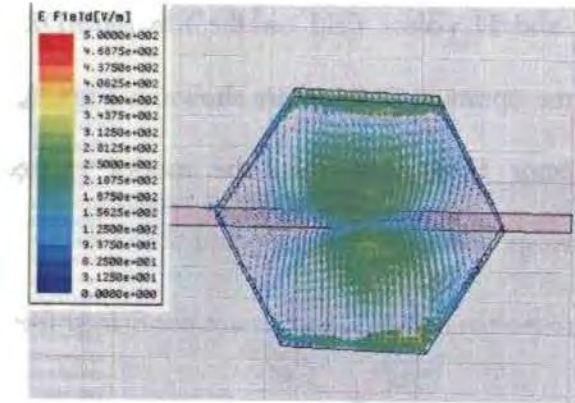


**(a) Vect-E (1.899 GHz)**

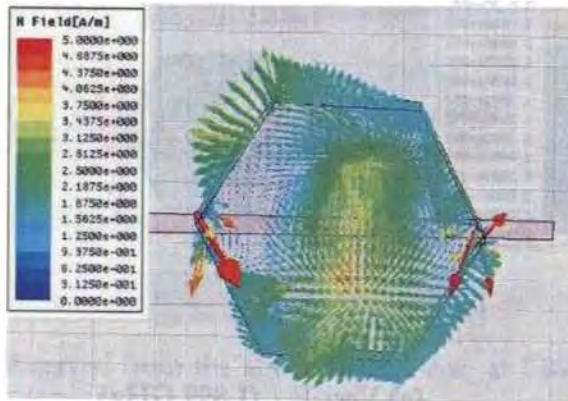


(b) Vect-H (1.899 GHz)

Fig 5.24 (a) & (b) Vector- E and Vector- H variation for 1.926GHz (HE<sub>11δ</sub> mode)



(c) Vect-E (2.432 GHz)

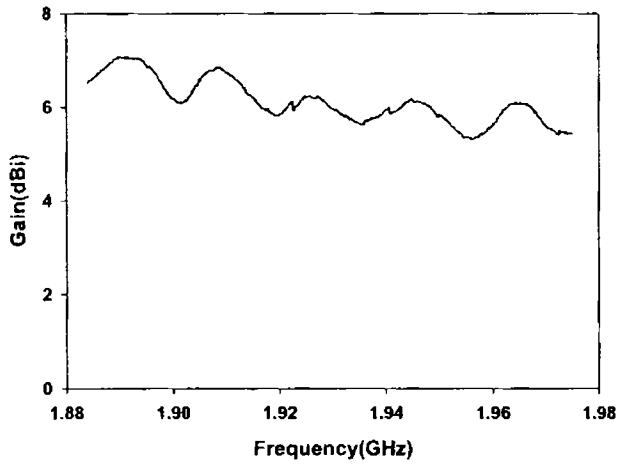


(d) Vect-H (2.432 GHz)

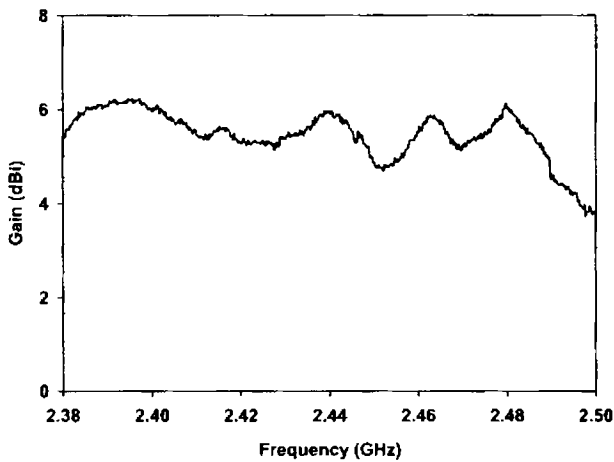
Fig 5.24 (c) & (d) Vector- E and Vector- H variation for 2.541GHz (HE<sub>12δ</sub> mode)

**(vi) Gain of the antenna**

The gain of the antenna is measured with respect to a standard circular patch antenna operating in the same resonant frequency (Gain transfer method). Measured gain at the I<sup>st</sup> and II<sup>nd</sup> bands are shown in **Figs. 5.25 (a) and (b)**. It is noted that the antenna offers an average gain of 6.1 dBi and 5.4 dBi respectively in the I<sup>st</sup> and II<sup>nd</sup> bands in the boresight direction.



**(a)**



**(b)**

**Fig. 5.25** Measured antenna gain at **(a)** I<sup>st</sup> band **(b)** II<sup>nd</sup> band

#### 5.4 Radiation efficiency of the HDRA

Efficiency of the antenna is defined theoretically as

$$\eta = P_{\text{rad}} / (P_{\text{rad}} + P_{\text{diss}})$$

Where  $P_{\text{rad}}$  is the total radiated power and  $P_{\text{diss}}$  is the power dissipated in the antenna structure.

The efficiency of the coaxial fed HDRA is calculated using HFSS and is found to be 93.34%, 90.41 % and 86.6 % respectively for 1.89 GHz, 2.56 GHz and 3.21 GHz. For microstrip fed HDRA, efficiency is found to be 98.3 % for the first resonant frequency of 1.926GHz and 97.19% for the second resonant frequency of 2.451 GHz.

#### 5.5 Comparison of antenna performance between HDRA and conventional Cylindrical DRA

Diagonal length of HDRA = Diameter of CDRA		
	HDRA	CDRA
1. Resonance	Multiple	Single
2. Pattern	Broadside, conical	Broadside, conical
3. Mode of excitation	HE <sub>118</sub> , HE <sub>128</sub> , HE <sub>138</sub> , TM <sub>018</sub>	HE <sub>118</sub> , TM <sub>018</sub>
4. Miniaturisation	High	Low

#### 5.6 Conclusion

This chapter discussed the experimental studies on a novel dielectric resonator antenna with hexagonal geometry. In the first section the characteristics of the antenna when excited with coaxial probe feed is described. The antenna performance is optimized for the probe length,

HDRA aspect ratio and probe feed location. All the characteristics of the HDRA are studied. It is observed that the antenna exhibits a maximum of three resonant frequencies with good gain and moderate bandwidth. The radiation pattern is observed to be broad and conical at different frequencies. A comparison with the simulated results using HFSS is also done and the results are discussed. Mode analysis is done by sketching the field distribution on HDRA using HFSS. The antenna exhibits good gain with the coaxial feed excitation.

In last section, the antenna is excited with microstrip feed and optimised for a position corresponds to dual frequency with good gain. It is observed that the dual frequency viz. 1.92 GHz and 2.451 GHz finds application in wireless communication. The first band covers the digital cordless Telephones (**DCT: 1.88GHz to 1.92 GHz**) band and almost all frequencies of personal communication systems (**PCS: 1.85 GHz to 1.99 GHz**). The second band covers the wireless local area network (**WLAN: 2.4 GHz to 2.484 GHz**) band. The antenna exhibits good gain, even though less than that of coaxial feed excitation. This antenna is unique in the sense that it is capable of producing multiple frequencies with a single feed, without using any hybrid structure [4-7]. A comparison between experimental and simulated results is included and discussed. Mode analysis is performed using HFSS on the basis of the field distribution on HDRA. The efficiency of the antenna is found to be around 98% for



microstrip feed and it vary from 86-94 % for the coaxial feed HDRA for different operating frequencies.

## **References**

1. A.A. Kishk, Yan Yin and A.W. Glisson, Conical dielectric resonator antenna for wideband applications, *IEEE Trans. Antennas Propagat.*, vol. 50, pp. 469-474, April 2002.
2. Darko Kajfez and A. A. Kishk, Dielectric Resonator Antenna-Possible Candidate For Adaptive Antenna Arrays, *Proceedings VITEL 2002, International Symposium on Telecommunications, Next Generation Networks and Beyond, Portoroz, Slovenia, May 13-14, 2002.*
3. Darko Kajfez, A.W. Glisson and Joseph James, Computed Modal Field Distributions for Isolated Dielectric Resonators, *IEEE Transactions on Microwave Theory and Techniques, Vol.MTT-32*, pp. 1609-1616, 1984l.
4. Tayeb A. Denidni, and Qinjiang Rao, Hybrid Dielectric Resonator Antennas With Radiating Slot for Dual-Frequency Operation, *IEEE Antennas and wireless propagation letters*, Vol. 3, pp. 321-323, 2004.
5. Sung, C. S. Ahn, and Y.-S. Kim, Microstripline fed dual frequency dielectric resonator antenna, *Microwave and optical technology letters*, Vol. 42, No. 5, pp. 388-390, 2004
6. Z.Fan and Y.M.M. Antar, Slot coupled DR antennas for dual frequency operation, *IEEE transactions on antennas and propagation*,Vol. 45, No. 2, pp. 306-308, 1997.
7. Qinjiang Rao, Tayeb A. Denidni, and abdel R. sebak, Hybrid Resonator Antenna suitable for wireless communication applications at 1.9 and 2.45GHz, *IEEE Antennas and wireless propagation letters*, Vol. 4, pp. 341-343, 2005.

**6.1 Introduction**

Maxwell's partial differential equations of electrodynamics represent a fundamental unification of electric and magnetic fields predicting electromagnetic wave phenomena which Nobel Laureate Richard Feynman has called the most outstanding achievement of 19<sup>th</sup> century science. Now engineers and scientists worldwide use computers of high configuration to obtain the solutions of these equations for the purpose of investigating electromagnetic wave guiding, radiation, scattering phenomena and technologies. Today, in the beginning of 21<sup>st</sup> century, it may seem a little odd to devote so much effort in solving the 19<sup>th</sup> century equations.

During the 1970 and 1980's several scientists working in these areas found the limitations of frequency domain integral equation solutions of Maxwell's equations. This led to a novel alternative approach: Finite Difference Time Domain (FDTD) method, introduced by Yee in 1966 [1, 2], was the first direct time domain solutions of Maxwell's differential (curl) equations on special grids or lattices. There are several reasons for the considerable interest in FDTD and related computational solution approaches of Maxwell's equations.

1. FDTD uses no linear algebra
2. FDTD is accurate and robust

3. FDTD treats impulsive behavior naturally
4. FDTD treats non linear behavior naturally
5. FDTD is a systematic approach
6. Computer memory capacities are increasing rapidly
7. Computer visualization capabilities are increasing rapidly

The classic Yee Finite-Difference Time-Domain (FDTD) algorithm employs standard central-differences to approximate both the spatial and temporal derivatives of the governing equations. For electromagnetic problems, Maxwell's coupled differential equations are approximated as coupled finite difference equations. The finite-difference equations are solved for the future fields in terms of known past fields. The coupled equations are then alternately solved to advance the fields in the time-domain. A simulation is obtained by marching the fields forward in time. However, because of the approximations inherent in the FDTD equations, fields accumulate errors as they propagate. The amount of error is dependent on the direction of propagation and the frequency, i.e., the error is both anisotropic and dispersive. Given unlimited computer resources, any desired model fidelity could be obtained. Because of memory and other computer limitations, one often cannot simply increase the discretization to achieve an acceptable level of error. Instead, a different FDTD algorithm can be employed which has superior error characteristics. Several such algorithms have been proposed in the

electromagnetic literature and a survey of many of the more promising ones can be found in [3].

**6.2 Electromagnetic analysis**

The FDTD technique is a computationally efficient means of directly solving Maxwell’s time dependent curl equations using finite difference technique. In this extensively computer based numerical method, the continuous distribution of electromagnetic fields in a finite volume of space is sampled at distinct points in a space and time lattice. The FDTD method is formulated by discretizing Maxwell's curl equations over a finite volume and approximating the derivatives with centered difference approximations. Conducting surfaces are treated by setting tangential electric field components to zero. The walls of the mesh, however, require special treatment to prevent reflections from the mesh termination.

**6.2.1 Governing Equations**

Formulation of the FDTD method begins by considering the differential form of Maxwell's two curl equations, which govern the propagation of fields in the structures. For simplicity, the media are assumed to be piecewise uniform, isotropic, and homogeneous. The structure is assumed to be loss less (i.e., no volume currents or finite Conductivity). With these assumptions, Maxwell's curl equations may be

written as  $\mu \frac{\partial H}{\partial t} = -\nabla \times E$  ----- (6.1)

$$\epsilon \frac{\partial E}{\partial t} = \nabla \times H$$
 ----- (6.2)

In order to find an approximate solution to this set of equations, the problem is discretized over a finite three-dimensional computational domain with appropriate boundary conditions enforced on the source, conductors, and mesh walls.

### **6.2.2 Finite-Difference Equations**

To obtain discrete approximations to these continuous partial differential equations the centered difference approximation is used on both the time and space first-order partial differentiations. For convenience, the six field locations are considered to be interleaved in space as shown in **Fig. 6.1**, which is a drawing of the FDTD unit cell [1]. The entire computational domain is obtained by stacking these rectangular cubes into a larger rectangular volume. The x, y, and z dimensions of the unit cell are  $\Delta x$ ,  $\Delta y$ , and  $\Delta z$  respectively. The advantages of this field arrangement are that centered differences are realized in the calculation of each field component and that continuity of tangential field components is automatically satisfied. Because there are only six unique field components within the unit cell, the six field components touching the shaded upper eighth of the unit cell in **Fig. 6.1** are considered to be a unit node with subscript indices  $i, j$  and  $k$  corresponding to the node numbers in the x, y, and z directions.

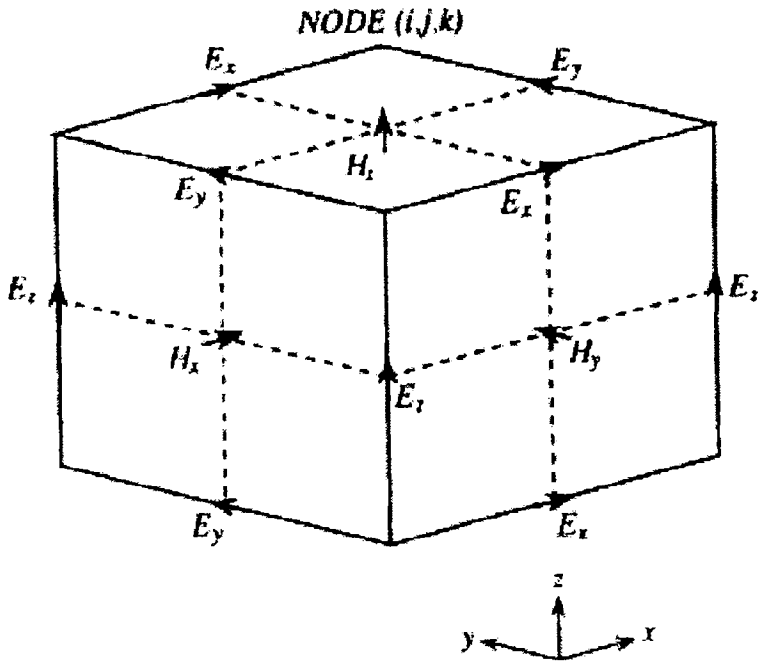


**Fig. 6.1** Field component placement in the FDTD unit cell

This notation implicitly assumes the  $\pm 1/2$  space indices and thus simplifies the notation, rendering the formulas directly implementable on the computer. The time steps are indicated with the superscript  $n$ . using this field component arrangement, the above notation, and the centered difference approximation, the explicit finite difference approximations to (6.1) and (6.2) are

$$Hx_{i,j,k}^{n+1/2} = Hx_{i,j,k}^{n-1/2} + \frac{\Delta t}{\mu \Delta z} (Ey_{i,j,k}^n - Ey_{i,j,k-1}^n) - \frac{\Delta t}{\mu \Delta y} (Ez_{i,j,k}^n - Ez_{i,j-1,k}^n) \text{-----} (6.3.1)$$

$$Hy_{i,j,k}^{n+1/2} = Hy_{i,j,k}^{n-1/2} + \frac{\Delta t}{\mu \Delta x} (Ez_{i,j,k}^n - Ez_{i-1,j,k}^n) - \frac{\Delta t}{\mu \Delta z} (Ex_{i,j,k}^n - Ex_{i,j,k-1}^n) \text{-----} (6.3.2)$$

$$Hz_{i,j,k}^{n+1/2} = Hz_{i,j,k}^{n-1/2} + \frac{\Delta t}{\mu \Delta y} (Ex_{i,j,k}^n - Ex_{i,j-1,k}^n) - \frac{\Delta t}{\mu \Delta x} (Ey_{i,j,k}^n - Ey_{i-1,j,k}^n) \text{-----} (6.3.3)$$

$$Ex_{i,j,k}^{n+1} = Ex_{i,j,k}^n + \frac{\Delta t}{\epsilon \Delta y} (Hz_{i,j+1,k}^{n+1/2} - Hz_{i,j,k}^{n+1/2}) - \frac{\Delta t}{\epsilon \Delta z} (Hy_{i,j,k+1}^{n+1/2} - Hy_{i,j,k}^{n+1/2}) \text{-----} (6.3.4) \text{---} (6.3)$$

$$Ey_{i,j,k}^{n+1} = Ey_{i,j,k}^n + \frac{\Delta t}{\epsilon \Delta z} (Hx_{i,j,k+1}^{n+1/2} - Hx_{i,j,k}^{n+1/2}) - \frac{\Delta t}{\epsilon \Delta x} (Hz_{i+1,j,k}^{n+1/2} - Hz_{i,j,k}^{n+1/2}) \text{-----} (6.3.5)$$

$$Ez_{i,j,k}^{n+1} = Ez_{i,j,k}^n + \frac{\Delta t}{\epsilon \Delta x} (Hy_{i,j+1,k}^{n+1/2} - Hy_{i,j,k}^{n+1/2}) - \frac{\Delta t}{\epsilon \Delta y} (Hx_{i,j+1,k}^{n+1/2} - Hx_{i,j,k}^{n+1/2}) \text{-----} (6.3.6)$$

The half time steps indicate that  $E$  and  $H$  are alternately calculated in order to achieve centered differences for the time derivatives. In these equations, the permittivity and the permeability are set to the appropriate values depending on the location of each field component. For the electric field components on the dielectric-air interface the average of the two permittivity,  $(\epsilon_1 + \epsilon_2)/2$ , is used. The validity of this treatment is explained in [4]. Due to the use of centered differences in these approximations, the error is second order in both the space and time steps; i.e., if  $\Delta x$ ,  $\Delta y$ ,  $\Delta z$ , and  $\Delta t$  are proportional to  $\Delta l$ , then the global error is  $O(\Delta l^2)$  [5]. The maximum time step that may be used is limited by the Courant stability restriction of the finite difference equations,

$$\Delta t \leq \frac{1}{v_{\max}} \left( \frac{1}{\Delta x^2} + \frac{1}{\Delta y^2} + \frac{1}{\Delta z^2} \right)^{-1/2} \text{-----} (6.4)$$

Where  $V_{max}$ , is the maximum velocity of light in the computational volume. Typically,  $V_{max}$  will be the velocity of light in free space unless the entire volume is filled with dielectric. These equations will allow the approximate solution of  $E(r, t)$  and  $H(r, t)$  in the volume of the computational domain or mesh; however, special consideration is required for the source, the conductors, and the mesh walls.

**6.2.3 Normalised Maxwell's equations**

This thesis uses the normalized general form of field variables, as used by Sullivan [6], for the simplicity of formulation.

$$\bar{E} = E / \eta \text{-----} (6.5)$$

$$\text{where...}\eta = \sqrt{\frac{\mu_0}{\epsilon_0}}$$

The normalised Maxwell's curl equations are

$$\frac{\partial \bar{D}}{\partial t} = \frac{1}{\sqrt{\epsilon_0 \mu_0}} \nabla \times \bar{H} \text{-----} (6.6)$$

$$\bar{D}(w) = \epsilon_r^*(w) \cdot \bar{E}(w) \text{-----} (6.7)$$

$$\frac{\partial \bar{H}}{\partial t} = -\frac{1}{\sqrt{\epsilon_0 \mu_0}} \nabla \times \bar{E} \text{-----} (6.8)$$

Normalisation is used for the field variables having the same order of magnitude, which is an advantage in formulating Perfect Matched Layer (PML), which is the crucial part of FDTD.



The above equations produce six scalar equations. All field variables  $D_x$ ,  $D_y$ ,  $D_z$  and  $H_x$ ,  $H_y$ ,  $H_z$  are normalized and we are eliminating dash symbol present in the field components of equation 6.6 and 6.8.

$$\frac{\partial D_x}{\partial t} = \frac{1}{\sqrt{\epsilon_0 \mu_0}} \left( \frac{\partial H_z}{\partial y} - \frac{\partial H_y}{\partial z} \right) \text{-----} (6.9.1)$$

$$\frac{\partial D_y}{\partial t} = \frac{1}{\sqrt{\epsilon_0 \mu_0}} \left( \frac{\partial H_x}{\partial z} - \frac{\partial H_z}{\partial x} \right) \text{-----} (6.9.2)$$

$$\frac{\partial D_z}{\partial t} = \frac{1}{\sqrt{\epsilon_0 \mu_0}} \left( \frac{\partial H_y}{\partial x} - \frac{\partial H_x}{\partial y} \right) \text{-----} (6.9.3) - (6.9)$$

$$\frac{\partial H_x}{\partial t} = \frac{1}{\sqrt{\epsilon_0 \mu_0}} \left( \frac{\partial E_y}{\partial z} - \frac{\partial E_z}{\partial y} \right) \text{-----} (6.9.4)$$

$$\frac{\partial H_y}{\partial t} = \frac{1}{\sqrt{\epsilon_0 \mu_0}} \left( \frac{\partial E_z}{\partial x} - \frac{\partial E_x}{\partial z} \right) \text{-----} (6.9.5)$$

$$\frac{\partial H_z}{\partial t} = \frac{1}{\sqrt{\epsilon_0 \mu_0}} \left( \frac{\partial E_x}{\partial y} - \frac{\partial E_y}{\partial x} \right) \text{-----} (6.9.6)$$

Discretizing the equations 6.9.3 and 6.9.6, ie for  $D_z$  and  $H_z$  is

$$D_{z,i,j,k+1/2}^{n+1/2} = D_{z,i,j,k+1/2}^{n-1/2} + \frac{\Delta t}{\sqrt{\mu_0 \epsilon_0} \Delta x} \{ H_{y,i+1/2,j,k+1/2}^n - H_{y,i-1/2,j,k+1/2}^n - H_{x,i,j+1/2,k+1/2}^n + H_{x,i,j-1/2,k+1/2}^n \} \text{-----} (6.10)$$

$$H_{z,i+1/2,j+1/2,k}^{n+1} = H_{z,i+1/2,j+1/2,k}^n - \frac{\Delta t}{\sqrt{\mu_0 \epsilon_0} \Delta x} \{ E_{y,i+1,j+1/2,k}^{n+1/2} - E_{y,i,j+1/2,k}^{n+1/2} - E_{x,i+1/2,j+1,k}^{n+1/2} + E_{x,i+1/2,j,k}^{n+1/2} \} \text{-----} (6.11)$$

Similarly we can write all the other difference equation also. From the above difference equation the computer code for all the six fields can be written as

$$dx(i,j,k) = dx(i,j,k) + 0.5 * (hz(i,j,k) - hz(i,j-1,k) - hy(i,j,k) + hy(i,j,k-1)); \text{-----} \quad (6.12.1)$$

$$dy(i,j,k) = dy(i,j,k) + 0.5 * (hx(i,j,k) - hx(i,j,k-1) - hz(i,j,k) + hz(i-1,j,k)); \text{-----} \quad (6.12.2)$$

$$dz(i,j,k) = dz(i,j,k) + 0.5 * (hy(i,j,k) - hy(i-1,j,k) - hx(i,j,k) + hx(i,j-1,k)); \text{-----} \quad (6.12.3)$$

$$ex(i,j,k) = gax(i,j,k) * dx(i,j,k); \text{-----} \quad (6.12.4)$$

$$ey(i,j,k) = gay(i,j,k) * dy(i,j,k); \text{-----} \quad (6.12.5) \quad \text{-----} \quad (6.12)$$

$$ez(i,j,k) = gaz(i,j,k) * dz(i,j,k); \text{-----} \quad (6.12.6)$$

$$hx(i,j,k) = hx(i,j,k) + 0.5 * (ey(i,j,k+1) - ey(i,j,k) - ez(i,j+1,k) + ez(i,j,k)); \text{-----} \quad (6.12.7)$$

$$hy(i,j,k) = hy(i,j,k) + 0.5 * (ez(i+1,j,k) - ez(i,j,k) - ex(i,j,k+1) + ex(i,j,k)); \text{-----} \quad (6.12.8)$$

$$hz(i,j,k) = hz(i,j,k) + 0.5 * (ex(i,j+1,k) - ex(i,j,k) - ey(i+1,j,k) + ey(i,j,k)); \text{-----} \quad (6.12.9)$$

Since the term =  $\frac{\Delta t}{\sqrt{\mu_0 \epsilon_0} \Delta x} = 0.5$

Where

$$gax(i,j,k) = gay(i,j,k) = gaz(i,j,k) = \frac{1}{\epsilon_r + \sigma dt / \epsilon_0} \text{---} \quad (6.13)$$

for free space its value is unity.

### 6.2.4 The Perfect Matched Layer (PML)

One of the most flexible and efficient Absorbing Boundary Conditions (ABCs) is the perfectly matched layer developed by Berenger [7]. The basic idea is, if a wave is propagating in medium A and it impinges upon medium B, the amount of reflection is dictated by the intrinsic impedances of the two media

$$\Gamma = \frac{\eta_A - \eta_B}{\eta_A + \eta_B} \text{-----} (6.14)$$

Which are determined by dielectric constant  $\epsilon$  and permeability  $\mu$  of the two media

$$\eta = \sqrt{\frac{\mu}{\epsilon}} \text{-----} (6.15)$$

When one of the medium parameter is a constant and the other changes, then there is a change in impedance and hence a portion of the wave reflected back. When  $\mu$  changes with  $\epsilon$ , then  $\eta$  remains constant and the reflection coefficient  $\Gamma$  become zero and no reflection will occur. But the pulse is continuously moving to new medium again the same problem occur and hence we want a medium that is lossy so that the pulse will die out before it hits the boundary. This is accomplished by making both  $\epsilon$  and  $\mu$  complex, because the imaginary part represents the part that causes decay.

Convert the Maxwell's equations to Fourier domain, then the two dimensional equations (eqn. 6.6, 6.7 and 6.8) becomes

$$j\omega Dz = C_0 \left( \frac{\partial Hy}{\partial x} - \frac{\partial Hx}{\partial y} \right) \text{-----} (6.16)$$

$$Dz(w) = \epsilon_r^*(w).Ez(w) \text{-----} (6.17)$$

$$j\omega Hx = -C_0 \frac{\partial Ez}{\partial y} \text{-----} (6.18)$$

$$j\omega Hy = C_0 \frac{\partial Ez}{\partial x} \text{-----} (6.19)$$

We are adding fictitious dielectric constants and permeability's [8]

$$\epsilon_{Fz}^*, \mu_{Fx}^*, \text{ and } \mu_{Fy}^*$$

Then the above equations become

$$j\omega Dz. \epsilon_{Fz}^*(x). \epsilon_{Fz}^*(y) = C_0 \left( \frac{\partial Hy}{\partial x} - \frac{\partial Hx}{\partial y} \right) \text{-----} (6.20)$$

$$Dz(w) = \epsilon_r^*(w).Ez(w) \text{-----} (6.21)$$

$$j\omega Hx. \mu_{Fx}^*(x). \mu_{Fx}^*(y) = -C_0 \frac{\partial Ez}{\partial y} \text{-----} (6.22)$$

$$j\omega Hy. \mu_{Fy}^*(x). \mu_{Fy}^*(y) = C_0 \frac{\partial Ez}{\partial x} \text{-----} (6.23)$$

There are two conditions to form a PML

1. The impedance going from the background medium to the PMI,

must be constant,

$$\eta_0 = \eta_m = \sqrt{\frac{\mu_{Fx}^*}{\epsilon_{Fx}^*}} = 1 \text{-----} (6.24)$$

the impedance is 1 because of our normalized units.

2. In the direction perpendicular to the boundary, the relative dielectric constant and relative permeability must be the inverse of those in the other direction. i.e

$$\left( \begin{array}{l} \epsilon_{Fx}^* = \frac{1}{\epsilon_{Fy}^*} \\ \mu_{Fx}^* = \frac{1}{\mu_{Fy}^*} \end{array} \right) \text{-----} (6.25)$$

Assume that each of these is a complex quantity of the form

$$\epsilon_{Fm}^* = \epsilon_{Fm} + \frac{\sigma_m}{j\omega\epsilon_0} \text{ for, } m = x \text{ or } y \text{-----} (6.26)$$

$$\mu_{Fm}^* = \mu_{Fm} + \frac{\sigma_m}{j\omega\epsilon_0} \text{ for, } m = x \text{ or } y \text{-----} (6.27)$$

The following selection of parameters satisfies the above eqn.[9]

$$\left\{ \begin{array}{l} \epsilon_{Fm} = \mu_{Fm} = 1 \\ \frac{\sigma_{Dm}}{\epsilon_0} = \frac{\sigma_{Hm}}{\mu_0} = \frac{\sigma_D}{\epsilon_0} \end{array} \right\} \text{-----} (6.28)$$

Substituting these values to the equation 6.24 for impedance is

$$\eta_0 = \eta_m = \sqrt{\frac{\mu_{Fx}^*}{\epsilon_{Fx}^*}} = \sqrt{\frac{1 + \frac{\sigma(x)}{j\omega\epsilon_0}}{1 + \frac{\sigma(x)}{j\omega\epsilon_0}}} = 1 \text{-----} (6.29)$$

This fulfills the first requirement. If  $\sigma$  increases gradually as it goes in to the PML, the field values  $Dz$  and  $Hx$  to be attenuated.

We will start by implementing PML only in the X direction. Thus we will retain only x dependent values of  $\epsilon_{Fz}^*$  and  $\mu_{Fx}^*$ . Eqn. 6.20 to 6.22 become

$$j\omega Dz \cdot \epsilon_{Fz}^*(x) = C_0 \cdot \left( \frac{\partial Hy}{\partial x} - \frac{\partial Hx}{\partial y} \right) \text{-----} (6.30)$$

$$j\omega Hx \cdot \mu_{Fx}^*(x) = -C_0 \frac{\partial Ez}{\partial y} \text{-----} (6.31)$$

$$j\omega Hy \cdot \mu_{Fy}^*(x) = C_0 \frac{\partial Ez}{\partial x} \text{-----} (6.32)$$

by using the values of eqn 6.28, the above equations become

$$j\omega \left( 1 + \frac{\sigma_D(x)}{j\omega \epsilon_0} \right) Dz = C_0 \cdot \left( \frac{\partial Hy}{\partial x} - \frac{\partial Hx}{\partial y} \right) \text{-----} (6.33)$$

$$j\omega \left( 1 + \frac{\sigma_D(x)}{j\omega \epsilon_0} \right)^{-1} Hx = -C_0 \frac{\partial Ez}{\partial y} \text{-----} (6.34)$$

$$j\omega \left( 1 + \frac{\sigma_D(x)}{j\omega \epsilon_0} \right) Hy = C_0 \frac{\partial Ez}{\partial x} \text{-----} (6.35)$$

Here the permeability of  $Hx$  in the above eqn 6.34 is the inverse of that of  $Hy$  in eqn. 6.35. Therefore we have fulfilled the second requirement for the PML.

Now the above eqns. is to be put in to the FDTD simulations. Take the left side of equation 6.33

$$j\omega\left(1 + \frac{\sigma_D(x)}{j\omega\epsilon_0}\right)Dz = j\omega Dz + \frac{\sigma_D(x)}{j\omega\epsilon_0} Dz \text{-----} (6.36)$$

Moving to the time domain and taking the finite difference approximations, we get the following

$$\begin{aligned} \frac{\partial Dz}{\partial t} + \frac{\sigma_D(i)}{\epsilon_0} Dz &\approx \frac{Dz_{ij}^{n+1/2} - Dz_{ij}^{n-1/2}}{\Delta t} + \frac{\sigma_D(i)}{\epsilon_0} \frac{Dz_{ij}^{n+1/2} + Dz_{ij}^{n-1/2}}{2} \\ &= Dz_{ij}^{n+1/2} \frac{1}{\Delta t} \left[1 + \frac{\sigma_D(i)}{2\epsilon_0} \Delta t\right] - Dz_{ij}^{n-1/2} \frac{1}{\Delta t} \left[1 - \frac{\sigma_D(i)}{2\epsilon_0} \Delta t\right] \text{-----} (6.37) \end{aligned}$$

Therefore the LHS and RHS of eqn. 6.33 is converted into FDTD as

$$\begin{aligned} Dz_{ij}^{n+1/2} &= gi3(i).Dz_{ij}^{n-1/2} + gi2(i).0.5.[Hy_{i+1/2,j}^n - Hy_{i-1/2,j}^n \\ &\quad - Hx_{i,j+1/2}^n + Hx_{i,j-1/2}^n] \text{-----} (6.38) \end{aligned}$$

Once again used the fact that

$$\frac{\Delta t}{\sqrt{\mu_0\epsilon_0}\Delta x} = \frac{\Delta t}{\Delta x} .C_0 = \frac{\Delta x/(2.C_0)}{\Delta x} .C_0 = 0.5$$

Where the new parameters gi2 and gi3 are given by

$$\left\{ \begin{aligned} gi2(i) &= \frac{1}{1 + \sigma_D(i).\Delta t/(2.\epsilon_0)} \\ gi3(i) &= \frac{1 - \sigma_D(i).\Delta t/(2.\epsilon_0)}{1 + \sigma_D(i).\Delta t/(2.\epsilon_0)} \end{aligned} \right\} \text{-----} (6.39)$$

Similarly the FDTD equation for Hy in eqn. 6.35 is

$$Hy_{i+1/2,j}^{n+1} = fi3(i+1/2).Hy_{i+1/2,j}^n + fi2(i+1/2).0.5.[Ez_{i+1,j}^{n+1/2} - Ez_{i,j}^{n+1/2}] \quad (6.40)$$

Where

$$\left\{ \begin{aligned} fi2(i+1/2) &= \frac{1}{1 + \sigma_D(i+1/2).\Delta t/(2.\epsilon_0)} \\ fi3(i+1/2) &= \frac{1 - \sigma_D(i+1/2).\Delta t/(2.\epsilon_0)}{1 + \sigma_D(i+1/2).\Delta t/(2.\epsilon_0)} \end{aligned} \right\} \quad \text{--- (6.41)}$$

Note that the above parameters are calculated at i+1/2 because of the position of Hy in the FDTD grid.

But the eqn for Hx in 6.34 require some other treatment than the other two. ie

$$j\omega Hx = -C_0 \left[ \frac{\partial Ez}{\partial y} + \frac{\sigma_D(x)}{j\omega\epsilon_0} \cdot \frac{\partial Ez}{\partial y} \right] \quad \text{--- (6.42)}$$

Here 1/jw is treated as an integral operator over time and jw as a derivative over time. The spatial derivative will be written as

$$\frac{\partial Ez}{\partial y} \sim \frac{Ez_{i,j+1}^{n+1/2} - Ez_{i,j}^{n+1/2}}{\Delta x} \sim \frac{curl \_e}{\Delta x}$$

Implanting this into FDTD formulation of eqn. 6.42 , Finally we get



$$\left\{ \begin{aligned} Hx_{i,j+1/2}^{n+1} &= Hx_{i,j+1/2}^n + \frac{C_0 \cdot \Delta t}{\Delta x} \text{curl}_- e + \frac{C_0 \cdot \Delta t}{\Delta x} \frac{\sigma_D(x) \Delta t}{\epsilon_0} I_{Hx(i,j+1/2)}^{n+1/2} \\ &= Hx_{i,j+1/2}^n + \frac{C_0 \cdot \Delta t}{\Delta x} \text{curl}_- e + \frac{\sigma_D(x) \cdot \Delta t}{2\epsilon_0} I_{Hx(i,j+1/2)}^{n+1/2} \\ I_{Hx(i,j+1/2)}^{n+1/2} &= I_{Hx(i,j+1/2)}^{n-1/2} + \text{curl}_- e \\ Hx_{i,j+1/2}^{n+1} &= Hx_{i,j+1/2}^n + 0.5 \cdot \text{curl}_- e + \text{fil}(i) \cdot I_{Hx(i,j+1/2)}^{n+1/2} \end{aligned} \right\} \quad (6.43)$$

$$\text{fil}(i) = \frac{\sigma(i) \cdot \Delta t}{2\epsilon_0}$$

Where

Calculating the f and g parameters, it is not necessary to actually vary conductivities. Instead, we calculate the auxiliary parameters,

$$xn = \frac{\sigma \cdot \Delta t}{2\epsilon_0}$$

that increases as it goes into the PML. The f and g parameters are calculated by [8]

$$\left\{ \begin{aligned} xn(i) &= 0.333 * \left( \frac{i}{\text{length\_pml}} \right)^3 \\ \text{where, } i &= 1, 2, \dots, \text{length\_pml} \\ gi2(i) &= \frac{1}{1 + xn(i)} \\ gi3(i) &= \frac{1 - xn(i)}{1 + xn(i)} \end{aligned} \right\} \quad \text{-----} (6.44)$$

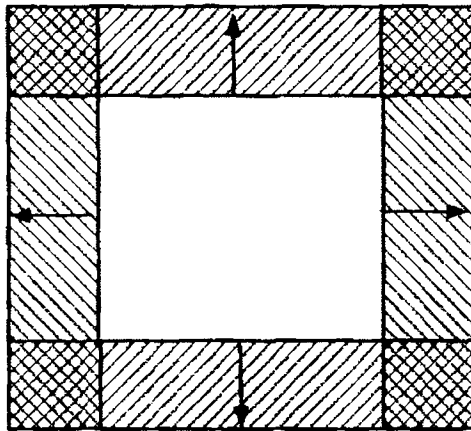
The parameter  $x_n(i)$  varies between 0 and 1. The factor .333 was found empirically to be the largest number that remained stable. The parameters vary in the following manner

$$\begin{aligned}
 f_{i1} & \text{ from } 0 \text{ to } 0.333 \\
 g_{i2} & \text{ from } 1 \text{ to } 0.75 \quad \text{-----(6.45)} \\
 g_{i3} & \text{ from } 1 \text{ to } 0.5
 \end{aligned}$$

Through out the problem space,  $f_{i1}$  is zero and  $g_{i2}$  and  $g_{i3}$  are one. Therefore there is a seamless transition from the main part of the problem space to the PML. (See Fig. 6.2).

The corners are an overlap of both sets of parameters

Decreasing values of  $f_{1j}$ ; increasing values of  $f_{2j}$ ,  $f_{3j}$ ,  $g_{2j}$ , and  $g_{3j}$



Decreasing values of  $f_{1i}$ ; increasing values of  $f_{2i}$ ,  $f_{3i}$ ,  $g_{2i}$ , and  $g_{3i}$

Fig. 6.2 Parameters related to the perfectly matched layer (PML)

Considering y direction also, ie two dimension, then similarly as equations 6.33, 6.34 and 6.35

$$j\omega\left(1 + \frac{\sigma_D(x)}{j\omega\epsilon_0}\right)\left(1 + \frac{\sigma_D(y)}{j\omega\epsilon_0}\right)Dz = C_0 \cdot \left(\frac{\partial Hy}{\partial x} - \frac{\partial Hx}{\partial y}\right) \text{---- (6.46)}$$

$$j\omega\left(1 + \frac{\sigma_D(x)}{j\omega\epsilon_0}\right)^{-1}\left(1 + \frac{\sigma_D(y)}{j\omega\epsilon_0}\right)Hx = -C_0 \frac{\partial Ez}{\partial y} \text{----- (6.47)}$$

$$j\omega\left(1 + \frac{\sigma_D(x)}{j\omega\epsilon_0}\right)\left(1 + \frac{\sigma_D(y)}{j\omega\epsilon_0}\right)^{-1}Hy = C_0 \frac{\partial Ez}{\partial x} \text{----- (6.48)}$$

Converting in to FDTD, For Dz, from equation 6.46

$$Dz_{ij}^{n+1/2} = gi3(i).gj3(j).Dz_{ij}^{n/2} + gi2(i).gj2(j)0.5.[Hy_{i+1/2,j}^n - Hy_{i-1/2,j}^n - Hx_{i,j+1/2}^n + Hx_{i,j-1/2}^n] \text{----- (6.49)}$$

For Hy, from equation 6.48

$$\left\{ \begin{array}{l} \text{curl } \underline{e} = Ez_{i+1,j}^{n+1/2} - Ez_{i,j}^{n+1/2} \\ I_{Hy(i+1/2,j)}^{n+1/2} = I_{Hy(i+1/2,j)}^{n-1/2} + \text{curl } \underline{e} \\ Hy_{i+1/2,j}^{n+1} = fi3(i+1/2).Hy_{i+1/2,j}^n \\ \quad - fi2(i+1/2).0.5.\text{curl } \underline{e} + fj1(j).I_{Hy(i+1/2,j)}^{n+1/2} \end{array} \right\} \text{--- (6.50)}$$

For Hx, from equation 6.47

$$\left\{ \begin{array}{l} \text{curl } _e = Ez_{i,j}^{n+1/2} - Ez_{i,j+1}^{n+1/2} \\ I_{Hx(i,j+1/2)}^{n+1/2} = I_{Hx(i,j+1/2)}^{n-1/2} + \text{curl } _e \\ Hx_{i,j+1/2}^{n+1} = fj3(j+1/2).Hx_{i,j+1/2}^n \\ \quad + fj2(j+1/2).0.5.\text{curl } _e + fil(i).I_{Hx(i,j+1/2)}^{n+1/2} \end{array} \right\} - (6.51)$$

Full set of parameters associated with PML are the following.

$$\begin{array}{ll} fil(i) \& fj1(j) & \text{from 0 to .333} \\ fj2(i), gi2(i), fj2(j), \& gj2(j) & \text{from 1 to .75} \\ fj3(i), gi3(i), fj3(j), \& gj3(j) & \text{from 1 to .5.} \end{array} \quad - (6.52)$$

Now consider for 3 dimensions, i.e. x, y and z directions. Similarly as in two dimensions, the full set of equations after adding PML is

$$\begin{array}{l} jw(1 + \frac{\sigma_x(x)}{jw\epsilon_0})^{-1}(1 + \frac{\sigma_y(y)}{jw\epsilon_0})^{-1}(1 + \frac{\sigma_z(z)}{jw\epsilon_0})Dx = C_0.(\frac{\partial Hz}{\partial y} - \frac{\partial Hy}{\partial z}) \\ jw(1 + \frac{\sigma_x(x)}{jw\epsilon_0})^{-1}(1 + \frac{\sigma_y(y)}{jw\epsilon_0})^{-1}(1 + \frac{\sigma_z(z)}{jw\epsilon_0})Dy = C_0.(\frac{\partial Hx}{\partial z} - \frac{\partial Hz}{\partial x}) \\ jw(1 + \frac{\sigma_x(x)}{jw\epsilon_0})^{-1}(1 + \frac{\sigma_y(y)}{jw\epsilon_0})^{-1}(1 + \frac{\sigma_z(z)}{jw\epsilon_0})^{-1}Dz = C_0.(\frac{\partial Hy}{\partial x} - \frac{\partial Hx}{\partial y}) - (6.53) \end{array}$$

$$\begin{array}{l} jw(1 + \frac{\sigma_x(x)}{jw\epsilon_0})^{-1}(1 + \frac{\sigma_y(y)}{jw\epsilon_0})^{-1}(1 + \frac{\sigma_z(z)}{jw\epsilon_0})Hx = C_0.(\frac{\partial Ey}{\partial z} - \frac{\partial Ez}{\partial y}) \\ jw(1 + \frac{\sigma_x(x)}{jw\epsilon_0})^{-1}(1 + \frac{\sigma_y(y)}{jw\epsilon_0})^{-1}(1 + \frac{\sigma_z(z)}{jw\epsilon_0})Hy = C_0.(\frac{\partial Ez}{\partial x} - \frac{\partial Ex}{\partial z}) \\ jw(1 + \frac{\sigma_x(x)}{jw\epsilon_0})^{-1}(1 + \frac{\sigma_y(y)}{jw\epsilon_0})^{-1}(1 + \frac{\sigma_z(z)}{jw\epsilon_0})^{-1}Hz = C_0.(\frac{\partial Ex}{\partial y} - \frac{\partial Ey}{\partial x}) \end{array}$$

Discretizing the equation for Dz is

$$\left\{ \begin{array}{l} j\omega(1 + \frac{\sigma_x(x)}{j\omega\epsilon_0})(1 + \frac{\sigma_y(y)}{j\omega\epsilon_0})(1 + \frac{\sigma_z(z)}{j\omega\epsilon_0})^{-1}Dz = C_0 \cdot (\frac{\partial Hy}{\partial x} - \frac{\partial Hx}{\partial y}) \\ j\omega(1 + \frac{\sigma_x(x)}{j\omega\epsilon_0})(1 + \frac{\sigma_y(y)}{j\omega\epsilon_0})Dz = C_0 \cdot (1 + \frac{\sigma_z(z)}{j\omega\epsilon_0})^{-1} (\frac{\partial Hy}{\partial x} - \frac{\partial Hx}{\partial y}) \\ = C_0 \cdot curl\_h + C_0 \cdot \frac{\sigma_z(z)}{j\omega\epsilon_0} curl\_h \\ I_{Dz} = \frac{1}{j\omega} curl\_h \\ j\omega(1 + \frac{\sigma_x(x)}{j\omega\epsilon_0})(1 + \frac{\sigma_y(y)}{j\omega\epsilon_0})Dz = C_0 \cdot (curl\_h + C_0 \cdot \frac{\sigma_z(z)}{\epsilon_0} I_{Dz}) \end{array} \right\} \quad (6.54)$$

Converting into FDTD eqns

$$\left\{ \begin{array}{l} curl\_h = Hy_{i+1/2,j,k+1/2}^n - Hy_{i-1/2,j,k+1/2}^n \\ \quad - Hx_{i,j+1/2,k+1/2}^n + Hx_{i,j-1/2,k+1/2}^n \\ I_{Dzi,j,k+1/2}^n = I_{Dzi,j,k+1/2}^{n-1} + curl\_h \\ Dz_{ij,k+1/2}^{n+1/2} = gi3(i).gj3(j).Dz_{ij,k+1/2}^{n-1/2} + \\ \quad gi2(i).gj2(j).0.5.[curl\_h + gk1(k).I_{Dzi,j,k+1/2}^n] \end{array} \right\} \quad (6.55)$$

Similarly all the FDTD equation for D, E and H fields for the three dimensional case are given below

$$\left\{ \begin{array}{l} \text{curl } _h = Hz_{i+1/2,j+1/2,k}^n - Hz_{i+1/2,j+1/2,k}^n - (Hy_{i+1/2,j,k+1/2}^n - Hy_{i+1/2,j,k-1/2}^n) \\ I_{Dxi+1/2,j,k}^n = I_{Dxi+1/2,j,k}^{n-1} + \text{curl } _h \\ Dx_{i+1/2,j,k}^{n+1/2} = gj3(j).gk3(k).Dx_{i+1/2,j,k}^{n-1/2} \\ \quad + gi2(j).gk2(k).0.5.[\text{curl } _h + gil(i).I_{Dxi+1/2,j,k}^n] \end{array} \right\}$$

$$\left\{ \begin{array}{l} \text{curl } _h = Hx_{i,j+1/2,k+1/2}^n - Hx_{i,j+1/2,k-1/2}^n - (Hz_{i+1/2,j+1/2,k}^n - Hz_{i-1/2,j+1/2,k}^n) \\ I_{Dyi,j+1/2,k}^n = I_{Dyi,j+1/2,k}^{n-1} + \text{curl } _h \\ Dy_{ij+1/2,k}^{n+1/2} = gi3(i).gk3(k).Dy_{ij+1/2,k}^{n-1/2} \\ \quad + gi2(i).gk2(k).0.5.[\text{curl } _h + gj1(j).I_{Dyi,j+1/2,k}^n] \end{array} \right\} \quad - (6.56)$$

$$\left\{ \begin{array}{l} \text{curl } _h = Hy_{i+1/2,j,k+1/2}^n - Hy_{i-1/2,j,k+1/2}^n - (Hx_{i,j+1/2,k+1/2}^n - Hx_{i,j-1/2,k+1/2}^n) \\ I_{Dzi,j,k+1/2}^n = I_{Dzi,j,k+1/2}^{n-1} + \text{curl } _h \\ Dz_{ij,k+1/2}^{n+1/2} = gi3(i).gj3(j).Dz_{ij,k+1/2}^{n-1/2} \\ \quad + gi2(i).gj2(j).0.5.[\text{curl } _h + gk1(k).I_{Dzi,j,k+1/2}^n] \end{array} \right\}$$

$$\left\{ \begin{array}{l} Ex_{i+1/2,j,k}^{n+1/2} = gax(i,j,k) * Dx_{i+1/2,j,k}^{n+1/2} \\ Ey_{ij+1/2,k}^{n+1/2} = gay(i,j,k) * Dy_{ij+1/2,k}^{n+1/2} \\ Ez_{ij,k+1/2}^{n+1/2} = gaz(i,j,k) * Dz_{ij,k+1/2}^{n+1/2} \end{array} \right\} \quad \text{--- (6.57)}$$

$gax(i,j,k) = gay(i,j,k) = gaz(i,j,k) = 1$  for free space

$gax(i,j,k) = gay(i,j,k) = gaz(i,j,k) = 1/\epsilon_1$  for free problem space

$$\left. \begin{aligned}
 \text{curl}_- e &= E_{y_{i,j+1/2,k+1}}^{n+1/2} - E_{y_{i,j+1/2,k}}^{n+1/2} - (E_{z_{i,j+1,k+1/2}}^{n+1/2} - E_{z_{i,j,k+1/2}}^{n+1/2}) \\
 I_{Hx_{i,j+1/2,k+1/2}}^{n+1/2} &= I_{Hx_{i,j+1/2,k+1/2}}^{n-1/2} + \text{curl}_- e \\
 Hx_{i,j+1/2,k+1/2}^{n+1} &= fj3(j).fk3(k).Hx_{i,j+1/2,k+1/2}^n \\
 &\quad + fj2(j).fk2(k).0.5.[\text{curl}_- e + fil(i).I_{Hx_{i,j+1/2,k+1/2}}^{n+1/2}]
 \end{aligned} \right\}$$

$$\left. \begin{aligned}
 \text{curl}_- e &= E_{z_{i+1,j,k+1/2}}^{n+1/2} - E_{z_{i,j,k+1/2}}^{n+1/2} - (E_{x_{i+1/2,j,k+1}}^{n+1/2} - E_{x_{i+1/2,j,k}}^{n+1/2}) \\
 I_{Hy_{i+1/2,j,k+1/2}}^{n+1/2} &= I_{Hy_{i+1/2,j,k+1/2}}^{n-1/2} + \text{curl}_- e \\
 Hy_{i+1/2,j,k+1/2}^{n+1} &= fi3(i).fk3(k).Hy_{i+1/2,j,k+1/2}^n \\
 &\quad + fi2(i).fk2(k).0.5.[\text{curl}_- e + fj1(j).I_{Hy_{i+1/2,j,k+1/2}}^{n+1/2}]
 \end{aligned} \right\} \text{--- (6.58)}$$

$$\left. \begin{aligned}
 \text{curl}_- e &= E_{x_{i+1/2,j+1,k}}^{n+1/2} - E_{x_{i+1/2,j,k}}^{n+1/2} - (E_{y_{i+1,j+1/2,k}}^{n+1/2} - E_{y_{i,j+1/2,k}}^{n+1/2}) \\
 I_{Hz_{i+1/2,j+1/2,k}}^{n+1/2} &= I_{Hz_{i+1/2,j+1/2,k}}^{n-1/2} + \text{curl}_- e \\
 Hz_{i+1/2,j+1/2,k}^{n+1} &= fi3(i).fj3(j).Hz_{i+1/2,j+1/2,k}^n \\
 &\quad + fi2(i).fj2(j).0.5.[\text{curl}_- e + fk1(k).I_{Hz_{i+1/2,j+1/2,k}}^{n+1/2}]
 \end{aligned} \right\}$$

The whole PML parameters are

$$\begin{aligned}
 &fil(i), fj1(j), fk1(k) \text{ \& } gil(i), gj1(j), gk1(k) \text{ --- from } 0 \text{ to } .333 \\
 &fi2(i), fj2(j), fk2 \text{ \& } gi2(i), gj2(j), gk2(k) \text{ --- from } 1 \text{ to } .75 \text{ --- (6.59)} \\
 &fi3(i) fj3(j), fk3(k) \text{ \& } gi3(i), gj3(j), gk3(k) \text{ --- from } 1 \text{ to } .5
 \end{aligned}$$

Which are calculated by the empirical formula derived by Sullivan [8], is

$$x_n = 0.333 * (i / \text{length\_pml})^3 \quad i=1,2,\dots,\text{length\_pml}$$

$$fi1 = fj1 = fk1 = x_n = gi1 = gj1 = gk1$$

$$gi2 = gj2 = gk2 = 1 / (1 + x_n) = fi2 = fj2 = fk2,$$

$$gi3 = gj3 = gk3 = (1 - x_n / (1 + x_n)) = fi3 = fj3 = fk3$$

Throughout the problem space,  $fi1 = fj1 = fk1 = gi1 = gj1 = gk1 = 0$  and

$g_i2=g_j2=g_k2=f_i2=f_j2=f_k2=g_i3=g_j3=g_k3=f_i3=f_j3=f_k3=1$ , Therefore there is a seamless transition from the main part of the program to the PML.

### 6.3 Description of the microstrip fed HDRA

**Fig. 6.3 (a)** illustrates the microstrip fed hexagonal dielectric resonator antenna to be analyzed. Since we are more interested in the internal properties of the antenna rather than in the resulting radiation pattern, so it will not be necessary to model a large part of the surrounding area. Since  $S_{11}$  depends on the geometry of the antenna, it is crucial that we model the HDRA to its dimensions as close as possible. Looking at the dimension of **Fig. 6.3 (a)**, it is obvious that we need FDTD cells of size about 0.5mm to accurately get these dimensions. Which is calculated from the fact that

$$\text{Cell size should be less than or equal to } \lambda/20$$

(for 2.45 GHz,  $\lambda/20 = 0.74\text{mm}$  and for 3.25GHz,  $\lambda/20=0.56\text{mm}$ )

For modeling the microstrip fed hexagonal dielectric resonator antenna, the HDRA is split into one rectangle with dimensions 14.4 mm X 26 mm X 11mm (length X breadth X thickness) and four triangles with dimensions 13 mm X 8 mm X 11mm (length X base X thickness) as shown in **Fig. 6.3 (d)**. The number of cells for the rectangular DRA is  $29 \Delta_y$ ,  $52 \Delta_x$  and  $22 \Delta_z$ . The slanted area of triangular DRA is modeled using stair case approximation, therefore the number of cells varies from 0 to  $16 \Delta_y$  as base when the length increases from 0 to  $26 \Delta_x$  and height of



triangular DRA is same as rectangular and same for all the other three triangles.

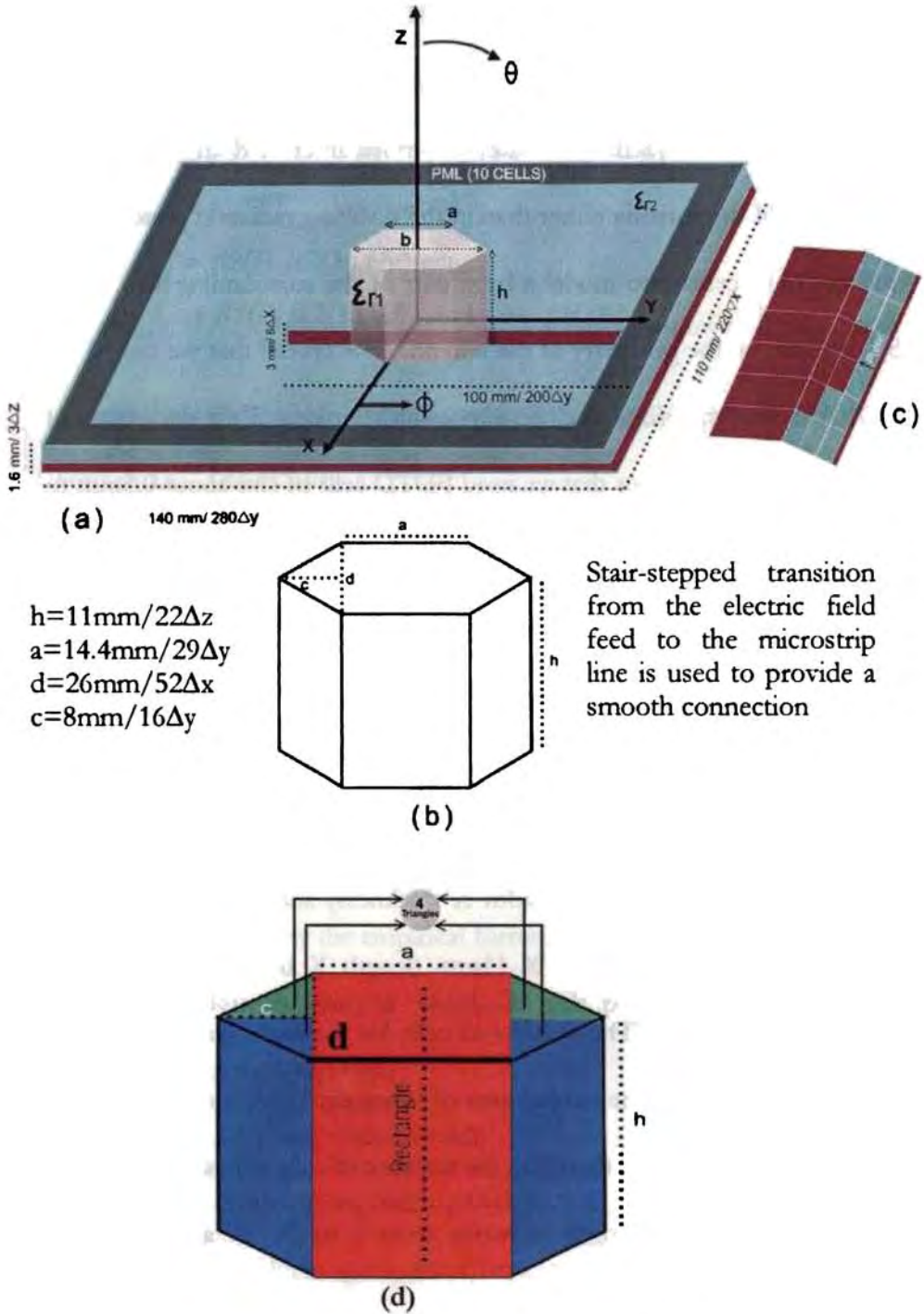


Fig. 6.3 Geometry of the computational domain

The microstrip feed line having a dimension of 3 mm X 100 mm and thus the no of cells for the microstrip feed is  $6 \Delta x \times 200 \Delta y$ . The dimension of the microstrip patch is 110 mm X 140 mm X 1.6 mm, there for the total no. of cells required is  $220 \Delta x$ ,  $280 \Delta y$  and  $3 \Delta z$ . There for the number of cells taken for the whole computational domain along X, Y and Z directions is  $220 \Delta x$ ,  $280 \Delta y$  and  $50 \Delta z$ . ( $50 \Delta z = 3 \Delta z$  for substrate +  $22 \Delta z$  for DRA +  $15 \Delta z$  air +  $10 \Delta z$  PMI.)

### 6.3.1 Modeling the materials

For modeling the whole structure, consists of 5 materials: ground plane metal, dielectric substrate, feed metal, dielectric material for DRA and free space. Assume that the substrate has a relative dielectric constant of 4 and DR has a relative dielectric constant of 69. Therefore the relationship between electric flux density and electric field is

$$e_x(i, j, k) = g_{ax}(i, j, k) * dx(i, j, k)$$

from eqn. 6.13,  $g_{ax}(i, j, k) = 1/4$  and  $g_{ax}(i, j, k) = 1/69$  respectively for substrate and DR. For metal, the E fields within those points corresponding to metal remain as zero. ie. simply put  $g_{ax}$ ,  $g_{ay}$  and  $g_{az}$  equal to zero at those points corresponds to the metal surface, we must be cognizant of the relative positions of the fields in the Yee Cell (Fig. 6.1). Suppose we are viewing the FDTD lattice under the antenna, looking in the X direction, is illustrated in Fig. 6.4. It is seen that the entire structure lays on a ground metal plane, and hence  $E_x$  and  $E_y$  values for  $k=1$  remains zero. Since the  $E_z$  values lays half cells above the  $k=1$

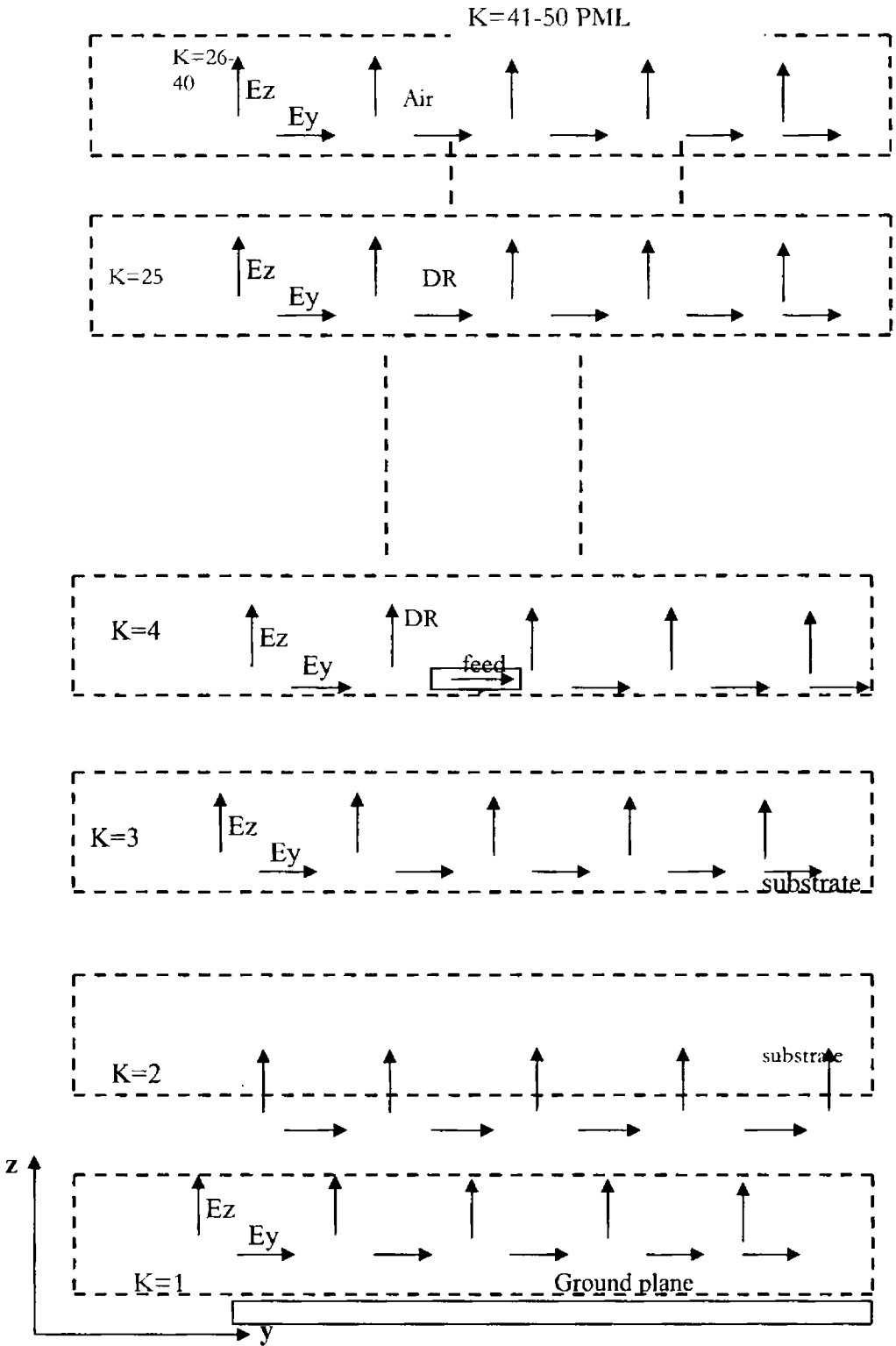


Fig. 6.4 Positions of E fields relative to the material being modeled.

plane, it will be in the substrate. Similarly for specifying the feed metal on the antenna in the  $k=4$  plane,  $E_x$  and  $E_y$  values corresponds to feed line are set to zero, but  $E_z$  values at  $k=4$  is in DR. Then upto 25 cells the material is DR and hence set the appropriate values for  $g_{ax}$ ,  $g_{ay}$  and  $g_{az}$  for getting E fields. After 25 cells and around the HDR, the medium is air, therefore set the appropriate values for  $g_{ax}$ ,  $g_{ay}$  and  $g_{az}$  for getting E fields corresponds to air. Also the permittivity of air – DR interface, substrate - DR interface and substrate – air interface are given as the average of the two medium and those cells are modeled appropriately [5].

### **6.3.2 Boundary conditions**

For this work, the PML explained in section 6.2.4 is used as absorbing boundary condition for both homogenous and non homogenous media. The main advantage of a PML is that it does not require substantial modification when there is a transition from one medium to another, but all other boundary conditions need modification. But we have implemented the PML using the PML parameters at all the problem space. Here used 10 cells as PML around the problem space (i.e. top and sides).

### 6.3.3 Source

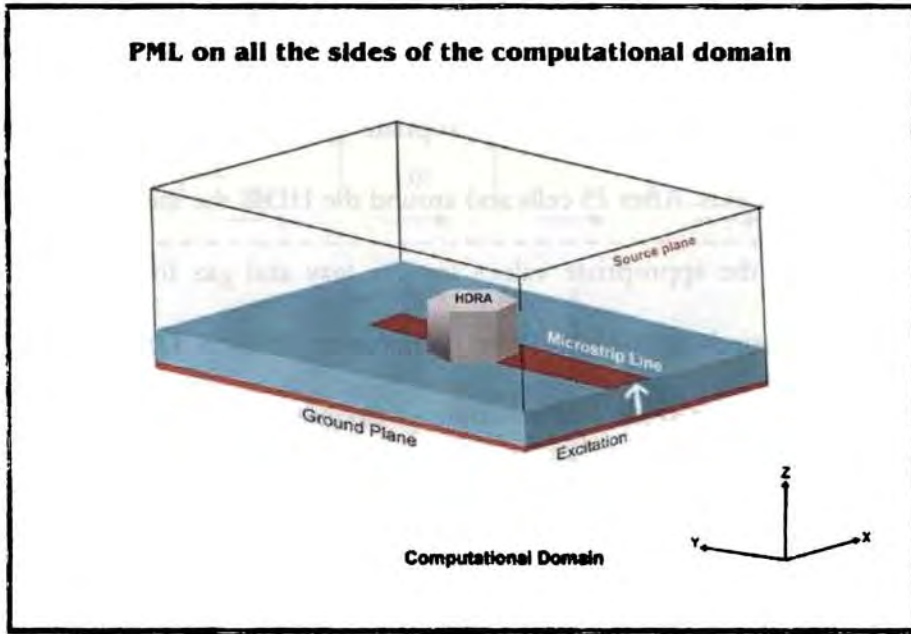


**Fig. 6.5** The computational volume for the microstrip fed HDRA circuit simulation

The volume in which the microstrip fed HDRA circuit simulation is to be performed is shown in **Fig. 6.5**. At  $t=0$  the fields are assumed to be zero throughout the computational domain. A Gaussian pulse is desirable as the excitation because its frequency spectrum is also Gaussian and will therefore provide frequency-domain information from dc to the desired cutoff frequency by adjusting the width of the pulse. In order to simulate a voltage source excitation it is necessary to impose the vertical electric flux density  $D_z$  in a rectangular region underneath port 1 as shown in **Fig. 6.5**. The remaining electric flux components on the source plane

must be specified or calculated. The source plane consists only of  $D_x$ , and  $D_z$  components, with the tangential magnetic field components offset  $\pm \Delta y / 2$ . The launched wave has nearly unit amplitude and is Gaussian in time and in the  $y$  direction: the width of the Gaussian pulse is chosen for at least 20 points per wavelength at the highest frequency represented significantly in the pulse.

$$Pulse = e^{-\frac{(dt - T - t_0)^2}{T^2}} \text{ --- (6.60)}$$

$T_1 = 20 \times 10^{-12}$  sec, width of the incident pulse.

$t_0 = 3 \times T_1$  center of the incident pulse

$dt = 6.922 \times 10^{-12}$  sec, which is the time required for passing the wave through half of the smallest cell.

Where  $dt$  is calculated from the eqn. 6.4 as

$$dt = \frac{\Delta z}{2C} \sqrt{\epsilon_r(\text{highest})}$$

### 6.3.4 Resistant source FDTD excitation

FDTD antenna calculations are often excited by a “hard” source described in [10, 11], that is the internal resistance is zero ohms. These sources are very easy to implement in an FDTD code. The electric field at the mesh edge where the source is located is determined by some function

of time rather than by the FDTD update equations. A common choice is a Gaussian pulse, but other functions may also be used. The Gaussian pulse is significantly greater than zero amplitude for only a very short fraction of the total computation time, especially for resonant geometries such as many antennas and microstrip circuits. Once the pulse amplitude drops the source voltage becomes essentially zero, the source effectively becoming a short circuit. Thus, any reflections from the antenna or microstrip circuit which return to the source are totally reflected. The only way the energy introduced into the calculation space can be dissipated is through radiation or by absorption by lossy media or lumped loads. For resonant structures, there are frequencies for which this radiation or absorption process requires a relatively long time to dissipate the excitation energy. Using a source with an internal resistance to excite the FDTD calculation provides an additional loss mechanism for the calculations.

Consider that it is desired to excite an FDTD calculation with a voltage source that corresponds to an electric field  $E$  in the  $z$  direction at a certain mesh location  $i_s \Delta x, j_s \Delta y, k_s \Delta z$ , described using the usual Yee notation. The corresponding equivalent circuit for a voltage source which includes an internal source resistance  $R_s$ , is illustrated in **Fig. 6.6**. If the source resistance  $R_s$ , is set to zero then the usual FDTD electric field at the source location is simply given by

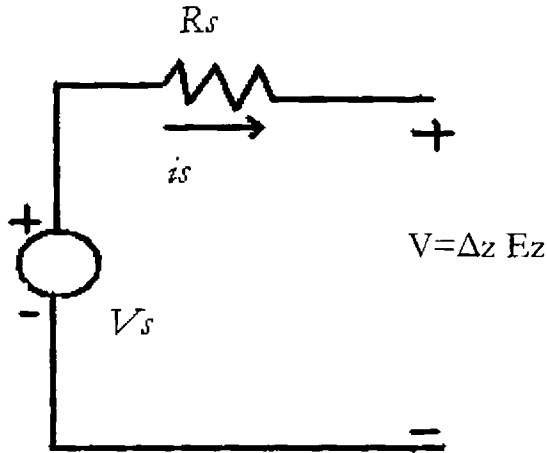


Fig. 6.6 FDTD source with source resistance  $R_s$  [10]

$$E_s(i_s, j_s, k_s) = V_s(n\Delta t) / \Delta z \text{-----(6.56)}$$

$V_s$  is any function of time-often a Gaussian pulse. However, with the source resistance included, the calculation of the source field  $E_s^n(i_s, j_s, k_s)$  at each time step is complicated slightly. To determine the terminal voltage  $V_s$  of Fig. 6.5 and, thus, the FDTD electric source field  $E_s^n(i_s, j_s, k_s)$ , the current through the source must be determined. This can be done by applying Ampere’s circuital law, taking the line integral of magnetic field around the electric field source location. The current through the source is then given by [12]

$$I_s^{n-1/2} = (Hx_{is,js-1,ks}^{n-1/2} - Hx_{is,js,ks}^{n-1/2})\Delta x + (Hy_{is-1,js,ks}^{n-1/2} - Hy_{is,js,ks}^{n-1/2})\Delta y \text{-----(6.61)}$$



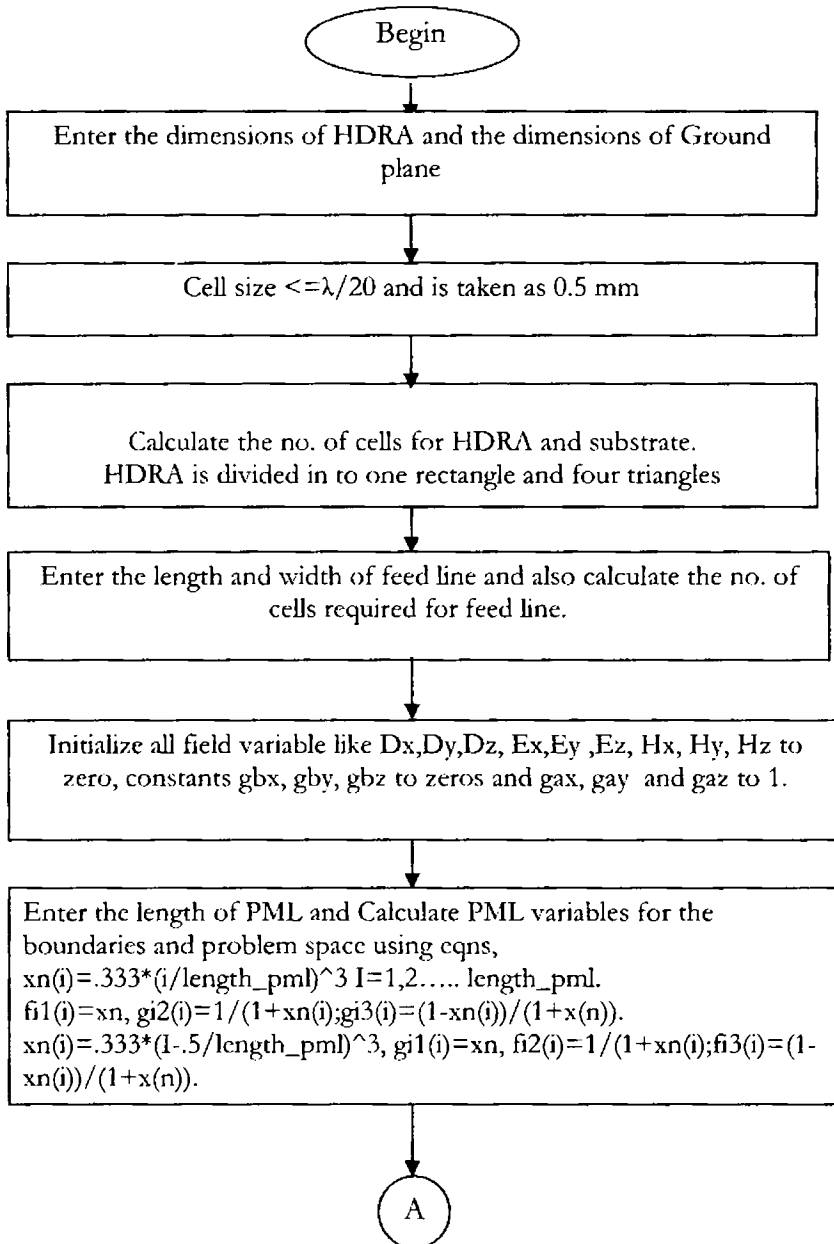
So that by applying Ohm's law to the circuit of **Fig. 6.6**, the electric source field is given by

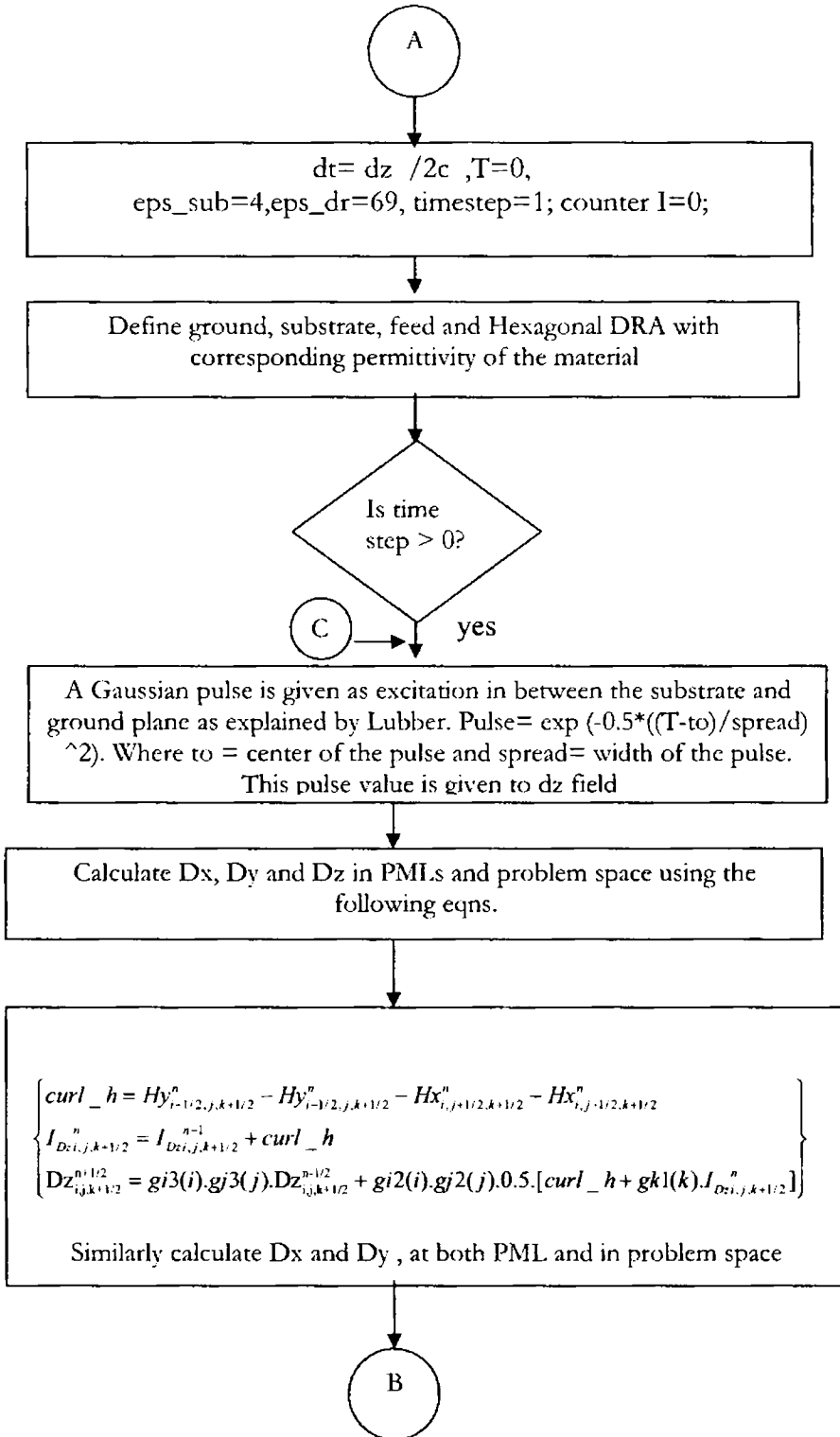
$$E_s^n(is, js, ks) = V_s(n\Delta t) / \Delta z + I_s^{n-1/2} R_s / \Delta z \text{ --- (6.62)}$$

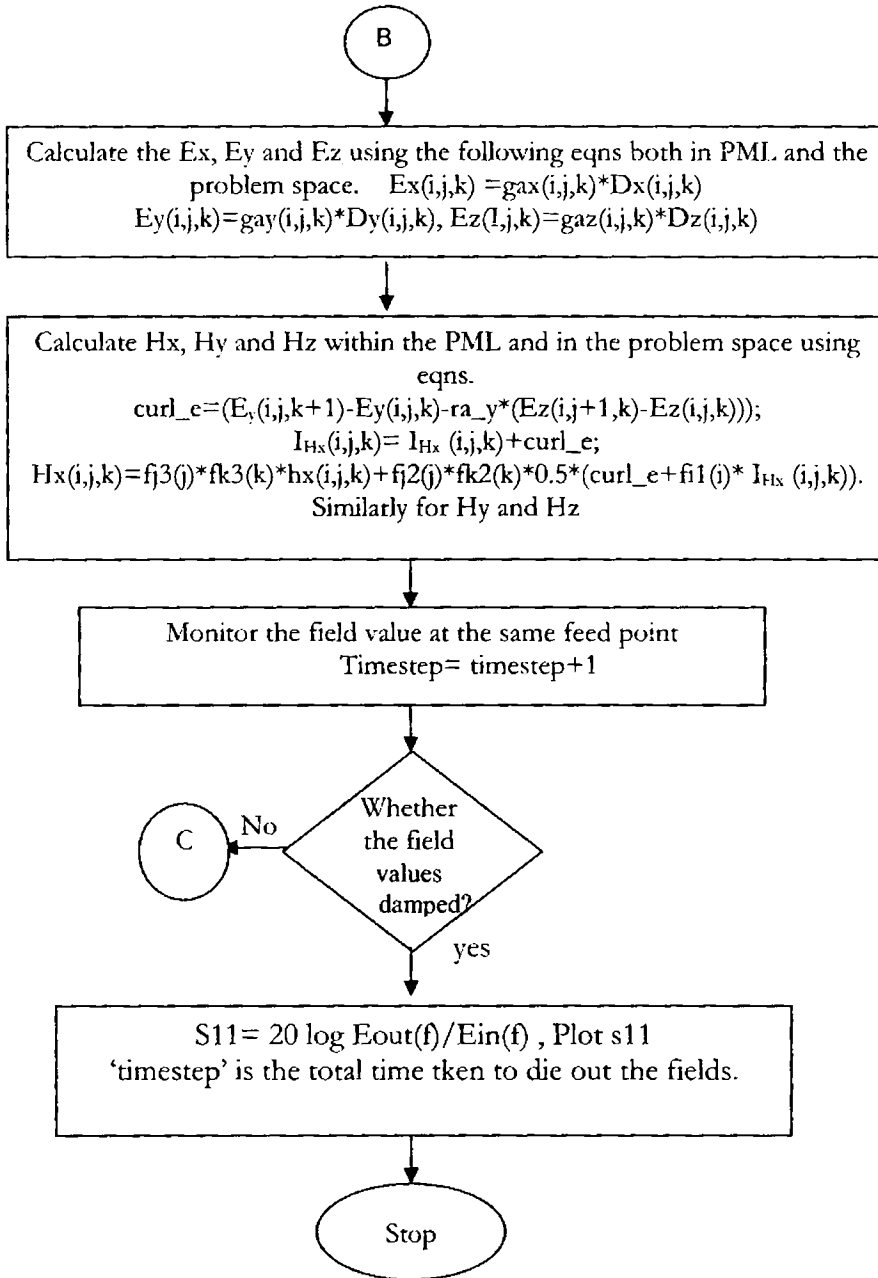
If  $R_s = 0$  in this equation, then the usual hard-voltage source results. The 1/2 time-step offset between the current and voltage used in the application of Ohm's law to determine the terminal voltage has not been observed to introduce any appreciable error into the FDTD impedance calculation. As an indication of this, in usual practice, the complex Fourier transforms of the source voltage and current are divided to produce the impedance without any correction needed for the 1/2 time step offset between them. The value of the internal resistance does not appear to be critical. A reasonable choice for  $R_s$  is to use the value of the characteristic impedance of the transmission line, coaxial cable, or microstrip, depending on the particular antenna geometry.

### 6.3.5 Flow chart for the simulation of HDRA

The following flow chart explains the steps used for developing the program for the simulation of microstrip fed Hexagonal dielectric resonator antenna.







### 6.3.6 FDTD Results

#### 6.3.6.1 Calculation of Return loss

Calculation of return loss ( $S_{11}$ ) is as follows

- 1) The information of interest is at a single point as opposed to calculating the resulting fields through out an entire area.

- 2) The frequency response is calculated over an entire range of frequencies, as opposed to getting the response at a few discrete frequencies.
- 3) Store the time domain data during the simulation and then calculate the frequency response after the simulation is over.

To compute  $S_{11}$  with an internal resistance, return loss versus frequency for a microstrip fed HDRA will be calculated. The problem space size is  $220 \times 280 \times 50$  cells. The antenna is fed using a z-directed electric field just above the ground plane and directly below the end of the stripline as marked in Fig. 6.3 (b). This electric field source location is then transitioned to the end of the microstrip feed line by additional FDTD mesh edges of perfect conductor as shown in the Fig. 6.3 (b). The perfectly conducting ground plane is at the bottom, the dielectric substrate is shown as light green squares, the mesh edge where the electric field feed is located is shown as an arrow, and the conducting meshes are shown filled wine red. The stair-stepped transition from the electric field feed (arrow) to the microstrip line at the top of **Fig. 6.3(a)** was used to provide a relatively smooth connection from the single electric feed location to the microstrip feed. The Gaussian voltage  $V$  which determines the FDTD source electric field versus time is shown in **Fig. 6.7**. The source voltage and current calculations with a source resistance  $R_s = 50$  Ohms are shown in **Fig. 6.9**. The same Gaussian pulse  $V$  was used for both calculations. It takes only 2500 time steps to damp the voltages and currents and hence to cover the

entire computational domain. Where as for the hard source, with no internal resistance, it takes more than 10000 time steps, and still the current has not completely dissipated.

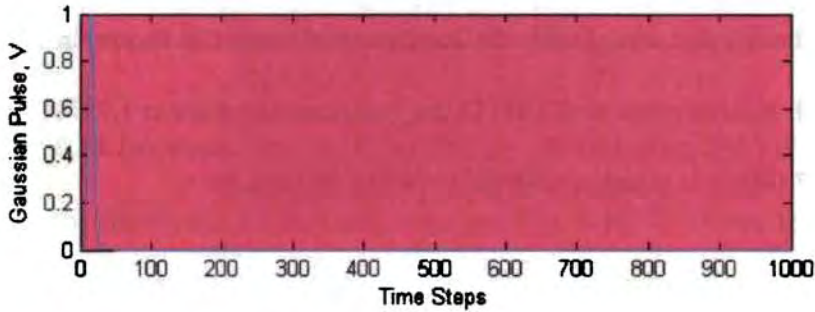


Fig. 6.7 Gaussian Pulse

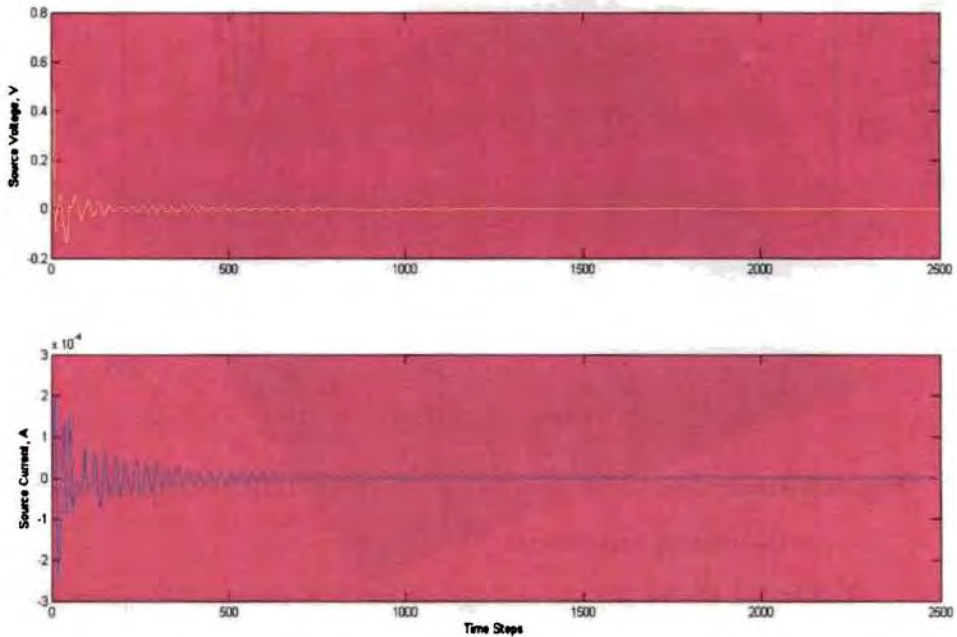
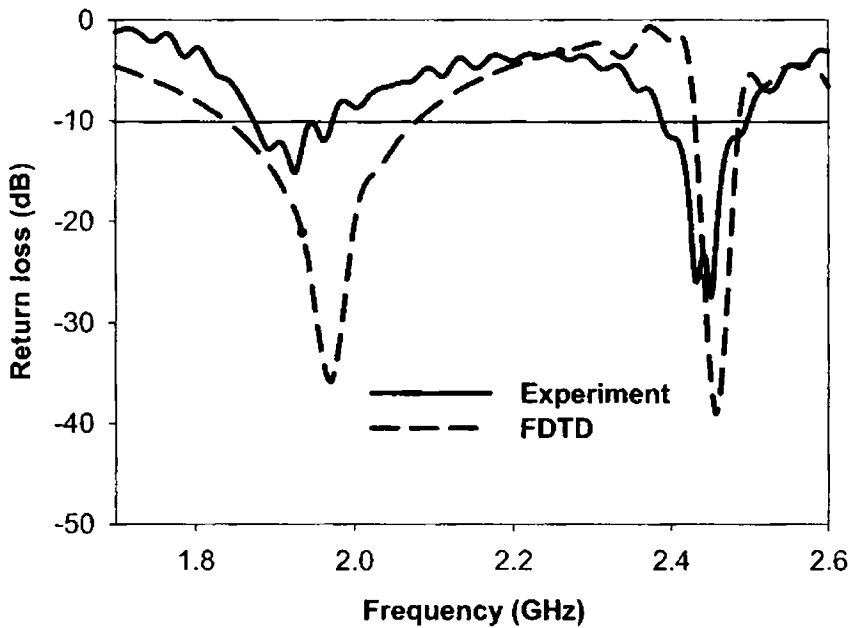


Fig. 6.8 HDR Antenna source voltage  $V_s$  and Source current  $I_s$  with source resistance  $R_s=50\text{ohms}$  ohms. All 2500 time steps are shown.

The return loss in dB is calculated by the following equation [6]

$$S_{11}(f) \text{ dB} = 20 \log_{10} [ E_{\text{out}}(f) / E_{\text{in}}(f) ].$$

Where  $E_{\text{out}}(f)$  and  $E_{\text{in}}(f)$  are the magnitude of the Fourier transform of the time domain output voltage  $V_{\text{out}}(t)$  and input supply Gaussian pulse  $V_{\text{in}}(t)$ . The  $S_{11}$  plot along with the experimental results is shown in **Fig. 6.9**, which indicates that with FDTD the two resonances are at 1.9871GHz and 2.457 GHz. It matches with the experimental results.



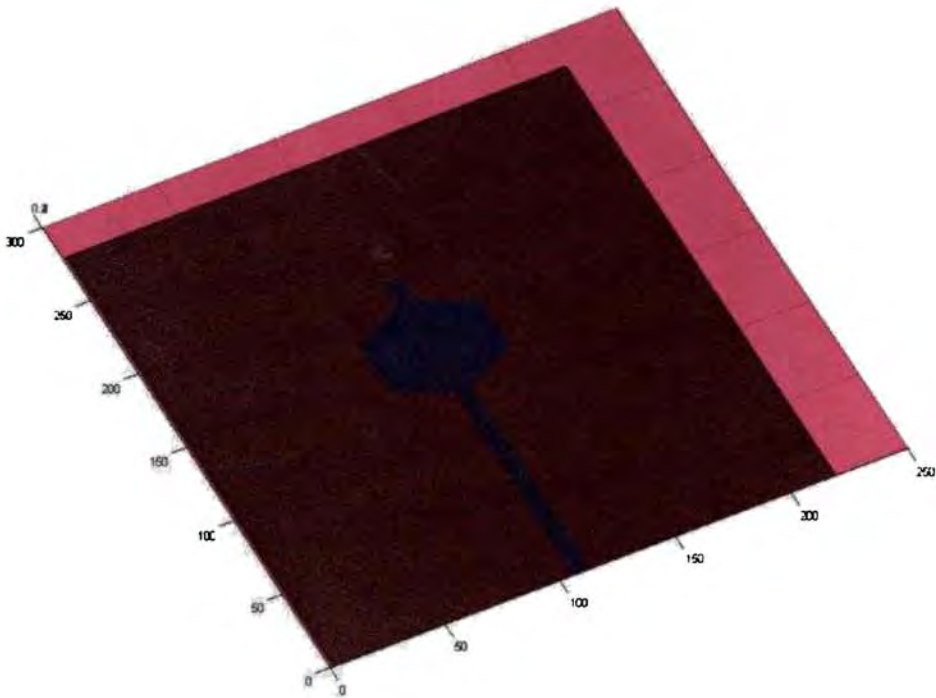
**Fig. 6.9** Return loss variation of microstrip fed HDRA-comparison of theory and experiment

**Table 6.1** shows the percentage of error in resonant frequencies between the FDTD and measured results. There is an error of 2.3% and 0.24% for the first and second resonant frequency respectively.

**Table 6.1:** Comparison of resonant frequencies with theory and experimental results of microstrip fed IIDRA

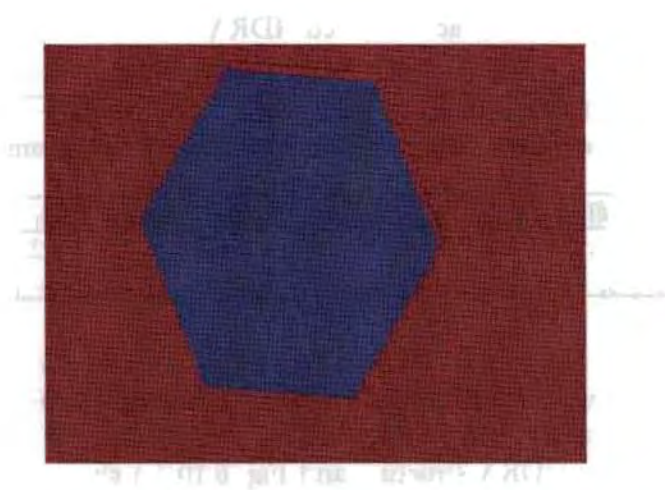
Antenna Position		FDTD method Frequency(GHz)		Experimental Frequency(GHz)		% error FDTD & Experiment	
$x_0$	$y_0$	f1	f2	f1	f2	f1	f2
13mm	8mm	1.971	2.457	1.926	2.451	2.3	0.24

**Fig. 6.10 (a)** shows the FDTD structure of microstrip fed IIDRA, Fig. 6.10 (b) shows the IIDRA structure and Fig. 6.10 (c) shows the slanted area of IIDRA simulated using staircase approximation.



(a)





(b)



(c)

**Fig. 6.10** FDTD structure of IIDRA

### 6.3.6.2 Calculation of Electric field distribution

For calculating the magnitude of electric field distribution on the top surface of HDRA for a particular frequency, instead of Gaussian pulse, one cycle of the following sinusoidal pulse is applied as excitation to the HDRA.

$$V(t) = \sin 2\pi f_0 t$$

Where  $f_0$  is the resonant frequency of interest

**Fig. 6.11(a) and (b)** shows the electric field distribution at the top surface of HDRA for the resonant frequencies 1.971 GHz and 2.457 GHz respectively. It is clear from **Fig. 6.11 (a)** that there is one intensity variation on top of HDRA which corresponds to the mode  $HE_{118}$ , which was the mode obtained in HFSS simulation also. In **Fig. 6.11 (b)**, there are two intensity variations on the top surface and thus the mode at this frequency is  $HE_{128}$ , which was obtained using HFSS simulation also.

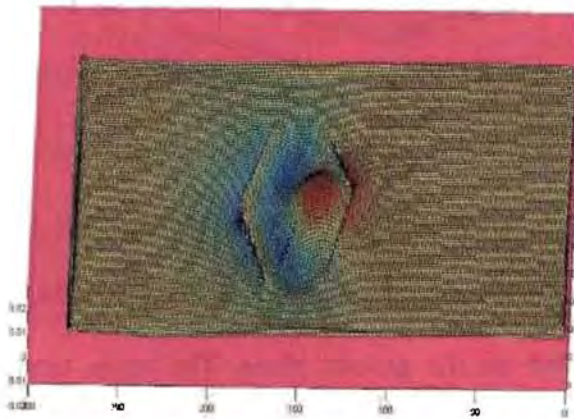


**Fig. 6.11(a)** Magnitude of Electric field distribution at 1.971 GHz

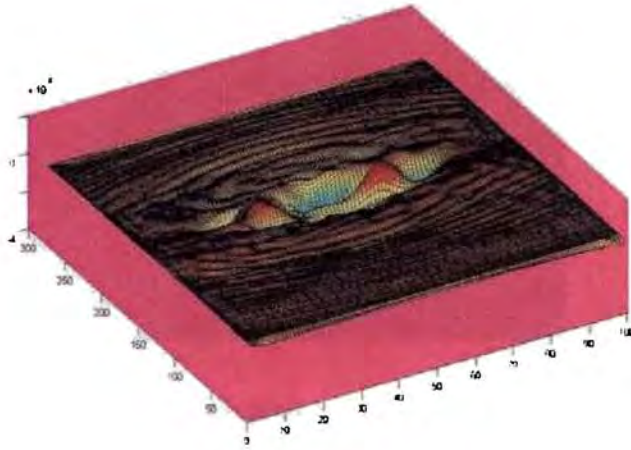


**Fig. 6.11 (b)** Magnitude of Electric field distribution at 2.457 GHz

#### 6.4 Description of Coaxial Fed HDRA

The volume for which the FDTD simulation of coaxial fed HDRA is performed is shown in **Fig.6.12 (a)**. It consists of a coaxial probe as feed to the HDRA and is placed on a conducting ground plane of dimension 100 mm X 100 mm. The total volume of the FDTD problem space is 200 X 200 X 48 cells. The cylindrical coaxial probe is approximately modeled with squared coaxial probe as shown in **Fig 6.12 (b)**. The length of the coaxial probe is 6mm and hence equivalent to  $12\Delta z$  and the thickness of the probe is 0.6mm, is divided as  $1 \Delta x$ ,  $1 \Delta y$ . The connector is modeled on the ground plane. The space between center conductor and the outer conductor of the connector is 3.5mm which is modeled as  $7 \Delta x$  or  $7 \Delta y$ . This cylindrical connector is as well modeled by

approximating to squared cells as shown in Fig. 6.13 (a) & (b). The excitation is given in between the dielectric and metal and using feed transition the field reaches to the probe as shown in Fig. 6.13 (b). The space between outer and inner conductor of the connector is filled with Teflon with permittivity of 2.2. At this juncture also feed transition with the concept of source internal resistance is used for reducing the number of time steps to cover the complete problem space. The same HDR, PML and Gaussian pulse, as used for the analysis of microstrip fed HDRA, are used for analysing the coaxial fed HDRA also.

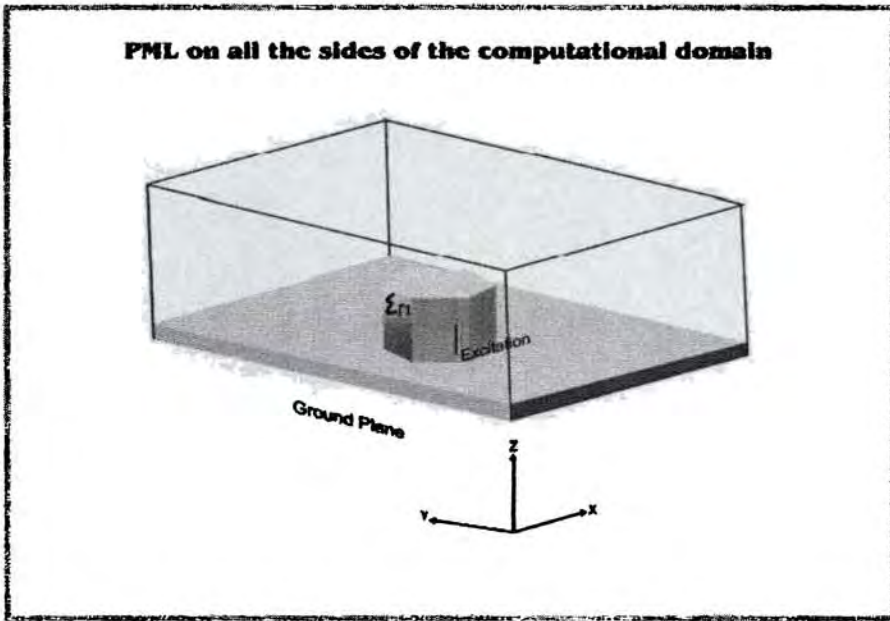


Fig.6.12 (a) The volume for which the FDTD simulation of coaxial fed HDRA is performed

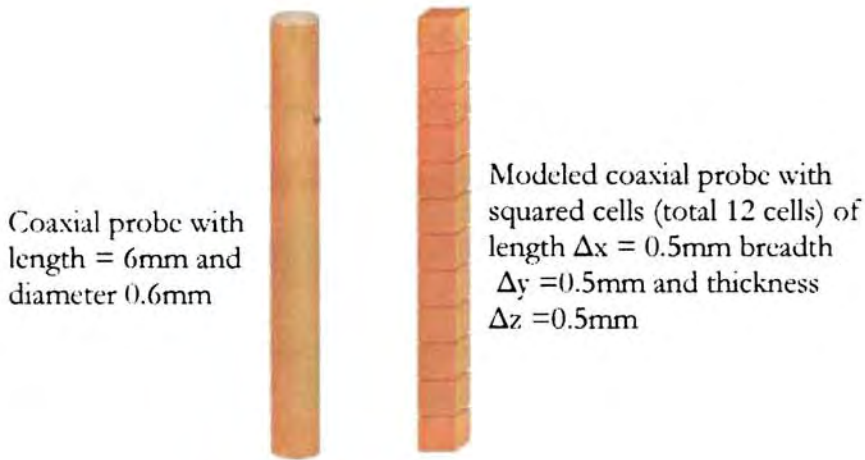


Fig.6.12 (b) FDTD modeled coaxial probe

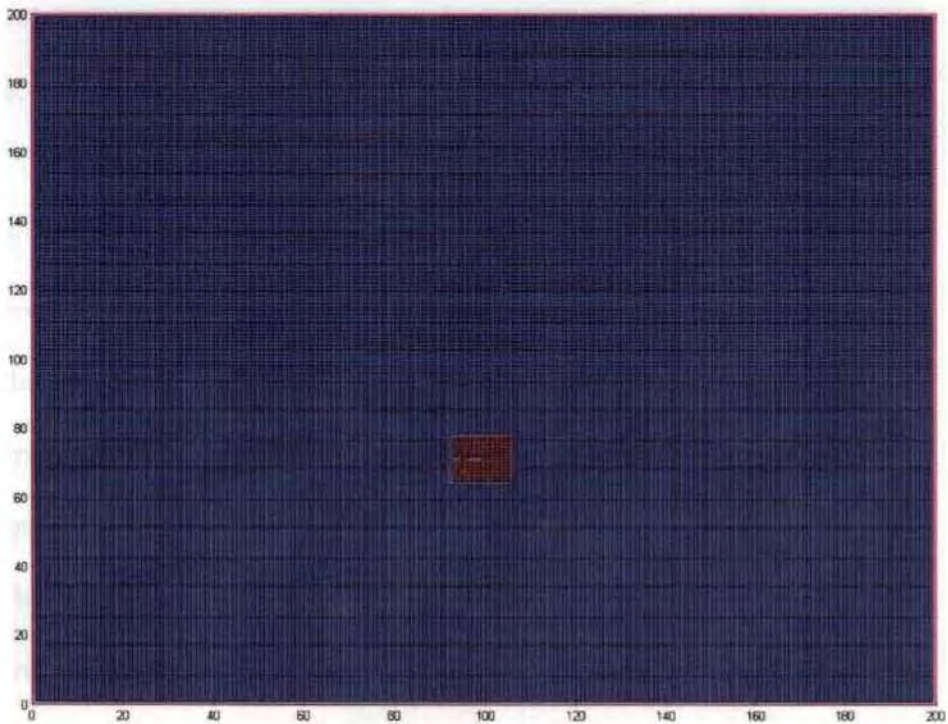
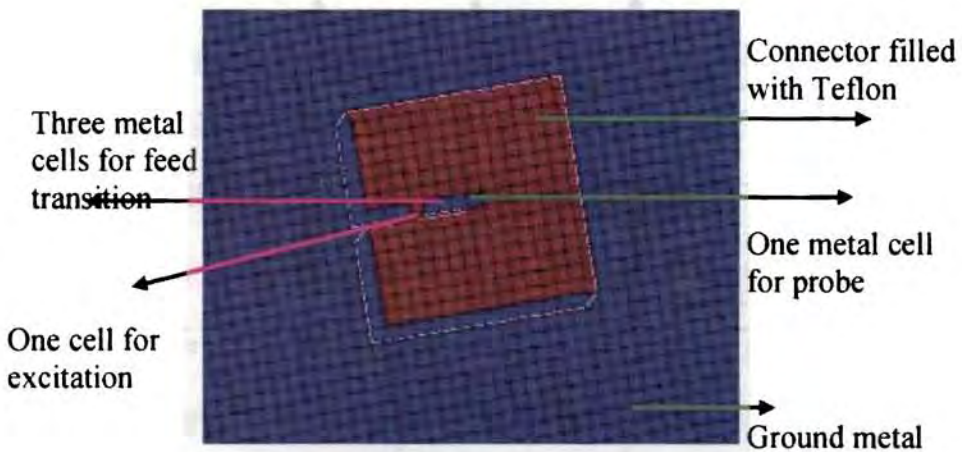


Fig.6.13 (a) connector is modeled on the ground plane with squared cells



**Fig.6.12 (b)** Expanded form of the SMA connector

#### 6.4.1 Modeling the materials

Modeling the whole structure consisting of ground plane metal, coaxial feed probe metal, dielectric material for DRA and free space is to be done. HDR has a relative dielectric constant of 69. Therefore the relationship between electric flux density and electric field is

$$e_x(i, j, k) = gax(i, j, k) * dx(i, j, k)$$

From equation 6.12,  $gax(i, j, k) = 1/69$  for DR. For metal, the E fields within those points corresponding to metal remain as zero. Suppose we are viewing the FDTD lattice under the antenna, looking in the X direction, is illustrated in **Fig. 6.13**. It is seen that the entire structure lays on a ground metal plane, and hence  $E_x$  and  $E_y$  values for  $k=1$  remains zero. Since the  $E_z$  values lays half cells above the  $k=1$  plane, it will be in the DR. Similarly for specifying the coaxial feed metal on the antenna

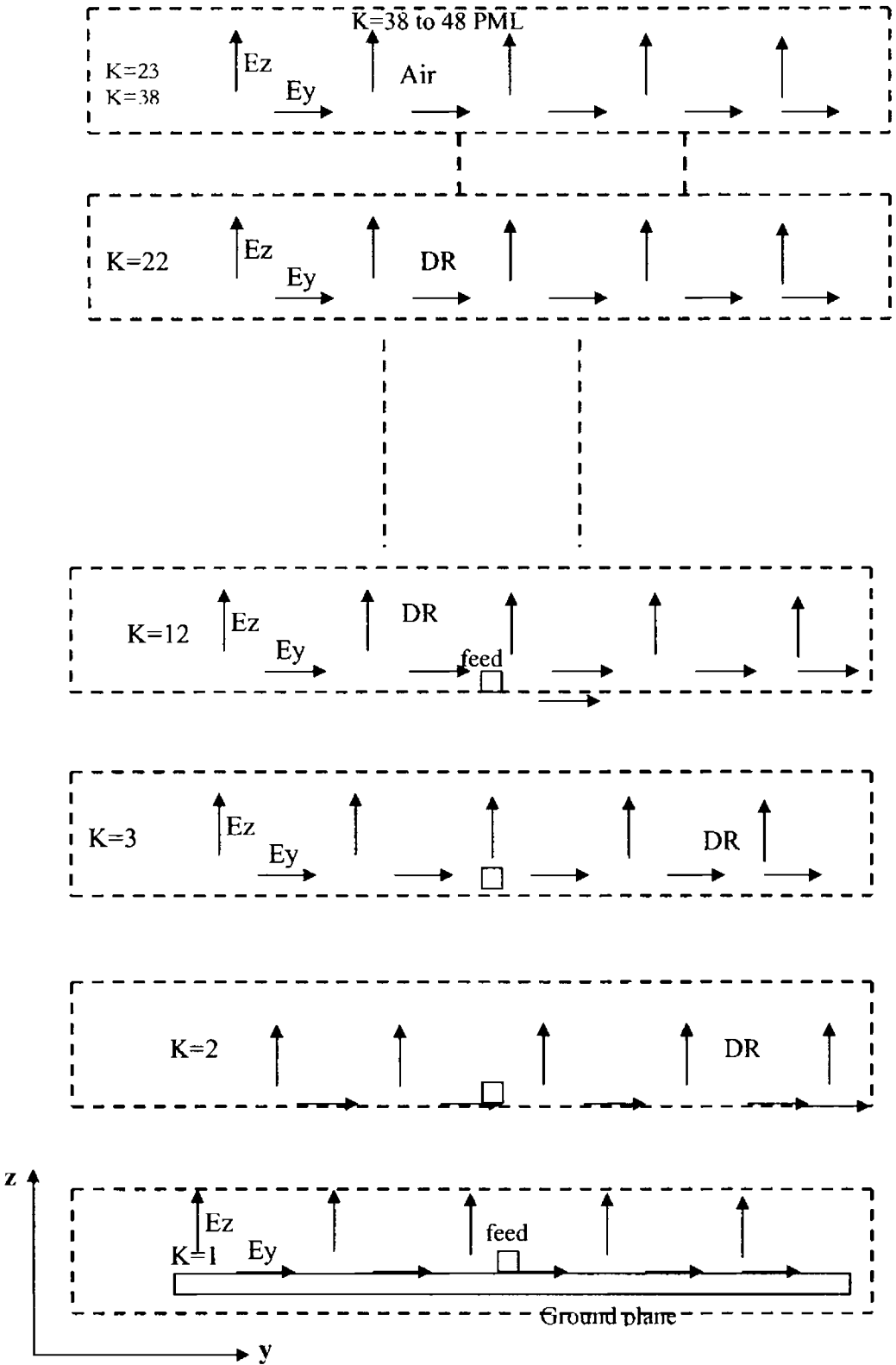


Fig. 6.13 Positions of E fields relative to the material being modeled.

starts from  $k=1$  to  $k=12$  with a thickness of one cell size,  $E_x$ ,  $E_y$  and  $E_z$  values corresponds to probe feed are set to zero, and the values around the probe corresponds to DR. Then upto  $k=22$  cells from  $k=1$ , the material is DR and hence set the appropriate values for  $g_{ax}$ ,  $g_{ay}$  and  $g_{az}$  for getting E fields. After 22 cells and around the HDR, the medium is air, and therefore set the appropriate values for  $g_{ax}$ ,  $g_{ay}$  and  $g_{az}$  for getting E fields corresponding to air. Also the permittivity of air-DR interface is given as the average of the two medium those cells are modeled appropriately. The return loss, incident and reflected voltage and currents are calculated and plotted similar to the microstrip fed DRA.

## **6.4.2 FDTD Results**

### **6.4.2.1 Calculation of Return loss**

The return loss variation of a coaxial fed HDRA is calculated in the same way as microstrip fed antenna as explained in the section 6.3.6.1. The source voltage and current calculations with a source resistance  $R_s = 50$  Ohms are shown in **Fig. 6.14**. The same Gaussian pulse  $V$  was used for both calculations. It takes only 1600 time steps to damp the voltages and currents and hence to cover the entire computational domain. Where as for the hard source, with no internal resistance, it takes more than 9000 time steps, and still the current has not completely dissipated.



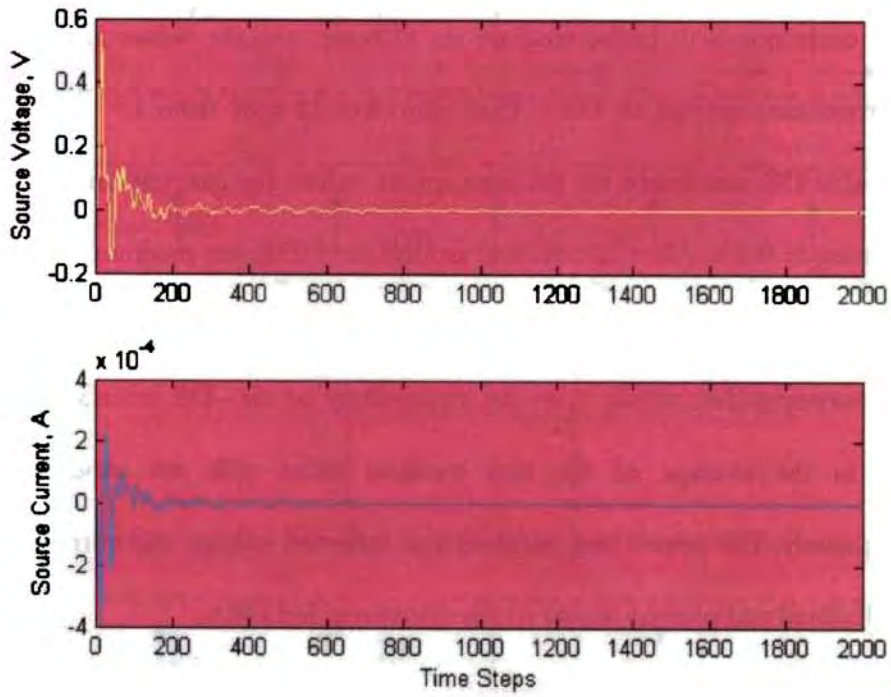


**Fig. 6.14** HDR Antenna source voltage  $V_s$  and Source current  $I_s$

The theoretical  $S_{11}$  plot along with the experimental one is shown in **Fig. 6.15**; it indicates that using FDTD the three resonances are obtained at 1.825GHz, 2.65 GHz and 3.318 GHz respectively.

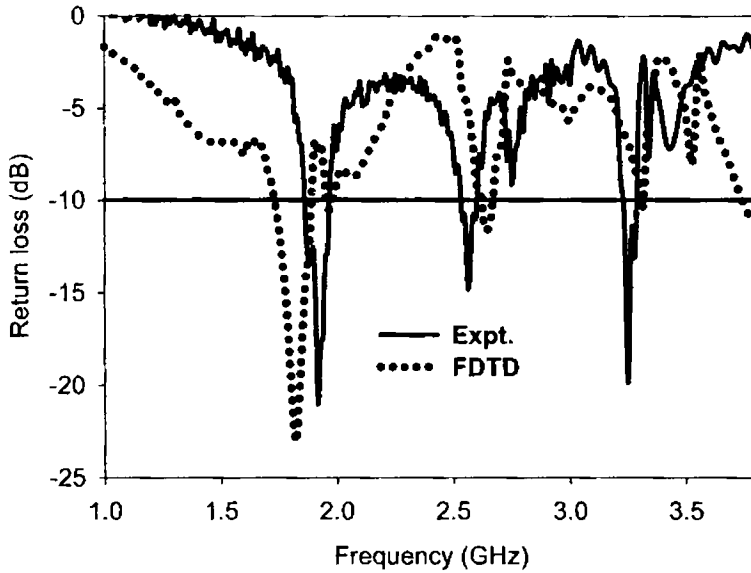


**Fig. 6.15** Return loss variation of coaxial probe fed HDRA- a comparison between theory and experiment

Table 6.2 shows the percentage of error in resonant frequencies between the FDTD and measured results. There is an error of 4.9%, 3.1% and 2.07% for the first, second and third resonant frequencies respectively.

Table 6.1: Comparison of resonant frequencies with theory and experimental results of coaxial fed HDRA

Antenna Position	FDTD method			Measured			% error FDTD & Experiment		
	Frequency (GHz)			Frequency (GHz)			f <sub>1</sub>	f <sub>2</sub>	f <sub>3</sub>
3	f <sub>1</sub>	f <sub>2</sub>	f <sub>3</sub>	f <sub>1</sub>	f <sub>2</sub>	f <sub>3</sub>	f <sub>1</sub>	f <sub>2</sub>	f <sub>3</sub>
	1.825	2.650	3.318	1.920	2.570	3.250	4.9	3.1	2.07

The error in this case is larger compared to microstrip fed HDRA due to the air gap between the coaxial probe and antenna, and the cylindrical coaxial probe is modeled with square probe. Fig. 6.16 (a) shows the FDTD

structure of coaxial fed IIDRA, Fig. 6.10 (b) shows the HDRA structure, and the slanted area of HDRA simulated using staircase approximation.

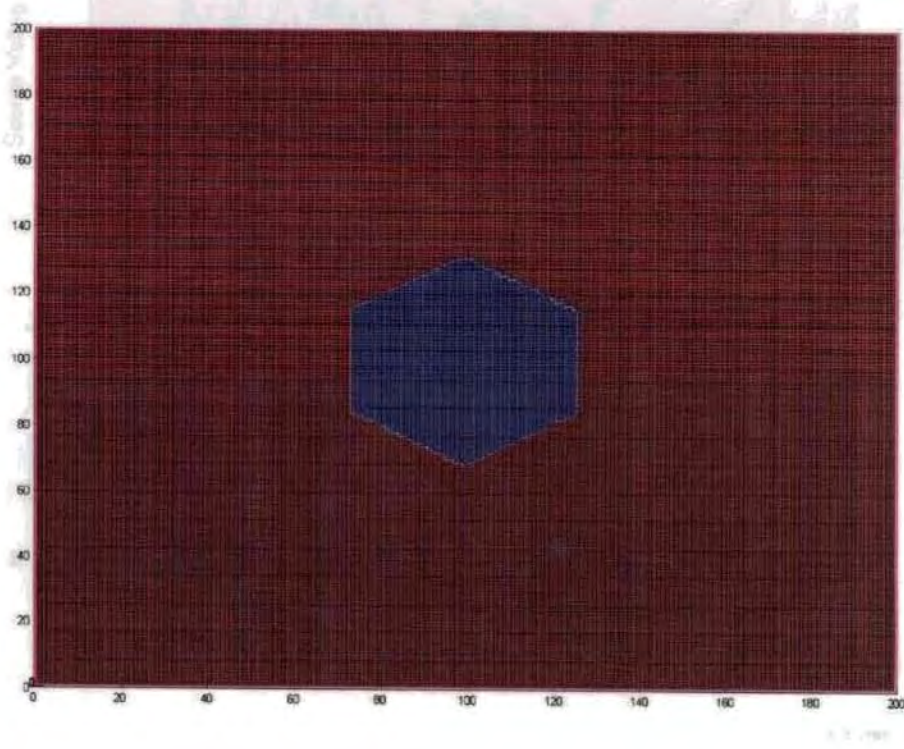


Fig. 6.16 (a)

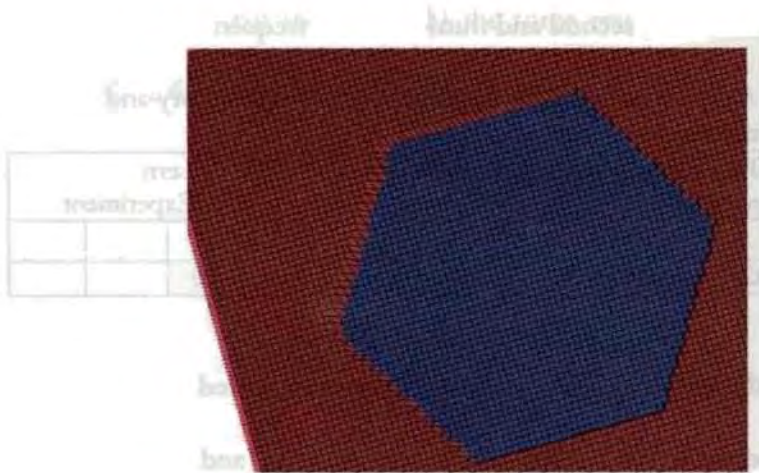


Fig. 6.16 (b)

Fig. 6.16 FDTD structure of coaxial fed IIDRA

## 6.5 Conclusion

This chapter explained the theoretical study of hexagonal dielectric resonator antenna using FDTD. The first part describes the development of FDTD equations for the antenna from basic Maxwell's curl equations. Here Perfect Matched Layer is used as Absorbing Boundary Condition. The FDTD modeling of Microstrip fed and Coaxial fed HDRA are described. A comparison between theoretical results with the measured results is also given.

## References

1. K. S. Yee, Numerical solution of initial boundary value problems involving Maxwell's equations in isotropic media, *IEEE Transactions on Antennas and Propagation*, vol. 14, pp. 302–307, Mar. 1966.
2. A. Taflove, Review of the formulation and applications of the finite-difference time domain method for numerical modeling of electromagnetic wave interactions with arbitrary structures, *Wave Motion*, vol. 10, no. 6, pp. 547–582, 1988.
3. K. L. Shlager and J. B. Schneider, Comparison of the dispersion properties of several Low-dispersion finite-difference time-domain algorithms, *IEEE Transactions on Antennas and Propagation*, vol. 51, pp. 642–653, Mar. 2003.
4. X. Zhang and K. K. Mei, Time domain finite difference approach to the calculation of the frequency dependent characteristics of microstrip discontinuities, *IEEE Trans. Microwave Theory Tech.*, vol. 36, pp. 1775-1787, Dec. 1988.
5. D. M. Sheen, S. M. Ali, M. D. Abouzahra, and J. A. Kong, Application of the three-dimensional finite-difference time-domain method to the analysis of planar microstrip circuits, *IEEE Trans. Microwave Theory Tech.*, vol. 38, pp. 849-857, July 1990.
6. Dennis M. Sullivan, *electromagnetic simulation using the FDTD method*, IEEE publishing press, 2000.
7. J.P. Berenger, A perfectly matched layer for the absorption of electromagnetic waves, *J. comput. Phys.*, Vol. 114, pp. 185-200, 1994.
8. D.M. Sullivan, A simplified PML for use with the FDTD method, *IEEE microw. And guided wave lettr.*, Vol.6, pp.97-99, Feb 1996.

9. D.M. Sullivan, An unsplit step 3D PMI. for use with the FDTD method, IEEE Microw. And guided wave lettr., Vol.7, pp.184-186, Jul 1997.
10. K. Kunz and R. Luebbers, The Finite Difference Time Domain Method for electromagnetics, Boca Rotan, FLCRC PRESS, pp.496, 1993.
- 11 R. Luebbers, L. Chen, T. Uno, and S. Adachi, FDTD calculation of radiation patterns, impedance, and gain for a monopole antenna on a conducting box, IEEE Trans. Antennas Propugat., vol. 40, pp. 1577-1583, Dec. 1992.
- 12 R.J Lubbers, and H.S Langdon, A simple feed model that reduces time steps needed for FDTD antenna and microstrip calculations, IEEE Trans. Antennas Propugat., vol. 44, pp. 1000-1004, July. 1996.

**FDTD code for D, E and H field with PML.**

```

% dz calculation for the three sections
% first PML
for i=2:IE
    for j=2:JE
        for k=2:ka-1
            curl_h=(ra_x*(hy(i,j,k)-hy(i-1,j,k))-ra_y*(hx(i,j,k)-hx(i,j-1,k)));
            idzl(i,j,k)=idzl(i,j,k)+curl_h;
            dz(i,j,k)=gi3(i)*gj3(j)*dz(i,j,k)+gi2(i)*gj2(j)*0.5*(curl_h+gk1(k)*i
            dzl(i,j,k));
        end
    end
end

% Problem space
for i=2:IE
    for j=2:JE
        for k=ka:kb
            curl_h=(ra_x*(hy(i,j,k)-hy(i-1,j,k))-ra_y*(hx(i,j,k)-hx(i,j-1,k)));
            dz(i,j,k)=gi3(i)*gj3(j)*dz(i,j,k)+gi2(i)*gj2(j)*0.5*curl_h;
        end
    end
end

% last PML

```

```

for i=2:IE
    for j=2:JE
        for k=kb+1:KE
            kzh=k-kb;
            curl_h=(ra_x*(hy(i,j,k)-hy(i-1,j,k))-ra_y*(hx(i,j,k)-hx(i,j-1,k)));
            idzh(i,j,kzh)=idzh(i,j,kzh)+curl_h;
            dz(i,j,k)=gj3(i)*gj3(j)*dz(i,j,k)+gj2(i)*gj2(j)*0.5*(curl_h+gk1(k)*i
            dzh(i,j,kzh));
        end
    end
end

```

Similarly for Dx and Dy is

```

% dx calculation for the three sections

% first PML

for i=2:ia-1
    for j=2:JE

        for k=2:KE
            curl_h=(ra_y*(hz(i,j,k)-hz(i,j-1,k))-hy(i,j,k)+hy(i,j,k-1));
            idxl(i,j,k)=idxl(i,j,k)+curl_h;
            dx(i,j,k)=gj3(j)*gk3(k)*dx(i,j,k)+gj2(j)*gk2(k)*0.5*(curl_h+gi1(i)
            *idxl(i,j,k));
        end
    end
end

% Problem space
for i=ia:ib
    for j=2:JE
        for k=2:KE
            curl_h=(ra_y*(hz(i,j,k)-hz(i,j-1,k))-hy(i,j,k)+hy(i,j,k-1));
            dx(i,j,k)=gj3(j)*gk3(k)*dx(i,j,k)+gj2(j)*gk2(k)*0.5*curl_h;

```

```

        end
    end
end
% last PML
for i=ib+1:IE
    ixh=i-ib;
    for j=2:JE
        for k=2:KE
            curl_h=(ra_y*(hz(i,j,k)-hz(i,j-1,k))-hy(i,j,k)+hy(i,j,k-1));
            idxh(ixh,j,k)=idxh(ixh,j,k)+curl_h;
            dx(i,j,k)=gi3(j)*gk3(k)*dx(i,j,k)+gj2(j)*gk2(k)*0.5*(curl_h+gj1(i)
            *idxh(ixh,j,k));
        end
    end
end

% dy calculation for the three sections
% first PML
for i=2:IE
    for j=2:ja-1
        for k=2:KE
            curl_h=(hx(i,j,k)-hx(i,j,k-1)-ra_x*(hz(i,j,k)-hz(i-1,j,k)));
            idyl(i,j,k)=idyl(i,j,k)+curl_h;
            dy(i,j,k)=gi3(i)*gk3(k)*dy(i,j,k)+gi2(i)*gk2(k)*0.5*(curl_h+gj1(j)
            *idyl(i,j,k));
        end
    end
end

% Problem space
for i=2:IE
    for j=ja:jb
        for k=2:KE
            curl_h=(hx(i,j,k)-hx(i,j,k-1)-ra_x*(hz(i,j,k)-hz(i-1,j,k)));
            dy(i,j,k)=gi3(i)*gk3(k)*dy(i,j,k)+gi2(i)*gk2(k)*0.5*curl_h;
        end
    end
end
end

```

```

% last PML
for i=2:IE
    for j=jb+1:JE
        jyh=j-jb;
        for k=2:KE
            curl_h=(hx(i,j,k)-hx(i,j,k-1)-ra_x*(hz(i,j,k)-hz(i-1,j,k)));
            idyh(i,jyh,k)=idyh(i,jyh,k)+curl_h;
            dy(i,j,k)=gi3(i)*gk3(k)*dy(i,j,k)+gi2(i)*gk2(k)*0.5*(curl_h+gj1(j)
            *idyh(i,jyh,k));
        end
    end
end
end

```

Calculation of Ex, Ey and Ez from Dx, Dy and Dz is

```

for i=2:IE
    for j=2:JE
        for k=2:KE

            ex(i,j,k)=gax(i,j,k)*dx(i,j,k);
            ey(i,j,k)=gay(i,j,k)*dy(i,j,k);
            ez(i,j,k)=gaz(i,j,k)*dz(i,j,k);

        end
    end
end

```

similarly for Hx, Hy and Hz is

```

%**** ***** Calculation of H fields %*****

```

```

% Calculation of Hx
%1st PML
for i=1:ia-1
    for j=1:JE-1
        for k=1:KE-1
            curl_e=(ey(i,j,k+1)-ey(i,j,k)-ra_y*(cz(i,j+1,k)-cz(i,j,k)));
            ihxl(i,j,k)=ihxl(i,j,k)+curl_e;

```



```

hx(i,j,k)=fj3(j)*fk3(k)*hx(i,j,k)+fj2(j)*fk2(k)*0.5*(curl_e+fi1(i)*i
hxl(i,j,k));

```

```

    end
  end
end

```

```

    % problem space
  for i=ia:ib
    for j=1:JE-1
      for k=1:KE-1
        curl_e=(ey(i,j,k+1)-ey(i,j,k)-ra_y*(ez(i,j+1,k)-ez(i,j,k)));
        hx(i,j,k)=fj3(j)*fk3(k)*hx(i,j,k)+fj2(j)*fk2(k)*0.5*curl_e;

        end
      end
    end
  end
end

```

```

    % 2Nd pml
  for i=ib+1:IE-1

    ixh=i-ib;
    for j=1:JE-1
      for k=1:KE-1
        curl_e=(ey(i,j,k+1)-ey(i,j,k)-ra_y*(ez(i,j+1,k)-ez(i,j,k)));
        ihxh(ixh,j,k)=ihxh(ixh,j,k)+curl_e;
        hx(i,j,k)=fj3(j)*fk3(k)*hx(i,j,k)+fj2(j)*fk2(k)*0.5*(curl_e+fi1(i)*i
        hxh(ixh,j,k));

        end
      end
    end
  end
end

```

```

    % Calculation of Hy
    %1st PML

```

```

  for i=1:IE-1
    for j=1:ja-1
      for k=1:KE-1

```

```

curl_e=(ra_x*(ez(i+1,j,k)-ez(i,j,k))-ex(i,j ,k+1)+ex(i,j,k));
ihyl(i,j,k)=ihyl(i,j,k)+curl_e;
hy(i,j,k)=fi3(i)*fk3(k)*hy(i,j,k)+fi2(i)*fk2(k)*0.5*(curl_e+fj1(j)*i
hyl(i,j,k));

```

```

    end
  end
end

```

```

% problem space

```

```

for i=1:IE-1

```

```

    for j=ja:jb

```

```

        for k=1:KE-1

```

```

curl_e=(ra_x*(ez(i+1,j,k)-ez(i,j,k))-ex(i,j,k+1)+ex(i,j,k));
hy(i,j,k)=fi3(i)*fk3(k)*hy(i,j,k)+fi2(i)*fk2(k)*0.5*curl_e;

```

```

        end
    end
end

```

```

% 2nd PML

```

```

for i=1:IE-1

```

```

    for j=jb+1:JE-1

```

```

        jyh=j-jb;

```

```

        for k=1:KE-1

```

```

curl_e=(ra_x*(ez(i+1,j,k)-ez(i,j,k))-ex(i,j ,k+1)+cx(i,j,k));
ihyh(i ,jyh,k)=ihyh(i ,jyh,k)+curl_e;
hy(i,j,k)=fi3(i)*fk3(k)*hy(i,j,k)+fi2(i)*fk2(k)*0.5*(curl_e+fj1(j)*i
hyh(i,jyh,k));

```

```

        end
    end
end

```

```

% Calculation of Hy

```

```

%1st PML

```

```

for i=1:IE-1
    for j=1:JE-1
        for k=1:ka-1
            curl_e=(ra_y*(ex(i,j+1,k)-ex(i,j,k))-ra_x*(ey(i+1,j,k)-ey(i,j,k)));
            ihzl(i,j,k)=ihzl(i,j,k)+curl_e;
            hz(i,j,k)=fi3(i)*fj3(j)*hz(i,j,k)+fi2(i)*fj2(j)*0.5*(curl_e+fk1(k)*ih
            zl(i,j,k));

            end
        end
    end

    % Problem space
    for i=1:IE-1
        for j=1:JE-1
            for k=ka:kb
                curl_e=(ra_y*(ex(i,j+1,k)-ex(i,j,k))-ra_x*(ey(i+1,j,k)-ey(i,j,k)));
                hz(i,j,k)=fi3(i)*fj3(j)*hz(i,j,k)+fi2(i)*fj2(j)*0.5*curl_e;
                end
            end
        end

    % 2nd PML
    for i=1:IE-1
        for j=1:JE-1
            for k=kb+1:KE-1
                kzh=k-kb;
                curl_e=(ra_y*(ex(i,j+1,k)-ex(i,j,k))-ra_x*(ey(i+1,j,k)-ey(i,j,k)));
                ihzh(i,j,kzh)=ihzh(i,j,kzh)+curl_e;
                hz(i,j,k)=fi3(i)*fj3(j)*hz(i,j,k)+fi2(i)*fj2(j)*0.5*(curl_e+fk1(k)*ih
                zh(i,j,kzh));

                end
            end
        end
    end

```

## **Chapter VII CONCLUSION AND FUTURE SCOPE OF THE WORK**

---

Investigations on the return loss, impedance and radiation characteristics of the new geometry hexagonal shaped dielectric resonator antenna clearly shows that this antenna produces multifrequency with a single feed of excitation independent of the coaxial probe or microstrip line feed. The main highlights of the study and possible applications are discussed in the following section.

### **7.1 Highlights of the work**

1. A new geometry of hexagonal shape DRA is introduced to the DRA shape community.
2. The material used for the fabrication is easily available and cheap.
3. Produced triple frequency resonances with coaxial feed excitation with moderate bandwidth, good radiation pattern and gain.
4. Excitation of three frequencies simultaneously with a single antenna facilitates the replacement of three individual antennas thereby miniaturization of the whole system.
5. Produced dual frequency with microstrip feed excitation with bandwidth suitable for DCT, almost all frequencies of PCS and WLAN applications. Radiation patterns also promising for

vehicular and broad pattern applications. Antenna exhibits good gain at both the bands.

6. Gain of HDRA is high compared to other shapes.
7. Efficiency of HDRA is around 98%
8. The theoretical FDTD results are in good agreement with experimental results in the case of microstrip HDRA. Where as there is slightly higher error in the results with the coaxial probe excitation, which is due to the air gap between the coaxial probe and HDRA during the experiment that is practically unavoidable.

## **7.2 Possible applications**

The HDRA find application in Personal Communication Systems (PCS), Digital Cordless Telephones (DCT), Wireless Local Area Networks (WLAN) and other wireless communications.

## **7.3 Scope of future work**

The new geometry hexagonal DRA is attractive due to its multiple resonances with a single feed of excitation. The scope of future work is

1. Effect of different material composition on the performance of HDRA.
2. Use two feeds simultaneously and test the validity of the HDRA for circular polarization.
3. Study the characteristics of the antenna with metal coating.
4. Size miniaturization using semi hexagonal DRA and sector HDRA.
5. Effect of other excitation methods on the performance of HDRA.

## 6. Bandwidth Enhancement

### 7.4 Concluding remarks

The development and analysis of novel geometry hexagonal shaped dielectric resonator antenna have been carried out in this thesis. The dependence of resonant frequency and radiation characteristics with the aspects ratio, coaxial feed location and microstrip feed excitation has been investigated and optimized. It is observed that the new antenna produces multiple frequencies with a single feed of excitation and hence find application as an ideal substitute for multifrequency wireless antennas.

## APPENDIX-A

### A MULTI- FREQUENCY COAXIAL FED METAL COATED DIELECTRIC RESONATOR ANTENNA

---

*A simple metal-coated dielectric resonator antenna with a coaxial feed producing multiple frequencies is reported. The characteristics of the antenna at all these frequencies are measured. The experimental result shows that, antenna produces broad patterns at all the operating frequencies. This antenna finds applications in frequency agile systems.*

#### **A-1 Introduction**

Dielectric resonator antennas (DRAs) have been of interest during the past few years due to its low loss, high permittivity, small size and broad beam characteristics. Ever since the development of direct fed coaxial probe DR antenna by S.A. Long et.al [1], various researchers had experimented the DR antenna coupling with microstrip lines [2]. The study on the input impedance characteristics of coaxial fed DRAs reveals that the peripheral coupling is most suited for effective radiation [3]. Recently, many investigators have reported dual-frequency operation using various methods, such as hybrid DRA with radiating slot, two microstrip feed and two feed slot-fed DRA [4]–[6]. Multiple frequencies using annular slot antenna and planar antenna were also reported [7]-[8]. However, these methods increase the size and the weight of DRAs and lead to complex

fabrication process. In this paper a single coaxial feed metal-coated dielectric resonator antenna (MDRA) with three 2:1 VSWR bands operating at 1.46GHz, 2.41GHz and 3.23GHz resonant frequencies are presented.

## A-2 Antenna structure

The multi frequency antenna structure is shown in **Fig 1**. The antenna is coated with a metal on the top surface of the dielectric resonator (DR) with a circular slot (opening) having 5mm diameter (2b) at the center as shown in the figure. The DR consists of a cylindrical block of ceramic material with permittivity  $\epsilon_r \sim 36$  and aspect ratio of less than unity (diameter  $2a = 27$  mm and length  $l = 12$  mm). The probe feed length is 5 mm for optimum matching. The DR is mounted on a ground plane having 170 mm diameter. The experimental set up consists of an HP 8510 C Network analyzer.

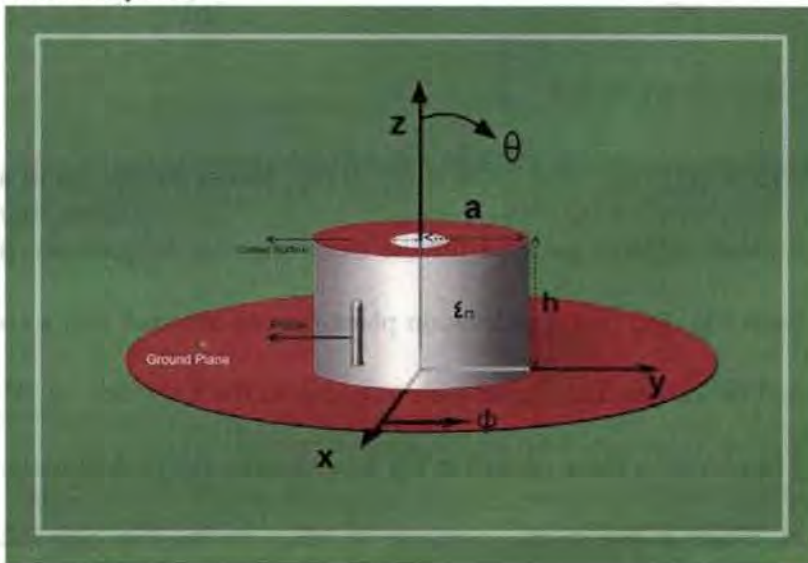


**Fig. 1** Antenna Structure



### A-3 Experimental results

Measured return loss is shown in **Fig. 2**. The experimental operating frequencies are centered at 1.46GHz, 2.41GHz and 3.23 GHz with 2:1 VSWR bandwidth of 1.489, 0.26 and 0.71% respectively.

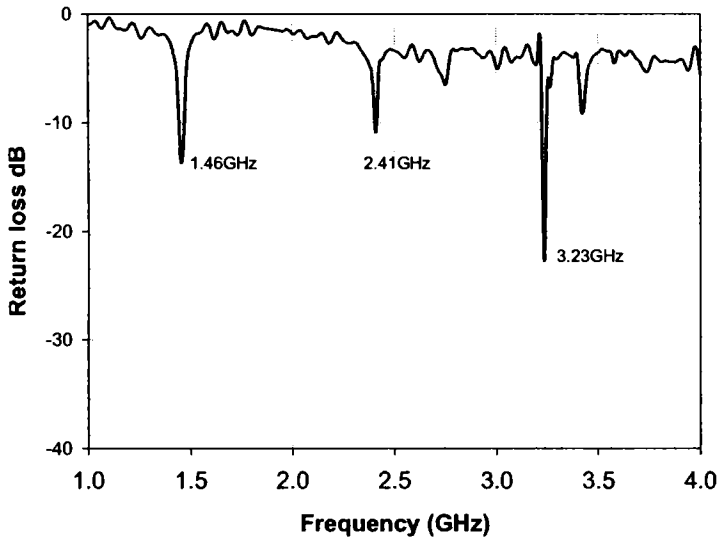


**Fig. 2** Measured return loss

Figs. 3 (a), 4 (a), 5 (a) and 3 (b), 4 (b), 5 (b) shows the elevation and azimuth plane radiation patterns for the three resonant frequencies. It is found from Fig. 3(a) that the elevation plane pattern is broad with a cross polar level of -20dB. This broad pattern is due to the excitation of HE<sub>116</sub> mode. The elevation plane pattern in Fig 4 (a) shows a dip in the broadside direction, which is due to the excitation of HE<sub>126</sub> mode. Fig. 5(a) shows almost broad pattern which is due to the excitation of HE<sub>136</sub> mode. The

half power beam widths (HPBW) are found to be  $76^\circ$ ,  $65^\circ$  and  $23^\circ$  at Elevation plane and  $64^\circ$ ,  $50^\circ$  and  $38^\circ$  at azimuth plane respectively against the frequencies 1.46, 2.41 and 3.23GHz. Table 1 summarises the measured results of the antenna.

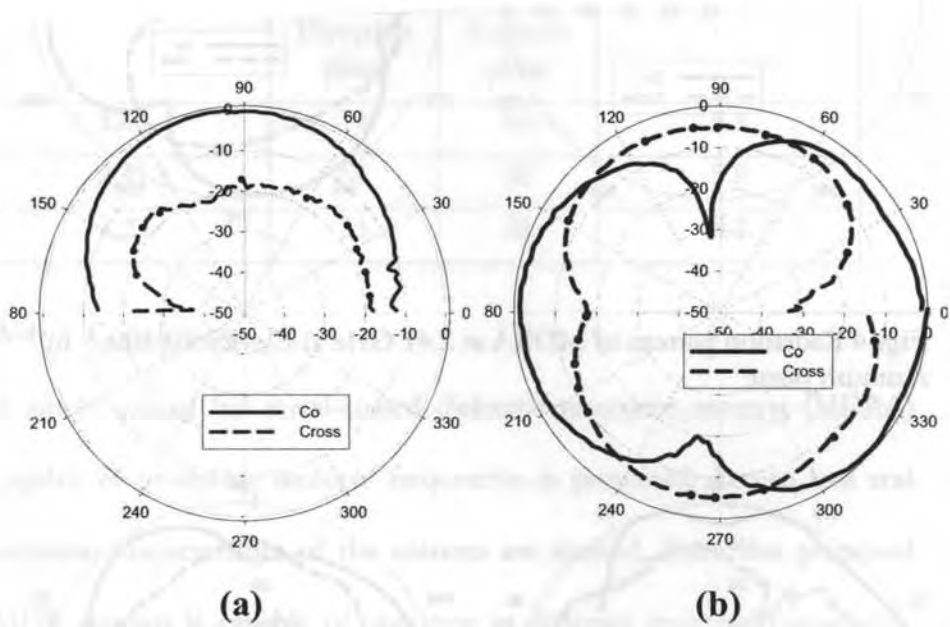


**Fig. 3** Radiation pattern of MDRA at 1.46 GHz a) Elevation plane (b) azimuth plane

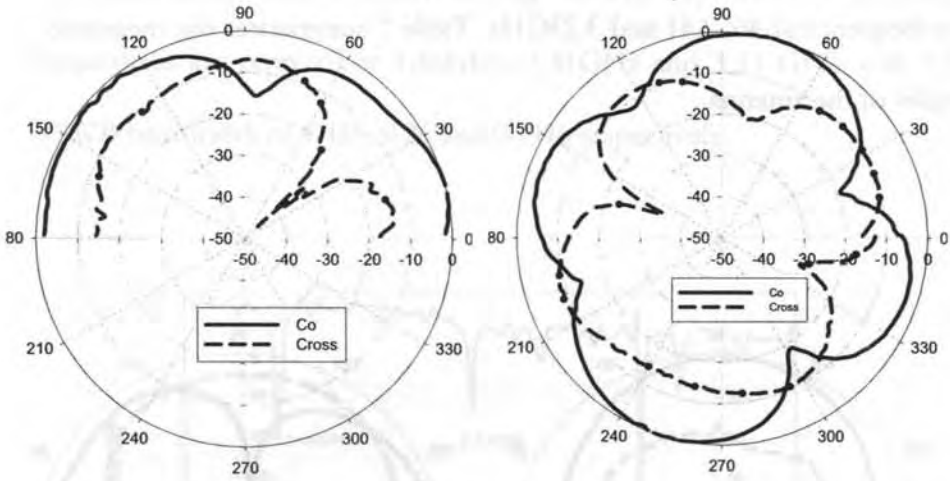


**Fig. 4** Radiation pattern of MDRA at 2.41 GHz a) Elevation plane b) Azimuth plane

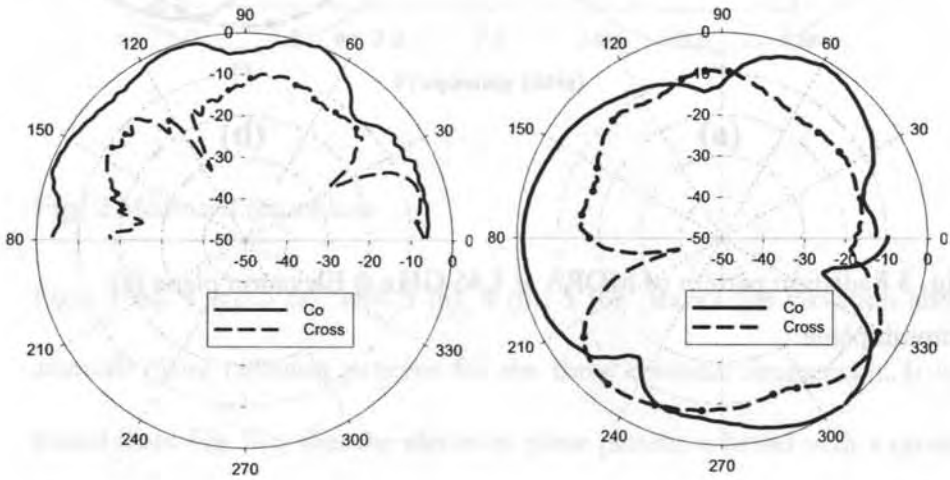


**Fig. 5** Radiation pattern of MDRA at 3.23 GHz a) Elevation plane b) Azimuth plane

Gain of the antenna is measured and the average gain is found to be 5.3dBi, 5.8dBi and 6.2dBi respectively at 1.46 GHz, 2.41GHz and 3.23GHz frequencies.

**Table 1** Characteristics of multi-frequency antenna

Operating frequency (GHz)	Measured (HPBW) in degrees		Average gain (dBi)
	Elevation plane	Azimuth plane	
1.46	74	64	5.3
2.41	65	50	5.8
3.23	23	38	6.2

#### A-4 Conclusion

A single coaxial fed metal-coated dielectric resonator antenna (MDRA) capable of producing multiple frequencies is presented. Return loss and radiation characteristics of the antenna are studied. Since this proposed MDR antenna is capable of operating at different resonant frequencies, individual antennas operating at these frequencies can be replaced by the above MDR antenna and find applications in frequency agile systems.

#### References

1. S. A. Long, M. W. McAllister, and L. C. Shen, The resonant cylindrical dielectric cavity antenna, *IEEE Trans. on Antennas and Propagation*, Vol. 31, pp. 406-412, 1983.
2. R. A. Kranenburg, and S. A. Long, Microstrip transmission line excitation of dielectric resonator antennas, *IEE Electronic Letters*, vol. 24, pp. 1156-1157, 1988.
3. G. P. Junker, A. A. Kishk, and A. W. Glisson, Input impedance of dielectric resonator antennas excited by a coaxial probe, *IEEE Trans. on Antennas and Propagation*, Vol. 42, pp. 960-965, 1994.

4. Tayeb A. Denidni, and Qinjiang Rao, Hybrid Dielectric Resonator Antennas With Radiating Slot for Dual-Frequency Operation, IEEE Antennas and wireless propagation letters, Vol. 3, pp. 321-323, 2004.
5. Y. Sung, C. S. Ahn, and Y.-S. Kim, Microstrip line fed dual frequency dielectric resonator antenna, Microwave and optical technology Letters, vol. 42, pp. 388-390, 2004.
6. Tayeb A. demidhi, qinjiang Rao, and abdel r. Sebak, Two-Ring slot-fed dielectric resonator antenna for dual frequency operation, Microwave and optical Technology Letters, Vol. 44, pp. 448-453, 2005.
7. Hooman Tehrani, and Kai Chang, A Multi-frequency Microstrip-fed Annular Slot Antenna, IEEE Int. APS Symp. Dig., pp. 632-635, 2000.
8. R.K. Raj, M. Joseph, B. Paul and P. Mohanan, Compact planar multiband antenna for GPS, DCS, 2.4/5.8 GHz WLAN applications, IEE Electronic letters, Vol. 41, pp. 3-4, 2005.

## **APPENDIX-B**

### **COUPLING MEDIUM FOR MICROWAVE MEDICAL IMAGING APPLICATIONS**

---

*An exhaustive study of the dielectric properties of sodium meta silicate (SMS) gel at the S band of the microwave frequencies is carried out using cavity perturbation technique. Dielectric parameters such as dielectric constant, dielectric loss, conductivity, heating coefficient and absorption coefficient are determined for gel samples of different relative density (RD) and pH value. It is observed that different combinations can achieve dielectric constants between 8 and 20, which matches well with the dielectric properties of various biological tissues. The material can find application as an efficient coupling medium and phantom model in microwave medical imaging.*

#### **B-1 Introduction.**

Microwave medical tomography is emerging as a novel non-hazardous method of imaging for the detection of tumours. This is efficient and beneficial mainly in the case of soft tissues [1]. Recently there has been intense research to develop a viable system for microwave medical tomography [2]. A prototype of the tomographic set up for active imaging of the breast has been developed and tested [3]. In all these systems the object to be imaged is placed at the centre of a chamber and the scattered microwave data from the sample is collected and analysed at the various locations of the receiver and the orientations of the object. Suitable

coupling media like water and saline solution have been in use for enhancing the coupling of electromagnetic energy as well as increasing the resolution. The dielectric constant of these conventionally used coupling media is the same and exhibits a high contrast with that of the different biological tissues. It has been reported that the ability to image internal structures and abnormalities can be considerably enhanced by reducing reflections at the surface by the use of a coupling medium matched to the tissue under study [3]. Besides, by employing media like water and saline, a better resolution and coupling is obtained only at the cost of large power loss within the coupling medium. Hence, the development of a suitable coupling medium, with appropriate surface dielectric properties of the various biological objects and low loss than the conventionally used medium is important. Also, the pursuit of a suitable and cost-effective material for developing phantom models of biological tissues or organs has been an active research area in microwave tomography. This work presents a study of the variation of dielectric properties of sodium meta silicate (SMS) gel with different concentration of SMS solution and oxalic acid. Gels are systems with two or more components; phases may show solid-like behaviour with respect to some components, but liquid-like behaviour with respect to others. The selective dielectric nature of this material is an attractive feature in using it as a coupling medium and phantom model in microwave medical tomographic applications.

**B-2 Sample preparation**

A definite amount of SMS powder is mixed with distilled water and its specific gravity/ relative density (RD) is calculated. A graph is drawn with RD as the Y intercept and the partial volume of distilled water as the X intercept. The gel formation occurs when RD of SMS solution is between 1.01 and 1.07. The exact amount of distilled water and SMS solution required for preparing SMS gel samples of various RD is found from the graph. One molar oxalic acid in distilled water is prepared, sterilized and filtered. The filtered SMS solution is mixed with oxalic acid for obtaining solutions of different pH value.

**B-3 Experimental Set up and Procedure**

The experimental set-up consists of a transmission type S-band rectangular cavity resonator, HP 8714 ET network analyzer and an interfacing computer [4] as shown in **Figs 1 and 2**. The cavity resonator is excited in the  $TE_{10p}$  mode. Initially, the resonant frequency  $f_0$  and the quality factor  $Q_0$  of each resonant peak of the cavity resonator with the empty sample holder placed at the maximum of electric field are determined. The sample holder is designed in the form of a capillary tube flared to a disk shaped bulb to facilitate its entry and easy movement through the cavity slot. The gel sample taken in the holder is introduced into the cavity resonator through the non-radiating slot. For a resonant frequency of the sample-loaded cavity, the position of the sample is



adjusted for maximum perturbation (i.e. maximum shift of resonant frequency with minimum amplitude for the peak). The new resonant frequency  $f_s$  and the quality factor  $Q_s$  are determined. The dielectric parameters at this frequency are calculated. The procedure is repeated for other resonant frequencies.

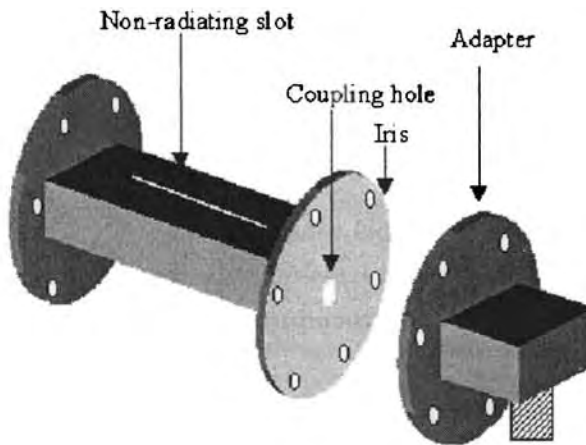


**Fig. 1** Schematic diagram of the cavity resonator

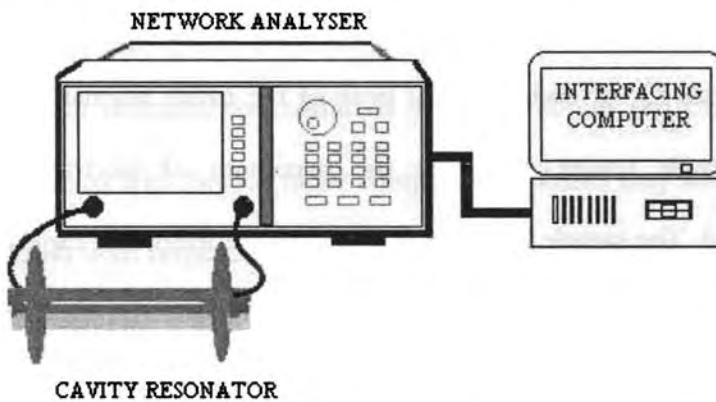


**Fig. 2** Network analyzer interfaced with cavity and computer

#### B-4 Theory

According to the theory of cavity perturbation [4], the real and imaginary parts of the complex permittivity are given as

$$\epsilon_r' - 1 = \frac{f_o - f_s}{2f_s} \left( \frac{V_c}{V_s} \right) \quad (1)$$

$$\epsilon_r'' = \frac{V_c}{4V_s} \left( \frac{Q_o - Q_s}{Q_o Q_s} \right) \quad (2)$$

Here,  $\bar{\epsilon}_r = \epsilon_r' - j\epsilon_r''$ ,  $\bar{\epsilon}_r$  is the relative complex permittivity of the sample,  $\epsilon_r'$  is the real part of the relative complex permittivity, which is known as dielectric constant.  $\epsilon_r''$  is the imaginary part of the relative complex permittivity associated with the dielectric loss of the material.  $V_s$  and  $V_c$  are the volumes of the sample and the cavity resonator respectively. The conductivity can be related to the imaginary part of the complex dielectric constant as

$$\sigma = \omega\epsilon'' = 2\pi f \epsilon_0 \epsilon_r'' \quad (3)$$

The heating coefficient J [5] is defined by

$$J = \frac{1}{\epsilon_r' \tan \delta} \quad (4)$$

Where  $\tan \delta$  is the loss tangent.

The absorption coefficient  $\alpha$  [5] of the material is given by

$$\alpha = \frac{\pi \epsilon_r'' f_0}{nc} \quad (5)$$

Where 'n' is the real part of the complex refractive index given by  $n = \sqrt{\epsilon_r^*}$ , and c is the velocity of light in free space.

### B-5 Results and discussion

The real and the imaginary parts of the complex dielectric permittivity of SMS gel with various RD and pH values at different frequencies are given in **Table 1**. It is observed that the selective range of dielectric constant is in conformity with those standard values for various tissues [6] as illustrated in **Table 2**. Hence it is a suitable material for making phantom models of corresponding biological tissues.

The conventional coupling media such as water and saline used for microwave medical imaging presents the same dielectric constant while used in various object environments. This results in different degrees of coupling electromagnetic energy to the object. One of the important factors on which the clarity of the reconstructed image depends is the scattered data obtained at the receivers, which in turn depends on the energy coupled to the object. Hence an efficient coupling medium should have a dielectric constant as close as that of the object. The selectivity of the dielectric constant due to the variation of RD and pH enables the material to be used as a very good coupling medium suitable for the various imaging tissues.

**Table 1** Real and imaginary parts of the complex dielectric permittivity of SMS Gel at S band

SMS gel		Frequency (GHz)	$\epsilon_r'$	$\epsilon_r''$
RD	pH			
1.01	4.5	2.24	8.21	0.608000
		2.44	8.38	0.586300
		2.68	8.69	0.586303
		2.97	8.54	0.594818
1.05	5	2.24	12.6	1.72000
		2.44	12.6	1.83329
		2.68	12.8	1.86790
		2.97	13.3	1.99851
1.069	3	2.24	13.5	1.82000
		2.44	11.8	2.02901
		2.68	13.1	1.98200
		2.97	14.4	2.25875
1.069	4.5	2.24	15.9	2.22000
		2.44	16.6	2.14058
		2.68	14.8	1.93403
		2.97	15.5	2.01196
1.02	3.5	2.24	14.7	2.83000
		2.44	17.2	3.15067
		2.68	16.5	2.84825
		2.97	17.3	2.76868
1.01	3	2.24	18.0	1.72000
		2.44	16.0	1.61759
		2.68	18.1	1.71305
		2.97	16.7	1.63445

**Table 2** Comparison between dielectric constants of various biological tissues and SMS gel

Biological Tissues	Frequency (GHz)	$\epsilon_r'$	SMS gel	
			RD	pH
Bladder, Human	2.07	16.5	1.069	4.5
	2.412	16.3		
	3.1	16.1		
Breast Fat, Human	3.2	9.8	1.01	4.5
Fat(Average Infiltrated), Ovine	1.08	9.71	1.01	4.5
	3.99	8.84		
Bone, Cancellous, Human	2.07	17.6	1.02	3.5
	2.53	17.38		
	3.10	17.14		
Bone, Cortical, Ovine	2.18	11.78	1.05	5
	2.67	11.54		
	3.26	11.299		
Lung inflated, Ovine	2.07	20.09	1.01	3
	2.95	19.59		
Bone, cortical, Human	2	8.4	1.01	4.5
	3	8.35		
Skull, Ovine	1.08	12.44	1.05	5
	3.99	10.96		
Bone marrow (infiltrated), Ovine	3.99	7.9	1.01	4.5
Bone Cancellous, Ovine (skull)	1.2	19.31	1.01	3
	4	17.76		
Bone marrow(Infiltrated), Calf (femur and tibia)	1	18.0	1.01	3

It is evident from table 1 that the dielectric loss factor of the proposed material is only around 2, while it is around 10 for the conventionally used coupling media viz. water at ISM band. The variation of conductivity with frequency is as shown in **Fig. 3**. It is observed that

the conductivity is consistent through out the band and so the material can be an effective coupling medium in multi-frequency imaging. Also the conductivity is found to be lesser than that of water, which indicates that the SMS gel samples are more efficient in coupling electromagnetic energy.

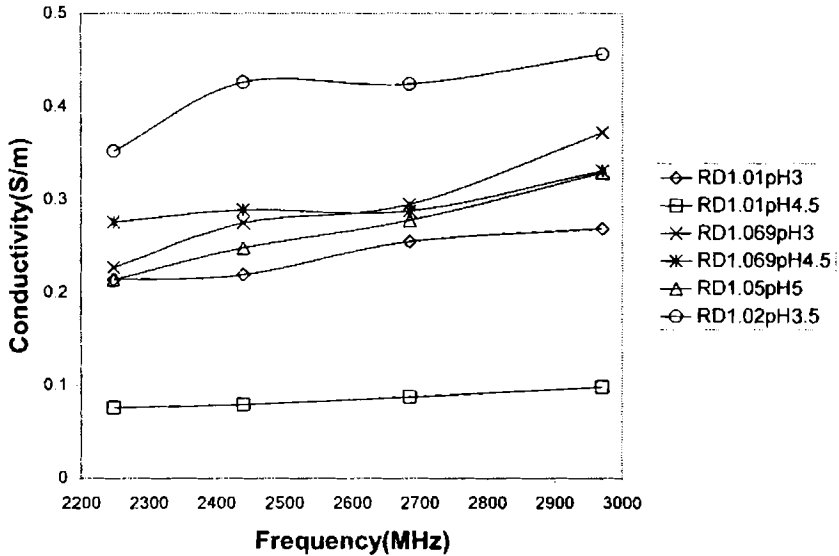


**Fig. 3** Variation of conductivity ( $\sigma$ ) with frequency

Variation of heating coefficient ( $\beta$ ) with frequency for different samples, which depicts the loss of energy due to dielectric heating, is as shown in **Fig 4**. Lower value of heating coefficient than that of water is indicative of more efficient transmission of energy through the medium.

Variation of absorption coefficient ( $\alpha$  in  $m^{-1}$ ) with frequency is shown in **Fig.5**. The absorption coefficient of a material is a measure of the transparency of the electromagnetic wave through it. The material shows a lower value of the coefficient indicating a better coupling of energy.

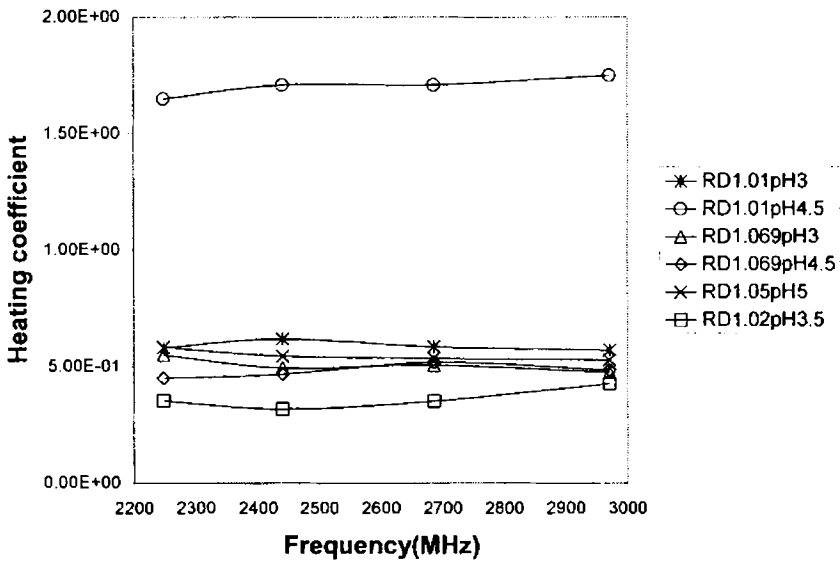


Fig. 4 Variation of heating coefficient ( $J$ ) with frequency

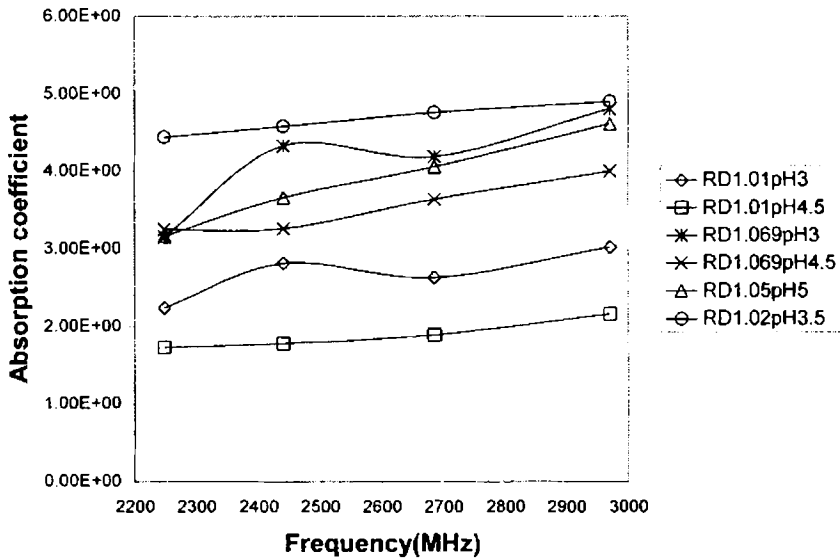


Fig. 5 Variation of absorption coefficient ( $\alpha$ ) with frequency

**B-6 Conclusion**

A study of dielectric properties of SMS gel at microwave frequencies (S band) is carried out. The dielectric constants are found to be in match with that of the various biological tissues. The properties of selectivity of dielectric constant coupled with low dielectric loss, conductivity, heating coefficient and absorption coefficient enable this material to be a very good coupling medium as well as a proper phantom model constituent for imaging purposes. The fact that the material can be easily prepared, cheap and non-toxic makes it an ideal candidate in microwave medical tomographic applications.

Besides, microwave medical tomography is promising as a novel non-hazardous method of imaging for the detection of tumors in soft tissues. The tomographic set up consists of antennas, coupling media and the object to be imaged. The antenna must be operated at ISM frequency. The purpose of coupling media is to enhance the coupling of electromagnetic energy between the antenna and the object to be imaged. The object is placed at the center of the imaging set up from where the scattered microwave data is collected and analyzed at the various locations of the receiver and the orientation of the object. As the HDRA antenna developed in the core work of the thesis operates at 2.4GHz-ISM frequency, with compact structure and low losses, it can be well used in tomographic set up as well.



## **References**

1. E.C. Fear, et al., Enhancing breast tumor detection with near-field imaging, *IEEE Microw. Mag.*, vol.3, pp. 48–56, 2002.
2. S.Y., Semanov et al., Three dimensional microwave tomography: experimental imaging of phantoms and biological objects, *IEEE Trans. Microw. Theory Tech.*, Vol. 48, pp. 1071–1074, 2000.
3. P.M., Meaney et al., A clinical prototype for active microwave imaging of the breast, *IEEE Trans. Microw. Theory Tech.*, Vol. 48, pp. 1841– 853, 2000.
4. K.T., Mathew and Raveendranath U., *Sensors update Wiley-VCH, Germany*, Vol. 7, pp. 185–210, 1999.
5. K.T. Mathew, S. Biju Kumar, Anil Lonappan, Joe Jacob, Thomas Kurian, Jacob Samuel and Thommachan Xavier, *Materials Chem. and Phy.*, Vol. 79, pp.187–190, 2002.
6. S., Gabriel, R.W., Lau, and C., Gabriel, The dielectric properties of biological tissues: II. Measurements in the frequency range 10 Hz to 20 GHz, *Phys. Med. Biol.*, vol. 41, pp. 2251–2269, 1996.

## PUBLICATIONS

## INTERNATIONAL JOURNALS

1. **V. Hamsakutty**, A.V. Praveen Kumar, Jaimon Yohannan, K. T. Mathew, "Hexagonal Dielectric Resonator Antenna for 2.4GHz WLAN Applications", **Microwave and Optical Technology Letters(USA)**, 20 Nov, 2006.
2. **V. Hamsakutty**, A.V. Praveen Kumar, Jaimon Yohannan, G. Bindu and K. T. Mathew, "Coaxial Fed Hexagonal Dielectric Resonator Antenna for multi- frequency operation", **Microwave and Optical Technology Letters(USA)**, Volume 48, Issue 5 , Pages 878 – 880, May 2006
3. **V. Hamsakutty**, A.V. Praveen Kumar, Jaimon Yohannan, K. T. Mathew, "Coaxial Fed Hexagonal Dielectric Resonator Antenna for Circular Polarization", **Microwave and Optical Technology Letters (USA)**, Volume 48, Issue 3 , Pages 581 – 582, March 2006
4. **V. Hamsakutty**, A.V. Praveen Kumar, G. Bindu, Vinu Thomas, Anil Lonappan, Jaimon Yohannan, K. T. Mathew "A Multi- Frequency Coaxial Fed Metal Coated Dielectric Resonator Antenna", **Microwave and Optical Technology Letters(USA)**, Volume 47, Issue 6 , Pages 573 - 575 Dec- 2005.
5. **V Hamsakutty**, Anil Lonappan, Joe Jacob, Jaimon Yohannan, Vinu Thomas, G.Bindu, K.T Mathew " A Novel Coupling medium for Microwave Medical Imaging" , **IEE Electronic Letters (UK)**, Vol. 39, No. 21, pp 1498-1499, 16th October 2003
6. A.V. Praveen Kumar, **V. Hamsakutty**, Jaimon Yohannan and K. T. Mathew, "A Wideband Conical Beam Cylindrical Dielectric Resonator Antenna's", **IEEE Antennas and Wireless Propagation Letters**, Vol.7, 2007
7. A. Lonappan, V. Thomas, G. Bindu, **V. Hamsakutty**, and K. T. Mathew "Analysis Of Human Breast Milk At Microwave Frequencies", **Progress in Electromagnetic Research (USA)**, 2005
8. A.V. Praveen Kumar, **V. Hamsakutty**, Jaimon Yohannan and K. T. Mathew, "A strip loaded dielectric resonator antenna for circular polarisation", **Microwave and Optical Technology Letters(USA)**, Volume 48, Issue 7 , Pages 1354 – 1356, July 2006.
9. A.V.Praveen Kumar, **V. Hamsakutty**, Jaimon Yohannan, K. T. Mathew Microstripline Fed Cylindrical Dielectric Resonator Antenna With a Coplanar Parasitic Strip", **Progress in Electromagnetic Research (USA)**,60,143-152,2006.
10. A. V. Praveen Kumar, **V. Hamsakutty**, Jaimon Yohannan, K. T. Mathew\*, "Microstripline fed Half-Cylindrical Dielectric Resonator Antenna for 2.4 GHz WLAN application", **Microwave and Optical**

- Technology Letters(USA)**, Volume 48, Issue 4 , Pages 724 – 726, April 2006
11. Vinu Thomas, C. Gopakumar, Jaimon Yohannan, Anil Lonappan, G. Bindu, A.V. Praveen Kumar, **V. Hamsakutty**, K. T. Mathew “A Novel Technique for Localizing the Scatterer in Inverse Profiling of Two Dimensional Circularly Symmetric Dielectric Scatterers Using Degree of Symmetry and Neural Networks” **Journal of Electromagnetic Waves and Applications(USA)**, Vol. 19, No. 15, 2113–2121, 2005
  12. G.Bindu , Anil Lonappan, Vinu Thomas, A. V. Praveen Kumar, **V Hamsakutty**, C.K. Aanandan, K.T Mathew “ Two Dimensional Microwave Tomographic Imaging of Low Water Content Tissues” , **Microwave and Optical Technology Letters (USA)** Vol. 46, No.6, pp 599-601, 20th September 2005
  13. Vinu Thomas, C. Gopakumar, A. V. Praveen Kumar, **V. Hamsakutty**, Anil Lonappan, G. Bindu, K. T. Mathew “A novel technique for reducing the imaging domain in microwave imaging of two dimensional circularly symmetric scatterers” , **Microwave and Optical Technology Letters (USA)** Vol. 44, No. 5, pp 423-427, 5th March 2005
  14. G.Bindu , Anil Lonappan, **V Hamsakutty**, Vinu Thomas, C.K. Aanandan, K.T Mathew “ Microwave Characterisation of Breast Phantom Materials” , **Microwave and Optical Technology Letters (USA)** Vol. 43, No.6, pp 506-508, 20th December 2004
  15. Vinu Thomas, C. Gopakumar, Anil Lonappan, G.Bindu, **V Hamsakutty**, K.T Mathew “ Microwave Imaging of Two-Dimensional Dielectric Cylinders with a Multiscaled Frequency Hopping Approach” , **Microwave and Optical Technology Letters (USA)** Vol. 43, No. 4, pp 353-355, 20th November 2004
  16. Anil Lonappan, **V Hamsakutty**, G.Bindu, Joe Jacob, Vinu Thomas, K.T Mathew “ Dielectric properties of human urine at microwave frequencies” , **Microwave and Optical Technology Letters (USA)** Vol. 42, No.6, pp 500-503, 20th September 2004
  17. G.Bindu ,**V Hamsakutty**, Anil Lonappan, Joe Jacob, Vinu Thomas, C.K. Aanandan, K.T Mathew “ Wide Band Bowtie Antenna with Coplanar Stripline Feed” , **Microwave and Optical Technology Letters (USA)** Vol. 42, No. 3, pp 222-224, 5th August 2004

### CONFERENCE PAPERS

1. **V. Hamsakutty** and K. T. Mathew, “ Dual frequency hexagonal dielectric resonator antenna for DCT and WLAN applications”, **National Symposium on Antennas & Propagation** December 14-

- 16, 2006, Department of Electronics, Cochin University of Science and Technology, Kochi-682 022, Kerala, India.
2. **V. Hamsakkutty**, A. V. Praveen Kumar, Jaimon Yohannan, K. T. Mathew, "Hexagonal dielectric resonator antenna for multifrequency operation", **IEEE AP-S International Symposium and USNC / URSI National Radio Science meeting, APS/URSI 2006**, July, 2006, Albuquerque, 9-13,USA.
  3. Jaimon Yohannan,**V. Hamsakkutty**, A. V. Praveen Kumar, Vinu Thomas, G. Bindu and K. T. Mathew, "A rectangular dielectric resonator band stop filter", **IEEE AP-S International Symposium and USNC / URSI National Radio Science meeting, APS/URSI** , 2006, July, 2006, Albuquerque, 9-13,USA.
  4. A. V. Praveen Kumar, **V. Hamsakkutty**, Jaimon Yohannan, K. T. Mathew, "Half split cylindrical dielectric resonator antenna for 2.4GHz wireless application", **IEEE AP-S International Symposium and USNC / URSI National Radio Science meeting, APS/URSI**, 2006, July, 2006, Albuquerque, 9-13,USA.
  5. **V. Hamsakutty**, A.V.Praveen Kumar, Jaimon Yohannan, Kattakkal Thomas Mathew, "Coaxial Fed Hexagonal Dielectric Resonator Antenna", **Asia Pacific Microwave conference**, Dec4-7 2005, china.
  6. Praveen Kumar A.V., **Hamsakutty V**, Jaimon Yohannan, Mathew K.T. "Microstripline Fed Cylindrical Sector Dielectric Resonator Antenna", **Asia Pacific Microwave conference**, Dec4-7 2005, china.
  7. G.Bindu, Anil Lonappan, Vinu Thomas, Jaimon Yohannan, **V. Hamsakutty**, C.K.Aanandan and K.T.Mathew, "coplanar stripline fed wide band bowtie antenna for ground penetrating radar", **URSI**, New Delhi 2005
  8. Jaimon Yohannan, A. V. Praveen Kumar, **V. Hamsakkutty**, Vinu Thomas and K. T. Mathew, "Synthesis of dielectric resonator for microwave filter designing", **Electromagnetic Research Symposium, PIERS 2005**, August 22-26, 2005, Hangzhou, China.
  9. Vinu Thomas, C. Gopakumar, Jaimon Yohannan, Anil Lonappan, G. Bindu, A.V. Praveen Kumar, **V. Hamsakutty**, K. T. Mathew\_"A Novel Technique for Localizing the Scatterer in Inverse Profiling of Two Dimensional Circularly Symmetric Dielectric Scatterers Using Degree of Symmetry and Neural Networks" **Electromagnetic Research Symposium, PIERS 2005**, August 22-26, 2005, Hangzhou, China
  10. Jaimon Yohannan, Vinu Thomas, **V. Hamsakkutty**, Praveen Kumar and K. T. Mathew," Microwave ceramic resonator antenna for communication applications", **IEEE AP-S International**

- Symposium and USNC / URSI National Radio Science meeting, APS/URSI 2005**, July 3-8, 2005, Washington DC, USA
11. A. V. Praveen Kumar, Jaimon Yohannan, Anil Lonappan, G. Bindu, Vinu Thomas, **V. Hamsakutty**, K. T. Mathew, "Microstripline Fed Circular Sector Dielectric Resonator Antenna", **IEEE AP-S International Symposium and USNC / URSI National Radio Science meeting, APS/URSI 2005**, July 3-8, 2005, Washington DC, USA
  12. Jaimon Yohannan, A. V. Praveen Kumar, Vinu Thomas, **V. Hamsakutty**, Anil Lonappan, K. T. Mathew "Half- Split Cylindrical Dielectric Resonator Antenna" **Fifth International Conference on Ferroelectrics, Ferroelectrics UK 2005**, April 26- 27, 2005, University of Paisley, Scotland, UK
  13. Vinu Thomas, C. Gopakumar, A.V. Praveen Kumar, **V. Hamsakutty**, Jaimon Yohannan, K. T. Mathew, "Imaging Domain Reduction in Microwave Imaging of Two Dimensional Circularly Symmetric Dielectric Scatters Using Degree Symmetry Vector" **International Conference on Photonics, Optoelectronics and Fiber optics**, SPIE 2004, December 9-11, 2004, Cochin, India
  14. **V Hamsakutty**, Anil Lonappan, Joe Jacob, G.Bindu , Vinu Thomas, A. V. Praveen Kumar, K.T Mathew " Biomedical Applications of Sodium Meta Silicate Gel as Coupling medium for Microwave Medical Imaging" , **IEEE AP-S International Symposium and USNC/URSI National Radio Science Meeting, APS/URSI 2004**, June 20-26, 2004, Monterey, California, USA
  15. Jaimon Yohannan, Vinu Thomas, **V. Hamsakutty**, Praveen Kumar , K. T. Mathew,"  $\text{Sr}_{(1-x/2)}\text{Na}_x\text{Nb}_2\text{O}_6$  ceramic dielectric resonator antennas", **National Symposium on Antennas & Propagation** December 21-23, 2004, Department of Electronics, Cochin University of Science and Technology, Kochi-682 022, Kerala, India.

## ERRATA

- 1) Since we had only one hexagonal die in our lab, we fabricated DRs of the same side length “a”, but of different heights throughout the thesis
- 2) pp. 24: Eqn. 1.1,  $X_{np}$  is the root of the characteristic equation  $J_n(X_{np}) = 0$  or  $J'_n(X_{np}) = 0$  and  $J_n$  is the  $n^{\text{th}}$  order Bessel function of the first kind,  $J'_n$  is the first derivative of  $J_n$
- 3) pp. 25, Ref. for Q-minimum, *Dielectric resonators*, Edited by D. Kajfez and Pierre Guillon, Artech House, 1986
- 4) pp. 27, Ref. for the relation between Q and dielectric constant: R. K Mongia and P. Bhartia, Dielectric Resonator Antennas-A Review and General Design Relations for Resonant Frequency and Bandwidth, Inter. Journal of Microwave and Millimeter-Wave Computer- aided Engineering, Vol.4, pp. 230-247, July 1994
- 5) pp. 28, 2<sup>nd</sup> sentence after Eq. 1.6: read as “Low Q-factor occurs for small values of dielectric constant”
- 6) pp. 36: Ref [9] should be read as Ref [11].
- 7) pp. 71, line 4 from the bottom, “special” should be replaced by “spatial”.
- 8) Section (3.4.4), The polarisation of the test antenna is measured by manually rotating the horn antenna about its axis, not by using the position controller.
- 9) pp. 76-79: “dye” should be replaced by “die” that is the device used for producing a shaped DR from the material powder.
- 10) For section (4.2) refer, A. J. Moulson and J. M. Herbert, Chapter 3 – Processing of Ceramics in *Electroceramics: Materials, Properties, Applications*, 2<sup>nd</sup> edition, Wiley
- 11) pp. 150: denominator of Eq. 6.42 is  $\Delta y$  instead of  $\Delta x$ .
- 12) pp. 159: Don't get confused with the sides of the cross section of the DR that seem unequal in Fig. 6.3 (d). All are of equal length “a”.

**V.HAMSAKUTTY**

Senior Research Fellow (FIP of UGC), Department of Electronics,  
Cochin University of Science and Technology, Cochin 682 022, Kerala, India

Phone: 91-484-2576418 Cell: 91-9446688782 Fax: 91-484-2575800

E-mail: [vhamsakutty@yahoo.com](mailto:vhamsakutty@yahoo.com), [hk@cusat.ac.in](mailto:hk@cusat.ac.in)

---

**PERSONAL**

Date of birth : 19<sup>th</sup> January 1976

Sex : Male

Languages Known : English and Malayalam

Nationality : Indian

Religion : Islam

Marital status : Married

Father's Name : V. Abdul Khader

Website : [www.freewebs.com/vhamsakutty](http://www.freewebs.com/vhamsakutty)

Permanent Address  
Vetikalladi House  
Pallikurup. P.O  
Mannarkkad  
Palakkad  
Kerala, India  
Phone: 91-4924-224923  
Cell: 91-94466688782  
E. mail : [vhamsakutty@yahoo.com](mailto:vhamsakutty@yahoo.com)  
[hk@cusat.ac.in](mailto:hk@cusat.ac.in)

Office Address  
FIP Teacher Fellow (FIP of UGC)  
Department of Electronics  
Cochin University of Science &  
Technology ,Cochin-682 022  
Kerala, India  
Phone : 91-484-2576418  
Cell: 91-9446764985  
Fax: 91-484-2575800

**SUMMARY**

- 5+ years of teaching experience at graduate level
- 4 years of research experience in Microwave Electronics, especially in dielectric resonator antennas
- Proficiency in Assembly Language programming (& Microprocessors) and high level programming
- 

**EDUCATION**

Course	Year	University	Institution	Class
Ph.D - Microwave Electronics (Synopsis submitted)	June 2002 to till date	Cochin University of Science and Technology, Cochin, Kerala, India	Department of Electronics, Kerala, India	--
M.Sc Electronics Science	1996-1999	Cochin University of Science and Technology, Cochin, Kerala, India	Department of Electronics, Kerala, India	<b>First Rank</b> with Distinction (84.5%) <b>CGPA-8.5</b>
B.Sc Physics	1993-1996	University of Calicut Kerala, India	M.E.S College, Mannarkkad, Kerala, India	<b>Topper</b> First class with Distinction (90.8%)

**HONORS, AWARDS & ACHIEVEMENTS**

1. Included in the **first edition of who's who in Asia** in the field of **Engineering** during the year 2006-2007.
2. Authored/co-authored **32 research papers** in International Journals such as IEEE Microwave and Wireless Component Letters, IEE Electronics Letters, Microwave and Optical Technology letters etc. and in conference proceedings.
3. Awarded research fellowship through **Faculty Improvement Programme (FIP)** for undertaking doctoral research work by University Grants Commission (UGC), under the Ministry of Human resources development, Govt. of India, India.(2005-2007)
4. Qualified **UGC-NET test for lecturers** conducted by University Grants Commission, Ministry of Human Recourses Development,



- Govt. of India. In India this test is compulsory for the post of Lecturer appointment in the Universities and Colleges.(2001)
5. **First Rank Holder**, M.Sc Electronics examination, Cochin University of Science and Technology ( CUSAT) Kochi, India (1999)
  6. Recipient of **K.G Nair Endowment Gold Medal** for securing first rank in Post graduation, which was one of the honorable award given to the most talented student of the Department of Electronics, CUSAT (1999)
  7. 1996-1998 **M.E.S Merit Scholarship** for studying Master of Science.
  8. **Topper in B.Sc Degree examination** at M.E.S College, Under University of Calicut, Mannarkkad, Kerala, India.

### **TECHNICAL SKILLS**

1. Experience in Antenna and RF/Microwave circuit design using **Ansoft HFSS**
2. Proficient in Finite Difference Time Domain (**FDTD**) method
3. Experienced in using **PNA 8362B** Network Analyzer, **Vector Network Analyzer HP 8510C and 8714ET**, Spectrum analyzer, Digital oscilloscope, Function generator .
4. Experience in carrying out antenna measurements in Anechoic Chambers
5. Hands-on experience in building of antenna prototypes using photolithography and antenna experimental work.
6. Experience in design and testing of Dielectric Resonator Antennas
7. Measurement of Dielectric constant and Loss tangent of a material using Cavity Perturbation Technique
8. Measurement of Dielectric constant using Hakki and Colemann set up.

### **PROGRAMMING SKILLS**

High-level languages:	C, C++, FORTRAN, BASIC, VHDL.
Operating systems:	Dos, Windows 98/2000/Xp, Linux.
Design automation tools:	Xilinx FPGA.
Algorithm development environments:	MATLAB
Assembly language:	8085
General Applications:	MS office

### **SCHOLARLY WORK AND SERVICES**

1. **Reviewer**, International Journal Progress in Electromagnetic Research and Electromagnetic Waves and Application (PIER & JEMWA).
2. **Chairman, board of Studies**, Electronics, University of Calicut, Kerala, India (since 2005)
3. **Member, board of Examination**, Electronics, University of Calicut, Kerala, India
4. **Member, board of Examination**, Electronics, Kannur University, Kerala, India.
5. **Subject expert** for appointing lecturers in colleges, University of Calicut, India.
6. **National Service Scheme programme officer**, W.M.O College, University of Calicut, India (2001-2003)
7. **National Service Scheme programme co-ordinator**, National integration camp, University of Calicut, India (2003)

### **WORK EXPERIENCE INCLUDING RESEARCH PROJECTS**

#### **RESEARCH / TEACHING EXPERIENCE**

1. Senior Research Fellow under faculty Improvement Programme of University Grants Commission at the Department of Electronics, Cochin University of Science and Technology, Cochin, from Feb 2005 to till date.
2. Lecturer at the Department of Electronics, W.M.O Govt. Aided College, Kalpetta, Wayanad, Kerala from Feb 2004 to Jan 2005.
3. Senior research fellow in a DST project of government of India at dept of Electronics, Cochin University of Science and Technology, Kochi, Kerala, India, July 2003 to Jan 2004
4. Lecturer at the Department of Electronics, W.M.O Govt. Aided College, Kalpetta, Kerala from July 1999 to June 2003.

**REFERENCES**

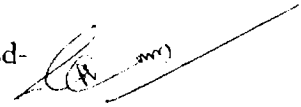
1. Prof. (Dr.) K.T. Mathew  
Professor & Dissertation Guide  
Department of Electronics  
Cochin University of Science and Technology, Kochi-22, India.  
Email: ktm@cusat.ac.in, Ph. 91-484-2576418, Fax : 91-484-2575800
  
2. Prof. (Dr.) K. Vasudevan  
Professor & Head  
Department of Electronics  
Cochin University of Science and Technology, Kochi-22, India.  
Email: vasudevan@cusat.ac.in, kv@cusat.ac.in,  
Ph. 91-484-2576418, Fax: 91-484-2575800
  
1. Dr. C.K Aanandan  
Reader  
Department of Electronics  
Cochin University of Science and Technology, Kochi-22, India.  
Email: anand@cusat.ac.in, Ph. 91-484-2576418, Fax: 91-484-2575800

I here by declare that all the information given above is true to the best of my Knowledge and belief.

Kochi

15-03-2007.

-sd-



V. Hamsakutty